PHOTOCATALYTIC DEGRADATION OF MICROPOLLUTANTS USING THIN FILMS FABRICATED WITH ADVANCED MATERIALS

A THESIS SUBMITTED IN PARTIAL FULFILMENT OF THE REQUIREMENTS FOR THE DEGREE OF DOCTOR OF PHILOSOPHY

CVL HMINGMAWIA

MZU REGISTRATION NUMBER : 1807307

Ph.D REGISTRATION NUMBER : MZU/Ph.D./1222 of 09.08.2018

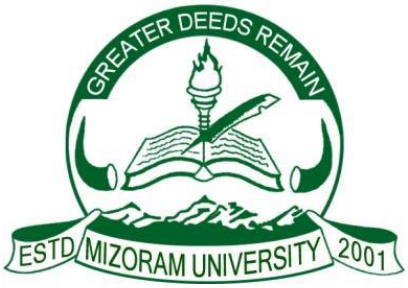

DEPARTMENT OF CHEMISTRY

SCHOOL OF PHYSICAL SCIENCES

SEPTEMBER, 2022

PHOTOCATALYTIC DEGRADATION OF MICROPOLLUTANTS USING THIN FILMS FABRICATED WITH ADVANCED MATERIALS

BY

CVL HMINGMAWIA

Department of Chemistry

Under the supervision of

Prof. DIWAKAR TIWARI

Submitted

In partial fulfilment of the requirement of the Degree of Doctor of Philosophy in Chemistry of Mizoram University, Aizawl.

MIZORAM UNIVERSITY
Department of Chemistry
(A DST-FIST Supported Department)
Tanhril, Aizawl, Mizoram. PIN: 796004

Prof. Diwakar Tiwari, Dean (SPS)

Thesis Certificate

This is to certify that the thesis entitled *'Photocatalytic degradation of micropollutants using thin films fabricated with advanced materials'* submitted by ***Mr. CVL Hmingmawia,*** for the degree of ***Doctor of Philosophy*** in the Mizoram University, Aizawl, Mizoram, embodies the record of original investigations carried out by him under my supervision. He has been duly registered and the thesis presented is worthy of being considered for the award of the Ph.D. degree. This work has not been submitted for any degree in any other university.

Dated: 22nd Sep, 2022.

(DIWAKAR TIWARI)
Supervisor

Tanhril Campus, Aizawl 796 004 Phone : 9862323015
Fax : (0389) 233 0834 E-mail : diw_tiwari@yahoo.com

DECLARATION OF THE CANDIDATE

Mizoram University

Sep, 2022

I, CVL Hmingmawia, hereby declare that the subject matter of this thesis is the record of work done by me, that the contents of this thesis did not form basis of the award of any previous degree to me or to do the best of my knowledge to anybody else, and that the thesis has not been submitted by me for any research degree in any other University/Institute.

This is being submitted to the Mizoram University for the degree of Doctor of Philosophy in Chemistry.

Dated: 22nd Sep, 2022

(CVL HMINGMAWIA)

Candidate

(Prof. MUTHUKUMARAN, R)

Head

(Prof. DIWAKAR TIWARI)

Supervisor

ACKNOWLEDGEMENT

First of all, I thank Almighty God for blessing me with the strength, health and wisdom to carry out this research and helping me to accomplish this work.

I would like to express my deepest and sincere gratitude to my research supervisor, *Prof. Diwakar Tiwari*, Department of Chemistry, Mizoram University, for giving me the opportunity to do research and giving helpful suggestions and guidance throughout this research. His vision, dynamism, motivation and sincerity have deeply encouraged me. He has been a great teacher, a friend and a guiding light to me. It was a great honor to work and study under his guidance. I would also like to express my gratitude for his compassion and good humor. I like to express my heartfelt thanks to his wife, family for their support, acceptance and endurance throughout the time he has devoted to my research work and thesis preparation.

I wish to express my heartiest gratitude to *Prof. Muthukumaran, R., Head, Department of Chemistry, MZU,* and other faculty members *viz., Dr. Zodinpuia Pachuau, Dr. N. Mohondas Singh, Dr. Ved Prakash Singh* and *Dr. A. Bimolini Devi*, for their support, encouragement and innovative suggestions during my research work. I would also like to convey my heartiest gratitude to *Dr. Lalhmunsiama,* Asst. Prof., Dept. of Industrial Chemistry, Mizoram University, for his helpful suggestions, support and patience in my research work. Despite his busy schedules, he is always open for help whenever I request him and I acknowledge and appreciate all his efforts.

I am delighted to appreciate the collaboration and assistance I got from all of my colleagues in the Department of Chemistry. I thank *Dr. R. Malsawmdawgnzela, Dr J. Lalmalsawmi, Dr. Levia Lalthazuala, Ms Ngainunsiami, Mr. Ricky Lalawmpuia, Mr. Sari kokba, Mr. Himangshu Dihingia, Ms. Lalmalsawmdawngliani, Mr. Lalruatkima Ralte, Ms. Melody Lalhruaitluangi, Ms. Swagata Goswami* for their support and helping hand, throughout my research work. I want to thank *Mr. Brojendro Singh Shagolsem*, Sr. Laboratory Technician, and *Mr. John Vanlalhruaia*, Technical Assistant, Chemistry Department for their helpful assistance. I express my heartfelt gratitude to them.

Last but not the least, my heartfelt gratitude to all of my family members for their everlasting prayers and constant support. They are always supportive and encouraged me throughout my academic and personal lives, and wished for this goal to become a reality.

(CVL HMINGMAWIA)

CONTENTS

List of Figures:

List of Tables:

INTRODUCTION

1. INTRODUCTION

1.1. Background

The most valuable natural resource on the planet is water. However, the water resources are unethically and improperly treated. Therefore, a reliable fresh and clean water resource remains a global concern. The entire amount of water available on Earth is estimated to be around 1.4 billion cubic kilometres. However, due to high saline levels in oceans and seas, approximately 97.5% is unfit for human consumption. A major portion (68.7%) of the available 2.5 percent fresh water is in the form of glaciers, ice caps, and permanent snow. Ground water (30.1%) and surface water (1.3%) are the only sources of available fresh water. Thus, only 20.56% of the accessible surface waters lying in rivers and lakes (i.e., 0.26% of total world fresh water reserves or 0.007% of the entire earth's water) is suitable for human consumption (Gleick et al., 2007). Meanwhile, these finite freshwater resources are under tremendous stress, which results in unsustainable exploitation and rising water demand for numerous human activities. Furthermore, global climate change, growing urbanisation, agricultural and industrial activity caused massive release of wastewater contained with refractory contaminants and solid wastes. Over the last few decades, the volume of hazardous wastes deposited in aquatic environments has increased dramatically (Jackson et al., 2001; Laws, 2000). According to the study published by the World Water Assessment Program (WWAP), about 14 billion pounds of hazardous wastes are dumped into the oceans each year and every day, about 2 million tonnes of human garbage is disposed-off into the water bodies (Dwivedi, 2017; Gleick, 2000). Furthermore, massive increase in pollutant load has resulted in widespread water quality degradation/deterioration around the world, limiting availability of clean or fresh water. 2 billion people lack access to clean/fresh water, according to the World Bank and the World Health Organization, and 1 billion people are unable to get their daily basic needs. Each year, 3.5 million people die in the developing nations as a result of insufficient water supply, sanitation, and hygiene difficulties (Gleick et al., 2007; Selene and Chou, 2003).

The increased amount of wastewater carrying a wide range of toxic and hazardous chemicals along with pathogens poses a serious threat to human health, aquatic life and the environment in general. Diarrheal illness is one of prominent water borne diseases; expected to cause 1.5 million children's death below the age of five years (Gleick, 2000; Kirstein et al., 2021; Y. Liu et al., 2021).

Furthermore, the increasing global shortage of clean water, as well as the catastrophic environmental repercussions of dirty wastewater, need an urgent treatment and reduction of such wastewaters. Due to rigorous environmental regulations and norms, it is now required that wastewater collected from municipalities and communities need to be appropriately treated in order to meet the mandated and stringent water quality requirements before being disposed-off into lakes or rivers (Laws, 2000).

Quality of the effluent, energy efficiency, cost-effectiveness and nutrient removal/recovery are the top concerns for wastewater treatment systems (WWT) (Kirstein et al., 2021). Despite advancements in wastewater treatment, conventional water treatment systems have limits in various parameters. Skimming/Screening is the first step in the wastewater treatment process, followed by chemical/biological treatment and advanced treatment with disinfections and mineralization are extensively included (Manea et al., 2016). As a result, the treatment process entails a number of time-consuming steps that necessitate the use of a range of chemicals. Perhaps the most important disadvantage is the potential for environmental issues to arise as a result of these activities. Hypochlorite, chlorine and ozone are among the chemical oxidants typically employed in wastewater treatment. Because of their easy availability, possibly cost effectiveness and relative efficiency as oxidants, these compounds are widely used (Brandt et al., 2017). However, the compounds and by-products produced appear to be hazardous, their application in such environmental remediation raises various health issues. Furthermore, the use of ozone and chlorine in wastewater treatment is linked to the formation of toxic disinfection by-products (DBPs) such as bromate and trihalomethanes (Krasner et al., 2009). Numerous by-products are potentially carcinogens or mutagens, making them potentially more dangerous than the original compound. Hypochlorite is also a source of concern; it is

utilised as a source of chlorine for treatment of water at smaller operations because it is affordable; hypochlorite is manufactured using chlorine gas and rapidly decomposes back into chlorine when heated or mishandled chemically (Backer, 2017).

Another disadvantage of current wastewater treatment systems is the production of excessive sludge, which frequently encompasses numerous types of harmful substances like organic matter and N, P, K and other nutrients, making its removal a serious concern. The vast amount of extra sludge created on a daily basis, on the other hand, has become the most problematic for environmental engineers to handle it amicably (T. Ahmad et al., 2016). Because of more strict legislation and social concerns for the environment, traditional sludge treatment and disposal options (e.g., compost and landfill) are facing a growing challenge. Additionally, many organic sulphides and amines formed during wastewater treatment contribute to *on-site* odours that bothers the population living around. This is necessitating the development of newer H_2S control methods in municipal sanitary sewer systems, treatment plants, and industrial waste treatment facilities (Pal, 2017). Furthermore, the presence of micropollutants, such as hormones, medicines, and personal care products, often known as emerging contaminants, are often detected in water bodies at lower levels. The existence of these persistent micropollutants in the aquatic environment is frequently linked to a variety of negative consequences, including short- and long-term toxicity, endocrine disruption, and antibiotic resistance in microbes (Chavoshani et al., 2020). These micro-pollutants are often detected in the effluent of conventional wastewater treatment plants (WWTPs); raising concerns of the aquatic environment.

Therefore, there is a growing concern on developing effective and efficient waste water treatment methods, which is feasible, cost-effective, environment friendly, and sustainable. "Advanced Oxidation Process (AOPs)" is one of alternative methods, which relies on heterogeneous photocatalysis and uses TiO_2 semiconductor as a photocatalyst (Angel et al., 2018; Pelaez et al., 2011; So et al., 2002). The basis of AOPs lies on the *in situ* formation of reactive species, such as hydroxyl radicals, which rapidly oxidises a variety of organic contaminants non-selectively (Linley et al., 2014; Falah et al., 2016). Titania (TiO_2) is having variety of applications, which is primarily due to its unique qualities, that include high thermal and chemical stability,

biocompatibility, low toxicity, cost effective, ease of manufacturing and tailored material. The use of TiO_2 semiconductor in photocatalytic processes is found to be a cost-effective, environment friendly, and long-term treatment technique that aligns with the 'zero' waste strategy (Chen et al., 2020).

1.2. Micropollutants in Aquatic Environment

1.2.1. Tetracycline (TC)

Tetracycline is a widely prescribed antibiotic for the treatment of bacterial infections like pneumonia, gonorrhoea, amoebic infections, respiratory tract infections, Rocky Mountain spotted fever and syphilis (Jiang et al., 2022). It is also used to treat acne vulgaris, as well as other skin conditions such as perioral dermatitis and rosacea (Farombi et al., 2008). Moreover, tetracycline is utilised to the aquaculture and the live stocks as an effective antibiotic (Niu et al., 2013). Moreover, according to the National Ambulatory Medical Care Survey (2007) of visits to office-based physicians in the United States, tetracycline is prescribed as a new or continuing medicine, among other similar drugs. Furthermore, because of its easy accessibility, availability, and cost effectiveness, the medicine has achieved widespread acceptability in third-world countries. As a result, the medicine is abused by self-prescriptions (Farombi et al., 2008).

Tetracycline enter the water bodies as active metabolites, unmetabolized drugs and breakdown products by excretion and direct runoff (Alotaibi and Mahmoud, 2022). Several monitoring studies (using GC/LC-MS) reveal that pharmaceuticals are widely detected into the water bodies. It is a known fact that over 90% of antibiotics are excreted through the urine and up to 75% in animal faeces, implying that 70%-80% of antibiotics enter into the sewage system in their parent form. However, the conventional sewage treatment system is unable to eliminate it completely; hence, resulting in the occurrence of residual antibiotics in the treated wastewater effluents. The tetracycline removal rate in the conventional wastewater treatment plants was reported to be 30% (Warner et al., 2022). This poses a serious threat to the entire ecosystem. Tetracycline is detected in the wastewater, surface water, drinking water as well as soils with measured concentrations ranging from ng L^{-1} – μg L^{-1} (Yang et

al., 2013). The presence of cumulated tetracycline in the environment causes genetic exchange, increasing bacteria's resistance to antibiotics, and posing a hazard to human health. Hence, developing novel and effective technology for removing tetracycline from aquatic habitats is critical and worth studying (C. Li et al., 2022).

Since its discovery in 1951, tetracycline is a known non-alcoholic steatohepatitis, or NASH (a condition where there is fats accumulation in the liver and accompanying liver diseases such as lipid peroxidation and cell necrosis/apoptosis) drug used in humans and rats (Lepper et al., 1951). Tetracycline-induced NASH was well-documented elsewhere (Shen et al., 2009). Tetracycline inhibits the tricarboxylic acid cycle and respiratory chain in rat mitochondria (Fromenty and Pessayre, 1995). In rats and humans, triglyceride build up and lipid peroxidation was discovered, followed by surge in serum alanine and aspartate aminotransferases. In vitro investigations using hepatocyte monolayers were used to partially demonstrate the tetracycline toxicity. Tetracycline-treated hepatocytes from rats and dogs showed impaired fatty acid metabolism and lipid build up, while oxidative stress was seen in both rat and human hepatocytes. Tetracycline therapy causes a reduction in mitochondrial membrane potential in human hepatocytes. Thus, these monolayer culture results addressed lipid build up, oxidative stress, or mitochondrial lesion, which only reflected a portion of cellular alterations (Xu et al., 2008).

Tetracycline also causes a variety of metabolic problems in animals and is suspected of causing testicular harm in humans. Tetracycline treatment resulted in a decrease in motility of epididymal sperm, sperm count, percentage of live spermatozoa, a rise in aberrant sperm morphology, and adverse histopathologic alterations in the testes (Zhong et al., 2022). Tetracycline also causes hepatotoxicity, which is associated with fatty infiltration and damage to liver parenchymal cells. The drug was also linked to hyperglycaemia and pancreas damage (Asha et al., 2007). The mechanisms by which tetracycline causes these effects are unknown, however reactive oxygen species (ROS) are suggested to be responsible (Li and Hu, 2016). Tetracycline produces oxidative stress in rats' liver and pancreas by lowering antioxidant enzymes and glutathione (GSH) levels while increasing the quantities of lipid peroxide produced (Asha et al., 2007). In the liver of rats given tetracycline antibiotics,

immunohistochemical expression of oxidative stress-related markers such as heme oxygenase-1, superoxide dismutase (SOD) and 8-hydroxy deoxyguanosine was predominantly detected (Kikkawa et al., 2006).

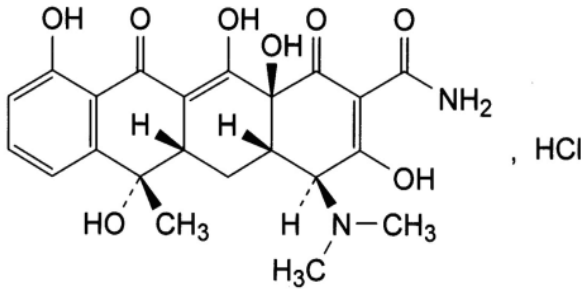

Figure 1.2.1: Structure of tetracycline

1.2.2. Sulfamethazine (SMZ)

Sulfamethazine (SMZ) belongs to the sulfonamide family. Sulfonamide drugs are a class of synthetic antimicrobials that possess a wide range of applications against Gram-positive and Gram-negative bacteria (H. Liu et al., 2021). These drugs were used in medical practice long before penicillin was discovered. They are derived from sulfanilamide (p-aminobenzenesulfonamide), a structural analogue of p-aminobenzoic acid (a component required in the production of folic acid in bacteria), the precursor of DNA, nucleic acids and purine. Therefore, sulfonamides are bacteriostatic medicines that suppress bacterial growth by interfering with bacterial folic acid production (Lin and Cheng, 2021). The drug disrupts the biosynthetic pathway for synthesis of folic acid, effectively preventing the conversion of p-aminobenzoic acid to folic acid (mediated by the enzyme dihydropteroate synthetase), making them antimetabolites. Sulfonamides showed antibacterial activity against *Proteus mirabilis*, enteric Gram-negative E. coli, Haemophilus influenzae, Neisseria, Nocardia, Listeria *monocytogenes*, *Streptococcus nonenterococcus*, *Staphylococcus aureus*, and a few species of anaerobic bacteria (Lin et al., 2022). They are most commonly used to treat toxoplasmosis, menigococcal disorders, streptococcal pharyngitis, infections caused by Nocardia asteroides, uncomplicated urinary tract infections and other infections. Long-term usage of these medications lead to development in drug resistance (He et al., 2022).

SMZ is often prescribed to human, animal, aquaculture and livestock production due to its low cost and broad-spectrum antibacterial efficacy (Ledjeri et al., 2017; Lin and Wu, 2018). The drug is partially metabolized once administered to humans or animals hence released in significant amounts through the faeces or urines and subsequently entering into the wastewaters (Yu et al., 2019). It was reported that SMZ is one of the most often detected antibiotics in water bodies (Li et al., 2021). It is potentially harmful to marine species, affects animal reproduction, and interrupts the human endocrine system, hence; the presence of SMZ in water bodies is a serious environmental concern (Perini et al., 2018). The presence of SMZ in the aquatic environment promotes the tolerance in microorganisms, lowering the drug effectiveness (Li et al., 2016). SMZ drug is usually detected at the range of ng/L to mg/L in aquatic environments (Wen et al., 2018; F. Wang et al., 2018b; X. Liu et al., 2019).

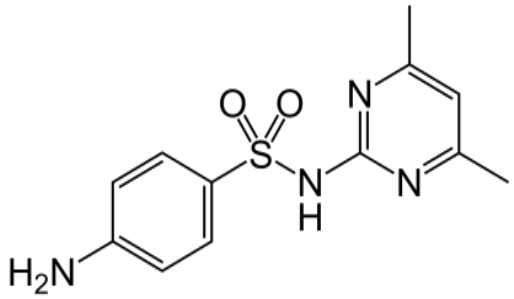

Figure 1.2.2: Structure of Sulfamethazine

1.2.3. Bisphenol A (BP-A)

Bisphenol A (4,4'-(propane-2,2-diyl)diphenol) is a common organic compound used as a raw material and intermediary in the production of epoxy resins, polycarbonate plastics and food packaging (Mutou et al., 2006). It has harmful effects on a variety of targets in the human body via estrogen response pathways (Ballesteros-Gómez et al., 2009). It is regarded as a typical chemical of endocrine disrupting chemicals (EDC) that leads to damage in the reproductive organs of aquatic organisms (Kang et al., 2006; Suzuki et al., 2004). It is evident that once EDCs enter into the body, interacts with the normal secretory substances, which effect the metabolism,

operation, release and synthesis process in the body. It causes inhibition in the action of endocrine system and also a variety of functional obstacles in the human body such as reproductivity disorder, immunity disorder and diseases related to the nervous system (Ismail et al., 2017). It is detected in natural surroundings such as foods, soil, water and air and finally enters the human tissues and fluids, at amounts ranging from PPM (parts-per-million) to PPB (parts-per-billion) levels. BP-A is released into the environment through wastewater discharge from BP-A-producing or BP-A-containing enterprises and industries (Ackerman et al., 2010; Yamamoto et al., 2001). As a result, BP-A pollution of the aquatic environment has become a global and serious health concern.

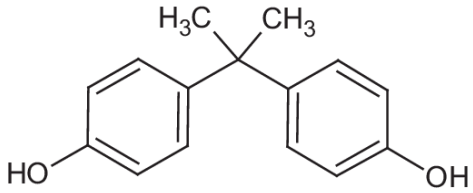

Figure 1.2.3: Structure of Bisphenol A

1.3. Dyes in Aquatic Environment

Dyes are water soluble organic compounds and used since human's civilization for a variety of purposes. Natural dyes were previously used on a small scale from naturally available materials such as plants and insects (Arora, 2014; Forgacs et al., 2004). It was considered that utilising natural dyes rather than synthetic dyes is a safer option for colouring the materials. Synthetic dyes are being used to colour printings, polymers, cosmetics, textiles, food materials etc. Because of the auxochrome (water soluble bonding chemicals) and chromophores (colour producing compounds) in nature, synthetic dye molecules are complex and stable in the ambient environment. However, auxochromes (colour helpers), such as sulfonic acid, hydroxyl, carboxylic acids, and amino groups, which aid in colour changes and offer dye solubility, are responsible for recalcitrant nature of these dye compounds (Carmen and Daniel, 2012). Because of the increased demand of synthetic dyes, large-scale production of synthetic dyes began and are extensively utilized in the pharmaceutical, food, cosmetic, textile,

paint, tannery, paper and pulp, and paper industries for dyeing the materials. Synthetic dyes enter the water bodies through effluent discharged by these industries, as well as those from dye manufacturing plants (Gürses et al., 2016). Therefore, the dye industries posing the serious environmental problems by discharging a massive amount of dye compounds into the aquatic environment and lead to a major threat to the aquatic environment's living species (Jung et al., 2016; Su et al., 2011; Muhd Julkapli et al., 2014). A rough estimate indicated that over 7 x 10^5 tons of dye produced each year having more that 10,000 types of dye compounds. Moreover, *Ca.* 10-15% of these dyes are used in dyeing operations and remaining are discharged through the effluents (Ali, 2010). These industrial effluents containing high concentrations of dye compounds showed a high chemical oxidation demand, high biological oxidation demand, high alkalinity and a high total dissolved solids content. Non-ionic dyes (disperse dyes), cationic dyes (basic dyes) and anionic dyes (direct, acid, and reactive dyes) are the three different types of dyes (Wainwright, 2011). Ionic and non-ionic dye chromophores are mostly composed of azo (-N=N-) groups or anthraquinone types. Because of their fused aromatic structures, anthraquinone-based dyes are more impervious to degradation. Metal complex dyes are primarily based on azo dyes and chromium, which are extensively used and account for 70% of total dye produced (Arora, 2014).

1.3.1. Mordant Orange-1 (MO1)

Mordant Orange-1 (MO1) is a water-soluble dye having complex aromatic structure and persistence in aqueous medium. It is also known as a 5-(4-Nitrophenylazo) salicylic acid sodium salt. Mordant orange-1 has an azo group and is a salicylic acid derivative. It is synthesized by the diazo coupling reaction and these compounds are not degraded efficiently with the conventional waste water treatment plants (Abdel-Messih et al., 2013). MO1 is primarily utilized to create yellow and orange hues. The presence of nitrogen double bonds (N=N-) distinguishes azo dyes (Sun et al., 2013). It is also utilized as an acid-base indicator. The azo bond is the chromophore part of the molecule, which reduces transmittance of water significantly and showed greater impact on aquatic life (Khan et al., 2019).

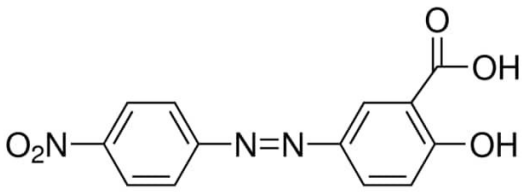

Figure 1.3.1: Structure of Mordant Orange 1

1.3.2. Rhodamine B (Rh-B)

Rhodamine B (N-[9-(ortho-carboxyphenyl)-6-(diethylamino)-3H-xanthen-3-ylidene] diethyl ammonium chloride) (Rh-B) is a red colour dye, which is highly soluble in water and belongs to the xanthene class (Jain et al., 2007). The dye is familiar water tracer fluorescent and is commonly used as a colorant in fabrics and foods (Richardson et al., 2004). It causes skin and eyes irritation and respiratory tract disorder when consumed by humans and animals (Rochat et al., 1978). Experimental evidence for its carcinogenic nature, toxicity in reproduction and developments and neurotoxicity in animals and human are some of known effects listed elsewhere (Kornbrust and Barfknecht, 1985; McGregor et al., 1991; Mirsalis et al., 1989).

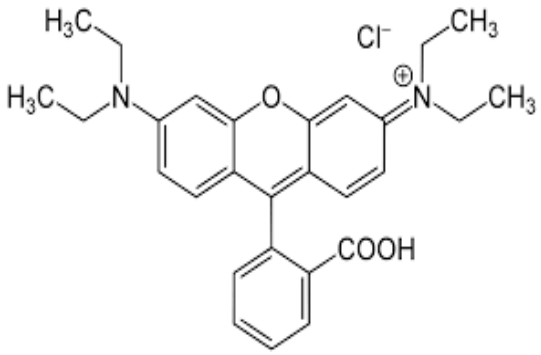

Figure 1.3.2: Structure of Rhodamine B

1.3.3. Rhodamine 6G (Rh-6G)

Rhodamine 6G (Rh-6G) is a synthetic dye, having fluorescent properties. Rh-6G is frequently used as a laser gain medium, tracer dyes, colouring agent in printing, etc. (Sabnis, 2015). It is a xanthene derivatives dye (Sabnis, 2015), which are highly corrosive to metals (Kang et al., 2015) and are known to be carcinogenic to humans

(Alford et al., 2009; Nestmann et al., 1979). Rh-6G is a fluorophore, which is not approved by the food and drug administration (FDA) and is reported to be toxic and mutagenic to cells, organs and organisms (Alford et al., 2009). Rh-6G is toxic to the tissues, triggering serious harm to ganglion cells of rat retinal (Thaler et al., 2008). Nestmann et al. reported that in mammalian and bacterial cultured cells, rhodamine 6G and rhodamine B are found to be genetically active. Rhodamine 6G is more mutagenic than rhodamine B (Nestmann et al., 1979).

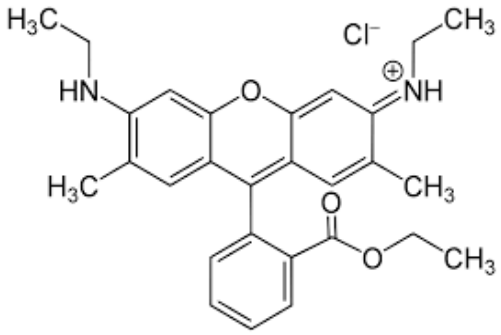

Figure 1.3.3: Structure of Rhodamine 6G

The complex aromatic structure makes dye compounds stable hence, persistent towards the biodegradation and led to make them relatively recalcitrance or persistent in soils and aquatic systems (Florenza et al., 2014; Forgacs et al., 2004). They are fairly stable even in the presence of numerous oxidising agents (Fu and Viraraghavan, 2001). As a result, dyes escaped from the existing wastewater treatment plants and wreaked havoc on the aquatic habitat once entered into the water bodies. The transmission of solar light is reduced in dye-contaminated water. As a result, photosynthesis is diminished or completely inhibited (Shawabkeh and Tutunji, 2003). Some dyes are highly toxic, bio accumulative and induce skin illnesses. Some Azo dyes are known to be mutagenic/carcinogenic and teratogenic (Dias et al., 2016). Their breakdown derivatives are also found to be harmful to aquatic life (fish, microorganisms, aquatic plants and mammals). Synthetic dyes compose of 3,3′-dimethylbenzidine, 3,3′-dimethoxybenzidine and benzidine are categorized as carcinogens of category 2, that is, "substances that should be considered as if they are carcinogenic to human" under current EU regulations. Furthermore, extensive research indicated that these dye compounds undergo biological and chemical assimilations, preventing re-oxygenation

in receiving streams, consume dissolved oxygen, causing eutrophication and have a proclivity to be sequestered by metal ions, thereby accelerating microtoxicity and genotoxicity (Walsh et al., 1980). In a broader sense, periodic and unwarranted exposure to coloured sewages causes a wide range of immune suppression, central nervous, circulatory, respiratory and neurobehavioral disorders, such as tissue necrosis, quadriplegia, jaundice, cyanosis, salivation, profuse diarrhoea, insomnia, hyperventilation, vomiting, leukaemia, multiple myeloma, autoimmune diseases, allergy (Verma et al., 2012; Foo and Hameed, 2010).

1.4. Micropollutant Removal in Wastewater Treatment Plants (WWTPs)

In general, public departments set up waste water treatment plants (WWTPs), but some organisations set up their private WWTPs to treat wastewaters from different sources, such as sewage, sanitation, laboratories, domestic etc. (Boehler et al., 2012; Z. Liu et al., 2009). Phosphorus, nitrogen, carbon, coliforms and pathogens in wastewaters are to be eliminated from the wastewaters using these conventional WWTPs. Furthermore, the sludge produced during the treatment was capable of removing a number of non-polar chemical compounds through the sorption process. In WWTPs, organic chemicals are removed through biotransformation/biodegradation and aeration (volatilization) (Sossalla et al., 2021). Some emerging micropollutants and several water contaminants on the other hand, are not eliminated and escape along with WWTP effluents, eventually enter into the receiving waters followed by the surface waters (Pintado-Herrera et al., 2014).

WWTPs are having limited capacity to efficiently remove the pharmaceutical compounds present in urban wastewaters, because some of these chemicals are ingested by microorganisms for their carbon source, and may restrict microorganism activity or cause bioaccumulation (Kosek et al., 2020). The concentration of pharmaceuticals in effluents from Waste Water Treatment Plants (WWTPs), Sewage Treatment Plants (STPs) and surface waters vary substantially, probably due to differences in pollutant loads in different regions and wastewater treatment plant effectiveness (Boehler et al., 2012). The treatment of wastewater in WWTPs is a time-consuming and complicated process. Moreover, prior to discharge the effluent of these

WWTPs into receiving waterways, wastewater need to be free from pollutant load to safeguard the living organisms in water bodies. If the treated wastewater contains with even low load of emerging pollutants viz., personal care products (PPCPs), pharmaceuticals and endocrine disrupting compounds (EDCs) reduced, binds to the soil or natural organic matter along the rivers or lakes, resulting in lowering of pollutant loads towards the downstream. These micropollutants are found in drinking water systems in the concentrations ranging from ug/L to ng/L. (Lara-Martín et al., 2014; Tuzen et al., 2017). Regulators, on the other hand, are not given any regulations for these growing contaminants in the drinking water system. There are very few measures and monitoring units in place to ensure these unregulated or emerging pollutants and associated by-products, particularly micro-range contaminants, are not released into the environment (Jafari Kang et al., 2017). The European Union Water Framework Directive (2000/60/EC) released an updated list of substances that are in priority every four years and has identified pharmaceutical compounds as potential pollutants under the precautionary measures (Rivera-Utrilla et al., 2013).

Chlorine is a widely used conventional treatment for drinking water disinfection. Several studies on the aromatic compounds chlorination revealed that the occurrence of different functional groups in the benzene ring could significantly affect the rate of chlorine reaction. In pharmaceutical products having amines, the reaction is usually fast, producing chlorinated compounds (Pinkston and Sedlak, 2004). These chlorinated by-products, however; are identified as toxic compounds (Lemus et al., 2012). Furthermore, the extent of mineralization attained in the majority of chlorination processes is not partial and inadequate (Dutschke et al., 2022).

Chlorine dioxide is a stronger oxidant as compared to chlorine and degrades a wider range of organic compounds through oxidation. It does not, however, react with chlorinated or ammonium organic substances, which is advantageous in terms of odour, taste and the generation of toxic organochlorinated species. Further, ClO_2 is only effective for a few antibiotics, including diclofenac, roxithromycin, 17-sulfamethoxazole and ethinylestradiol (Donohue, 2003). This is because ClO_2 reacts selectively with functional groups having high electron density, such as phenoxides

and tertiary amines, which limits the use of ClO_2 in broader wastewater treatment strategies (Ran et al., 2019).

Municipal wastewater treatment plants are designed to regulate a wide variety of substances, including pathogens, nutrients, carbonaceous substances and particulates. On the other hand, the micropollutants are not removed efficiently. As a result, evaluating the efficacy of removal of micropollutants during wastewater treatment was critical for optimizing treatment processes in preventing the discharge of potentially unsafe micropollutants (Chaidez et al., 2014).

In most cases, wastewater treatment plants use a primary, secondary, and tertiary (optional) treatment process. The primary step targets to eliminate the wastewater's solid content (grit, sand, grease, oils and fats and settle-able solids). This step, which is carried out completely mechanically through sedimentation and filtration, is found in all WWTPs (Ding et al., 2022; Moran, 2018; Mudge and Ball, 1964). Primary treatment process eliminates suspended solids that are present in water bodies but are ineffective in removing most micropollutants (Ding et al., 2022). Micropollutants are primarily removed by primary sludge through sorption. Dissemination of a compound into an organic (lipophilic) layer is the most common method of sorption (Lucas et al., 2011). As a result of high partition coefficients between the liquid phases and solid, fragrances are often to be removed efficiently (40%) during primary treatment (Carballa et al., 2004). Some EDCs are also eliminated in the primary treatment with the percentage elimination of *Ca*13% to *Ca* 43% in case of nonylphenol monoethoxylate and Bisphenol A (Ding et al., 2022). However, primary treatment in an aerated grit chamber results in a substantial upsurge in phenolic compounds, such as nonylphenol and bisphenol A, since the compounds initially stick at the grits and readily falls off due to grit chamber air agitation (Bilgin et al., 2020). The removal efficiency of hormones and pharmaceuticals in primary treatment is only up to 28% (estriol and diclofenac), implying that the compounds adsorb to the sludge particles is very limited (Behera et al., 2011). Estrone, sulfamethoxazol, naproxen and Ibuprofen are insignificantly removed (Carballa et al., 2004).

Pollutants undergo a variety of processes in the secondary treatment process, including abiotic transformation, biodegradation, partitioning, dilution and dispersion. Secondary treatment usually involves breaking down from a parent compound due to various chemical and physical alterations, biodegradation, and sorption to solids (Wang et al., 2020). The two main removal steps during biological treatment are sorption and biodegradation/biotransformation, with volatilization occurring to a smaller level (Jayakumar et al., 2021). Micropollutants are degraded to various extent during secondary treatment, leading to mineralization or partial degradation (by-products). Biological treatment is grounded on microorganisms' natural ability to stop elemental cycles such as P, N and C (Silva et al., 2012), which is associated with their biodegradation capability. Thus, the biodegradation process involves transformation of microbial organisms and alteration of chemical structure introduced into the environment (via enzymatic or metabolic action) (Li et al., 2022). Micropollutant biodegradation takes place through several mechanisms: (i) single substrate growth of a small subset of specialist oligotrophic organisms, which is not much popular in WWTPs and more probable to takes place in sediment or receiving water (Daughton and Ternes, 1999); and (ii) co-metabolism, where micropollutants are degraded by enzymes produced for other primary substances (e.g. ammonia monooxygenase (Vader et al., 2000) (iii) mixed substrate growth, where micropollutants are utilized as energy source and carbon and is mineralized (Luo et al., 2014).

Pollutants' sorption is primarily accomplished through (i) absorption, which involves hydrophobic interactions between aromatic groups and aliphatic group of a compound and the microorganism's lipophilic cell membrane as well as the sludge; (ii) adsorption, which involves electrostatic interactions of negatively charged microorganisms surfaces and positively charged groups (e.g., amino groups) (Kubota et al., 2005). Further, the biodegradation products of several micropollutants like estrogens are more unsafe as compared to the parent compound (Pawlak, 2003). As a result, conventional biological treatment processes are not efficient to remove the majority of these emerging micropollutants because they persisted in WWTP effluents and polluted ground and surface waters, which are the main feed of sources of drinking water. To comply with increasingly stringent legislation, more efficient and specific

treatments are obligatory to reduce the environmental pollution and possible aftereffects of the effluents (Chen et al., 2021). In recent years, various advanced treatment technologies are tested and proposed to meet both current and anticipated treatment requirements in order to address these new challenges and use more sustainable and efficient processes. Advanced oxidation processes (AOPs), membrane processes and adsorption on activated carbons are among those that are successfully demonstrated to remove a wide variety of potential water contaminants and are highly promising for water and wastewater treatment technologies.

1.5. Advancement in the Treatment of Waste Water

1.5.1 Activated Carbon Adsorption

Adsorption by activated carbons (ACs) is a common material for regulating the odour and taste of drinking water. AC showed high potential to treat the secondary effluent and was found more efficient in eliminating micropollutants than coagulation-flocculation processes (Choi et al., 2008). AC is widely used in packed bed filters as a powder feed (powdered activated carbon, PAC) or in granular form (granular activated carbon, GAC) (Liu et al., 2009). One benefit of using PAC is that it gives continuous fresh carbon hence, utilized as and when needed (Newcombe, 2006). Kovalova et al. (2013) examined the removal of several micropollutants such as sulfametoxazole, propranolol, carbamezapine and diclofenac with PAC treatment (PAC doses of 43, 23 and 8 mg/L) at a retention time of 2 days (Kovalova et al., 2013). The results revealed that the total load of selected metabolites and pharmaceuticals was reduced by approximately 86%. Hernández-Leal et al. (2011) showed an effective removal (>94 percent) of several micropollutants (nonylphenol, bisphenol A and personal care products) by means of PAC treatment with the starting pollutant concentrations of 100–1600 g/L at a contact time of 5 min with a PAC dose of 1.25 g/L (Hernández-Leal et al., 2011). The effectiveness of PAC in removing micropollutants is determined by the dose of PAC, water/wastewater composition, the molecular behavior and structure of the targeted molecules and their contact time (Boehler et al., 2012). Longer contact times or higher doses are found efficient in removing these micropollutants (Westerhoff et al., 2005).

In general, effective micropollutant removal by adsorption using PAC or GAC is possibly attainable when the pollutants are non-polar (KOW > 2) and the pore shape/size are matched with the pollutant molecular sizes (Rossner et al., 2009). However, the occurrence of natural organic matter (NOM), which strives for binding sites and thus blocks the accessible pores, causes significant decrease in removal efficiency of activated carbon. Furthermore, contact time, GAC regeneration and PAC dose all play significant roles in the effective elimination of micropollutants (Luo et al., 2014).

1.5.2. Membrane Process

Membrane filtration is a separation process carried out in a semi-permeable membrane, which separates pollutants based on the variance in their chemical or physical properties of two phases. Membrane is used as a separating wall, allowing some substances to pass through while others are blocked (Silva et al., 2012). Membrane processes such as reverse osmosis (RO), nanofiltration (NF), ultrafiltration (UF) and microfiltration (MF) are known processes widely employed for the removal of potential pollutants from wastewaters (Bolong et al., 2009). In general, micropollutant retention in membrane processes is accomplished through charge repulsion, adsorption onto membrane and size exclusion. Further, the energy consumption, pressure requirements and rejection, followed the order MF < UF < NF < RO, implying that RO provided nearly complete removal but due to its high energy consumption, restricts its large scale applications (Liu et al., 2009). NF/RO are most widely used membranes for the micropollutants removal from water, in which the rejection efficacy greatly influenced by several parameters (such as pressure, temperature and pH), membrane fouling, membrane properties (e.g., hydrophilicity/hydrophobicity, surface charge, pore size and permeability), membrane operating conditions (e.g., water feed quality and flux), physicochemical properties of pollutant (e.g., electrostatic properties, solubility, water partition coefficient and molecular weight). Additional factors that impact the operation of RO membranes is fouling, which has a variety of negative consequences, including reduction in permeate quality and membrane degradation. The RO membrane fouling causes significant decrease in estrogens removal (Ng and Elimelech, 2004).

1.5.3 Ozonation

Ozone (O_3) is a strong oxidizing agent (E_0 = 2.08 eV), due to the *in situ* generation of reactive •OH radicals in water, which are strong oxidizing agents than the parent ozone. The ozone induces indirect oxidation of specific functional groups of organic molecules via an electrophilic mechanism (Mantzavinos and Psillakis, 2004). Traditionally, ozonation is used in the treatment of drinking water for disinfection, taste control and odour (Hua et al., 2006). The main disadvantage of ozonation is limited mineralization of organic pollutants. Moreover, presence of bromide ions in water is oxidised and forming the highly toxic bromate ions and other toxic organic bromated byproducts (Ozekin et al., 1998; Singer, 1990). The International Agency for Research on Cancer has classified bromate ions as potentially carcinogenic (IARC). Aside from its high input cost, ozone is having low stability and solubility in water. Furthermore, ozone shows a slow reaction rate with several organic compounds, such as saturated carboxylic acids or inactive aromatic compounds (Beltrán et al., 1994). These drawbacks limited the wider use of ozone in wastewater treatment (Mehrjouei et al., 2015).

1.5.4 Advanced Oxidation Processes (AOPs)

Advanced oxidation process is widely employed in the water treatment which is carried out at near-ambient pressure and temperature that involves *in situ* formation of very reactive species e.g., hydroxyl radicals (•OH). The hydroxyl radicals readily oxidize a wide range of organic compounds non-selectively (Glaze et al., 1987). Hydroxyl radical (•OH) (E^0= 2.8V) is very strong oxidizing agent (Pera-Titus et al., 2004), that readily attacks most of the organic compound having rate constants typically in the order of 10^6–10^9 L mol^{-1} s^{-1} (Hoigné, 1997). Depending on the compound to be oxidized, •OH reacts 10^6-10^{12} times faster than the ozone (Munter, 2001). The advantage of AOPs is due to the fact that they provide multiple ways for producing hydroxyl radicals, permitting better acquiescence with the requirements in the treatment process. Some examples of AOPs are sonolysis, electrochemical, photo-Fenton (H_2O_2+Fe^{2+}/Fe^{3+}+UV), Fenton (H_2O_2+Fe^{2+}/Fe^{3+}), H_2O_2/UV, O_3/UV, O_3/H_2O_2, photolysis (UV/VUV) (Saharan et al., 2014).

1.5.4.1. UV/Vacuum UV Photolysis

Photolysis entails the interaction of light radiation with the target compound, which initiates the photochemical reactions and results with breaking down of organic compounds to its intermediate products or complete decomposition of compounds (Doll and Frimmel, 2003). UV treatment is traditionally used for drinking water purification and disinfection as the disinfection by-products are much less as compared to chlorination (Pereira et al., 2007). UV photolysis produces highly reactive species such as hydrogen atoms (•H) and hydroxyl radical (•OH) from water molecules (Arany et al., 2013). These radicals will further interact with the pollutant molecules in the presence of water molecules, which further results in the degradation of pollutant molecules. The application of photolysis in water treatment is limited by smaller molar absorptivity of the target molecules and its low quantum yield (Alapi and Dombi, 2007).

1.5.4.2. Ozone-Ultraviolet Radiation - (O_3-UV)

In O_3-UV process ozone molecules are activated by UV photons which results in the generation of hydroxyl radicals (Lu et al., 2022). Here the most common light source used is a mercury lamp at medium-pressure covered in a quartz sleeve (produces UV light with a wavelength of 200–280 nm). This is because ozone molecules show λ_{max} at 253.7 nm. The O_3-UV process is widely used to oxidize aromatic and aliphatic chlorinated organic compounds, as well as pesticides and natural organic matter (NOM) (Lu et al., 2022; Rajabizadeh et al., 2020). In terms of removal efficiency and reaction rate, the results frequently show that the O_3-UV process is more efficient than ozone alone. By the early 1980s, it was commercialized for the treatment of groundwater contaminated with perchloroethylene (PCE) and trichloroethylene (TCE). However, in most cases, the O_3-UV process is now observed as less efficient as compared to the H_2O_2-UV and O_3-H_2O_2 processes (Mansouri et al., 2019).

1.5.4.3. Hydrogen Peroxide - Ultraviolet (H_2O_2-UV)

When exposed to UV light, H_2O_2 leads to the formation of two hydroxyl radicals. The hydroxyl radicals formed then reacted with the target organic compounds or recombines to form again the H_2O_2 molecule, hence; a decomposition–formation cycle proceeds (Xiang et al., 2020). In comparison with ozone, H_2O_2 is a very low molar absorptivity within the wavelength range of 200–300 nm. As a result, it is highly vulnerable to the competing organic compound's absorption in UV and also solids suspended in water. If an organic molecule is more quickly reacted with H_2O_2 after activation, it is expected that this type of direct photo-oxidation contributes significantly to degrade the organic compounds in the H_2O_2-UV system. The H_2O_2-UV process is primarily used to oxidize the stable and recalcitrant compounds. Liu et al. (2017) investigated the oxidation process for volatile organic compounds (VOCs) using H_2O_2-UV. The degradation percentage was reported to be 80% within 120 minutes of treatment. It was also reported that •OH was ascribed for the rapid oxidation of VOCs in aqueous solutions (G. Liu et al., 2017).

1.5.4.4. Ozone - Hydrogen Peroxide (Peroxone)

Though H_2O_2 reaction with O_3 molecules in water is very slow, however, the conjugate base (HO_2^-) quickly interacts with ozone molecules, generates hydroxyl radicals in only two steps (Merényi et al., 2010). Except the ozonation, the O_3-H_2O_2 process, also known as the peroxone process. The peroxone is extensively used among the AOPs due to their simplicity and cost effectiveness. The O_3-H_2O_2 process is primarily used in water treatment for the oxidation degradation of micropollutants, pesticides and controlling the taste and odor due to such compounds (Mansouri et al., 2019). The ideal H_2O_2/O_3 molar ratio is usually between 0.3 and 0.6. Kepa et al. investigated the elimination of cyanide from water using the peroxone process. It was found that the O_3-H_2O_2 process could efficiently remove cyanide with almost 100% of efficiency (Kepa et al., 2008).

1.5.4.5. Fenton Oxidation

Fenton oxidation takes place in the occurrence of ferric ions or ferrous with H_2O_2 through a chain reaction of free radicals that generates reactive hydroxyl radicals (•OH). It is classified as an oxidation reaction catalyzed by metal, with iron serving as

the catalyst (Ameta et al., 2018). The efficiency of this process is directly related to the pH of the solution, which is between pH 2-4. Furthermore, using UV irradiation, more hydroxyl radicals (•OH) are generated in what was named photo-Fenton reaction as compared to the dark Fenton reaction (Karale et al., 2014). At atmospheric pressure and room temperature, the Fenton reaction is carried out. The Fenton process is relatively clean, safe, simple and the required reagents are readily available (Bauer and Fallmann, 1997). The application of photo-Fenton processes in the degradation of pesticides, 2,4-dichlorophenol from aqueous solutions was demonstrated elsewhere (Wadley and Waite, 2002). The results reveal that 91% mineralization was achieved within 2h of treatment. Usually, Fenton process is able to mineralize a significant portion of the target pollutant, resulting in less toxic effluents, which is easily eliminated by simple post-treatment (Dong et al., 2020). Perini et al., 2017 investigated the photo-Fenton reaction for the degradation of pharmaceuticals fluoxetine and ciprofloxacin. The results revealed that 50 % degradation of both pharmaceuticals were achieved after 90 min of photo-Fenton oxidation (Perini et al., 2017). Nonetheless, the main disadvantages of Fenton process are the small range of pH for operation, to evade the generation and consequent precipitation of iron oxyhydroxides, as well as the necessity to recuperate dissolved ions from the solution, which are already treated, which necessitates additional treatment methods (Zhang et al., 2019).

1.5.4.6. Electrochemical Oxidation

The degradation of various organic-pollutants was conducted on the suitable anode made up of PbO_2, IrO_2, TiO_2, Pt, graphite, some alloys based on Ti, and also boron-doped diamond (BDD) with appropriate electrolyte (NaCl) (Wang and Stahl, 2020). The electrochemical oxidation takes place usually by two mechanisms: direct anodic oxidation, in which the target compounds are adsorbed onto the anode surface and degraded by the application of anodic electron transfer reaction. Further, the indirect oxidation, in which the reactive species such as hydrogen peroxide, ozone, hydroxyl radicals, hypochlorite, chlorine are formed at the electrode surface, which facilitates the oxidation of target molecules. The applied current, the type of supporting electrolytes, and the working electrode are crucial operating parameters that influence

the overall performance. The initial pollutant concentrations and pH of the pollutant solution are the other factors that control the efficiency of the degradation reaction (Weber and Ramasamy, 2020). BDD anode received greater attention in the decontamination of a variety of pollutants in aqueous solutions because they exhibit significantly good conductivity, electrochemical and chemical stability and improved mineralization rate with very high current efficiencies (Abdelhay et al., 2020). NaCl is a common supporting electrolyte used to increase the effluent conductivity and to provide secondary oxidants as chlorine. However, the usage of NaCl gives rise to the formation of toxic organo-chlorinated compounds that are formed as byproducts of the reaction (Scialdone et al., 2009).

1.5.4.7. Ultrasound Irradiation (Sonolysis)

Ultrasound irradiation, also known as sonolysis, is widely used as an advanced oxidation process (AOP) for the treatment of waste water in recent years. Sonochemical reactions are initiated using acoustic irradiation of liquids at high-intensity at cavitation-producing frequencies (usually in the 20–1000 kHz range). Thus, cavitation is used to concentrate the ultrasound diffused energy into micro-reactors with concurrent formation of reactive hydroxyl radicals (•OH), in which the reactor serves as a hotspot (Ono et al., 2020). The bulk solutions, the interfacial region between the surrounding liquids and the bubble, and the cavitation bubble itself are the three potential sites for sonochemical reactions. The two main mechanisms of sonochemical degradation are solution radical chemistry and pyrolytic reactions near or inside the bubble (Madhavan et al., 2019). Organic compounds with high volatility or less solubility are more probable to undergo sonochemical degradation quickly due to their tendency to accumulate near or inside the liquid-gas interface. The water matrix, bulk temperature, nature and type of contaminant, reactor geometry and intensity and frequency of ultrasounds are the common factors that control the sonolysis process. The occurrence of solids or dissolved gases typically enhances the performance of sonolysis, which supplements extra nucleation centers (Qiu et al., 2018).

1.6. Heterogeneous Photocatalysis

The heterogeneous photocatalysis using semiconductor, mainly ZnO and TiO_2 and utilizing the ultraviolet (UV) or solar irradiation is the most common method of AOPs. When the photocatalyst is irradiated with the UV light, electron/hole pairs (e^-/h^+) are readily generated, which quickly move to the surface and induce redox reactions with suitable substrates. Over the catalyst, oxygen serves as an electron acceptor, forming superoxide radicals, while adsorbed H_2O molecules and OH^- act as electron donors, forming •OH radical (Antonelli and Ying, 1995; Chen et al., 2020; Xu et al., 2014). The photocatalytic degradation of several organic pollutants is thoroughly studied using semiconductor-assisted photocatalytic processes (Chen et al., 2020).

1.7. Photocatalysis with Heterogeneous TiO_2

TiO_2 semiconductor based advanced oxidation process (AOP) is the most effective and eco-friendly wastewater treatment strategy. The photo-induced electron-hole pairs (e^-/h^+) allow the reduction and oxidation of pollutants adsorbed on the TiO_2 surface. The radical species formed by e^- and h^+ are peroxide radical ($•O_2^-$) and hydroxyl radicals (•OH). Hydroxyl radicals have relatively high redox potential (E_0 = +2.80 V), which effectively degrades an even highly stable organic compound,/species in the aqueous medium (Angel et al., 2018; Boxi and Paria, 2015).

The photocatalytic process has numerous advantages over other existing techniques, including the fact that it effectively degrades pollutants rather than simply transformed them in to alternative phase (e.g., gas sparging, adsorption with activated carbon) and does not require the use of possibly hazardous substances (e.g., chlorination, ozone) (Pulido Melián et al., 2013). It is primarily carried out at room temperature (solar light can act as the light source and oxygen from the atmosphere is utilized as oxidant) and it generally results in the complete mineralization of organic compounds into H_2O, CO_2 and other mineralized by-products (Gao et al., 2015). Furthermore, TiO_2 is considered to be the most suitable photocatalyst, if not an ideal photocatalyst, owing to its relatively high chemical stability, suitable flat band potential, high photo-catalytic activity, low energy consumption, low operation temperature, biological inertness, ease of availability, photo-stability, ability to prevent

the formation of unwanted by-products and water insolubility under room temperature (Sonawane et al., 2003; Yasumori et al., 1994).

1.8. Photocatalysis with Heterogeneous Noble Metal Doped TiO_2

Despite numerous advantages, TiO_2 has a number of limitations that limit its wider implications in the treatment processes. TiO_2 is having a large band gap energy (3.2 eV) that requires harmful UV-C radiation to excite the semiconductor. Moreover, a high electron-hole pair recombination rate limits the efficiency of catalysts in wastewater treatment processes (Jang et al., 2012). The e^-/h^+ pairs are having very short lifespans, and without the presence of suitable scavengers, recombination dissipates the stored energy within a few nanoseconds. However, a suitable modification improves the applicability of TiO_2 in the wastewater treatment. Several modifications are demonstrated to improve the photocatalytic activity by reducing the band gap energy and minimising the electron-hole recombination reactions by doping the noble metals within the titania network (Mogal et al., 2014).

Doping of Ag or Au nanoparticles with TiO_2 has shown a substantial importance due to the known surface plasmon resonance (SPR) phenomenon. Due to the surface plasmon resonance, Ag or Au nanoparticles decorated TiO_2 are able to absorb light towards the visible range, which causes a localised electric field near TiO_2 surface, resulting in the efficient generation of electron-hole pairs at the TiO_2 surface (Ge et al., 2006; Rengaraj and Li, 2006). Furthermore, the noble metal nanoparticles on TiO_2 surface operate as a co-catalyst, assisting with efficient separations of electron and hole (Zangeneh et al. 2015). The photocatalytic activity and the plasmon resonance effect are mostly determined by the geometry, the particle size and the extent of doping of noble metal nanoparticles to its sphere (Rengaraj and Li, 2006). This obviously overcomes the prevalent limits in the application of bare TiO_2 and allows the solar visible light radiation. This lowers the cost of operation and provides a more viable option for the treatment of wastewater for real implications (Lee et al., 2014; Liu et al., 2013).

The presence of Ag^0(NPs) effectively restricts the electrons excited from TiO_2 and leave the holes for further organic compound degradation reactions (Cao et al.,

2014; Sofianou et al., 2014). It also causes a delay in their wavelength response when they approach the visible range (Leong et al., 2014). Furthermore, silver nanoparticles efficiently promote electron excitation by generating a local electric field, with surface plasmon resonance effect in metallic silver nanoparticles, which show an enhanced electric field (Dinh et al., 2014; Tsukamoto et al., 2012). Chao et al. investigated the effect of doping Ag on TiO_2 and its photocatalytic activity when exposed to UV light. The Ag(NPs) doped TiO_2 showed an increased specific surface area and exhibited excellent photocatalytic activity of the catalyst (Chao et al., 2003)..

Similarly, the Au^0(NPs) doped TiO_2 exhibit a high visible light absorption and the surface plasmon resonance effect (SPR) of their free electrons (Sousa-Castillo et al., 2016). Using visible light irradiation, the plasmonic photocatalyst Au-TiO_2 demonstrates remarkable degradation efficiency of micropollutants such as methylene blue (Jin et al., 2016), Rhodamine B (RhB) (Wang et al., 2015), methyl orange (Fu et al., 2017), metronidazole (Shoueir et al., 2019), tetracycline (Li et al., 2019). The Au-TiO_2 was successfully used to reduce CO_2 using either visible (532 nm) light or UV (245, 365 nm) light radiations (Hou et al., 2011). Visible and UV light induced water splitting was demonstrated using the Au(NP) doped TiO_2 catalyst to generate the O_2 and H_2 (Ni et al., 2007).

1.8.1. Factors Influencing TiO_2 Photocatalysis

Various operational parameters, including solution pH, pollutant concentrations, temperature, presence of the interfering ions, light intensity, nature and type of photocatalyst are significantly affecting the efficiency and oxidation rate of pollutants in the heterogeneous photocatalysis reactions.

1.8.1.1. pH of the Solution

pH is an important parameter that influences the heterogeneous photocatalytic treatment process. The speciation of organic pollutants, the sizes of aggregates it forms and surface charge of the catalyst or the isoelectric point are all determined by varying the solution pH. The adsorption of pollutant molecules at the surface of catalyst causes

is greatly impacted with solution pH hence, the photocatalytic reaction rate (Alkaim et al., 2014).

The surface of TiO_2 develops positively charged in an acidic medium ($pH < pH_{pzc}$) and attracts the anionic species due to the electrostatic attractive force; however, in alkaline conditions, the surface of TiO_2 develops negatively charged ($pH > pH_{pzc}$) and attracts the cationic species and repels the anionic species (Constantin et al., 2018) (*Cf* Equation 1.1-1.2).

$$pH < pH_{pzc} : TiOH + H^+ \rightarrow TiOH_2^+ \quad \ldots(1.1)$$

$$pH > pH_{pzc}: TiOH + OH^- \rightarrow TiO^- + H_2O \quad \ldots(1.2)$$

1.8.1.2. Pollutant Concentration and Nature

From the standpoint of practical implication, the initial pollutant concentration in the photocatalytic reaction is critical and determines the reaction mechanism. It is demonstrated that increasing the initial pollutant concentration reduces the percentage degradation at a constant dose of catalyst (Bendjabeur et al., 2017). This is explained by the fact that at high initial pollutant concentrations, more pollutant molecules are adsorbed on the TiO_2 surface; on the other hand, fewer photons are available to reach the surface of the catalyst and thus forms lesser number of •OH, resulting in a decrease in degradation percentage (Reza et al., 2017; Sowmya et al., 2018).

Further, the chemical nature speciation of pollutant molecules also affected the photocatalytic degradation efficiency, in addition to their initial concentrations. The substituent group showed significant impact on the photocatalytic degradation of aromatic compounds (Gaya and Abdullah, 2008). In comparison with the electron donating groups, the compounds with electron withdrawing nature (benzoic acid, nitrobenzene) firmly sorbed on to the photocatalyst and are thus seemingly undergo direct oxidation (Bhatkhande et al., 2004). Therefore, the sorption of pollutant molecules on the photocatalyst surface impacts the degradation efficiency of pollutants in aqueous medium.

1.8.1.3. Photocatalyst Nature and Type

TiO_2 photocatalytic activity is determined by its structural properties and surface structure, which include surface hydroxyl density, band gap, porosity, particle size distribution, surface area and crystal composition. The average size of a crystal is critical because it is related directly to a catalyst's efficiency via its specific surface area. In most cases, the anatase form of TiO_2 is a more efficient photocatalyst as compared to the rutile phase (Luttrell et al., 2014), in which the rate of electron-hole recombination is high (Ozawa et al., 2014). TiO_2 photocatalyst is used in either immobilized form on a supporting material or in powder form. Degussa P-25 is the most common powder form of TiO_2 available commercially. It consists of approximately 20% rutile and 80% anatase mineral phases and showed reasonably good catalytic activity (Ohno et al., 2001). Furthermore, the concentration of the catalyst is directly related to the overall degradation reaction rate. On the other hand, to some extent, agglomeration of crystallites reduces the available surface area for light absorption, resulting in a decrease in the rate of photocatalytic degradation (Li et al., 2010).

1.8.1.4. Intensity of Light

The intensity of the light is one of the important parameter; influencing the extent of photocatalytic degradation of pollutants. Formation of electron-hole pairs in the photochemical reaction and the rate of photocatalysis are highly dependent on intensity of light (Kusiak-Nejman and Morawski, 2019). To attain a high rate of photocatalytic reaction, a moderately high intensity of light is required to produce sufficient photon energy to the surface of TiO_2 (Ye et al., 2015). According to reports, the rate of organic pollutant degradation is directly related to the radiant flux (Φ) (Lin, 2013). Further, the linear dependence of the photocatalytic reaction rate on radiant flux (Φ) is reported as a square root dependency of $\Phi^{0.5}$ above a certain value (Malato et al., 2009). The increase in rate of degradation of organic compounds at higher radiant flux is due to the reason that at higher light intensity, the absorption of photons by the catalyst is more, which results in an increase of electron-hole pairs on the surface of the catalyst. This enhances the formation of more hydroxyl radicals hence, to achieve an enhanced degradation efficiency (Cervantes-Avilés et al., 2017; Mallakpour and Nikkhoo, 2014). However, excessively high radiant flux may increase the

recombination of electron-hole pairs and thus the catalytic activity is deactivated hence, lead to decrease in degradation rate of pollutant molecules (Lee et al., 2018).

1.8.1.5. Interfering Ions

The presence of several co-existing cations and anions is common in the wastewaters, ground waters and surface waters, which controls the photocatalytic processes in the degradation of pollutants in such complex matrices. The coexisting ions have a major impact on the efficiency of photocatalysis for pollutant degradation (Xu et al., 2015; Yuan et al., 2019). The interfering ions preferentially occupy the catalyst active sites and lowers the catalytic activity. There are several species which preferentially scavenge the hydroxyl radicals or other oxidant, thereby slowing down the rate of pollutant degradation (Thompson and Yates, 2006). The anions or cations, on the other hand, may be converted into active radicals or form an electrostatic field near the catalyst to support the electron and hole separation (Siqi et al., 2012).

The existence of the coexisting ions during the removal of the pollutants provides useful input data for determining the degradation mechanism and for mimicking the treatment of real water samples. The studies are carried out in the presence of several coexisting ions such as oxalic acid, glycine, $ZnCl_2$, NaCl, $NaNO_2$, $NaNO_3$, EDTA, and $CuSO_4$ under light irradiation utilizing the photocatalyst. These ions compete with the pollutant molecules for sorption on the photocatalyst surface. Hence, it can prevent the target molecule from reaching the photocatalyst surface and can hinder the photocatalytic degradation of pollutant molecules.

1.8.1.6. Effect of Temperature

The influence of temperature on the rate of photocatalytic degradation was previously reported (Yamamoto et al., 2013). Using Ag-doped TiO_2 nanostructures, Barakat et al. revealed the effect of temperature on the photodegradation of rhodamine B (Barakat et al., 2013). The photocatalytic activity of Ag/TiO_2 is favoured by an increase in temperature, and at 55°C the highest degradation rates of rhodamine B was achieved. However, the other studies showed increase in temperature caused for decrease in degradation of rhodamine B dye using the nanofibrous shape Ag-doped

TiO_2. It was demonstrated that the kinetic energy of the pollutant molecules were increased at higher temperatures, which caused molecules to detach from the photocatalyst's surface. The influence of reaction temperature (298-353 K) on photocatalytic H_2 generation using the Pt/TiO_2 suspensions were examined previously (Kim et al., 2016) and showed that increasing the temperature from 298 K to 323 K, the H_2 generation rates was increased by 7.8 folds. At higher temperatures, interfacial charge transfer and charge carrier mobility both improved and favoured the reaction rates. At various temperatures, the photocatalytic elimination of organic compounds was studied using the TiO_2/sepiolite composite, which showed that the increase in temperature favoured the reaction rates (Zhang et al., 2011). An excellent overview of photo-thermal catalysis was published elsewhere (Nakano et al., 2004). Photo-thermal catalysis accelerates reaction rates through the synergistic interaction of sunlight photons and thermo-chemical contributions.

It was further shown that very high temperature promotes significantly the recombination and adsorption of charge carriers, which results in decline of photocatalytic activity (Chen and Hsu, 2021). This is consistent with the Arrhenius equation, which states that an apparent first order rate constant k_{app} linearly increases with $\exp^{(-1/T)}$ (Barakat et al., 2020).

1.9. Literature Review

Titanium dioxide (TiO_2) semiconductor is widely used in photocatalysis (Fujishima and Honda, 1972; Nakata and Fujishima, 2012; Ni et al., 2007). The properties of TiO_2 as a semiconductor was first pointed out and pioneered by Honda and Fujishima in the generation of oxygen from water in electrocatalysis assisted with photon energy (Fujishima and Honda, 1972). The study paves the way for the 'advanced treatment' of wastewater under the photocatalytic processes. The photocatalysis was also intended to split the water to obtain H_2 and O_2 (Fajrina and Tahir, 2019). Various structural forms of TiO_2 such as nanosheets, nanorods, nanowires, nanoparticles etc., showed a range of applications in the technological developments (Reghunath et al., 2021). TiO_2 is extensively studied as a photocatalyst for the oxidative removal of organic contaminants from aqueous wastes (Zhao et al.,

2018). Anatase and rutile are two of the three crystalline forms of TiO_2 and are significantly promising in photocatalysis. The anatase phase is more efficient than the rutile phase. The TiO_2 photocatalyst is widely used in batch reactor operations to treat the photocatalysis of numerous micropollutants, dyes, pesticide and herbicide derivatives that are prevalent in wastewater effluents (Reghunath et al., 2021).

Heterogeneous photocatalysis is technological advancement in oxidation methods that rely on the semiconductor, which facilitates *in situ* the generation of reactive species (Emeline et al., 2013). After the discovery of photoinduced water splitting on TiO_2 electrodes about five decades ago, researchers began investigating heterogeneous photocatalysis (Fujishima and Honda, 1972). Practical use of TiO_2 photocatalysts was applied both in outdoor and indoor applications during the last couple of decades (Nakata and Fujishima, 2012). Photo induced oxidation, gaseous pollution removal, water detoxification, anticancer therapy, disinfection, hydrogen transfer, water splitting and organic synthesis are all areas where photocatalysis is being studied extensively (Fajrina and Tahir, 2019; Forgacs et al., 2004; Malato et al., 2009; Reza et al., 2017; Zhao et al., 2018). Heterogeneous photocatalysis is a highly effective and efficient means to purify both air and water, and TiO_2 is widely used as an efficient catalyst that allows the formation of charge carriers, which facilitates the oxidative and reductive reactions (Emeline et al., 2013).

The principles of photocatalysis with heterogeneous TiO_2 involves the absorption of light radiation having energy higher than or equal to TiO_2 band-gap energy (3.0 eV (rutile) and 3.2 eV (anatase)) on its surface, after which valence band (VB) electrons jump to the vacant conduction band (CB) with in femtoseconds produces a hole (h^+) in the valence band (VB), leading to the formation of electron-hole pair (e^- - h^+) (Equation 1.3) (Jang et al., 2012). The wavelength of light having sufficient photon energy for the electronic excitation is typically $\lambda < 400$ nm. The energised light source and a photocatalyst along with an oxidising agent, such as oxygen or air, are all involved in the photocatalytic oxidation process. Furthermore, photon energies less than the band gap energy (i.e., longer wavelengths), are then dissipated as heat. The holes generated in the VB moves to the surface of the catalyst and undergoes reaction with the water molecules forming •OH radical (Kusiak-

Nejman and Morawski, 2019). The organic molecules on the vicinity of TiO_2 surface are then oxidized by •OH radicals and photogenerated holes. In the meantime, electrons excited in the CB react with the adsorbed oxygen molecules (O_2) to form superoxide radical anions (Nakata and Fujishima, 2012) (Equation 1.4). The major oxidant is the hydroxyl radicals (•OH). The oxidative photocatalytic degradation of numerous organic contaminants by TiO_2 was extensively researched (Guo et al., 2019). Figure 1.9.1. depict the mechanism of electron-hole pair production and pollutant removal on the surface of photo-irradiated TiO_2.

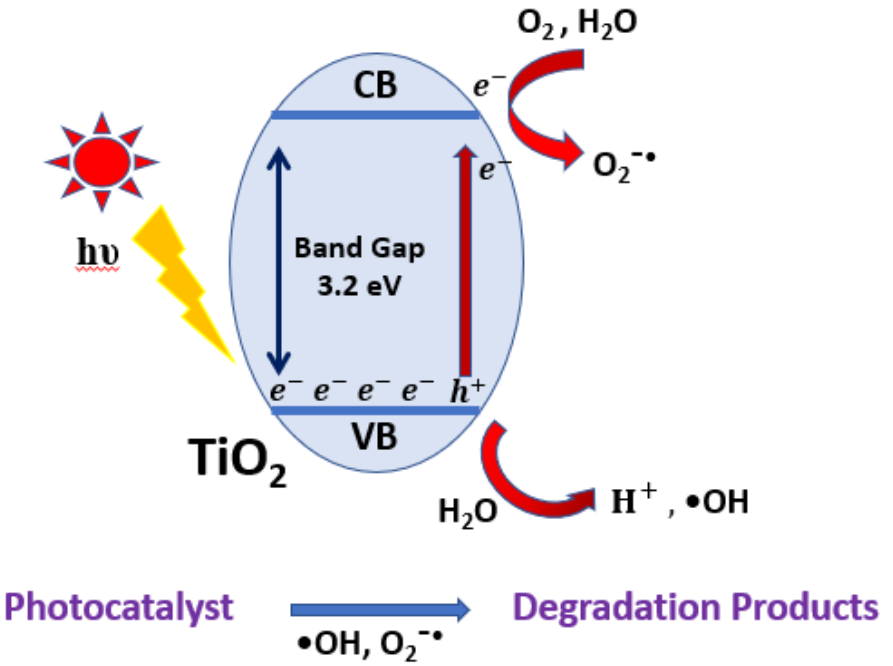

Figure 1.9.1.: Schematic illustration on photocatalytic degradation of organic pollutants through the formation of photoinduced charge carriers (e^- / h^+) in the surface of semiconductor TiO_2.

On the surface of TiO_2, a series of chain reductive and oxidative processes take place, and are given below (Equation 1.3-1.9): (Chong et al., 2010)

Photo induced excitation: $$TiO_2 + h\nu \longrightarrow e^- + h^+ \quad \ldots(1.3)$$

Superoxide radical formation: $(O_2)_{ads} + e^- \longrightarrow O_2^{\bullet -}$ …(1.4)

Formation of hydroxyl radical: $OH^- + h^+ \longrightarrow OH^\bullet$ … (1.5)

Formation of hydroperoxyl radical: $O_2^{\bullet -} + OH^\bullet \longrightarrow HOO^\bullet$ …(1.6)

Hydroperoxyl radical as e^- scavenger: $HOO^\bullet + e^- \rightarrow HO_2^-$ …(1.7)

Formation of hydrogen peroxide: $HOO^- + H^+ \rightarrow H_2O_2$ …(1.8)

Photodegradation by hydroxyl radical: $RH + OH^\bullet \longrightarrow R'^\bullet + H_2O$ ...(1.9)

If electron scavengers are not present, the photo-excited electron recombines with the valence band hole within nanoseconds with concomitant dissipation of thermal energy. As a result, the occurrence of electron scavengers is critical for slowing down the recombination rate and ensuring efficient photocatalysis. Oxygen plays important role to restrict efficiently the recombination of electron and hole by allowing the generation of superoxide radicals ($O_2^{\bullet -}$) as seen in equation (1.4). Oxygen traps the electrons and forms the superoxide radicals. The superoxide radical ($O_2^{\bullet -}$) further protonated to produce the hydroperoxyl radical ($\bullet O_2H$) followed by H_2O_2 as demonstrated in equation (1.6) and (1.7). The hydroperoxyl radical has scavenging properties, which implies that co-occurrence of these radical species further delays the recombination time in the entire photo-catalysis reactions. However, the presence of both water molecules and dissolved oxygen (DO) is responsible for continuing these reactions in the photo-catalysis process. The extremely reactive hydroxyl radicals (•OH) is not generated in absence of water molecules (Chong et al., 2010). However, in the absence of water molecules, some simple organic molecules (e.g., formic acid and oxalate) are mineralized via direct electrochemical oxidation, in which the surface trapped electron is scavenged by metal ions in the system (Eggins, 1998). Many basic mechanistic investigations on photocatalytic degradation of several organic molecules (e.g. EDTA, oxalic acid) by TiO_2 are previously investigated (Xu et al., 2015; Yuan et al., 2019). The reactive hydroxyl radical (•OH), hydroxylates aromatic compounds causing sequential oxidation/addition and ultimately the ring opening of organic

compound. The intermediates produced, predominantly aldehydes and carboxylic acids, are carboxylated further to produce the carbon dioxide and water (Schneider et al., 2014). As the photo-catalysis reaction takes place on TiO_2 surface activated by photon energy, understanding the reaction mechanism that entail photo-degradation of organic compounds is critical for kinetic studies. If the irradiation time is increased for heterogeneous photo-catalysis, the liquid phase organic molecules are degraded to their respective intermediates and then mineralized to carbon dioxide and water (Equation 1.10).

$$\text{Organic pollutant} \xrightarrow[O_2]{TiO_2/h\nu} \text{Reaction Intermediate(s)} \rightarrow H_2O + CO_2 \qquad \ldots(1.10)$$

The synthesis of porous TiO_2 thin films with large specific surface area received greater attention (Angulo-Ibáñez et al., 2021; Grosso et al., 2003). The structural and surface characteristics of the photocatalyst showed impact on the photocatalytic efficiency. The shape and size of the catalyst affect the extent of adsorption of pollutants, recombination rate and life time of electron-hole pairs and the degradation intermediates (Wojcieszak et al., 2015). Photocatalytic process contains several chemical reactions that take place on the catalyst surface, increasing the surface area of the catalyst and improves the efficiency of the photocatalytic process by exposing more pollutant molecules at the surface (Thomas and Natarajan, 2018). Particle size is also an important characteristic in heterogeneous catalysis since it is directly related to a catalyst's efficiency with its specific surface area (Kočí et al., 2009). Quantum size shows an impact on the photo-induced phenomena. As the size of the TiO_2 particles gets smaller, a blue shift and an increase in reaction yield and photocatalytic activity was observed (Demir Kivrak et al., 2021). This was attributed to the reduction of radiation-less transfer and the simultaneous augmentation of charge carrier activity. Traditional alkoxide sol-gel technique with the addition of surfactants or templating membranes was used to produce porous inorganic TiO_2 (anatase) films (Bashiri et al., 2017). The template enables the porous TiO_2. Due to efficient decomposition of polyethylene glycol even relatively at low temperatures, it is suitable for achieving the porous structure of coatings (Nawawi et al., 2016). Controlling the synthesis and deposition steps is highly important for producing surface coatings that

are uniform, regular, even and crack-free. Band gap, porosity, morphology, particle aggregation, surface OH groups, specific surface area and crystalline phase are the factors that influence titania's photocatalytic efficiency (Solonenko et al., 2018). However, the literature reports a wide range of results. Some researchers stress upon the importance of large surface area in increasing efficiency (Kočí et al., 2009), others point to the particle size and crystallinity (Demir Kivrak et al., 2021).

The utilisation of TiO_2-based photocatalysis has a number of disadvantages, including moderately high electron-hole recombination rate and difficulties in phase separation. As a result, the efficiency of photocatalysts was hampered. Furthermore, the wide energy band gap (3.2 eV), TiO_2 is only effective when exposed to a UV light source (wavelength of less than 400 nm), which is less than 4% of the total solar radiation (Jang et al., 2012). To increase the photocatalytic activity of the photocatalyst, greater suppression of electron-hole pairs is attributed. Hence, the doping of TiO_2 with noble metals lowers the recombination rate substantially. Several investigations showed that the TiO_2 network doped with noble metals. This results in a decrease in band gap energy below the titanium dioxide's conduction band energy. The dopant metal traps electrons, holding electrons for a short time before being transferred to an acceptor on the surface of the catalyst. As a result, electrons and holes are free to participate in additional oxidative degradation reactions (Ge et al., 2006; Rengaraj and Li, 2006). Furthermore, some doped metals with TiO_2 networks cause an oxygen vacancy in the titania lattice or even a defect in the lattice. Introducing the impurity causes imbalanced charge and strain, resulting in oxygen vacancy. This vacancy then traps electrons and significantly prevents the recombination of electron and hole pairs. Several investigations are undertaken to dope various metals with TiO_2 networks to increase their photocatalytic activity under UV to visible light irradiations. Because of the probable transition of d and f orbital electrons, transition metals have long been used as dopants. As they are good electron acceptors, thus prevent the recombination of photo-induced electron-hole pairs (Zangeneh et al., 2015).

Among the dopant metals, noble metals (Ag, Au, Pd and Pt) have shown high Schottky barriers which helps trapping of electrons, facilitating separation of electron-hole pairs (Gwo et al., 2016). They also exhibit surface plasmon resonance (SPR)

effect which facilitates TiO_2 photocatalysts to utilise light toward the visible region by reducing the band gap and to enhance the excitation of electrons at the catalyst surface (Ge et al., 2006; Rengaraj and Li, 2006). It also increases the lifetime of electron and hole pairs, which results in an increase of photocatalytic efficiency of noble metal doped TiO_2 (Zangeneh et al., 2015).

Plasmonic noble metal nanoparticles exhibit localized surface plasmon resonance (LSPR) due to their interaction with electromagnetic light radiation. This effect developed due to the electron oscillates in the conduction band at the interface of plasmonic metal-dielectric (Gwo et al., 2016). When light radiation hits the plasmonic metals, electrons get excited from their ground states. Rapid collective oscillation of electron density occurs on the noble metals, which results in the induction of localized surface plasmon resonance (D. Wang et al., 2018a). This generates an electromagnetic field near the metal nanoparticles (Lal et al., 2007). Thus, absorption and scattering of the incoming electromagnetic wave at frequencies close to the LSPR and the generation of strong electric fields near the surface of the nanoparticles (Zhou et al., 2012). Due to the excitation of LSPR, metal nanoparticles behave as nano-antennas, gathering energy from light and converting it into an intense, localized electric field. (Rycenga et al., 2011). Metal nanoparticles that induce LSPR excitation in the visible or near-IR regions are usually termed plasmonic nanoparticles. Plasmonic photocatalysis and conventional photocatalysis are almost similar processes (Li and Li, 2001; Yun et al., 2009). However, in plasmonic photocatalysis, the doped noble metals show plasmonic effect, which enhances the overall performance of the photocatalysts in the process. It leads to the formation of Schotty junction, which exists in between the semiconductor and the doped noble metal (Zhang et al., 2013). It is a space-charge layer through which the excited electrons are moved from the conduction band of TiO_2 to metal nanoparticles. It occurs from the variance in energy level between the Fermi level of the semiconductor CB and the metal, and is commonly named as the Schottky barrier energy (Tatsuma et al., 2017). Noble metal nanoparticles store and shuttle photo-generated electrons from the vicinity of the TiO_2 surface to the acceptor (Xiong et al., 2011). The noble metal on TiO_2 photocatalyst modifies the surface properties of the photocatalyst, which further facilitate the generation of

hydroxyl radicals by interaction with hydrogen peroxide through the photo reduction of oxygen (Oros-Ruiz et al., 2013).

Among all the noble metals, silver (Ag) nanoparticles show intense surface plasmon resonance (SPR) at the wavelength of 320-450nm which is near to the corresponding TiO_2 band gap absorption energy (~3.2 eV, 388 nm). In Ag/TiO_2 photocatalyst, movement of electrons from the conduction band of TiO_2 to Ag nanoparticles is thermodynamically favoured. This is due to the reason that the Fermi level of Ag metal is lower as compared to the TiO_2 (Rengaraj and Li, 2006). As a result, Schottky barrier is formed easily at metal-semiconductor (Lee et al., 2014; Liu et al., 2013). Thus Ag/TiO_2 is a promising photocatalyst for photocatalytic reactions and is shown to have high efficiency in the removal of different pollutants as compared to the bare TiO_2 nanomaterial (Cao et al., 2014; Sofianou et al., 2014). Absorption wavelength of this nanomaterial is predominantly in the visible region (Leong et al., 2014). Doping of Ag nanoparticles with titania results in an increase in the efficiency of photocatalytic degradation of several pollutants, as Ag nanoparticles efficiently traps the electrons and restricts the recombination of the electron-hole pairs (Cao et al., 2014; Sofianou et al., 2014) (Figure 1.9.2.). Because of their inexpensive cost and efficient photocatalytic capabilities, Ag nanoparticles show widespread applications (Handoko et al., 2019). The free electrons of metal collectively oscillate when stimulated by light irradiation. It was also shown that the extent of noble metal nanoparticles doped to TiO_2 sphere, geometry and particle size showed a significant role in the catalytic performance, hence; the plasmon resonance (Li and Li, 2001; Yun et al., 2009). Doping with noble metals thus overcomes the limitations of TiO_2, which was applicable only under UV-C light radiations. Hence, the catalyst is useful in the solar visible light radiations, which accounts for about 40% of solar radiation. This lowers the cost of the operation and makes it more practicable in terms of treatment methods.

The SPR band of metallic Au(NPs) is less intense as compared to the metallic Ag(NPs). However, Au nanoparticles showed high stability and intense broad visible light absorption band due to SPR, which makes it more promising for industrial applications (Dinh et al., 2014; Tsukamoto et al., 2012). Other studies suggest that the

combination of Au and TiO_2 results in a dual perimeter site in which the activation of molecular oxygen takes place (Green et al., 2012). As a result, Au doped TiO_2 is a promising photocatalyst for photocatalytic reactions.

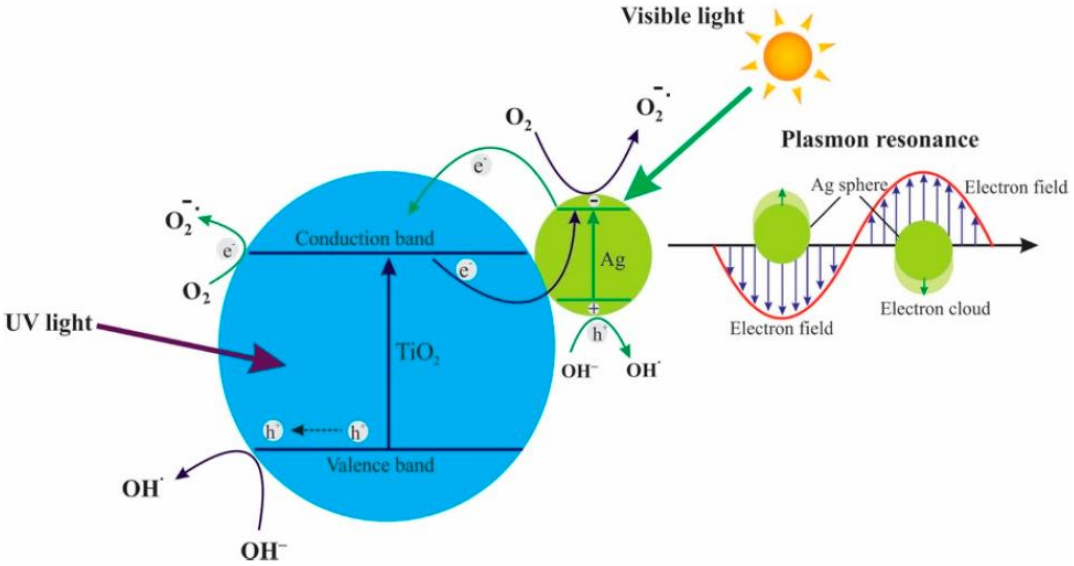

Figure 1.9.2.: Localised surface plasmon resonance (LSPR) effect of Ag doped TiO_2 (Handoko et al., 2019)

Leong et al. (2014) used a non-hydrolytic sol-gel approach to synthesize the TiO_2 nanomaterials, and Ag doped TiO_2 nanomaterials with ethylene glycol and silver nitrate as precursor materials. Under a 500 W tungsten halogen lamp having UV cut-off filter for visible light source, nanocomposite Ag-TiO_2 photocatalyst and TiO_2 were used to degrade amoxicillin. The diffuse surface reflectance data showed that the band gap energy of Ag doped TiO_2 nanomaterial is decreased significantly as compared to the bare TiO_2. Further, a significant degradation of amoxicillin was obtained using the Ag-TiO_2 nanomaterial under the visible light (Leong et al., 2014). Boxi and Paria (2015) used the sol-gel process to obtain the Ag(NPs) doped hollow TiO_2 nanocomposite using AgBr as the sacrificial core. The formation of Ag doped hollow TiO_2 nanomaterials showed considerably high BET specific surface area as compared to the TiO_2 solid. Moreover, the Ag doped hollow TiO_2 showed enhanced photocatalytic degradation of metronidazole. Further, the recyclability of

nanocomposite material showed only *Ca* 10% decrease in the removal efficiency of metronidazole at the end of sixth repeated cycles (S. S. Boxi and Paria, 2015). The effect of Ag doping with TiO_2 caused to change the mineral phase of TiO_2 from anatase to rutile (Chao et al., 2003). Further, the oxidative degradation of 2-propanol, Ag deposition, is used to enhance the photocatalytic activity of rutile TiO_2 (Sclafani and Herrmann, 1998). Ag-TiO_2NAs@GOCF (Ag-TiO_2 nanowire arrays graphene oxide coated carbon fibers) composite obtained by the facile self-template method was utilised for the elimination of tetracycline under visible light and UV light. Photocatalytic efficiency of 86.66% and 95.73% were obtained under visible light and UV light, respectively (Wang et al., 2017). Photo-oxidation of phenol as a probe molecule, Au-NPs with a small sized distribution supported on TiO_2 nanocrystal were utilised. The catalyst shows efficient long-lasting photoactivity, since *Ca* 90% of the phenol was mineralized (Su et al., 2012). The oxidation of 2,3,6-trimethyl phenol and 2,6-di-tert-butyl phenol (as two different substituted phenols) with aqueous H_2O_2 was efficiently catalysed by Au-NPs doped TiO_2 (Cheneviere et al., 2010). In a photocatalytic reactor with fixed bed flow chamber, the TiO_2 modified with extremely small concentrations of Au-NPs was used to photocatalyze the oxidation of methyl tert-butyl ether (MTBE) (Orlov et al., 2006). The Au-NPs improves the TiO_2 photocatalytic efficacy for the removal of MTBE.

The photocatalytic performance of Au/TiO_2 prepared by the sol-gel method, is active under visible light irradiations. The results of optical absorption spectra and UV-visible diffuse reflection spectra (DRS) revealed that a new energy level lower than 3.2 eV was formed in the Au/Au^{3+}-TiO_2, which promotes light absorption toward the lower energy region of the electromagnetic spectrum. Thus, energy corresponding to visible light is adequate to excite the photocatalyst as the band gap energy was reduced significantly ($E < 3.2$ eV). Further, methylene blue was taken as a model pollutant and was treated under 110 W visible light. The photocatalytic degradation allowed for the removal of the TOC of 73.6 % using the 0.5% Au^{3+}-TiO_2 (Li and Li, 2001). The reactivity of the surface of the plasmonic Au@TiO_2 photocatalyst was tailored using bio-based chitosan fibre fabricated by adopting an ionic gelation process (Shoueir et

al. 2019). The Au/TiO_2 fibre is highly efficient for removing methylene blue, metronidazole, and carbofuran within 250 min of operation under 25W visible light.

The catalytic activity of plasmonic materials depends partly on the size and shape of noble metal particles in the bulk substrate. The fabrication of Au-nanoparticles/TiO_2 hybrid films on Ti wires using electrochemical methods was reported by Fu et al. The efficiency of the fabricated material was studied by treating methyl orange dye. The percent degradation with TiO_2 nanotubes, Au/TiO_2/Au/TiO_2, TiO_2/Au/TiO_2 and Au/TiO_2 were reported to be 39.2%, 68.1%, 39.2% and 17.0%, respectively after 30 min of irradiation. The increased catalytic activity of the hybrid material was due to the reduced size of the Au particles. As a result, the surface area to volume ratio rises, further increasing the separation of electron and hole. Additionally, the Au nanoparticles exhibit electro-catalysis oxidation properties for biological and organic species (Fu et al. 2017).

Interest lies in the advanced nanocomposite material based on the natural clay and TiO_2 to remove a variety of micropollutants (Miyoshi et al., 2002; Wu et al., 1999; Fukugami and Sato, 2000). Bentonite clay is an aluminium silicate composite material in which two tetrahedral silica sheets are fused to one alumina octahedral sheet. Clay is a porous material showing a high surface area, which offers excellent support materials. Moreover, clays are abundant, non-toxic, cost-effective, and more importantly, environmentally friendly materials. The exchangeable cations (Na, K and Ca) present at the interlayer of clay structure compensate for the excess charge of the clay sheet (Sun et al., 2002; Liu and Zhang, 2014). Moreover, this allows the intercalation of charged inorganic or organic compounds within the interlayer by the exchange process (Amin et al., 2009; Fu et al., 2005; Wu et al., 2010; J. Li et al., 2009). Previously, the preparation of Ag/TiO_2/Bentonite powder nanocomposite material using the facile thermal decomposition method was reported. The material showed increased antibacterial activities against Gram-negative (*E. coli*) bacteria and Gram-positive (*S. aureus*) bacteria using the suitable diffusion method (Krishnan and Mahalingam, 2017). Clay-based TiO_2 composites thin film, prepared using the melt blending method, increases the photocatalytic efficiency in removing ethylene and enhances the antimicrobial activity against *Rhodotorula mucilaginosa* and

Pseudomonas spp. using 8 W ultraviolet (UV) lamps (Bodaghi et al., 2015). Bentonite clay modified cetyl-trimethyl ammonium bromide loaded TiO_2 (TiO_2/CTAB-Bt) was successfully utilized to treat refinery wastewater such as benzene, toluene, phenol, and naphthalene, through simultaneous photocatalytic oxidation under UV light and adsorption (Ulhaq et al., 2021).

1.10. Objectives and Scope of the Current Investigation

Environmental pollution from micropollutants and dyes, especially personal care products, pharmaceuticals, antibiotics and hormones has become a major environmental concern around the world, as several micropollutants are highly toxic, low biodegradable and persistent at low levels. Most of these micro-pollutants and dyes are incompletely or partially removed/degraded by wastewater treatment plants, raising severe concerns of deleterious water quality hence, the human health (Lara-Martín et al., 2014; Tuzen et al., 2017). Further, the residual untreated pollutants escape through the running water and causing several health issues in the aquatic environment (e.g., infertility etc.) and also posing a risk to human health (e.g., resistance to antibiotic) (Jafari-Kang et al., 2017). As a result, fine tuning and upgradation of the existing wastewater treatment plants (WWTPs) is a demand of the hour.

The advanced oxidation process (AOPs) using heterogeneous TiO_2 photocatalysis is highly efficient and relatively greener treatment processes to be employed in the waste water treatments. The principle of AOPs lies on the *in situ* formation of reactive hydroxyl radicals, which readily oxidizes even persistent compounds in aqueous wastes. Further, widespread use of TiO_2 as the heterogeneous catalyst is because of its unique properties *viz*., excellent thermal and chemical stability, biocompatibility, low toxicity, low cost, easy fabrication, engineered material etc. However, the bare titanium dioxide possessed a wide band gap energy and showed a rapid charge recombination rate, which restricted its implications in the treatment processes. Therefore, alternatively the doping of titanium dioxide with noble metals reduces significantly the band gap energy which allows readily to absorb toward visible light (Mogal et al., 2014). The doped titanium dioxide shows an enhanced reactivity in the photocatalytic processes using the visible light or even to harness the

solar radiations (Ge et al., 2006; Rengaraj and Li, 2006). Noble metals (Ag, or Au) show unusually high Schottky barriers which helps trapping of electrons and reduces the electron-hole pairs recombination. They also exhibit surface plasmon resonance (SPR) effect which enables titanium dioxide catalysts to absorb light at the visible region and enhances the excitation of electrons and increases the photocatalytic efficiency (Selvaraj and Li, 2006). Silver (Ag) nanoparticles show enormously intense surface plasmon resonance (SPR) effect at the wavelength of 320-450 nm near the band gap energy of titanium dioxide (~3.2 eV, 388 nm) (Rengaraj and Li, 2006). In Ag^0 TiO_2 photocatalyst, movement of electrons between the conduction band of titanium dioxide and Ag nanoparticles is favourable since Fermi level of silver metal is lowered as compared to the titanium dioxide (Selvaraj and Li, 2006). This causes the generation of Schottky barriers within the metal-semiconductor, and enables the excited electrons to move toward the electric field and the holes toward the opposite direction of the electric field. This inhibits the fast electron-hole pair recombination (Lee et al., 2014; Liu et al., 2013).

The interest lies in the advanced nanocomposite material based on the natural clay and TiO_2 for the removal of micro-pollutants (Miyoshi et al., 2002; Wu et al., 1999; Fukugami and Sato, 2000). Bentonite clay is an aluminium silicate composite material in which two silica tetrahedral sheets fused to one alumina octahedral sheet. Clay is a porous material showing high surface area which offers excellent support materials. Moreover, clays are abundant, non-toxic, cost effective, and more importantly are found to be environmental friendly (Sun et al., 2002; Liu and Zhang, 2014).

The present research work deals with an alternative waste water treatment methods *viz.*, the advanced oxidation process, which aimed at a highly efficient degradation of several organic micropollutants such as tetracycline, sulfamethazine, bisphenol A and some of the dyes including mordant orange, rhodamine B and rhodamine 6G. The process involves oxidation of target pollutants using immobilised clay supported Ag or Au nanoparticles doped TiO_2 thin films using PEG (Polyethylene glycol) as templating agent. Numerous physico-chemical parametric investigations are being carried out in depth in order to gain a better understanding of the photocatalytic

degradation of these pollutants. pH-dependent photocatalytic degradation of pollutants were carried out at a wide range of pH. It demonstrates the degradation mechanisms of pollutants at the surface of a photocatalyst. Concentration dependent studies were carried out within a wide range of pollutant concentration (0.5-20mg/L). Further, the kinetic studies were carried out to determine the effectiveness of the photocatalyst, efficiency of pollutant degradation and to determine the rate constant in the photocatalytic degradation reaction. Furthermore, in order to propose a plausible mechanism in the photocatalytic degradation of pollutants, the reactive radical scavengers studies were carried out. The reusability of the thin film photocatalyst in the repetitive photocatalytic degradation of the contaminants in an aqueous solution is investigated in order to demonstrate the practical implication of the thin film. Moreover, the real water implications further added the utility of novel photocatalysts in the scaling up of the process for technology development.

METHODOLOGY

2. METHODOLOGY

2.1 Materials

2.1.1. Chemicals and Apparatus

Analytical Reagent (AR) /Guaranteed Reagent (GR) grade chemicals are preferably used in the entire experimentation. Tetracycline hydrochloride ($C_{22}H_{25}ClN_2O_8$) (≥95.0%) (CAS No. : 3380-34-5), sulfamethazine ($C_{12}H_{14}N_4O_2S$) (≥99.0%) (CAS No. : 57-68-1), bisphenol A ($C_{15}H_{16}O_2$) (≥99.0%) (CAS No. : 99 80-05-7), Mordant Orange-1 ($C_{13}H_9N_3O_5$) (CAS No. : 2243-76-7), Rhodamine B ($C_{28}H_{31}ClN_2O_3$) (50%) (CAS No. : 81-88-9), Rhodamine 6G ($C_{28}H_{31}N_2O_3Cl$)(99%) (CAS No. : 989-38-8), polyethylene glycol ($C_{2n}H_{4n+2}O_{n+1}$) (PEG) (CAS No. : 25322-68-3), titanium (IV) isopropoxide ($Ti(OCH(CH_3)_2)_4$) (99%) (CAS No. : 97 546-68-9), gold chloride hydrate ($HAuCl_4.xH_2O$) (99.9%) (CAS No. : 27988-77-8), silver sulphate (Ag_2SO_4) (99.9%) (CAS No. : 10294-26-5), and sodium borohydride ($NaBH_4$) (99.9%) (CAS No. : 16940-66-2) were purchased from Sigma Aldrich. Co., USA. Acetic acid (CH_3COOH) (99.9%) (CAS No. : 64-19-7) and ethylenediamine tetra-acetic acid (EDTA) ($C_{10}H_{16}N_2O_8$) (98.0%) (CAS No. : 60-00-4) were obtained from the Loba Chemicals, India. Ethanol anhydrous (CH_3CH_2OH) (99.9%) (CAS No. : 64-17-5) was obtained from the Changshu Yangyuan Chemicals, China. 2-propanol ($CH_3CHOHCH_3$) (99.7%) (CAS No. : 67-63-0), acetylacetone ($CH_3COCH_2COCH_3$) (CAS No. : 123-54-6), sodium azide (NaN_3) (99.0%) (CAS No. : 26628-22-8), sodium chloride (NaCl) (99.0%) (CAS No. : 7440-23-5), sodium nitrate ($NaNO_3$) (99.0%) (CAS No. : 7631-99-4), copper sulphate ($CuSO_4$) (99.0%) (CAS No. : 7758-99-8), oxalic acid dihydrate ($C_2H_2O_4.2H_2O$) (99.0%) (CAS No. : 6153-56-6), glycine ($C_2H_5NO_2$) (99.0%) (CAS No. : 56-40-6), nickel chloride ($NiCl_2$) (95.0%) (CAS No. : 7718-54-9), hydrochloric acid (HCl) (CAS No. : 7647-01-0), and sodium hydroxide (NaOH) (CAS No. : 1310-73-2) were obtained from the Merck India Ltd., India. Bentonite clay (BN) was obtained from a commercial supplier, which was collected near Bhuj, Gujarat, India. The clay was used after simple washing with purified water without any further purification, dried in an oven at 90°C and crushed to obtain 100 BSS (British Standard Sieve). A circular borosilicate glass disk with a diameter and

thickness of 2.3 cm and 0.5 mm respectively was utilised for fabricating the thin film nanocomposite.

Water was purified by the Sartorius water Purification System (model: Pore Size of 0.45 + 0.2 mm, Sartopore 2150, Sterile Plus, Arium Mini Plus UV Lab., Germany). The conductivity of the purified water was 0.05 µS/cm. An electric furnace was utilised for annealing materials (Nabertherm, Germany; Model No. LT/15/12/P330). A pH-meter with glass and calomel electrode assembled (Thermo Scientific, Sn B43460) was used for all the pH measurements in aqueous solutions. Using the standard buffer solutions, the pH meter was carefully calibrated before using it. A Light-emitting diode (LED) (visible light) bulb (Havells- Adore LED 20 W, 50 Hz, India) and UV-A lamp (λ_{max} = 360 nm (Philips, Model: 9W, PLS9W BLB/2P 1CT, Hansung UV Pvt. Co. Ltd., Korea) were employed in the photoreactor.

2.1.2. Reagents

i) Sample stock solutions: 50.0 mg/L solution of different micropollutants and dyes were prepared in purified water. The stock solutions were prepared by dissolving an accurate amount of analyte in the purified water. The solubility of pollutants were enhanced using the sonication bath.
ii) Standard Buffers (pH 4.01, 7.00 & 12.45) (Hanna Instruments) were utilised for the calibration of pH meter.
iii) Standard HCl and NaOH (0.1 mol/L) solutions were used for adjusting the pH of the sample solutions.

2.1.3. Instruments

A UV-Visible Spectrophotometer (Thermo Electron Corporation, England; Model: Thermo Spectronic UV1) was used to investigate the kinetics of organic compound degradation by measuring the variation in absorbance at a fixed wavelength or scanning over a range in the spectrum. The TOC Analyzer (*Shimadzu, Japan; Model: TOC-VCPH/CPN*) was used to determine the total organic carbon content data. The change in NPOC (Non-Purgeable Organic Carbon) values with the photocatalytic treatment provided the mineralization of the pollutants under the photocatalytic

operations. Moreover, the natural water samples were subjected for the TOC measurements to obtain the inorganic and organic carbon content present in the natural water samples. Calibration was done using standard potassium hydrogen phthalate solutions to obtain the required carbon concentrations. The TOC Analyzer (Shimadzu, Japan; Model: TOC-VCPH/CPN) used in this study is based on catalytic oxidation/NDIR (680^0C combustion) method and is highly responsive and reliable for analysing parameters such as TC, IC, TOC, and NPOC with measuring ranges and detection limits of TC: 4 ng/L to 25000 mg/L and IC: 4 ng/L to 30000 mg/L. Atomic Absorption Spectrometer (Shimadzu, Japan; Model: AA-7000) was used for the quantitative determination of metals such as Zn, Ni, Cu, Pb, Mn, Fe, etc. Liquid chromatograph-mass spectrometric (LC-MS) (LCMS-8040, Shimadzu) analysis was performed for the treated pollutant samples in order to study the possible reaction pathways in the degradation of pollutant molecules and to provide the degradation by-products. The positive ion mode mass spectra were used to identify the compounds present in solution.

Scanning Electron Microscope (SEM) (FESEM: JEOL JSM 7100F; Oxford Xmax) (Operation condition: SEI Resolution used: 15kV, Magnification: 10-1000000, Accelerating Voltage: 0.2-30 kV, Probe Current: 1pA-400nA and Electron Gun used: In-Lens Schottky field emission gun) was utilized to obtain the surface morphology of nanocomposite thin films viz., Ag^0(NPs)/TiO_2, Clay/Ag/TiO_2, Clay/Ag/TiO_2(T), Clay/Au/TiO_2 and Clay/Au/TiO_2(T). Similarly, all the nanocomposite powder samples were subjected for the TEM (Transmission Electron Microscopic) analysis using the TEM Analyser (HRTEM/EDX: JEOL, JEM 2100; Oxford Xtreme) (Operation condition: Magnification: X40K, Accelerating Voltage: 200 kV, Emission Current (status): 113 μA, Spot size (diameter): TEM Spot 1, Alpha 3, Current density: 0.3 pA/cm^2, Experiment time: 0.3 sec.). TEM-EDX (Processing option : All elements analyzed (Normalised), Number of iterations = 3) was used to depict the percentage distribution spectra of the elements. Additionally, the TEM-EDX elemental mapping was conducted for the elements Ti, O, Si, Al, Ag and Au. Furthermore, the interplanar distance of Ag(NP) or Au(NP) was calculated, and the size of the particles was obtained. Atomic Force Microscope (AFM) (NT MDT Moscow; Ntegra Aura)

operated under Semi contact mode and silicon nitride as a probe was used to produce three-dimensional topographical images of the thin-films.

Brunauer-Emmett-Teller (BET) surface area analyses were conducted using a BET Surface Area Analyser (Micromeritics) based on liquid N_2 adsorption and desorption isotherms. The BET results provided the pore size, specific surface area and pore volumes of Ag^0(NPs)/TiO_2, Clay/Ag/TiO_2, Clay/Ag/TiO_2(T), Clay/Au/TiO_2 and Clay/Au/TiO_2(T) powders. The X-ray diffraction machine (PANalytical, Netherland; Model X'Pert PRO MPD) was used to obtain the X-ray diffraction (XRD) pattern of the Ag^0(NPs)/TiO_2, Clay/Ag/TiO_2, Clay/Ag/TiO_2(T), Clay/Au/TiO_2 and Clay/Au/TiO_2(T) powder nanocomposite materials. The X-ray diffraction data was recorded at the scan rate of 0.033 of 20 illumination and the generator was set at 30 mA, 40 kV. The Cu $K_{\alpha 1}$ and Cu $K_{\alpha 2}$ radiations were utilised, which have the wavelengths of 1.5406 and 1.54443 Å. Diffuse reflectance spectra (DRS) of the powder samples viz., Ag^0(NPs)/TiO_2, Clay/Ag/TiO_2, Clay/Ag/TiO_2(T), Clay/Au/TiO_2 and Clay/Au/TiO_2(T) were obtained using a UV-Vis spectrophotometer (Evolution 220; Thermo Scientific). DRS results were used to calculate the bandgap energies of these solids. The data was taken at a bandwidth of 1 nm over a wavelength range of 200 to 800 nm.

2.2. Methods

2.2.1. Synthesis of Ag Nanoparticles

Ag^0-nanoparticle was obtained by a simple chemical reduction process (Tiwari et al., 2018). In brief: 30 mL of $NaBH_4$ solution (0.2 mmol/L) was taken in a beaker, and kept in an ice bath. Further, 20 mL of Ag_2SO_4 solution (0.5 mmol/L) was slowly added to the sodium borohydride solution under constant and vigorous stirring. The reduction of Ag(I) to Ag(0) occurred, and the colloidal solution of silver was formed. This is confirmed by the colour change of the precursor solution from colourless to bright yellow (Figure 2.2.1.).

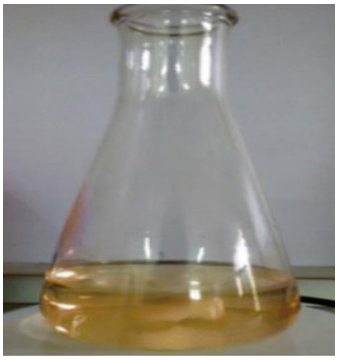

Figure 2.2.1.: Ag Nanoparticle colloidal solution.

2.2.2. Synthesis of Au Nanoparticles

The Au nanoparticles were obtained using a known chemical reduction process as described elsewhere (McFarland et al., 2004). In summary: 0.5 mmol/L of $AuCl_3$ solution was prepared in purified water. 50 mL of $AuCl_3$ solution taken in a conical flask and under stirring heated at ~80°C using the hot plate. Then 2.0 mL of 1% trisodium citrate solution was swiftly added to the $AuCl_3$ solution under stirring. The Au(III) is rapidly reduced to Au(0), and forms the colloidal Au(0) solution. The heating was stopped. The Au(0) solution turned to deep red in colour as shown in Figure 2.2.2.

Figure 2.2.2.: Au Nanoparticle colloidal solution.

2.2.3. Preparation of Ag^0(NPs)/TiO_2 Sol Solution

The nanocomposite Ag^0(NPs)/TiO_2 was synthesized by a facile sol gel process. Polyethylene glycol (PEG) was used as a templating agent to obtain the nanostructured titania network (Rtimi et al., 2013). 2.92 mL of titanium isopropoxide $Ti[OCH(CH_3)_2]_4$

(TISP) and 2.0 g of poly(ethylene glycol) (PEG) was added to 1.3 mL acetyl-acetone (AcAc). Instantly, 10.0 mL of freshly prepared Ag^0(NP) solution was dispersed to this solution mixture. The titanium solution was gently mixed with a solution mixture of 23.3 mL ethanol (EtOH), 0.55 mL acetic acid (AcOH), and 2.25 mL distilled water (H_2O). This results in the initiation of hydrolysis and condensation reactions. The resulting Ag^0(NPs)/TiO_2 solution mixture was vigorously stirred for 2 hrs. Then the sol solution was sonicated for 30 minutes in a sonication bath. A clear sol solution was obtained, it was then left for *Ca*. 24 hrs for aging (*Cf* Figure 2.2.3.). The sol was used for fabrication of thin films.

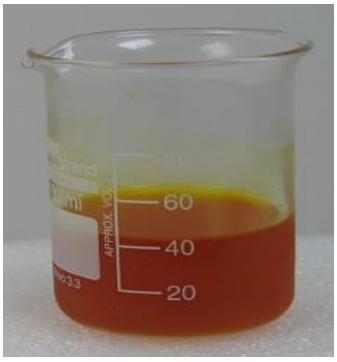

Figure 2.2.3.: Ag^0(NPs)/TiO_2 sol solution.

2.2.4. Preparation of Bentonite Clay Supported Ag^0(NPs)/TiO_2 Sol Solution

Preparation of nano-structured TiO_2 was carried out using a synthetic template route. The polyethylene glycol was used as a templating agent in the propagation of titania network. 1.3 mL of acetyl-acetone was added to a mixture of 2.9 mL TISP (titanium isopropoxide) and 2.0 g PEG (poly-ethylene glycol). The solution mixture was then stirred for 10 min followed by the addition of 10.0 mL of freshly prepared Ag^0(NP) colloidal solution. The solution mixture of H_2O (distilled water), EtOH (ethanol), and AcOH (acetic acid) having the volume of 2.25 mL, 23.3 mL, and 0.55 mL, respectively, were added to the reaction mixture. The condensation and hydrolysis reactions commenced. The solution mixture was stirred for about 2 hrs. Further, the sol solution of Ag/TiO_2 was introduced with the bentonite. 20.0 mg of bentonite clay was dispersed into the 20.0 mL of Ag/TiO_2 sol solution. The mixture was stirred for 2 hrs and then placed in a sonication bath for 30 min. The resulting Clay/Ag/TiO_2

nanocomposite was kept for 24 hrs for possible aging of the material (*Cf* Figure 2.2.4.). Similarly, the non-template Clay/Ag/TiO_2 was prepared using the same procedure without introducing the PEG. The non-template and template Clay/Ag^0(NP)/titania materials were labelled as Clay/Ag/TiO_2 and Clay/Ag/TiO_2(T) respectively.

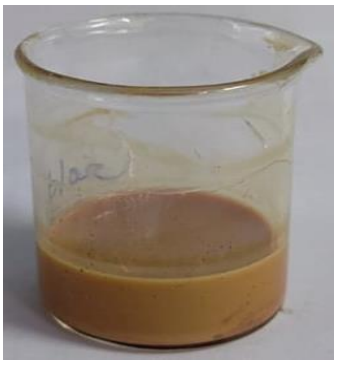

Figure 2.2.4.: Bentonite clay supported Ag^0(NPs)/TiO_2 suspension.

2.2.5. Preparation of Bentonite Clay Supported Au^0(NPs)/TiO_2 Sol Solution

The sol-gel process was adopted to synthesize the template TiO_2-nanocomposite. The titania network was obtained by utilising the polyethylene glycol (PEG) as templating agent. The precise procedure is followed as: 2.9 mL of titanium isopropoxide (TISP) was mixed with 2.0 g PEG in acetyl-acetone (AcAc). Instantaneously, 10.0 mL of freshly prepared Au^0(NPs) colloidal solution was added to this solution mixture. Furthermore, a solution containing distilled water (2.25 mL), acetic acid (0.55 mL) and ethanol (23.3 mL) was gently added to the titanium solution, allowing the condensation and hydrolysis reactions to initiate. After 2 hrs of stirring, 10 mg of bentonite clay was added per 10 mL of the titania solution. The mixture was vigorously stirred for another 2 hrs before being sonicated in a sonication bath for 30 min. A sol solution thus formed was then aged for 24 hrs at room temperature (*Cf* Figure 2.2.5.). The sol was then used to fabricate the thin films. Likewise, a non-template Clay/Au/TiO_2 sol was prepared without the use of PEG solid. The template and non-template Au-nanoparticle titania sols were given the names Clay/Au/TiO_2(T) and Clay/Au/TiO_2, respectively.

Figure 2.2.5.: Bentonite clay supported Au^0(NPs)/TiO_2 suspension.

2.2.6. Fabrication of Thin Films

The borosilicate glass disk was washed with HNO_3 (0.1 mol/L) and rinsed with plenty of purified water. The disk was dried at 100°C in a drying oven. The dried and cleaned circular borosilicate glass disk was fabricated with titania solution using the dip coating method. The disks were slowly introduced in the Ag^0(NPs)/TiO_2, Clay/Ag/TiO_2, Clay/Ag/TiO_2(T), Clay/Au/TiO_2 and Clay/Au/TiO_2(T) sol solutions and held vertically for 1 hrs. The disks were then taken out from the sol solutions and left to dry in air for 12 hrs followed by drying at 100°C for 1 hrs in a drying oven. The dried disks were then annealed at 500°C for 3 hrs using an electric furnace (Model No. LT/15/12/P330, Nabertherm; Germany). This results in the formation of an extremely fine nanocomposite thin film coating on the borosilicate glass substrate. The same procedure was repeated for three consecutive times to obtain a fine thin layer deposition of nanocomposite onto the glass substrate (Figure 2.2.6.). The fabricated thin films were kept in a sealed, dry container for later usage in photocatalytic operations.

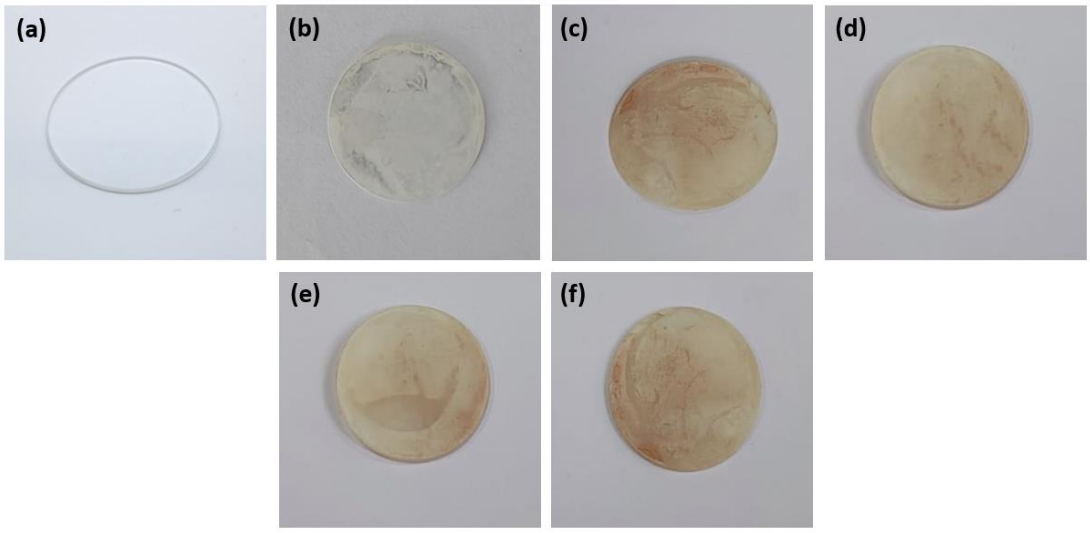

Figure 2.2.6.: (a) Borosilicate glass disk; (b) Ag^0(NPs)/TiO_2; (c) Clay/Ag/TiO_2; (d) Clay/Ag/TiO_2(T); (e) Clay/Au/TiO_2 and (f) Clay/Au/TiO_2(T) thin film.

2.2.7. Preparation of Nanocomposite Powders

The nanocomposite powders were obtained from the previously prepared sol solution of nanocomposites *viz.*, Ag^0(NPs)/TiO_2, Clay/Ag/TiO_2, Clay/Ag/TiO_2(T), Clay/Au/TiO_2 and Clay/Au/TiO_2(T). Firstly, the sol solutions were heated at 105°C for 1 hrs to evaporate the solvents and then annealed at 500 °C for 3 hrs in an electric furnace to get the powders of Ag^0(NPs)/TiO_2, Clay/Ag/TiO_2, Clay/Ag/TiO_2(T), Clay/Au/TiO_2 and Clay/Au/TiO_2(T). The solid powders were obtained by crushing the solids in a mortar. The powders were stored in an air tight bottles for further characterization purposes.

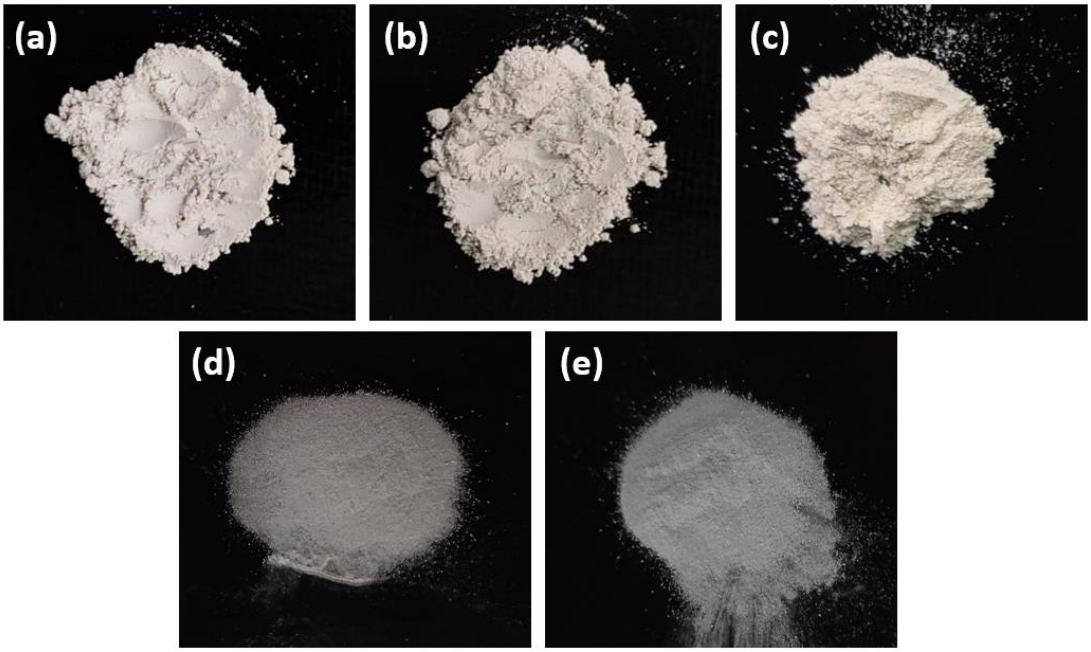

Figure 2.2.7.: The nanocomposite powders of **(**a) Ag^0(NPs)/TiO_2; (b) Clay/Ag/TiO_2; (c) Clay/Ag/TiO_2(T); (d) Clay/Au/TiO_2 and (e) Clay/Au/TiO_2(T).

2.2.8. Determination of pH_{PZC} of the Solids and Speciation Studies

The point of zero charge is the pH value at which the solid surface carries no net charge (pH_{pzc}). As a result, the solid's surface possessed net positive charge at pH < pH_{pzc} and a negative charge at pH > pH_{pzc} (Kragovic et al., 2019). The pH_{pzc} was measured using the drift method as described elsewhere (Lalhmunsiama et al., 2013).The detailed procedure is: In order to remove the dissolved CO_2, 500 mL of distilled water was added to a 1000 mL Erlenmeyer flask, the top was covered with cotton, and the water was gently and steadily heated till boiling for 20 minutes. The flask was quickly covered to stop the re-absorption of atmospheric CO_2. 50 mL of 0.01 mol/L NaCl solutions were prepared using the CO_2 free water. The solution pH in each flask was then adjusted to various pH values of 2.0, 4.0, 6.0, 8.0, 10.0, and 12.0 by dropwise addition of 0.1 mol/L HCl or 0.1 mol/L NaOH solutions. 100 mg of the solid sample was taken to each flask, which was then tightly closed before being shaken for 24 hours at 25°C. The solutions' final pH was recorded, and graphs were drawn

between $pH_{Initial}$ and pH_{Final}. The point of intersection of these curves where the $pH_{Initial}$ and pH_{Final} gave the point of zero charge.

The speciation study was conducted for the molecules TC, SMZ, BP-A, MO-1, R-B and R-6G from their known pk_a values (Table 2.2.8) using Microsoft Excel self-made programs. The species distribution of TC, SMZ, BP-A, MO-1, R-B and R-6G as a function of pH were graphically presented in the results and discussion section.

Table 2.2.8: pk_a values of various micro-pollutants.

Name of Micro-Pollutants	**pk_a Values**			**References**
	pk_a^1	**pk_a^2**	**pk_a^3**	
Mordant Orange 1 (MO-1)	5.0	11.0	-	(Nazar et al., 2010)
Tetracycline (TC)	3.3	7.7	9.7	(Liu et al., 2012)
Sulfamethazine (SMZ)	2.28	7.42	-	(Liu et al., 2017; Fukahori et al., 2011)
Bisphenol A (BP-A)	9.59	10.2	-	(Wang et al., 2021)
Rhodamine B (R-B)	4.2	-	-	(Maurya et al., 2006)
Rhodamine 6G (R-6G)	6.13	-	-	(Rajoriya et al., 2016)

2.2.9. Batch Reactor Studies

2.2.9.1. Photocatalytic Degradation Experiment

Stock solutions of tetracycline (TC) (50.0 mg/L), sulfamethazine (SMZ) (50.0 mg/L), bisphenol A (BP-A) (20.0 mg/L), Mordant Orange 1 (MO-1) (50.0 mg/L), Rhodamine B (R-B) (50.0 mg/L), Rhodamine 6G (R-6G) (50.0 mg/L) were prepared using purified water. To maximize the solubility of these pollutants in purified water, the solutions were sonicated for 10 minutes. Furthermore, the experimental concentrations were obtained by diluting the stock solutions successively. Drop by drop addition of HCl (1 mol/L)/or NaOH (1 mol/L) solutions enabled to adjust the pH of these solutions from pH 4.0-12.0. A pH-meter assembled with glass and calomel electrodes was used to measure the pH of these solutions. The concentration-dependent studies were carried out varying the initial pollutants' concentrations from 0.5 to 20.0

mg/L for each. The λ_{max} for TC, SMZ, BP-A, MO-1, R-B and R-6G were determined to be 360, 260, 293.5, 360, 553 and 526 nm, respectively (Yang et al., 2013; Li et al., 2021; Ackerman et al., 2010; Nestmann et al., 1979). The calibration curve was obtained using the standard solutions of each pollutant at different pollutant concentrations (0.5 to 20.0 mg/L). Batch reactor experiments were conducted to evaluate the photocatalytic degradation of these pollutants. The reactor was placed inside the black box having a dimension of 60 x 50 x 50 cm. Inside this black box, a reactor made up with borosilicate glass having the capacity of 100 mL was carefully placed. The pollutant solution (50.0 mL) was taken in the reactor vessel and a thin film photocatalyst was placed horizontally at the middle and bottom of the pollutant solution. At 10 cm above the reactor, a LED (visible light) or UV-A lamp was mounted carefully to ensure greater illumination of the photocatalyst. The samples were treated for 2 hrs for TC, MO-1, R-B, and R-6G; 3hrs for SMZ and 4 hrs for BP-A under LED (Visible Light)/or UV-A light using the thin-film photocatalysts. The photocatalytic oxidation reaction begins as light radiation reaches the thin-film photocatalyst in the pollutant solutions. The reaction temperature was maintained at 25±1°C throughout the experiment using a self-assembled water bath. The samples were oxygenated by bubbling the reaction mixture using an aquarium air pump. At predetermined times, pollutant samples were taken from the reactor, and the pollutant concentrations were measured using a UV-Vis spectrophotometer. Always blank studies were carried out under light irradiation using the same glass disk but not coated with nanocomposite materials. The efficiency of degradation for different pollutants were calculated using the equation (2.1.):

$$\text{Removal efficiency (\%)} = \frac{C_i - C_f}{C_i} x\ 100 \qquad \ldots(2.1.)$$

where C_i and C_f are the initial and final pollutant concentrations, respectively, i.e., before and after the photolytic/or photocatalytic treatment of pollutant solutions.

2.2.9.2. Effect of Solution pH

pH is an essential parameter in the photocatalytic process, which demonstrates an apparent mechanism involved at the interface i.e., the catalyst surface and the

pollutant species in aqueous medium. It also determines the degradation mechanisms of contaminants at the catalyst surface. The surface charge of the catalyst and the size of the catalyst aggregates are influenced by the pH of the solution (Sithamparanathan et al., 2021). The sorption of pollutants on the surface of the thin-film catalyst showed a significant impact on photocatalytic activity. The sorption process is strongly determined by the pH of sorptive solutions (Chong et al., 2010). Therefore, the pH-dependent degradation of micropollutants and dyes were carried out at a wide range of pH 4.0 to 12.0. The results were expressed as pollutant degradation percentage as a function of solution pH.

2.2.9.3. Effect of Concentration of Pollutant

The photocatalytic degradation of organic pollutants is a surface phenomenon, and organic pollutants that are adsorbed at the surface of a photocatalyst are more vulnerable to direct oxidation. Therefore, the initial concentration of pollutant in any photocatalytic reaction is an important parameter that demonstrates the mechanistic aspects of degradation (Nasseri et al., 2017). In general, the percentage photocatalytic degradation of pollutants was increased at a lower initial concentration and decreased with an increase in pollutant concentrations. Therefore, at constant solution pH, the effect of initial concentration of pollutant in photocatalytic degradation of organic pollutants was investigated increasing the initial concentration from 0.5 mg/L to 20.0 mg/L for TC, SMZ, MO-1, R-B, and R-6G and from 1.0 to 20 mg/L for BP-A. After a specified time period i.e., 2 hrs for TC, MO-1, R-B, and R-6G; 3 hrs for SMZ and 4 hrs for BP-A) treatment, the results were provided as percent pollutant degradation as a function of pollutants' initial concentrations.

2.2.9.4. Degradation Kinetics

In order to study the kinetics of the degradation process that occur between adsorbed organic pollutants and the surface reactive species, photocatalytic degradation kinetic study was carried. Further, the kinetic studies determine the effectiveness and efficiency of the photocatalyst and the time dependence elimination of pollutants provides an apparent rate constant values in the photocatalytic degradation of these organic pollutants. The time dependence change in the pollutant

concentration is monitored and modelled to the known kinetic equations. The pseudo-first order rate equation is utilized as shown in Eq. 2.2:

$$r = -\frac{d[C]}{dt} = k_{app}\left[k_{photolysis} + k_{photocatalysis}\right][C] = k_{app}\,[C] \qquad \ldots(2.2.)$$

where [C] is the micropollutant concentration and k_{app} is the pseudo-first-order rate constant. Equation 2.2 is integrated with the extreme conditions, i.e., at t=0, [C]=C_0. As a result, the equation 2.2 becomes:

$$ln\left(\frac{C_0}{C_t}\right) = k_{app} \cdot t \qquad \ldots(2.3)$$

The values of LN (C_o/C_t) were plotted against the time 't'. The apparent first order rate constant for the elimination of organic pollutant was obtained by the slope of the straight line.

Further, the photocatalytic oxidation of the pollutants was modelled with the Langmuir–Hinshelwood (L-H) isotherm. This demonstrates the adsorption properties of the sorbing species to the photocatalyst surface. The derived equation was used to its linear form:

$$r_0 = \frac{k_r . K . C_0}{1 + K . C_0} \qquad \ldots(2.4.)$$

or $$\frac{1}{r_0} = \frac{1}{K . k_r} . \frac{1}{C_0} + \frac{1}{k_r} \qquad \ldots(2.5.)$$

where '$1/r_0$' is a dependent variable, '$1/C_0$' is an independent variable, $1/k_r$ is the linear coefficient and ($1/(K.k_r)$) the angular coefficient of the straight line. From this model, the L-H adsorption constant and the rate constant were obtained by plotting $1/r_0$ against $1/C_0$ (Mendioroz et al., 1987).

2.2.9.5. Effect of Coexisting ions and Scavengers

Wastewater consists of a variety of dissolved inorganic/or organic cations and anions that affect the rate of photocatalytic degradation of organic pollutants in either a negative or positive way (Xu et al., 2015; Yuan et al., 2019). Some of the compounds are known scavengers of reactive species, that demonstrates even the mechanism of

photocatalytic degradation. To replicate the natural wastewater matrix, studies were carried out in the presence of several coexisting ions viz., oxalic acid, glycine, EDTA, $ZnCl_2$, NaCl, $NaNO_2$, $NaNO_3$, and $CuSO_4$ and scavengers viz., 2-propanol, $NaHCO_3$ and NaN_3 in the photocatalytic degradation of different organic pollutants under visible light irradiations utilizing the thin film catalyst. The initial pollutant concentrations were taken as 10.0 mg/L at a constant pH (TC: pH-10; SMZ: pH-6; BP-A: pH-8; MO-1: pH-6; R-B: pH-6; and R-6G: pH-6). Each coexisting ion concentration was taken as 100.0 mg/L and the scavengers concentration was taken as 1000.0 mg/L.

2.2.9.6. Mineralization Study

The extent of mineralization of pollutants in the photocatalytic treatment demonstrates the efficiency/applicability of operation as it indicates total elimination of dissolved harmful organic compounds from the contaminated aqueous solutions. As a result, the TOC (total organic carbon) analyser was used to measure the extent of mineralization in the photocatalytic degradation process. The mineralization of pollutants were obtained at different initial concentrations of pollutant (0.5 – 20.0 mg/L) for BP-A and (0.5 – 20 mg/L) for TC, SMZ, MO-1, RB and R6G, at a constant solution pH (TC: pH-10; SMZ: pH-6; BP-A: pH-8; MO-1: pH-6; R-B: pH-6; and R-6G: pH-6). The NPOC (Non-Purgeable Organic Carbon) values were obtained for the treated and untreated pollutant solutions, hence; the percentage removal of NPOC was calculated. Further, the percentage mineralization was plotted against the initial pollutants' concentrations.

2.2.10. Reusability of Thin Film Photocatalyst

The applicability of photocatalysts largely depends on extended and recurrent photocatalytic operations. This includes the stability of nanocomposite materials. As a result, the thin film photocatalysts were employed for the repeated catalytic operations in the batch reactor. The photocatalytic degradation of mordant orange 1, tetracycline, sulfamethazine, bisphenol A, rhodamine B and rhodamine 6G in an aqueous solution were carried out under LED (Visible Light) irradiation repeatedly for 6 times. After each cycle of operation, the thin film was cleaned with distilled water and then dried

for 1 hrs at 300°C in a drying oven. The catalyst was cooled at room temperature and again employed for the next photocatalytic cycle. The initial concentration (5.0 mg/L for MO-1 and 10 mg/L for TC; SMZ; BP-A; MO-1; R-B and R-6G) and pH (TC: pH-10; SMZ: pH-6; BP-A: pH-8; MO-1: pH-6; R-B: pH-6; and R-6G: pH-6) of the solution were kept constant for each cycle of operations.

RESULTS AND DISCUSSION

3. RESULTS AND DISCUSSIONS

3.1. Characterization of Samples

The materials synthesized *viz.*, Ag^0(NPs)/TiO_2, Clay/Ag/TiO_2, Clay/Ag/TiO_2(T), Clay/Au/TiO_2 and Clay/Au/TiO_2(T) were successfully characterized using various advanced analytical methods. Surface morphology was carried out using scanning electron microscope (SEM), transmission electron microscope (TEM)/EDX/Elemental Mapping and atomic force microscopy analyses (AFM). Further the materials were characterised using X-ray diffraction (XRD), Brunauer-Emmett-Teller (BET) surface area analysis and diffuse reflectance spectroscopic (DRS) techniques.

3.1.1. Scanning Electron Microscopic (SEM) Analysis

SEM micrograph of Ag^0(NP)/TiO_2 is shown in Figure 3.1.1(i). The result showed that small sized TiO_2 particles are distributed uniformly onto the silicate glass and formed a uniform thin film of nanocomposite. However, at some places, cracks are observed on the surface. Further, it is interesting to observe that the titanium dioxide is not agglomerated on the surface. This is because of template synthesis of titania. The EDX analysis of the thin film sample shown in Figure 3.1.1(i)(Inset). It is evident from the figure that the silver is incorporated within the titania network since a prominent Ag peak is observed in the EDX spectra.

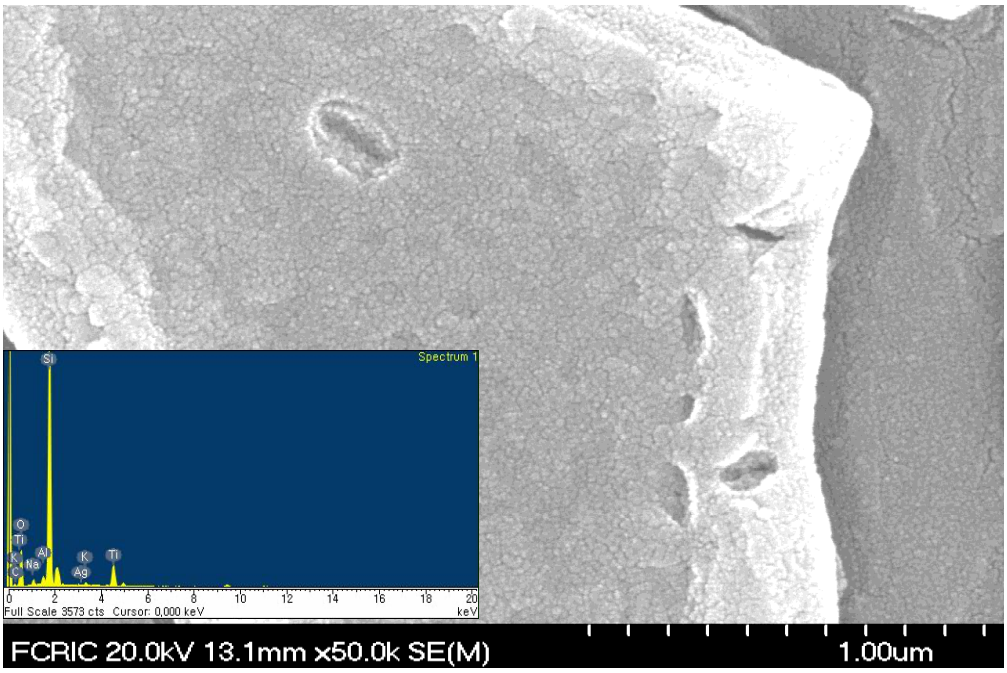

Figure 3.1.1(i): Scanning electron microscopic images of Ag^0(NP)/TiO_2 and SEM-EDX analysis of Ag^0(NP)/TiO_2 thin film (Inset).

Figure 3.1.1(ii) illustrates the SEM images of Clay/Ag/TiO_2 and Clay/Ag/TiO_2(T) thin films. Both the thin films showed that the fine grains of TiO_2 are evenly aggregated on the surface of borosilicate glass, and the particles form a uniform layer on the surface. The material prepared without the template showed fine particles and no cracks were observed on the surface. On the other hand, the material synthesized with PEG showed uniform dispersion of grains on the thin film surface. However, the grain size was significantly increased using the template. Moreover, some cracks are also observed on the surface. Similarly, Ag^0(NP)/TiO_2 nanocomposite thin-film prepared using the synthetic template method was reported to have fine grains of TiO_2 dispersed evenly on the surface of the supporting glass (Tiwari et al., 2018). Tahir et al. 2016 used phytochemicals to make a comparable Au(NPs)/TiO_2 nanocomposite and the TiO_2 was somewhat aggregated, and Au was evenly dispersed with the titanium dioxide (Tahir et al., 2016).

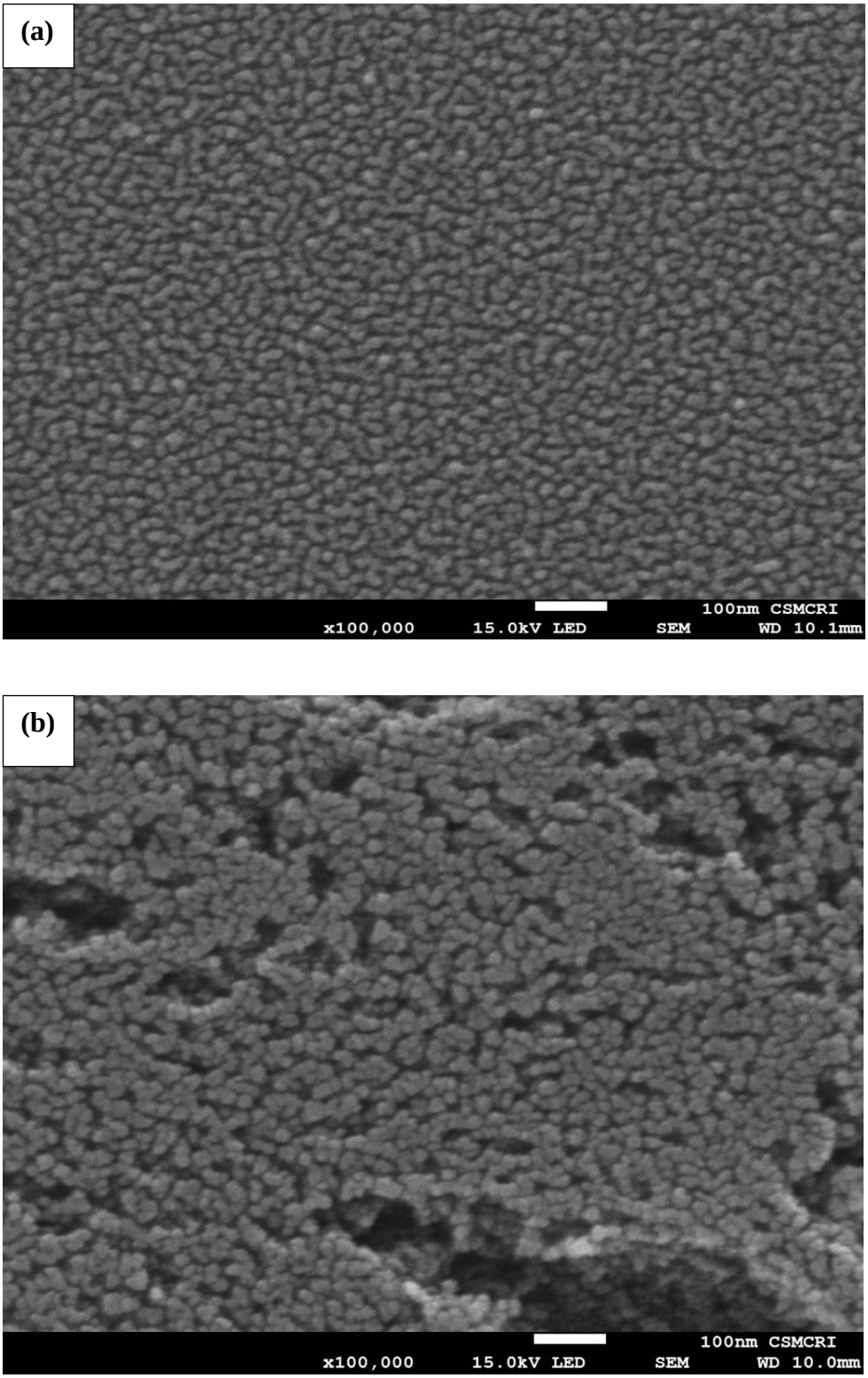

Figure 3.1.1(ii): Scanning electron microscopic images of (a) Clay/Ag/TiO_2 and (b) Clay/Ag/TiO_2(T) thin films.

Figure 3.1.1(iii) displays SEM images of Clay/Au/TiO_2 and Clay/Au/TiO_2(T) nanocomposite thin films. In both samples, Au/TiO_2 particles were equally disseminated on the substrate surface, as shown in Figure 3.1.1(iii). It is also worth noting that Au/TiO_2 forms a heterogeneous structure on the surface of the disk, and the TiO_2 particles are not aggregated. The surface of the Clay/Au/TiO_2(T) thin film exhibited a very dense surface structure with minor cracks. The titania is lumped at the surface and forms a very disordered surface structure.

The Clay/Au/TiO_2 thin-film exhibited uniform surface coverage with no cracks. Moreover, the grains are dispersed very evenly on the substrate surface. Furthermore, the grain size was significantly larger in the templated solid i.e., Clay/Au/TiO_2(T) as compared to the Clay/Au/TiO_2. Similar findings are obtained in Au-nanopillars dopes TiO_2 meso-porous thin films prepared using a sol-gel preparation method and was successfully utilised in the removal of tetracycline under UV-A irradiation (Tiwari et al., 2019). Furthermore, Au@TiO_2 nanohybrids showing spherical shape, with no aggregation and uniformly-distributed (monodispersed), having a grain size of around 40 nm were also reported to efficiently degrade methylene blue dye and was also shown to have improved antimicrobial activities (Sagadevan et al., 2020).

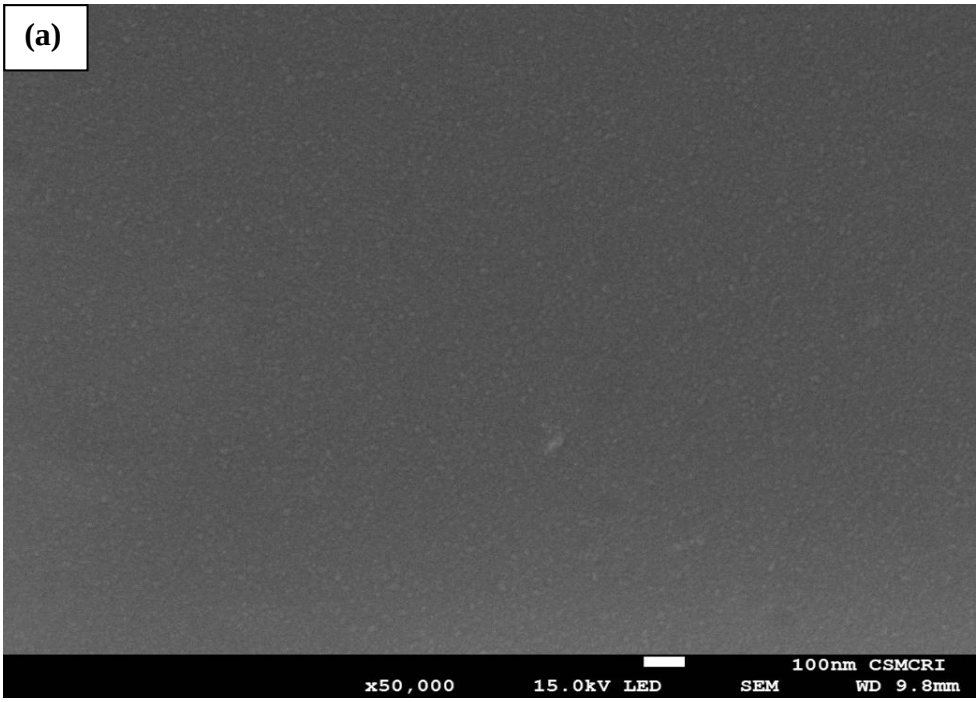

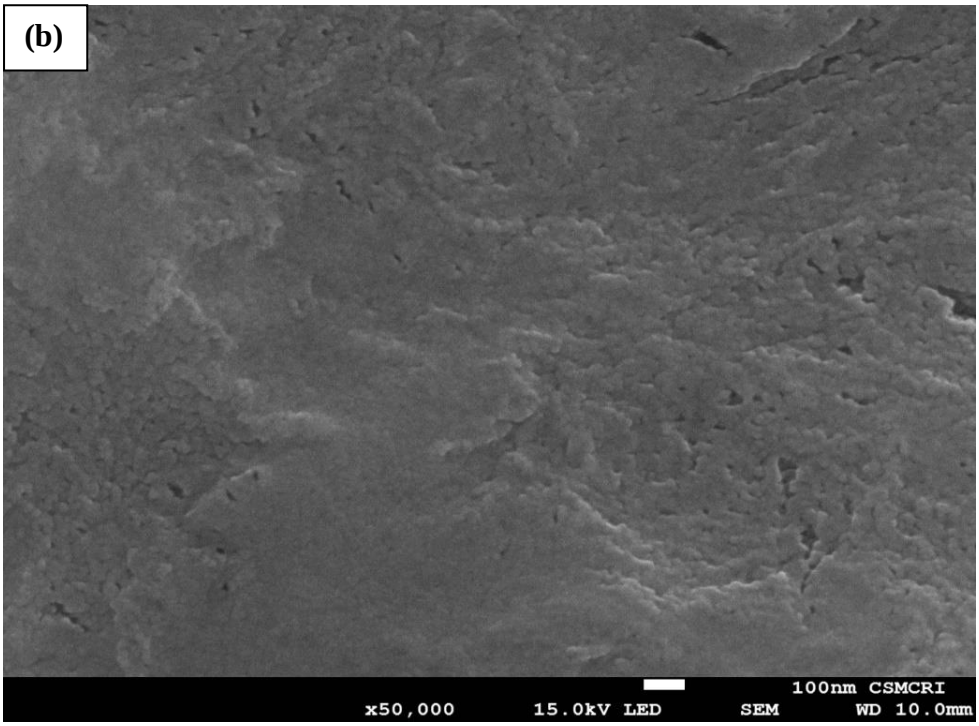

Figure 3.1.1(iii): Scanning electron microscopic images of (a) Clay/Au/TiO_2 and (b) Clay/Au/TiO_2(T) nano-composite thin film.

3.1.2. Transmission Electron Microscopic (TEM) Analysis

The TEM image of the Ag^0(NP)/TiO_2 nanocomposite is shown in Figure 3.1.2(i). The high-resolution TEM image clearly showed the fringes of Ag nanoparticles and it is uniformly distributed with TiO_2 structure. Moreover, the interplanar distance of the Ag^0(NP) is estimated to be 0.15 nm.

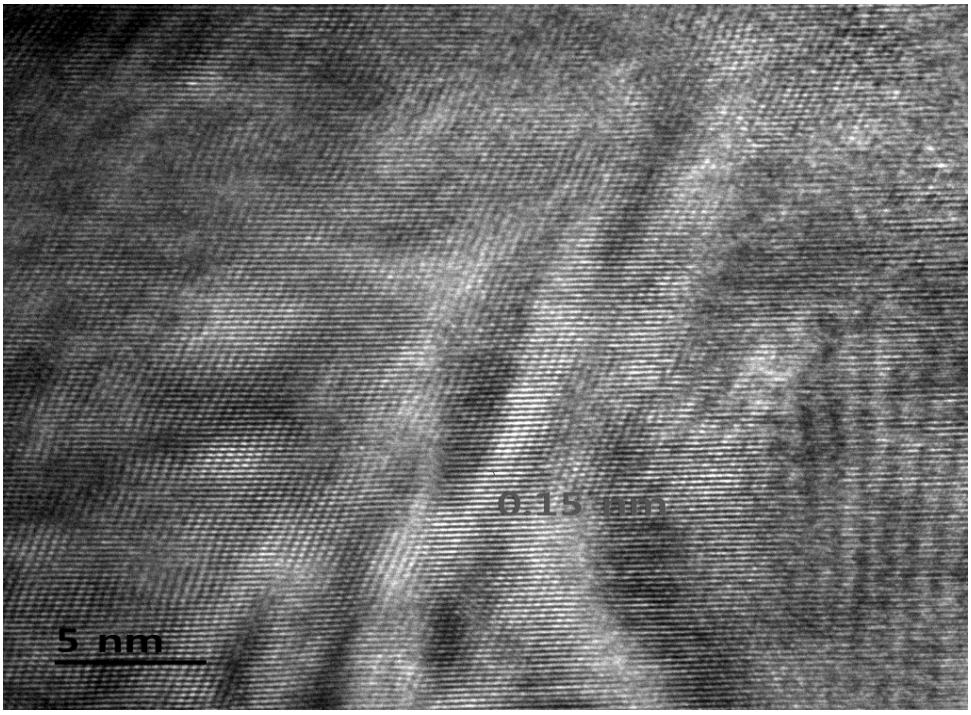

Figure 3.1.2(i): Transmission electron microscopic images of Ag^0(NP)/TiO_2 nanocomposite.

Further, the high-resolution TEM images of the Clay/Ag/TiO_2 and Clay/Ag/TiO_2(T) nanocomposite powders are shown in Figure 3.1.2(ii)(a) and (b). TEM results showed different morphological results of the nanocomposites prepared by the template and non-template methods. The silver nanoparticles' shape and sizes are significantly changed using the template. The non-template synthesis of Clay/Ag/TiO_2 showed a uniform and spherical Ag(NP) distribution within the titanium dioxide. The average size of the nanoparticles was in the range of 5-10 nm. Moreover, the particles are dispersed and not aggregated on the surface. On the other hand, the powder Clay/Ag/TiO_2(T) showed a unique cubical formation of Ag(NP). The cubical particles are uniformly distributed within the titania network. Further, the average size of the nanoparticles was in the range of 10-15 nm. It was reported previously that the grains of TiO_2 possess a spherical shape in the nanocomposite of silver-modified TiO_2/Halloysite. The size of the TiO_2 was ranged between 12 to 16 nm. Furthermore, the TiO_2 was aggregated on the surface of support media (Panagiotaras et al., 2014).

The TEM-EDX spectra for both the solids *viz.*, Clay/Ag/TiO_2 and Clay/Ag/TiO_2(T) are shown in Figure 3.1.2(ii)(c) and (d). Spectra clearly showed the

presence of Si, Al, O, and Ag elements in both materials. The results confirmed again that the Ag(NP) are decorated with the composite materials (Clay/TiO_2).

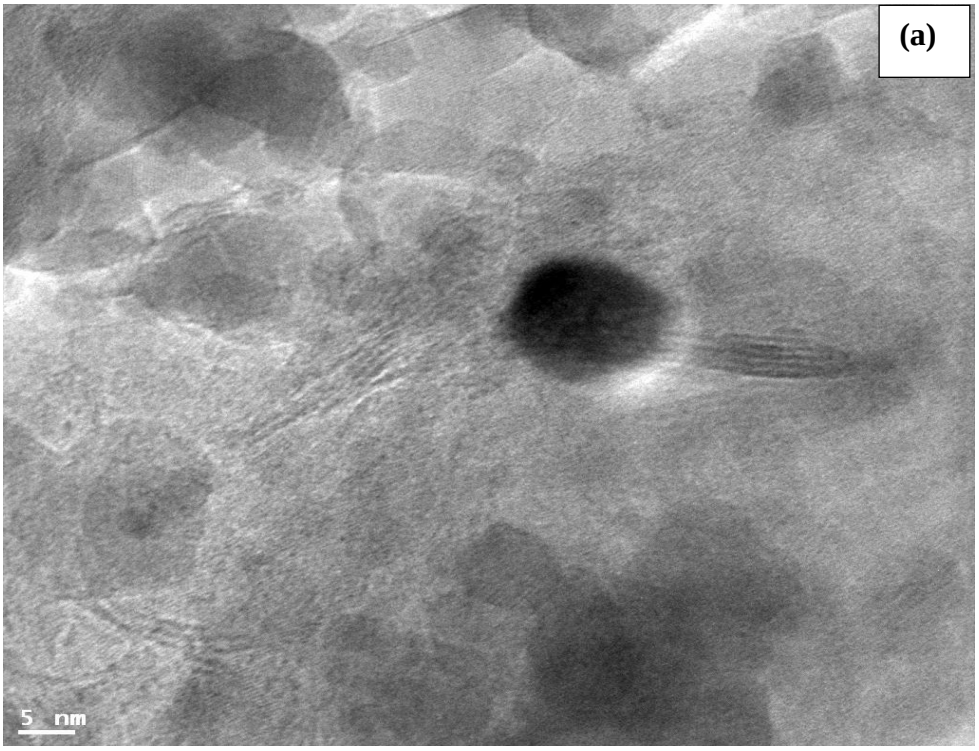

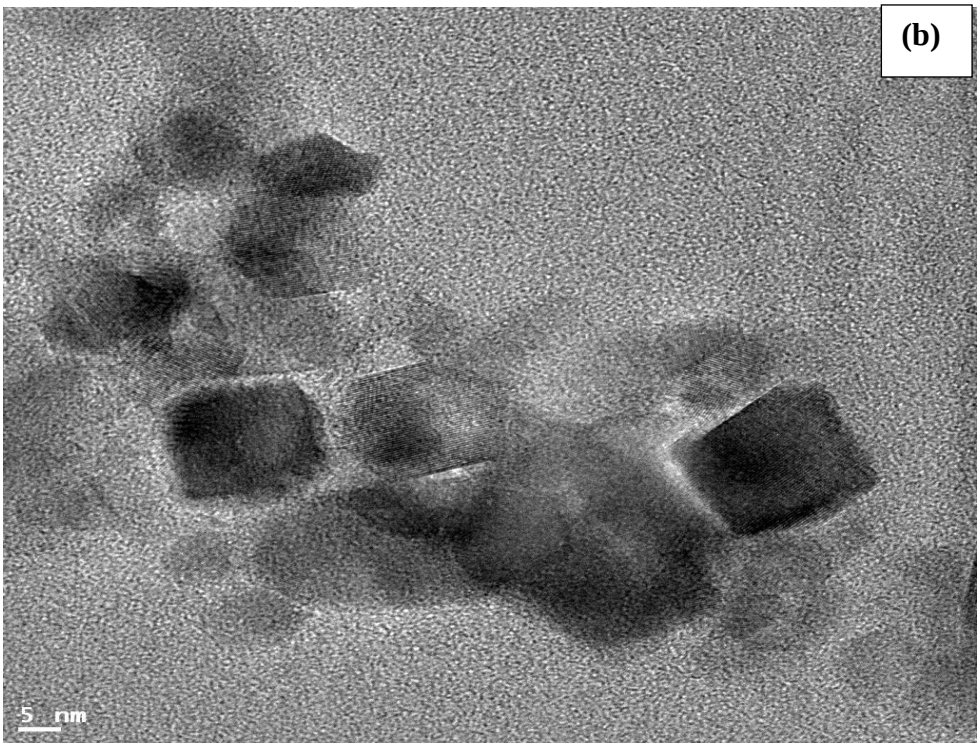

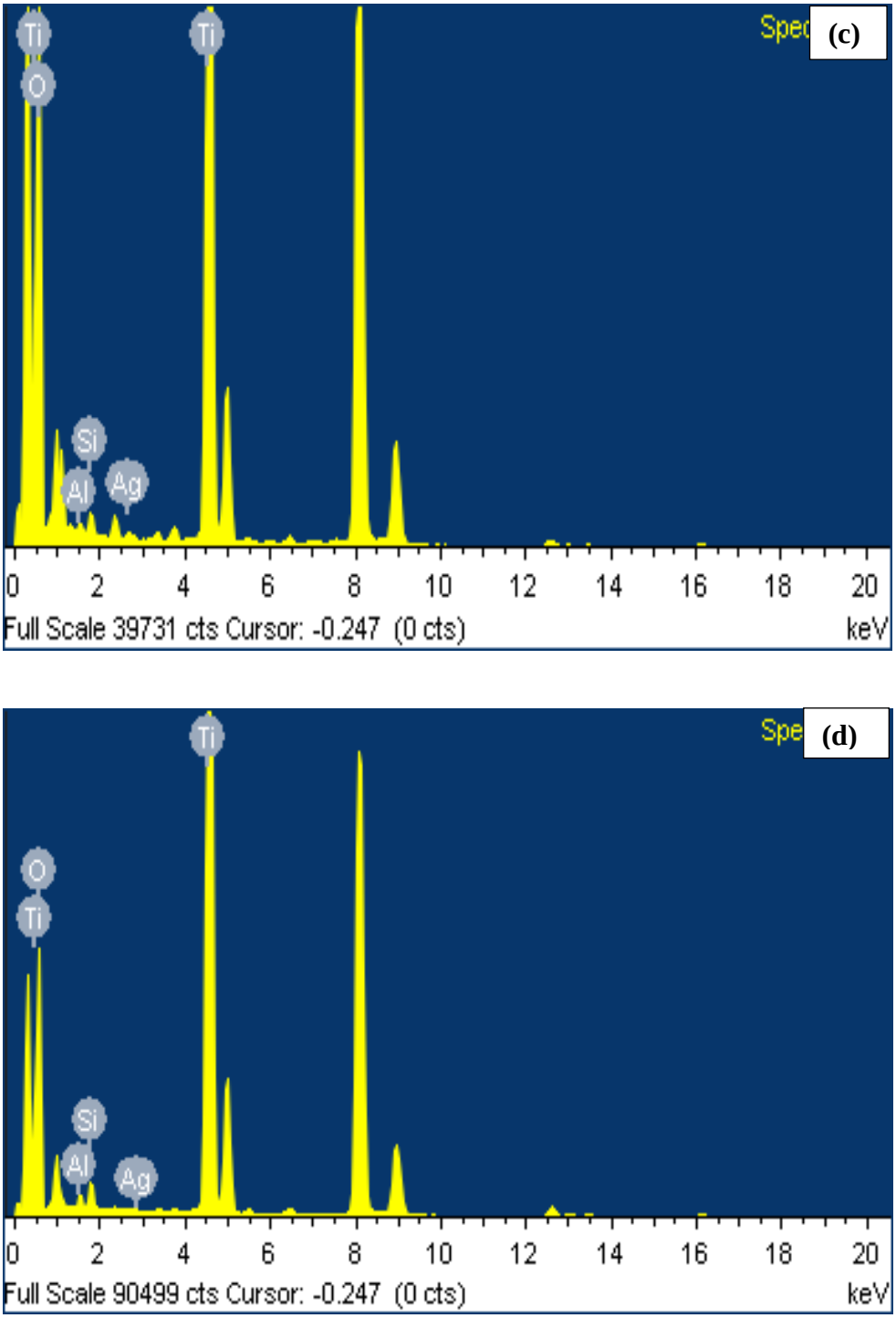

Figure 3.1.2(ii): Transmission electron microscopic images of (a) Clay/Ag/TiO_2 and (b) Clay/Ag/TiO_2(T) nanocomposite powders; TEM-EDX spectra for (c) Clay/Ag/TiO_2 and (d) Clay/Ag/TiO_2(T) nanocomposite.

In Figure 3.1.2(iii)(a) and (b), TEM pictures of nanocomposites Clay/Au/TiO_2 and Clay/Au/TiO_2(T) are shown. The TEM images clearly indicates that the cubical Au(NP) is distributed within the titania network and the average particle size is from 10 to 20 nm. For both the samples, it is also observed that fine disordered and heterogeneous surface structures are obtained. It was reported previously that Au/TiO_2/Au nanocomposite has TiO_2 nanosheets middle layer thickness of about 5 nm and was successfully employed as a plasmonic coupling photocatalyst (Wang et al., 2012). Furthermore, the heterogeneous nanocomposite Au^0(NPs)/TiO_2 with a particle size from 20-25 nm was obtained using the sol-gel method (Lalliansanga et al., 2020). The TEM-EDX of Clay/Au/TiO_2 and Clay/Au/TiO_2(T) were obtained and the results are depicted in Figure 3.1.2(iii)(c) and (d). Figure shows that Au^0(NP) are finely distributed within the titania network.

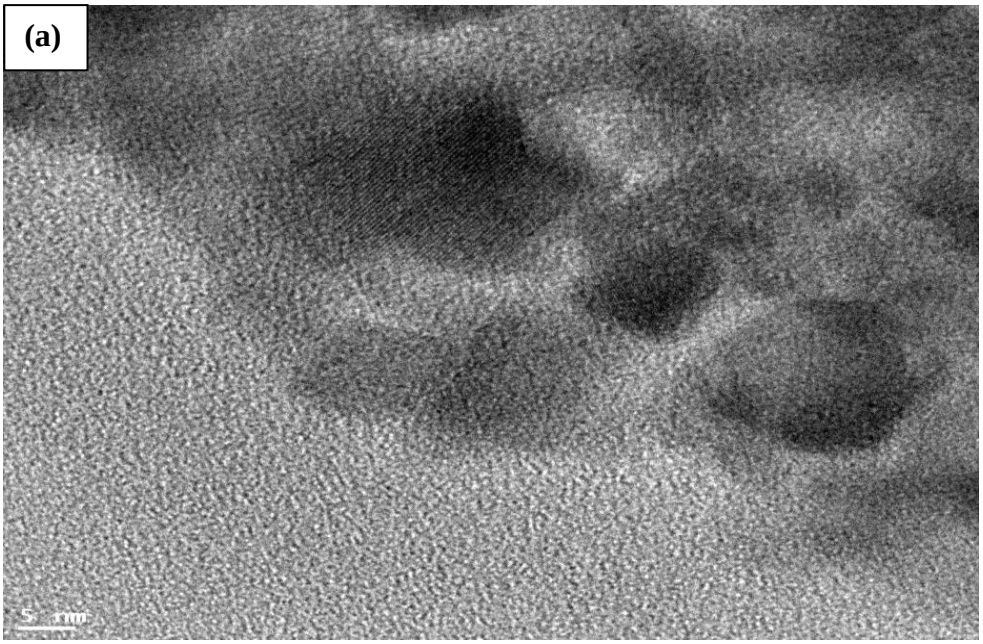

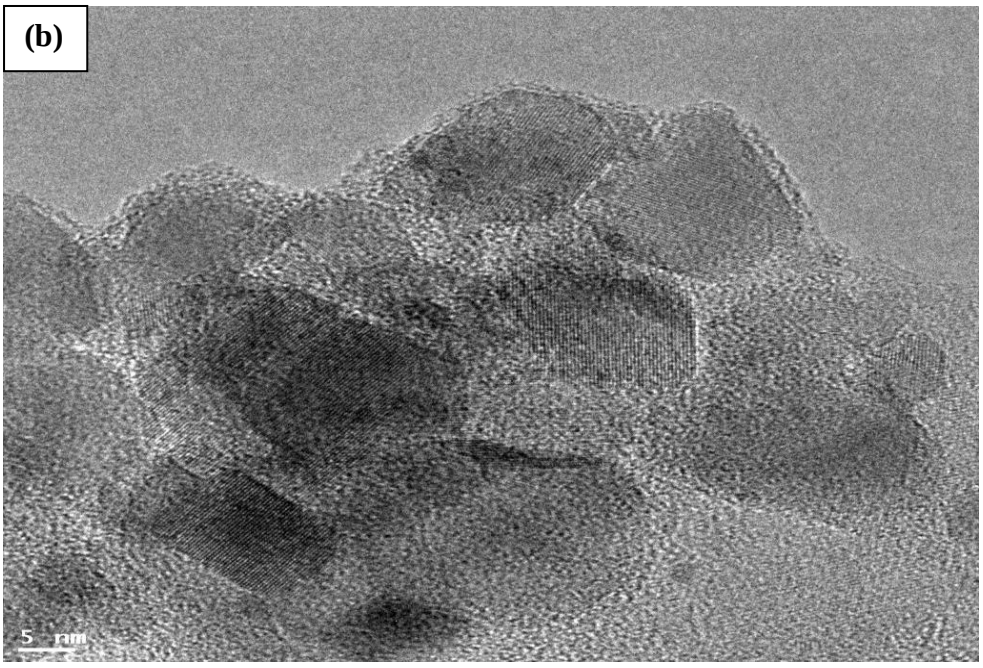
(b)
5 nm

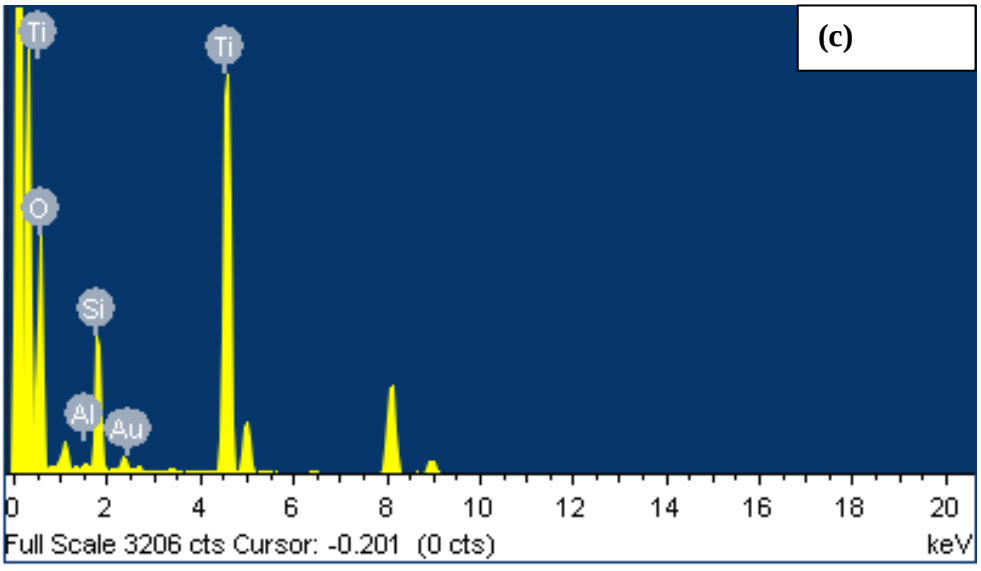
(c)
Ti
Ti
O
Si
Al
Au
0
2
4
6
8
10
12
14
16
18
20
Full Scale 3206 cts Cursor: -0.201 (0 cts)
keV

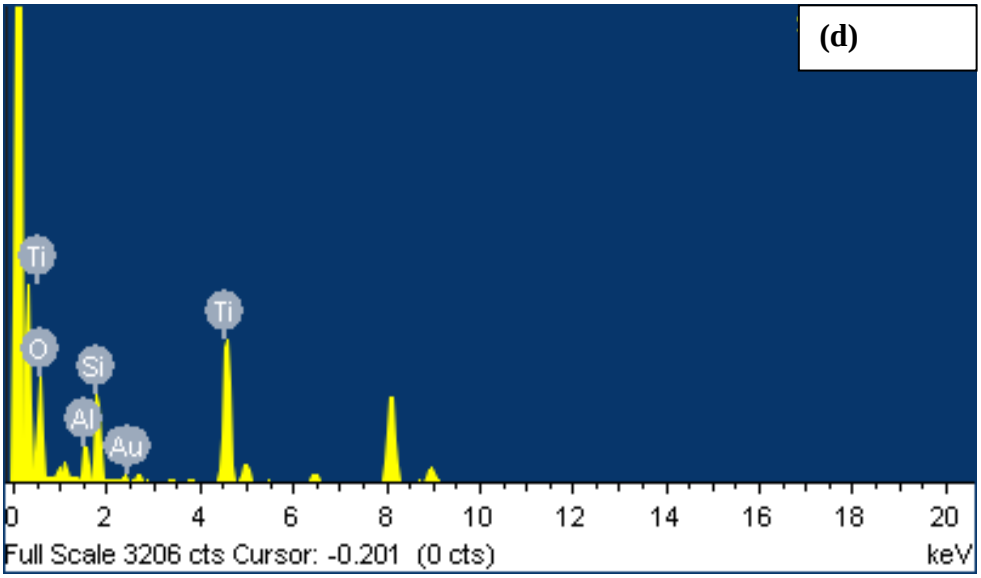

Figure 3.1.2(iii): Transmission electron microscopic images of (a) Clay/Au/TiO_2 and (b) Clay/Au/TiO_2(T) nanocomposite powders; TEM-EDX spectra for (c) Clay/Au/TiO_2 and (d) Clay/Au/TiO_2(T) nanocomposite.

The TEM-elemental mapping of Clay/Au/TiO_2 and Clay/Au/TiO_2(T) are displayed in Figure 3.1.2(iv). It is worth observing that the clay is distributed uniformly as Si and Al and provides a good support material. Further, the titania is dispersed on the support material. The O atom is intimately bonded with the Ti, which confirmed the formation of the Ti-O bond in both the materials, possibly forming the TiO_2. Further, the Au(NPs) are decorated within the titania network and uniformly disseminated. Moreover, the spatial and orderly distribution of Au(NPs) indicated that the Au(NPs) are not aggregated on the surface.

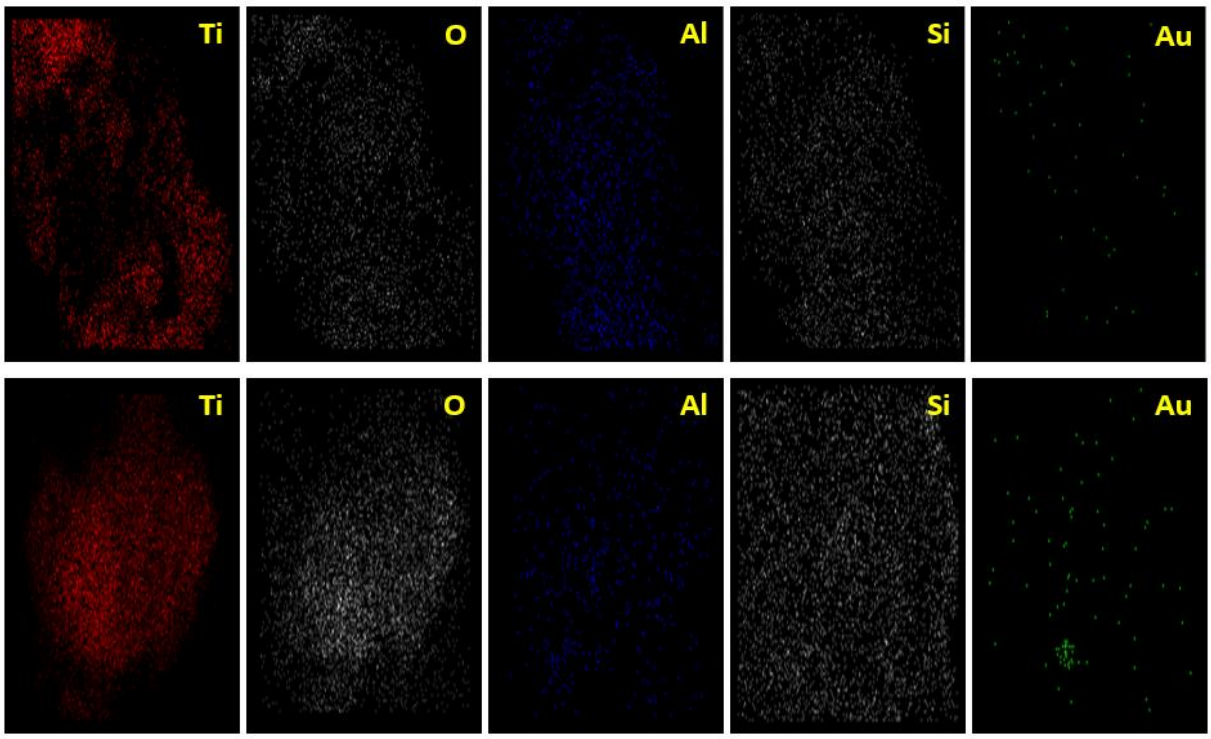

Figure 3.1.2(iv): TEM-elemental mapping of the nanocomposites Clay/Au/TiO_2(T) (upper side) and Clay/Au/TiO_2 (Lower side).

3.1.3. Atomic Force Microscopic (AFM) Analysis

The AFM image of Ag^0(NP)/TiO_2 nanocomposite thin film is shown as in Figure 3.1.3(i). AFM image infers that the surface of thin film of photocatalyst is highly uneven or heterogeneous in nature and the surface is possessed with small-sized pillars of titanium dioxide having maximum height of *Ca*. 350 nm. Further, the root mean square roughness (R_q) and mean roughness (R_a) of thin film is 16.952 nm and 12.250 nm, respectively.

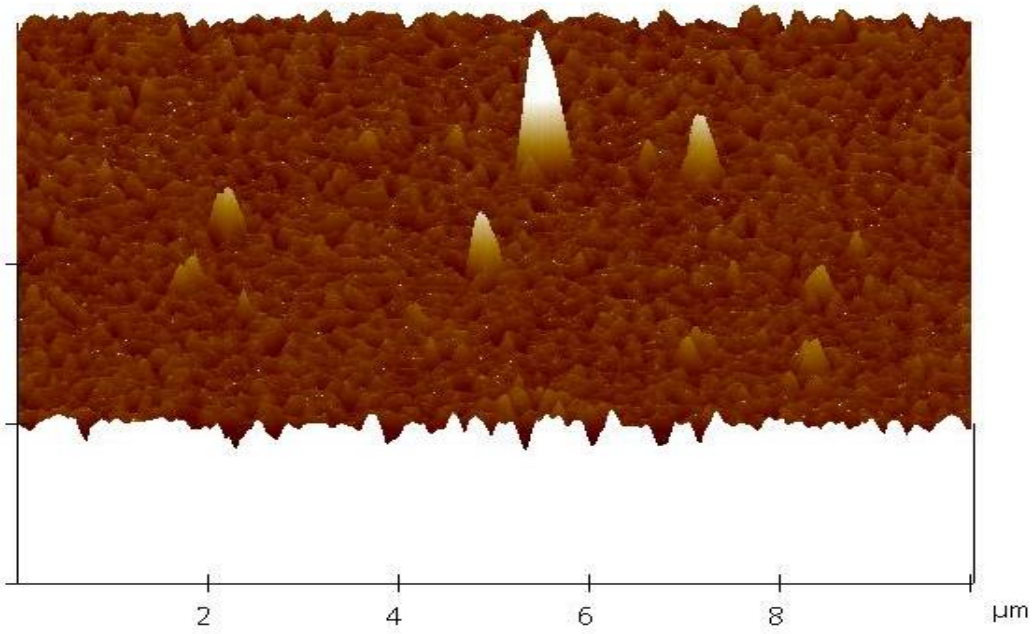

Figure 3.1.3(i): Atomic Force Microscopic (AFM) image of Ag^0(NP)/TiO_2 nanocomposite thin film.

The three-dimensional atomic force microscopic images of the Clay/Ag/TiO_2 and Clay/Ag/TiO_2(T) thin-films are illustrated in Figure 3.1.3(ii) (a) and (b) respectively. Both the materials showed heterogeneous surface structure and forming pillars on the substrate. Relatively, the Clay/Ag/TiO_2 surface showed a smoother surface compared to the templated nanocomposite material Clay/Ag/TiO_2(T). Furthermore, the mean roughness (R_a) and the root mean square roughness (R_q) of Clay/Ag/TiO_2 samples were found to be 6.879 nm and 9.012 nm, respectively. On the other hand, the Clay/Ag/TiO_2(T) thin-film showed the R_a and R_q, respectively 52.831 nm and 100.102 nm. These results evidenced that nanocomposite template synthesis enabled the enhancement of the surface heterogeneity.

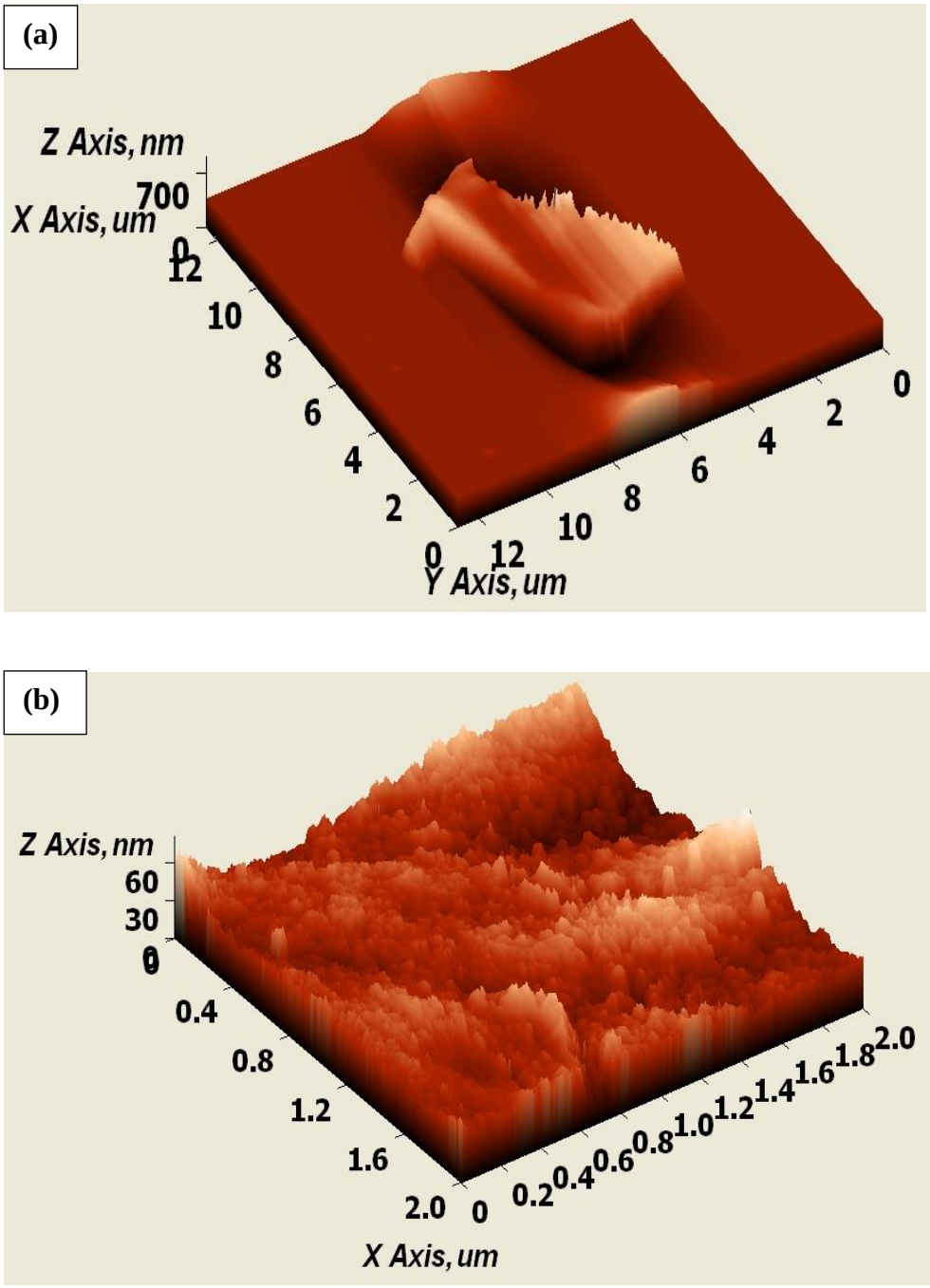

Figure 3.1.3(ii): Atomic force microscopic images of (a) Clay/Ag/TiO_2; and (b) Clay/Ag/TiO_2(T)

The 3D-AFM images of nanocomposite Clay/Au/TiO_2 and Clay/Au/TiO_2(T) are depicted in Figure 3.1.3(iii) (a) and (b). Both samples showed heterogeneous and disordered structures on their respective surfaces. Moreover, the Clay/Au/TiO_2 nanocomposite thin film showed a more dense surface structure. The template

synthesis enabled to create the dense titania network on the substrate surface. The TiO_2 pillared on the substrate surface and the pillar height is 8 and 4 nm, for the Clay/Au/TiO_2(T) and Clay/Au/TiO_2, respectively. The mean roughness (R_a) and the root mean square roughness (R_q) of Clay/Au/TiO_2(T) were obtained to be 1.165 nm and 1.454 nm, respectively, and 0.386 nm and 0.572 nm, respectively for Clay/Au/TiO_2. This inferred that the template synthetic process allowed for greater heterogeneity. The non-templated TiO_2 nanocomposite, on the other hand, has a relatively smoother surface compared to the templated TiO_2.

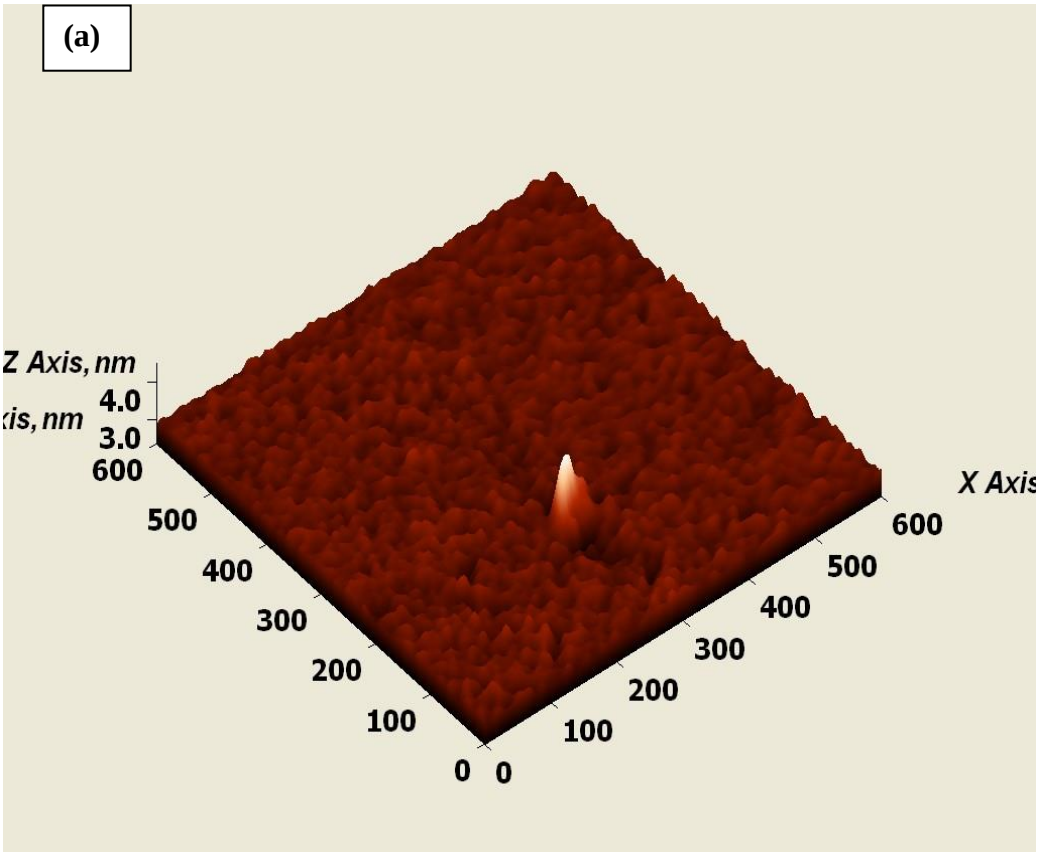

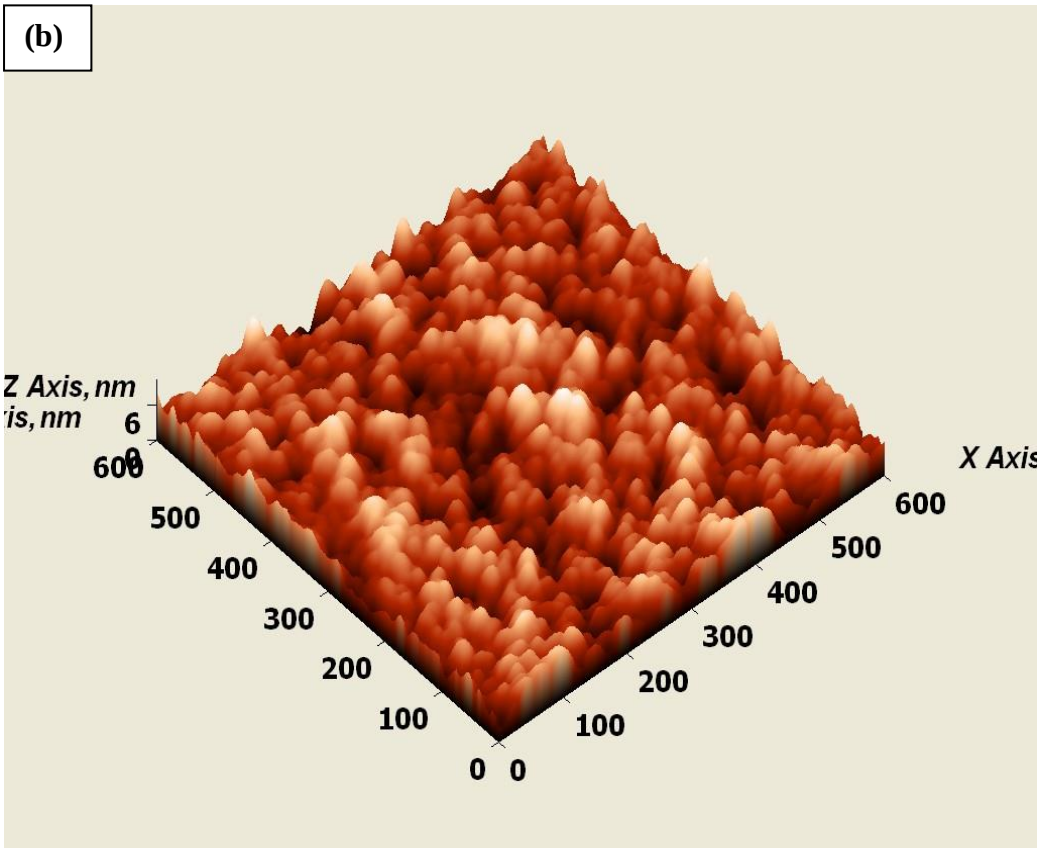

Figure 3.1.3(iii): Atomic force microscopic images of (a) Clay/Au/TiO_2 and (b) Clay/Au/TiO_2(T).

3.1.4. X-ray Diffraction (XRD) Analysis

XRD patterns of the nanocomposite powders revealed that both materials have crystalline structure (Fig. 3.1.4(i)). Both powders have distinct and characteristic diffraction peaks at the 2θ values of 25.42°, 37.90°, 48.12°, 54.02°, 55.14°, and 62.61° which confirmed the predominant occurrence of anatase phase of TiO_2 (JCPDS Card No.: 21-1272). Relatively less intensive diffraction peaks of Ag(NP) were observed at the 2θ values of 38.39°, 44.45°, 64.37°, and 77.53° referring to the (111), (200), (220), and (311) planes (JCPDS Card No.: 01-087-0719). However, these diffraction peaks are not predominant due to the low content of silver nanoparticles in the materials and also the peaks are merged with the predominant peaks of TiO_2 or bentonite.

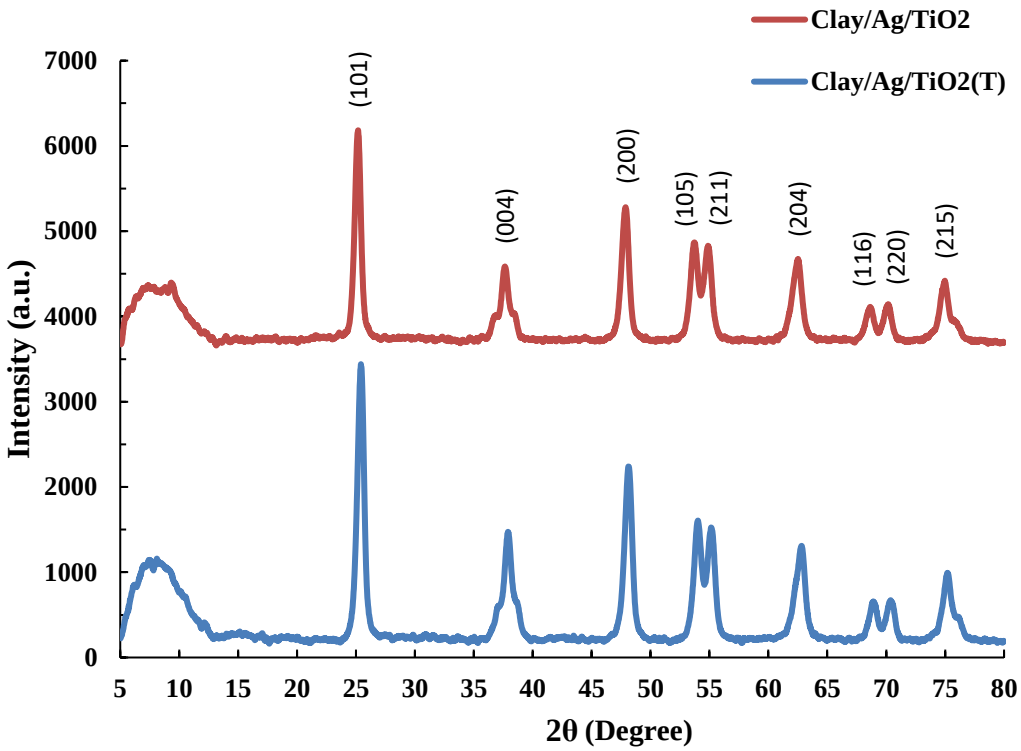

Figure 3.1.4.(i): X-ray diffraction pattern for Clay/Ag/TiO_2 and Clay/Ag/TiO_2(T) nanocomposite powders

XRD patterns of the two nanocomposite materials, Clay/Au/TiO_2 and Clay/Au/TiO_2(T) are given in Figure 3.1.4.(ii). TiO_2 is predominantly present in the anatase mineral phase in both the materials. The distinct peaks at the 2θ values of 25.42, 37.90, 48.12, 54.02, 55.14, and 62.61 are due to the anatase phase of TiO_2 (JCPDS Card No. 21-1272). On the other hand, the Au(NPs) Peaks are not quite visible in the spectra. Hence, the diffraction intensity was enhanced, as shown in figure 3.1.4.(ii) (Inset). It is apparent from the XRD pattern that the distinct diffraction pattern of Au(NPs) is obtained at the 2θ values of 38.34, 44.25, 64.34, and 77.32 (JCPDS Card No. 04-0784). This again confirmed the presence of Au^0(NP) in the solid samples.

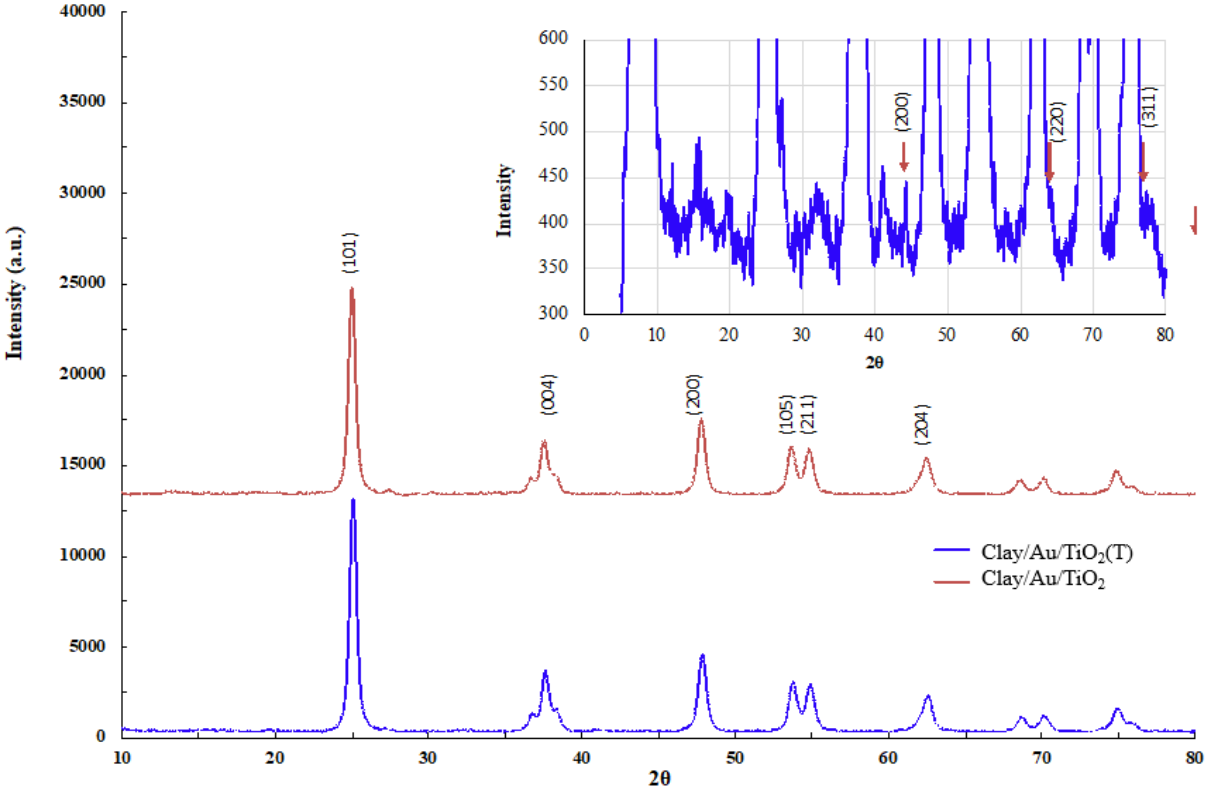

Figure 3.1.4.(ii): X-ray diffraction pattern for Clay/Au/TiO_2 and Clay/Au/TiO_2(T) nanocomposite powders [Inset: the expanded XRD pattern of Clay/Au/TiO_2(T) solid].

3.1.5. Brunauer–Emmett–Teller (BET) Analysis

The N_2 adsorption/desorption data are utilized to demonstrate the physical characteristics of Clay/Ag/TiO_2, and Clay/Ag/TiO_2(T) solids along with the determination of pore volume, pore size and specific surface area. Figure 3.1.5.(i) depicts the N_2 adsorption/desorption results. The results indicated that both the solids showed H1 type hysteresis loops, which stated the porous nature of solid and solid composed with a regular array of uniform spheres (Sing, 1984). Further, Table 3.1.5.(i) included the pore volume, pore size and specific surface area of the two materials. It revealed that both solids Clay/Ag/TiO_2 and Clay/Ag/TiO_2(T) possessed mesoporous structure. The sample Clay/Ag/TiO_2(T) showed relatively enhanced specific surface area as compared to the non-template Clay/Ag/TiO_2 solid. These results are consistent with the results obtained by the SEM and TEM analyses.

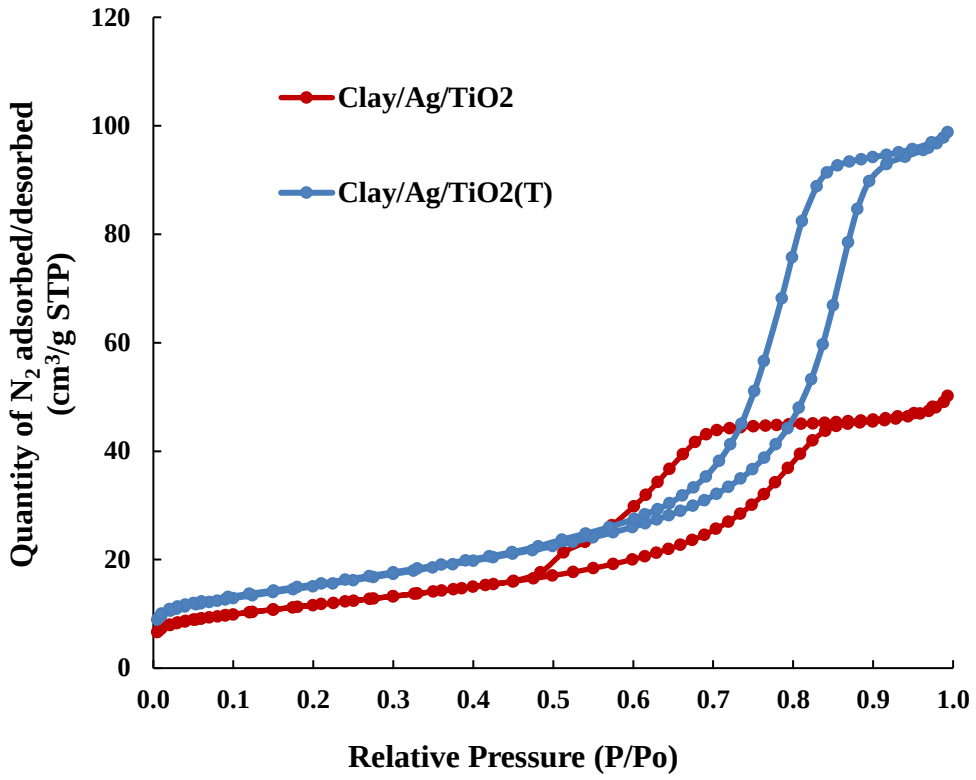

Figure 3.1.5.(i): (a) Nitrogen adsorption-desorption isotherms of Clay/Ag/TiO_2 and Clay/Ag/TiO_2(T) solids

Table 3.1.5.(i): BET pore size, pore volume and specific surface area of the Clay/Ag/TiO_2 and Clay/Ag/TiO_2(T) solids.

Sample	BJH adsorption pore size (nm)	BJH adsorption pore volume (cm^3/g)	BET specific surface area (m^2/g)
Clay/Ag/TiO_2	7.561	0.077	41.413
Clay/Ag/TiO_2(T)	11.438	0.153	53.951

Similarly, figure 3.1.5.(ii) shows the BET analysis results for Clay/Au/TiO_2 and Clay/Au/TiO_2(T). The pore sizes, pore volume and specific surface area of the nanocomposite materials were determined using N_2 adsorption/desorption data and the findings are shown in Table 3.1.5.(ii). The adsorption/desorption isotherm curves for Clay/Au/TiO_2(T) followed hysteresis loops of H1 type, which revealed that the material is highly porous and consists of the orderly distribution of even spheres. Alternatively, the Clay/Au/TiO_2 exhibited a hysteresis loop of H2 type, which revealed

that the materials' pores are associated with slender mouths with an even channel-like network (Sing, 1984). The H2 type loop indicated the particles were non-uniform shaped and sized (Sangiorgi et al., 2017). Moreover, the BET surface area of Clay/Au/TiO_2(T) is almost double compared to Clay/Au/TiO_2. The template synthesis enabled to enhance the surface area of the solid.

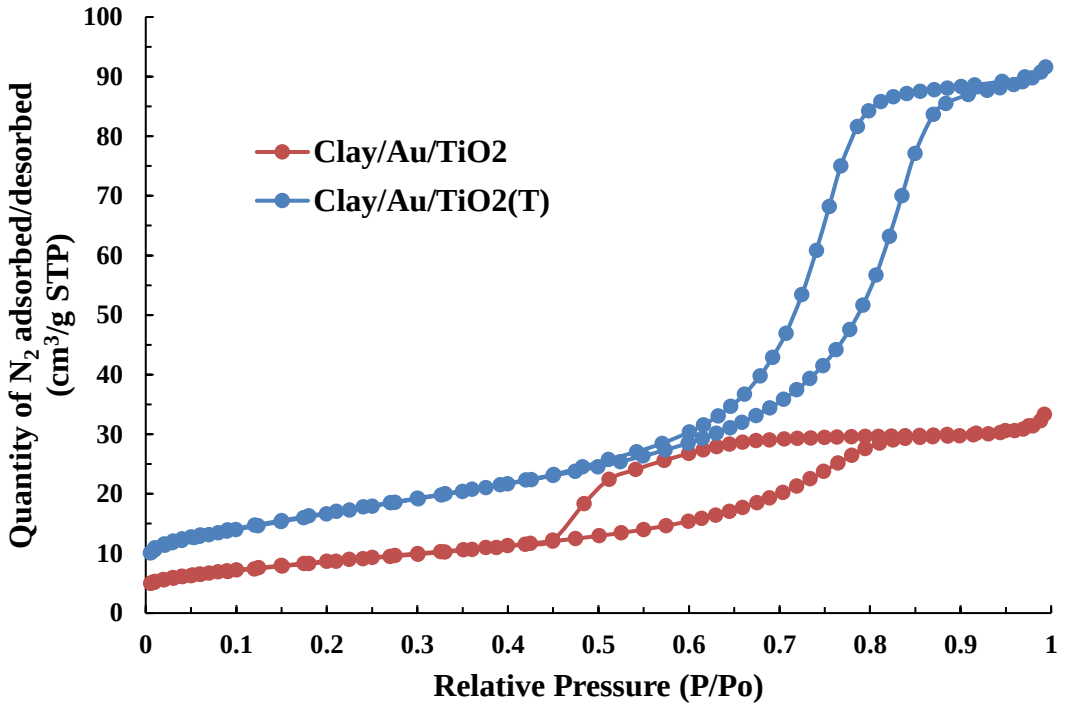

Figure 3.1.5.(ii): Nitrogen adsorption-desorption isotherms of Clay/Au/TiO_2 and Clay/Au/TiO_2(T) solids

Table 3.1.5.(ii): BET pore size, pore volume and specific surface area of Clay/Au/TiO_2 and Clay/Au/TiO_2(T) solids

Sample	BJH adsorption pore size (nm)	BJH adsorption pore volume (cm^3/g)	BET specific surface area (m^2/g)
Clay/Au/TiO_2(T)	94.88	0.142	60.12
Clay/Au/TiO_2	66.08	0.052	31.42

3.1.6. Diffuse Reflectance Spectroscopy (DRS) Analysis

Spectroscopic measurement of diffuse reflectance in UV-Vis spectral range is a standard technique to determine powder samples' bandgap (Pal et al., 2012). Thus UV-Vis spectrophotometer was used to produce diffuse reflectance spectra (DRS) for powder photocatalysts. The solid band gap energy was estimated by obtaining the adsorption coefficient from diffuse reflectance data utilizing the Kubelka-Munk equation (Equation. 3.1.). Using the Kubelka-Munk equation the reflectance was converted into a Kubelka-Munk function (equivalent to the absorption coefficient), F(R) (Hamrouni et al., 2020; Sangiorgi et al., 2017). The values of F(R) are directly proportional to the absorbance. The band gap energy of the materials can be found using Tauc plot i.e. by extrapolating the linear portion of a graph of $(F(R)xh\nu)^{1/2}$ vs the energy of photon of light.

$$F(R) = (1 - R)^2 / 2R \qquad \ldots(3.1.)$$

where R is the reflectance of a given sample concerning a reference at each wavelength.

The band gap energies for TiO_2 and Ag^0(NPs)/TiO_2 were compared and were determined to be 3.28 and 2.9 eV respectively. This clearly indicates that the presence of Ag^0(NPs) greatly reduced the band gap energy of the Ag^0(NPs)/TiO_2 nanocomposite material. The resulting Tauc plot was depicted in Figure 3.1.6.(i).

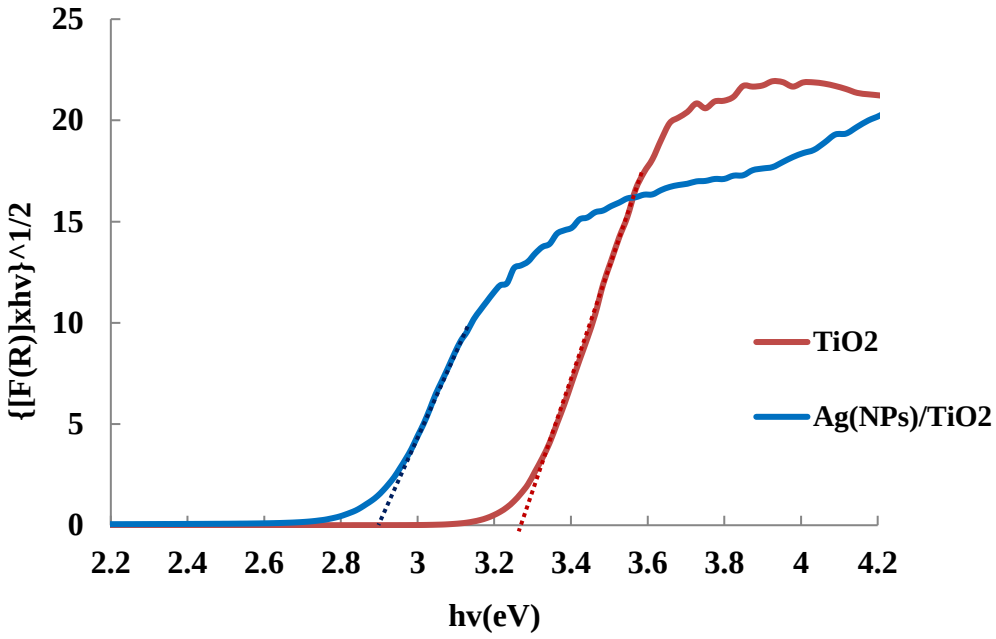

Figure 3.1.6.(i): Tauc plots for TiO_2 and Ag^0(NPs)/TiO_2.

Diffuse reflectance spectra (DRS) of the Clay/Ag/TiO_2 and Clay/Ag/TiO_2(T) solids were also obtained using the UV-Visible spectrophotometer. Further, using *Tauc's* relation, plots were obtained between the hν *vs.* $(F(R)xh\nu)^{1/2}$ as depicted in Figure 3.1.6.(ii) (Sangiorgi et al., 2017). The intermediate band gap energies (E_g) were obtained by extrapolating the flat portion of the plot to its zero value. The band gap energies of bare TiO_2, Clay/Ag/TiO_2, and Clay/Ag/TiO_2(T) were determined to be 3.28, 2.86, and 2.88 eV, respectively. This specifies that the presence of Clay/Ag(NP) significantly lowered the energy of the bandgap of the nanocomposite material. The low bandgap energy of nanocomposite is helpful in the visible-light-induced photocatalytic degradation processes (Mugunthan et al., 2018).

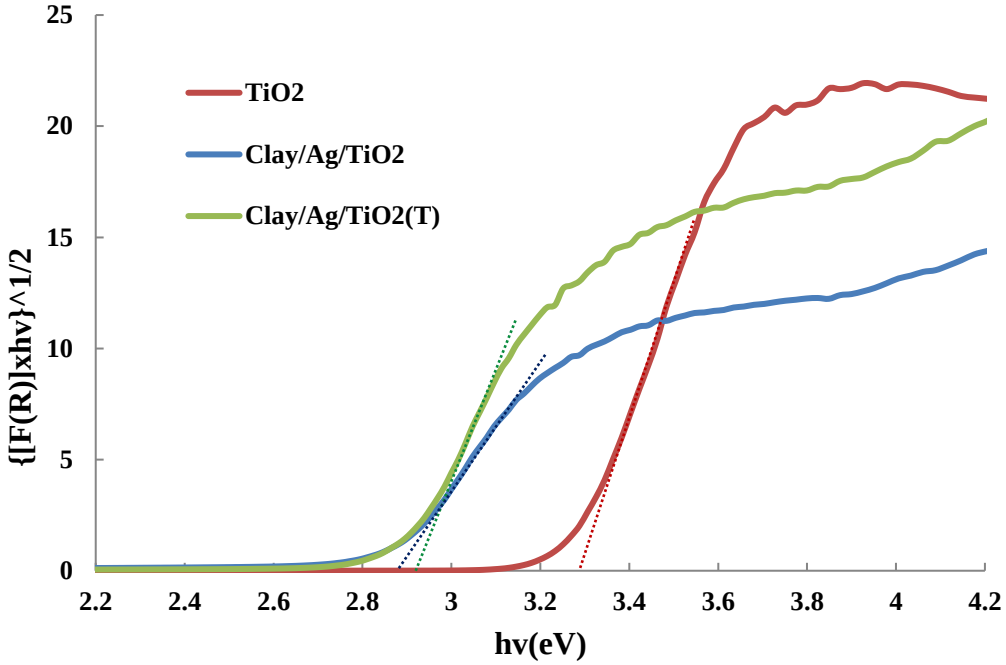

Figure 3.1.6.(ii): Tauc plots of TiO_2, Clay/Ag/TiO_2 and Clay/Ag/TiO_2(T) solids.

Further, Diffuse reflectance spectra (DRS) of the Clay/Au/TiO_2 and Clay/Au/TiO_2(T) solids are also obtained using the UV-Visible spectrophotometer. The absorption spectra of TiO_2, Clay/Au/TiO_2 and Clay/Au/TiO_2(T) are given in Figure 3.1.6.(iii). The energy of the band gap of the bare TiO_2, Clay/Au/TiO_2(T) and Clay/Au/TiO_2 solids were determined to be 3.24, 2.85, and 2.88 eV, respectively. This indicated that the occurrence of Au nanoparticles significantly lowered the band gap energy of these materials. Ben Saber et al. reported that Au@TiO_2/reduced graphene oxide (rGO) obtained by the solvothermal process possessed the band gap energy of 3.43eV (Ben Saber et al., 2021). Similarly, Au/TiO_2 (NPs) were obtained using a hydrothermal process. The materials have band gap energy within 3.1 – 3.15 eV as varied with the weight percentage of Au and Ti. The materials are efficient in the photocatalytic degradation of resorcinol under UV-A irradiation (Al-Hajji et al., 2020).

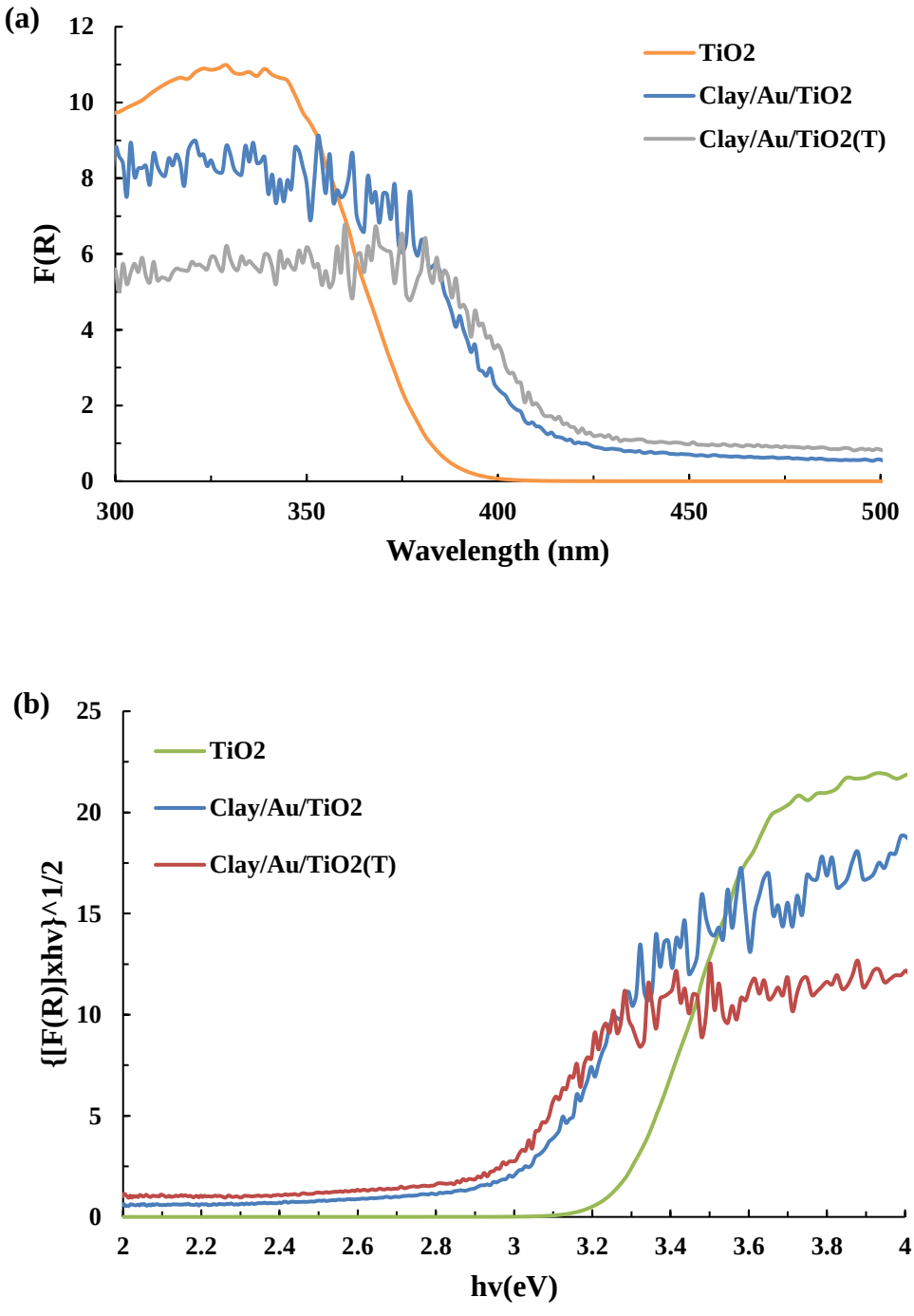

Figure 3.1.6.(iii): a) UV-vis absorption spectra for TiO_2, Clay/Au/TiO_2 and Clay/Au/TiO_2(T) b) Tauc plot for TiO_2, Clay/Au/TiO_2 and Clay/Au/TiO_2(T)

3.2. Photocatalytic Degradation of Micropollutants and Dyes Using Thin Film Photocatalysts (Mordant Orange 1 by Ag^0(NP)/TiO_2; Tetracycline, Sulfamethazine and Bisphenol-A by Clay/Ag/TiO_2 and Clay/Ag/TiO_2(T); Rhodamine B and Rhodamine 6G by Clay/Au/TiO_2 and Clay/Au/TiO_2(T)).

3.2.1. Batch Reactor Studies

3.2.1.1. Effect of pH in the Photocatalytic Degradation of Mordant Orange 1 (MO1)

Effect of pH is a useful parameter that demonstrates the mechanism of photocatalytic elimination of pollutant molecules. This is mainly due to the pH dependence transitions in pollutant species as well as the surface properties of active sites of photocatalysts (Lalhriatpuia et al., 2015). Therefore, the pH influences significantly the overall efficiency of the photocatalyst in the degradation of pollutant molecules (Zucca et al., 2008). Photocatalytic elimination of MO1 is carried out for a wide range of pH **(**4.0-10.0) using Ag^0(NP)/TiO_2 and results are depicted in Figure 3.2.1.1. The percentage removal of the MO1 was obtained after the 2 hrs irradiation. Results clearly showed that the decrease in pH i.e., pH 10.0 to 4.0 has caused an increase in elimination of MO1. Quantitatively, with a decrease in solution pH from 10.0 to 4.0, the corresponding increase in percentage removal of MO1 is from 29.15 to 61.3% (for UV-A) and 16.65 to 35.81% (for LED light) using nanocomposite thin film photocatalyst. The MO1 molecule contains two dissociable hydrogens one from the carboxylic group and second is due to the phenolic group which are having the pk_a values of 5.0 and 11.0 (Nazar et al., 2010). Therefore, within the pH region 6.0-10.0, the MO1 molecule usually exists as a mono-anionic species. However, the phenolic and carboxylic groups forming the hydrogen bonding result in a non-ionic species. Hence, in this pH range the MO1 molecule exists in equilibrium between the mono-anionic species (*Cf* Figure 3.2.1.1 (Inset)) (Nazar et al., 2010). Further, pH >10.0, both the protons of MO1 molecule are dissociated hence, the mono-anionic MO1 molecule becomes di-anionic species. Thus, the net charge of the MO1 species carries extra negative charge at and above pH 10.0. On the other hand, the pH_{pzc} of nanocomposite was obtained 6.8. This infers that the thin film possesses net positive charge pH <6.8 whereas its surface possesses negative charges pH >6.8. These studies showed that

increasing the pH gradually enhances the net negative charges both on the nanocomposite surface and MO1 species. This eventually caused an enhanced coulombic repulsion between the MO1 species and nanocomposite surface, which resulted in gradual decrease of MO1 removal at pH>6.0 (pH 6~10). Photocatalytic removal of Alizarin Yellow using the catalyst Au^0(NPs)/TiO_2 thin film showed similar removal behaviour (Lalliansanga et al., 2019). Copper deposited TiO_2 nanoparticles (Cu_2O-CuO/TiO_2) prepared by using a combination of impregnation and precipitation-deposition method utilized in the pH dependent photocatalytic degradation of commercial dyes such as Reactive Blue 49 (RB 49), Reactive Red 24 (RR 24) and Reactive Yellow 160 (RY 160) under UV irradiation (Ajmal et al., 2016). The nanocomposite catalyst greatly favoured the elimination of MO1 in aqueous media by UV-A or LED lights. Further, compared to the UV-A and LED light illumination, the UV-A light showed relatively higher degradation of MO1 throughout the studied pH.

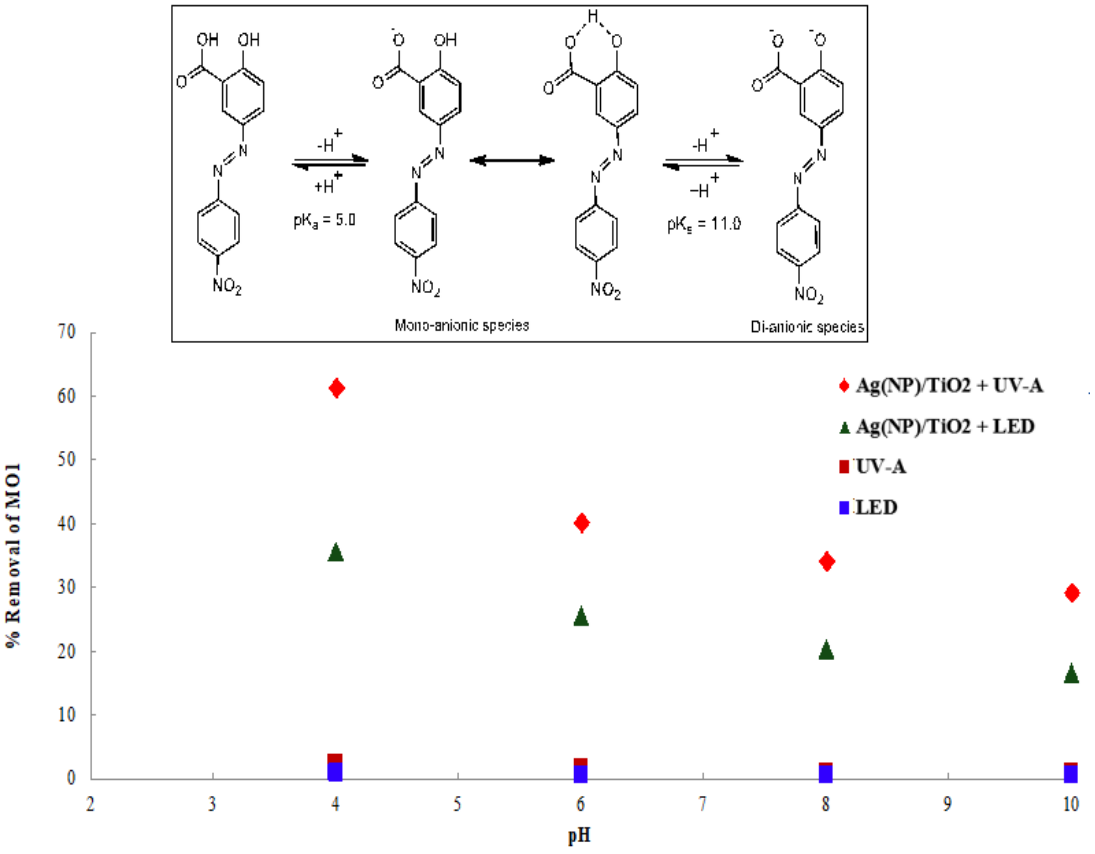

Figure 3.2.1.1: Effect of pH in the photocatalytic degradation of MO1 (Initial concentration of MO1: 5.0 mg/L) and the Inset, equilibrium of MO1 as function of pH.

3.2.1.2. Effect of pH in the Photocatalytic Degradation of Tetracycline (TC) and Sulfamethazine (SMZ)

pH dependence degradation of pollutant molecules greatly demonstrates the degradation mechanisms of contaminants at the surface of photocatalyst. The sorption of pollutants on the surface of the thin-film catalyst showed a significant impact on photocatalytic activity. The sorption process is strongly determined by the pH of pollutant solutions (Chong et al., 2010). Therefore, the pH-dependent degradation of TC and SMZ was carried out at a wide range of pH i.e., pH 4.0 to 10.0 using Clay/Ag/TiO_2 and Clay/Ag/TiO_2(T). The pollutant samples were treated for 2 hrs and 3 hrs respectively for TC and SMZ under LED (Visible Light) and UV-A light using the thin-film photocatalysts. The results are shown in Figure 3.2.1.2. Initial TC and SMZ concentrations were taken 5.0 mg/L. In general, oxidation of TC was favoured at higher pH (pH 10.0), while in the case of SMZ, the oxidation was favoured at pH 6.0, as shown in Figure 3.2.1.2. More specifically, in the case of TC, increasing the solution pH from 4.0 to 10.0 increased the percentage elimination of TC from 32.4 % to 50.4 % under LED (visible light) and 54.0 % to 72.4 % under UV-A light using Clay/Ag/TiO_2(T). On the other hand, the SMZ removal efficiency was increased from 28.46 % to 31.74%, with the increase in pH from 4.0 to 6.0 and a further increase in pH from pH 6.0 to 10.0 caused to decrease the removal efficiency of SMZ from 31.7 to 21.5% under LED (visible light) using the Clay/Ag/TiO_2(T) solid. Similarly, under the UV-A irradiation, the removal efficiency of SMZ was increased from 54.3% to 58.3 % with an increase in pH from 4.0 to 6.0. However, further increase in the pH from 6.0 to 10.0 had caused the removal efficiency to decrease from 58.3 to 42.7% using the Clay/Ag/TiO_2(T) solid.

In addition, the photolytic reaction was carried out in the absence of a photocatalyst by irradiating the TC and SMZ for 2 hrs and 3 hrs, respectively under LED (visible light) and UV-A light sources. The removal efficiency of TC and SMZ

was recorded as 1.1% (pH 10.0) and 1.1% (pH 6.0) respectively under LED (visible light). Similarly, under UV-A irradiation, the removal efficiency of TC and SMZ was found to be 26.3 % (pH 10.0) and 15.3 % (pH 6.0), respectively. The results indicated that minimal removal efficiency was obtained in removing TC and SMZ under the photolytic process. However, a significant increase in removal efficiency was recorded in the photocatalytic process. This inferred the potential use of catalyst in the degradation of recalcitrant water contaminants efficiently.

The photocatalytic degradation of micro-pollutants is highly influenced by the surface properties of the catalyst and its interaction with the micro-pollutants. The pH_{PZC} of powder Clay/Ag/TiO_2 and Clay/Ag/TiO_2(T) were determined to be 6.3. Thus in acidic conditions (pH<6.3), the catalyst surface carries a net positive charge, whereas in pH>6.3, the catalyst surface possesses net negative charge. On the other hand, the pollutant molecule TC is a triprotic compound, which means it has three dissociable hydrogens with dissociation constant values of 3.3, 7.7, and 9.7 correspond to the pk_a^1, pk_a^2, and pk_a^3, respectively and the percentage species distribution at varied pH is shown in Figure 3.2.1.2(a)(Inset)) (Liu et al., 2012) . Furthermore, due to the deprotonation from the phenolic diketone moiety, TC existed to its zwitterion (TCH_2^0 or TCH_2^{0+-}) configuration within the pH 3.3–7.7. At pH>7.7, TC molecules exist in anionic species (TCH^- or $TCH^{+\ -\ -}$) by deprotonation reaction. Therefore, with the deprotonation of the third proton from the tri-carbonyl group and the phenolic diketone group at pH>9.7, the TC molecule existed as a di-anionic species (Kang et al., 2010). Hence, the thin-film catalyst and TC molecules carried a net negative charge at higher pH values. This possibly repels the TC molecule at the catalyst surface, hence; relatively less sorption is expected. However, the increase in percentage degradation of TC at higher pH values is primarily due to the fact that the TC molecule showed higher affinity towards the catalyst surface and enabled to enhance the removal efficiency of TC in the photocatalytic process. Similar results were obtained previously, where TC was treated using Ag^0(NP)/TiO_2 nanocomposite thin film under UV-A irradiation (Tiwari et al., 2018).

On the other hand, the SMZ molecule has two dissociable hydrogens with pk_a^1 and pk_a^2 values of 2.28 and 7.42, respectively. It can acquire cationic, neutral, or

anionic forms depending on pH. The speciation of the SMZ showed that SMZ molecule predominantly present with the anionic species of SMZ^{-} and SMZ^{--} within the studied pH region, i.e., pH 4.0-10.0 (*Cf* Figure 3.2.1.2(b)(Inset)). (Liu et al., 2017; Fukahori et al., 2011). The photocatalyst possessed a net positive charge at pH<6.3. Hence, the negatively charged SMZ molecules are preferably attracted by catalyst until pH 6.3 and showed enhanced removal efficiency of SMZ. However, with a further increase in pH>6.3, the SMZ and catalyst surface are negatively charged. Hence, repulsive forces between the solid surface and pollutant molecules resulted from a decrease in removal efficiency of SMZ at pH>6.0. Bendjabeur et al. demonstrated that electrostatic attraction and repulsion occurred between the target pollutant and the photocatalyst (Gentian Violet and TiO_2) with the change in the solution's pH significantly affected the efficiency of the photocatalytic degradation of the pollutant molecules using a UV irradiation (Bendjabeur et al., 2017).

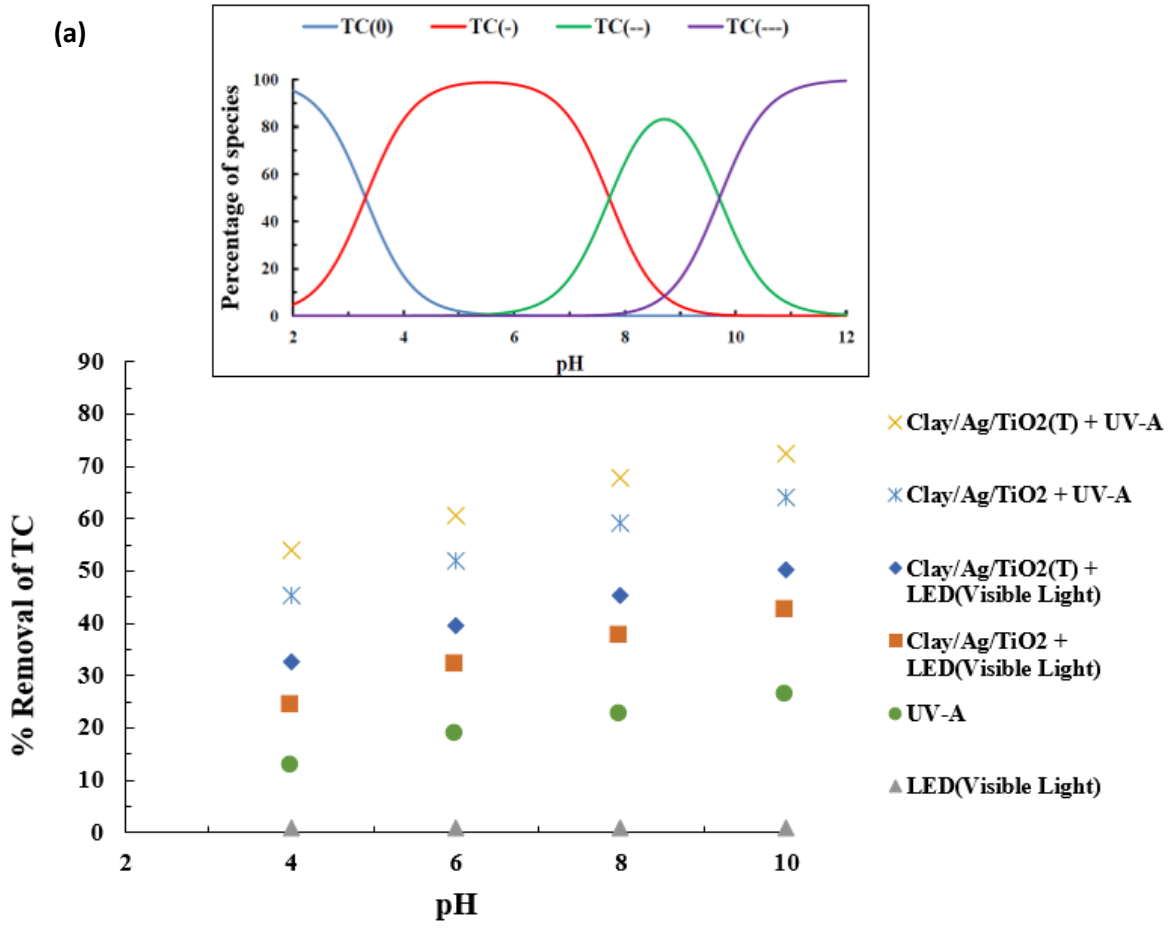

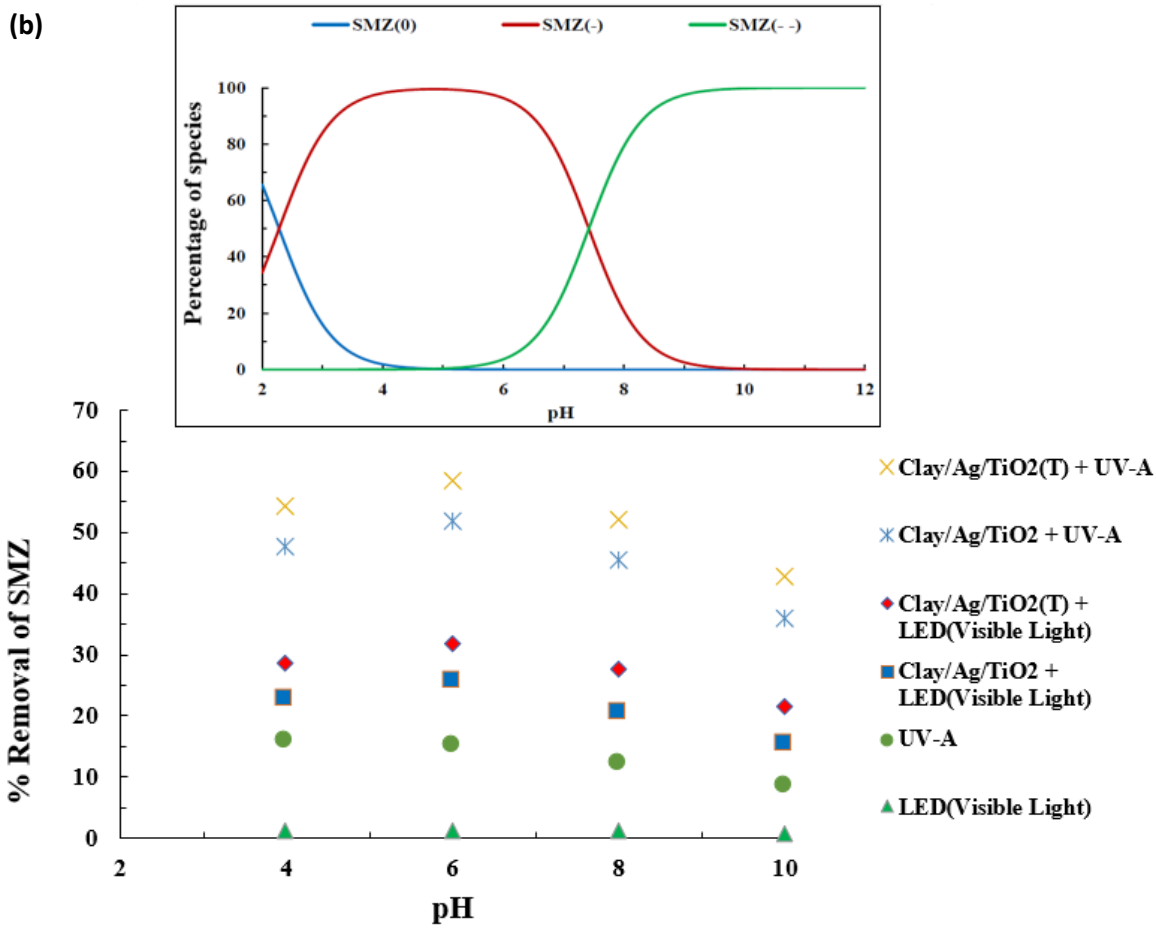

Figure 3.2.1.2: Effect of pH in the photocatalytic degradation of **(a)** tetracycline (TC) (Initial concentration of TC: 5.0 mg/L) and the Inset, species distribution of TC as a function of pH (5.0 mg/L; Temperature: 25°C) and **(b)** sulfamethazine (SMZ) (Initial concentration of SMZ: 5.0 mg/L) and the Inset, species distribution of SMZ as a function of pH (5.0 mg/L; Temperature: 25°C)

3.2.1.3. Effect of pH in the Photocatalytic Degradation of Bisphenol A (BP-A)

The pH-dependent degradation of BP-A was studied over a wide range of pH from 6.0 to 12.0 using photocatalyst Clay/Ag/TiO_2 and Clay/Ag/TiO_2(T). The pollutant samples were treated for 4 hrs under LED (Visible Light) and UV-A light irradiation. The initial concentration of BP-A was taken 5.0 mg/L and the pH dependence removal of BP-A is shown in Figure 3.2.1.3. BP-A oxidation is generally favoured at lower pH (pH 6), as shown in Figure 3.2.1.3. More specifically, increasing the solution pH from 6 to 12, caused to decrease the percentage removal of BP-A from

46.31% to 20.24% under LED (Visible Light) and 68.3% to 40.6% under UV-A light using the photocatalyst Clay/Ag/TiO_2(T). In addition, without using the photocatalyst, a photolytic reaction was carried out under UV-A irradiation for 4 hrs and results showed that A minimal percentage degradation of BP-A was obtained under the photolytic reaction (*Cf* Figure 3.2.1.3).

The surface characteristics of the photocatalyst and its interaction with the pollutants, possibly, impact the percentage degradation of pollutants in the photocatalytic process. The surface of the photocatalyst develops a partial positive charge in acidic conditions, i.e., when the solution pH is lower than the pH 6.3, whereas it develops a partial negative charge in alkaline conditions, i.e., when the solution pH is higher than pH 6.3. BP-A consists of two dissociable hydrogens having the pk_a^1 and pk_a^2 values of 9.59 and 10.2, respectively (Wang et al., 2021). Thus, below pH 9.59 BP-A existed as a neutral compound and it began to deprotonate to a negatively charged species above pH 9.59. Further at pH 10.2, BP-A exists predominantly as anionic species ($BP\text{-}A^{2-}$) (*Cf* Figure 3.2.1.3(Inset)). Thus, at lower pH (acidic conditions) pH~6.3, the neutral molecules of BP-A showed higher affinity towards the surface of the catalyst, hence causing enhanced elimination of BP-A at this pH. However, with a gradual increase in pH (pH >8), the catalyst surface carries net negative charge and the pollutant molecules also gradually dissociate the dissociable hydrogens which causes gradual increase in surface negative charge. Therefore, due to the electrostatic repulsion between the catalyst surface and the pollutant molecules, a gradual decrease in elimination of BP-A was recorded at higher pH values. Similar results were obtained by Moussavi et al., during the photochemical decomposition and detoxification of bisphenol A using vacuum UV (VUV)/H_2O_2 process (Moussavi et al., 2018). Additionally, the pH of solution influences the generation of hydroxyl radicals, hence; the degradation efficiency (Kuo et al., 2010). The oxidation potential of hydroxyl radicals is decreased significantly with an increase in the solution pH (Buxton et al., 1988). Therefore, the reduced photocatalytic degradation of BP-A was recorded. A similar result was shown for the elimination of BP-A using the TiO_2 catalyst (Kuo et al., 2010). Moreover, comparatively less degradation of BP-A at

higher pH was stated due to the negative charge on the surface of TiO_2 and the generation of carbonate ions during the BPA oxidation (Chiang et al., 2004).

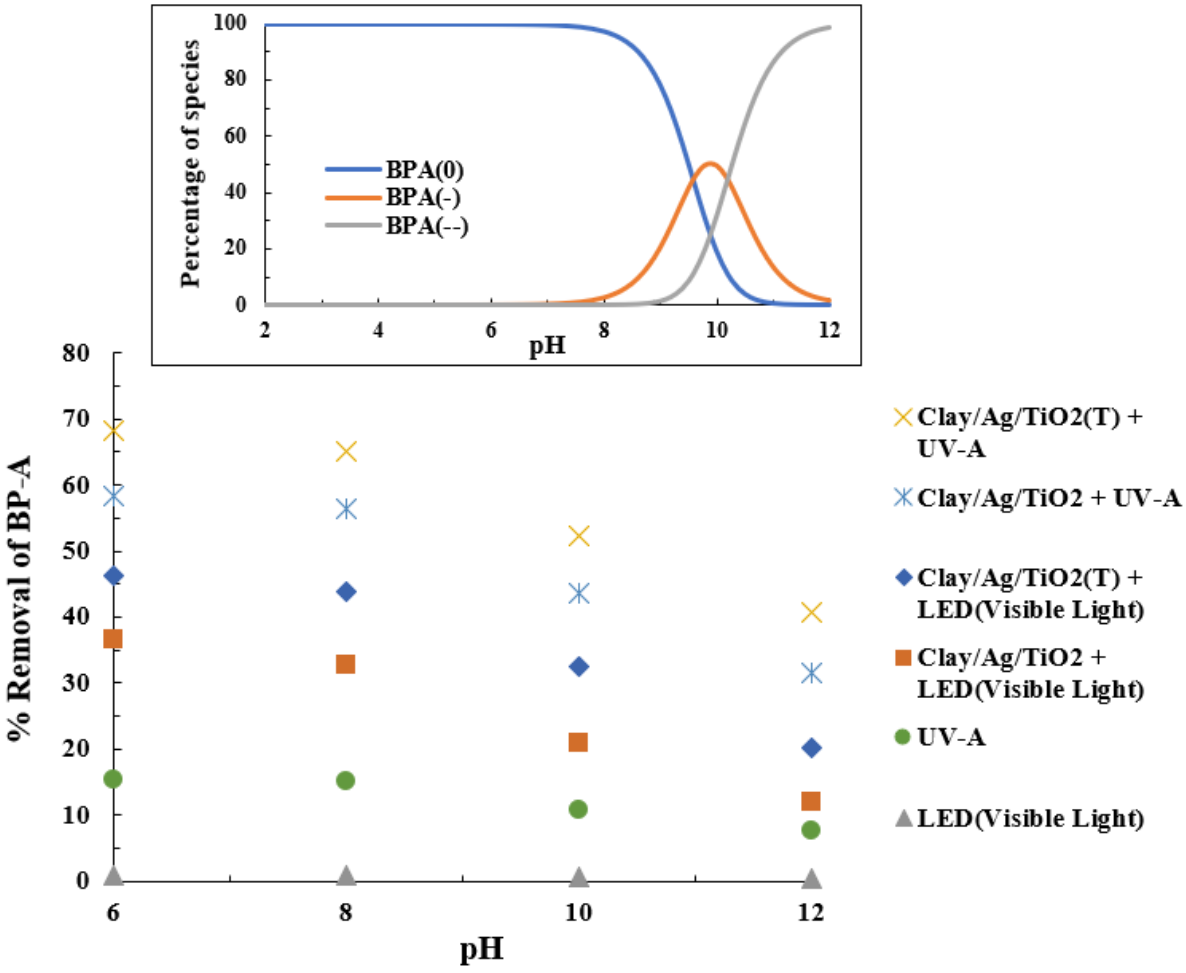

Figure 3.2.1.3: Effect of pH in the photocatalytic degradation of BP-A (Initial concentration of BP-A: 5.0 mg/L) and the Inset, species distribution of BP-A as a function of pH (5.0 mg/L; Temperature: 25°C)

3.2.1.4. Effect of pH in the Photocatalytic Degradation of Rhodamine B (Rh-B) and Rhodamine 6G (Rh-6G)

The pH dependence removal of Rh-B and Rh-6G was investigated by altering the pH of the dye solutions from pH 4.0 to 10.0 at a constant dye concentration (5.0 mg/L) using Clay/Au/TiO_2 and Clay/Au/TiO_2(T) photocatalyst. Figure 3.2.1.4. shows

the percentage degradation of Rh-B and Rh-6G as a function of pH. In case of Rh-B, it is clearly shown that with an increase in pH from pH 4 to 6, the percentage degradation is increased from 34.38 to 35.62 under visible light irradiation and from 55.35 to 56.74 under UV-A light using Clay/Au/TiO_2(T). However, further increase in pH from pH 6.0 to 10.0, the rate of percentage degradation is decreased from 35.62 to 21.84, respectively under visible light irradiation and from 56.74 to 38.33, respectively under UV-A light (Figure 3.2.1.4.(a)). In case of Rh-6G, increasing pH from pH 4 to 8, results in up surging in the degradation percentage from 25.38 to 36.03, respectively under visible light and from 46.35 to 60.46, respectively under UV-A light using Clay/Au/TiO_2(T). However, further increase in pH from pH 8.0 to 10.0 results in decline in the rate of percentage degradation from 36.03 to 18.84, respectively under visible light and from 60.46 to 36.33, respectively under UV-A light (Figure 3.2.1.4.(b)). The pH_{PZC} of both the catalysts was 6.5, hence, both the thin films have a net positive charge below this pH value (pH < 6.5) and become negatively charged above it (pH > 6.5).

Rh-B is having a dissociable hydrogen with pk_a value of 4.2 (Maurya et al., 2006). Therefore, the speciation studies indicated that the negatively charged species of Rh-B is gradually increasing with increase in the pH (pH>4.2) (Figure 3.2.1.4(a)(Inset)). However, relatively higher percentage removal of Rh-B within the pH region 4.2 - 6.5, implied that a strong affinity of pollutant molecules towards the positively charged surface of the catalyst. Moreover, the oxidation potential of hydroxyl radical is relatively higher at lower pH values, which favoured the elimination of Rh-B within this pH region 4.2 - 6.5. Further increase in pH pH >6.5, relatively stronger electrostatic repulsion occurred between the thin film catalyst and anionic species of Rh-B molecules, which resulted in lesser percentage removal of Rh-B. Similar results were reported in the photocatalytic degradation of Rh-B using Fe-Doped TiO_2 anchored on Reduced Graphene Oxide (Fe-TiO_2 /rGO) (Isari et al., 2018).

Similarly, the R-6G has the acid dissociation constant (pk_a) value 6.13 (Rajoriya et al., 2016). This showed that the undissociated R-6G molecule is predominating at pH<6.13 and a dissociated negatively charged R-6G at pH>6.13. However, a very high percentage removal of R-6G is observed within the pH region

6.0-8.0, indicating a strong affinity of catalyst towards the pollutant molecules (Figure 3.2.1.4.(b)). Further, at an extremely high pH value (pH 10.0), a sharp decline in percentage removal of R-6G is because of the strong repulsive forces between the pollutant molecules and the solid surface. Moreover, in a highly alkaline solution, the hydroxyl radical formation rate is decreased significantly due to the formation of hydroxyl ions (Khlyustova et al., 2016).

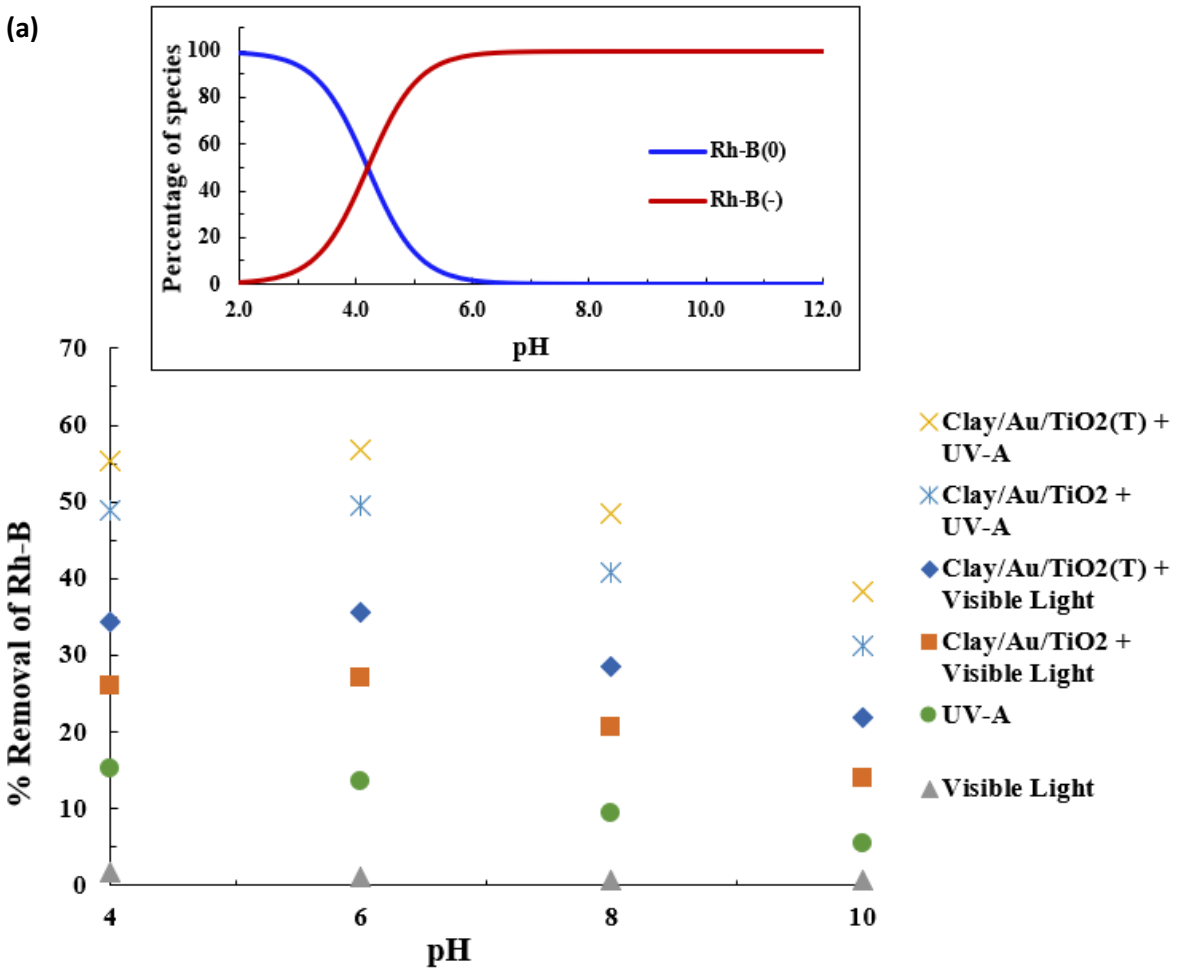

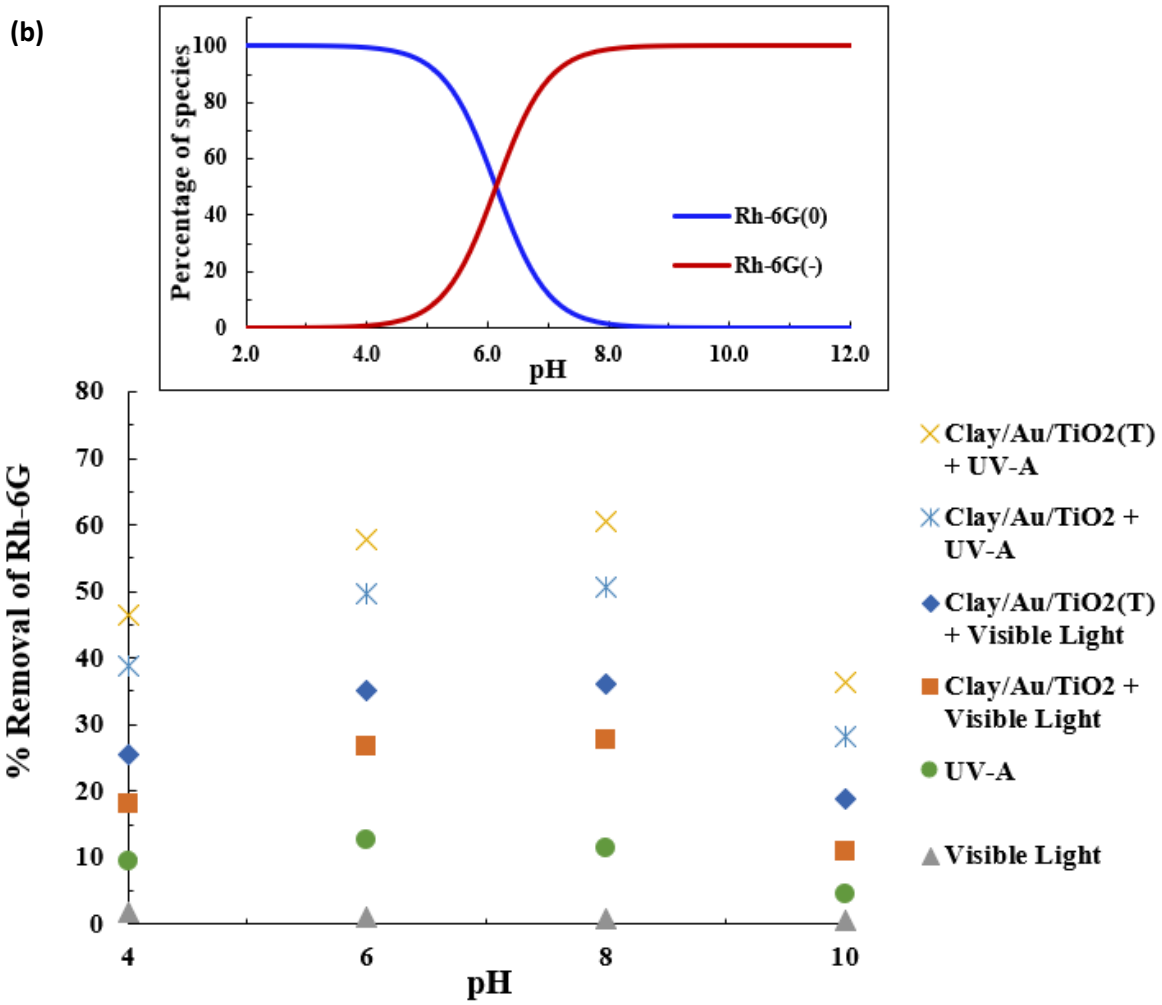

Figure 3.2.1.4.: Effect of pH in the photocatalytic degradation of **(a)** Rh-B (Initial concentration of Rh-B: 5.0 mg/L) and the Inset, species distribution of Rh-B as a function of pH (5.0 mg/L; Temperature: 25°C) and **(b)** Rh-6G (Initial concentration of Rh-6G: 5.0 mg/L) and the Inset, species distribution of Rh-6G as a function of pH (5.0 mg/L; Temperature: 25°C)

3.2.1.5. Effect of Concentration in the Photocatalytic Degradation of Mordant Orange 1 (MO1)

Concentration dependent elimination of MO1 is analysed for varied concentrations of MO1 (0.5 - 20.0 mg/L; pH 6.0) using thin film catalyst $Ag^0(NP)/TiO_2$, and results are illustrated in Figure 3.2.1.5. It demonstrates that decrease in concentration greatly favoured the removal efficiency of MO1. Decreasing

the concentration of MO1 from 20.0 to 0.5 mg/L has enabled to increase the percentage degradation of MO1 from 13.7 to 60.6% (for UV-A) and 6.5 to 38.14% (LED light), respectively. The decrease in degradation efficiency with an increase in concentration of MO1 is, perhaps, due to the reason that the contact possibility of MO1 at the photocatalyst surface was relatively less at higher concentration of MO1 dye (Tiwari et al., 2015). It is also evident that at high concentration of MO1, the scavenging effect increases, which possibly results in decrease of percentage removal of the MO1 (Nasseri et al., 2017). These results are in line with the results obtained in the photocatalytic degradation of Reactive Green 12(RG 12) using TiO_2 impregnated polyester in which the dye removal was significantly reduced with an increase in RG 12 concentration. At lower concentration of RG 12, the solution was more transparent, that penetration of light on the photocatalyst surface was more hence, favoured the formation of more reactive species (Hichem et al., 2017). Furthermore, a dark reaction is performed employing the catalyst Ag^0(NPs)/TiO_2 at various concentrations of MO1 (0.5–20.0 mg/L; pH 6.0). It is observed that almost negligible amounts of MO1 were removed even after 12 hrs of contact. Therefore, this indicated that the surface adsorption is almost negligible however, surface attraction favoured the degradation of MO1 under the photocatalytic process.

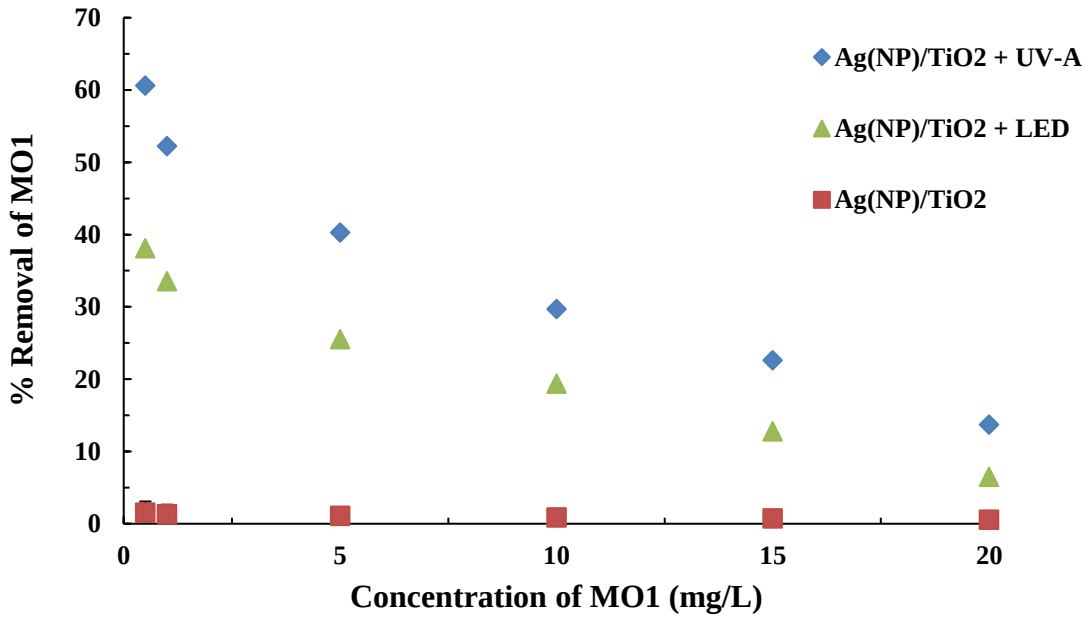

Figure 3.2.1.5.: Effect of concentration in the photocatalytic degradation of (MO1) [pH of solution: 6.0].

3.2.1.6. Effect of Concentration in the Photocatalytic Degradation of Tetracycline (TC) and Sulfamethazine (SMZ)

The initial concentration of TC and SMZ was varied from 0.5 mg/L to 20.0 mg/L in the removal of TC and SMZ at constant pH (pH 10.0 for TC and pH 6.0 for SMZ). The LED (Visible Light)/or UV-A light irradiation was used to treat the TC and SMZ solution for a total of 2 hrs and 3 hrs, respectively using Clay/Ag/TiO_2 and Clay/Ag/TiO_2(T) thin film catalysts. Figure 3.2.1.6. shows the percentage degradation of TC and SMZ as a function of initial antibiotic concentration. In brief, the percentage photocatalytic degradation of TC and SMZ was higher at lower initial antibiotic concentrations (Figure 3.2.1.6.). More specifically, using Clay/Ag/TiO_2(T) thin-film under LED (Visible Light), the degradation percentage of TC was decreased from 57.89 % to 34.46%, with an increase in the initial concentration of TC from 0.5 mg/L to 20.0 mg/L, respectively. Under UV-A light with Clay/Ag/TiO_2(T) thin film, increasing the initial concentration of TC from 0.5 mg/L to 20.0 mg/L, resulted in a decrease in percentage degradation of TC from 81.13% to 50.36%, respectively. Similarly, using Clay/Ag/TiO_2(T) thin-film under LED (Visible Light), the degradation percentage of SMZ was decreased from 37.83 % to 18.42%, with an increase in the initial concentration of SMZ from 0.5 mg/L to 20.0 mg/L, respectively. Under UV-A light with Clay/Ag/TiO_2(T) thin film, increasing the initial concentration of SMZ from 0.5 mg/L to 20.0 mg/L, caused a decrease of SMZ percentage degradation from 64.58% to 36.21%, respectively. Thus, for both TC and SMZ, a higher degradation percentage at lower antibiotic concentrations was due to the fact that at lower antibiotic concentrations, the catalyst surface possesses relatively more number of accessible surface active sites (Bendjabeur et al., 2017). At the same time, at higher concentrations, the accumulation of pollutant molecules on the surface of the thin film hinders the penetration of light radiation onto the photocatalyst resulting in a lesser percentage of removal (Tiwari et al., 2015; Augugliaro et al., 2002). It was previously reported that increasing pollutant concentrations caused an increase in the

scavenging effect, and resulted in a drop in pollutant removal efficiency (Omrani and Nezamzadeh-Ejhieh, 2020).

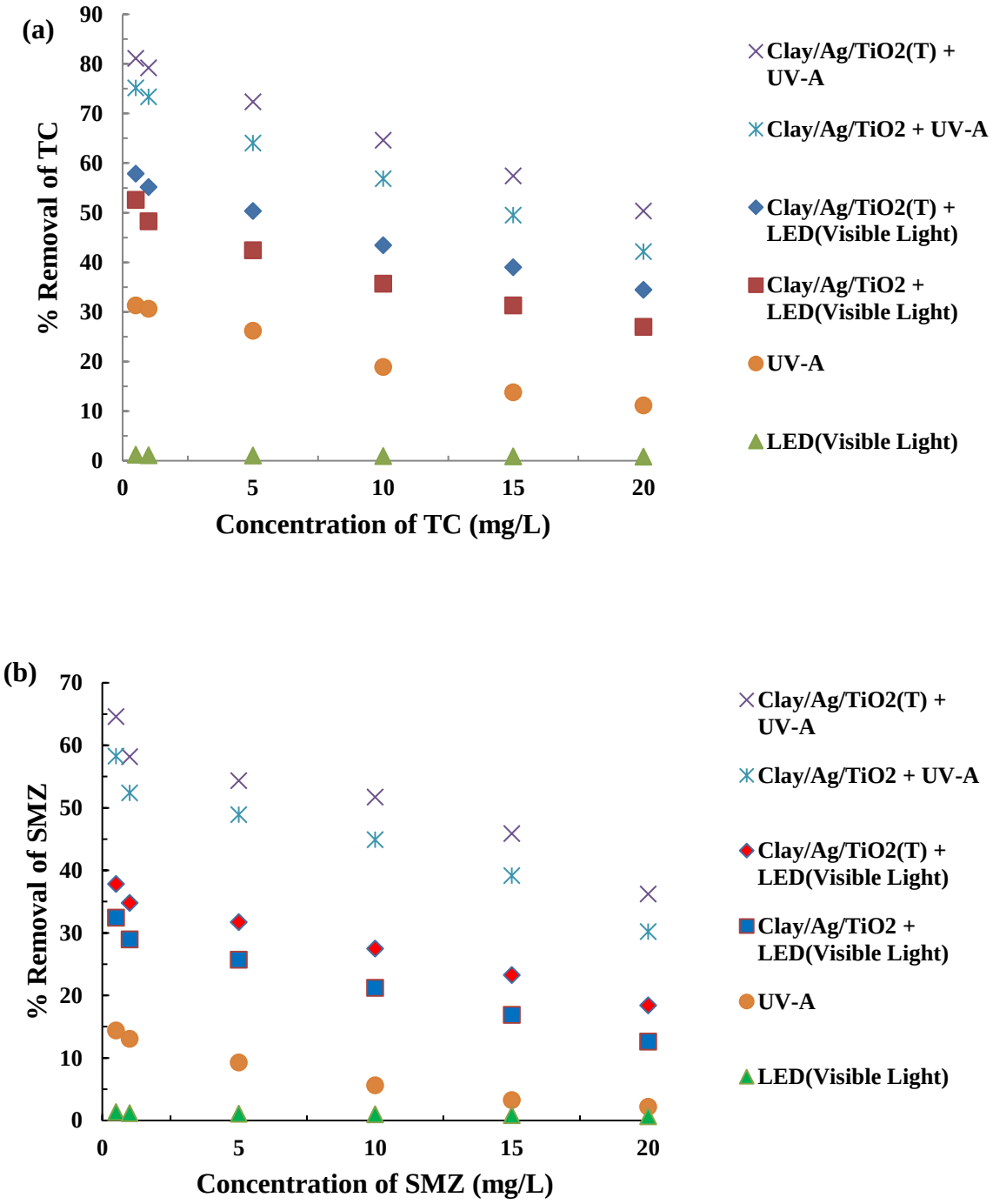

Figure 3.2.1.6.: Effect of concentration in the photocatalytic degradation of (a) TC (pH 10.0) and (b) SMZ (pH 6.0).

3.2.1.7. Effect of Concentration in the Photocatalytic Degradation of Bisphenol A (BP-A)

BP-A concentrations ranging from 1.0 mg/L to 20.0 mg/L were taken at constant pH 8. LED (Visible Light) and UV-A lamps were utilized to treat the pollutant solutions for 4 hrs using Clay/Ag/TiO_2 and Clay/Ag/TiO_2(T) thin film catalysts. The degradation percentage of BP-A as a function of initial BP-A concentration is shown in Figure 3.2.1.7. The percentage of photocatalytic degradation of BP-A is higher at lower initial pollutant concentrations. However, increasing the initial concentration of BP-A from 1.0 mg/L to 20.0 mg/L, the percentage removal of BP-A was decreased from 50.0% to 25.35% under LED (Visible Light) and 75.3% to 40.6% under UV-A light irradiation using the photocatalyst Clay/Ag/TiO_2(T). A gradual decrease in percentage degradation of BP-A with an increase in initial concentration of BP-A is because, at lower concentrations, the catalyst surface has more accessible active sites on the surface hence, favoured the percentage removal at lower BP-A concentration. However, relatively lesser active sites are available for the large number of BP-A molecules at higher concentration of BP-A, which caused a gradual decrease in percentage removal of BP-A at higher BP-A concentration. Additionally, at higher concentrations of BP-A, the pollutant molecules restricting the penetration of light on the thin film surface, which hindered the efficiency of photocatalyst in photocatalytic process (Bendjabeur et al., 2017; Lalhriatpuia et al., 2015). It was also reported that increasing the concentration of BP-A, caused to enhance the scavenging effect, hence relatively lesser percentage removal of BP-A was obtained at higher BP-A concentration (Jia et al., 2012).

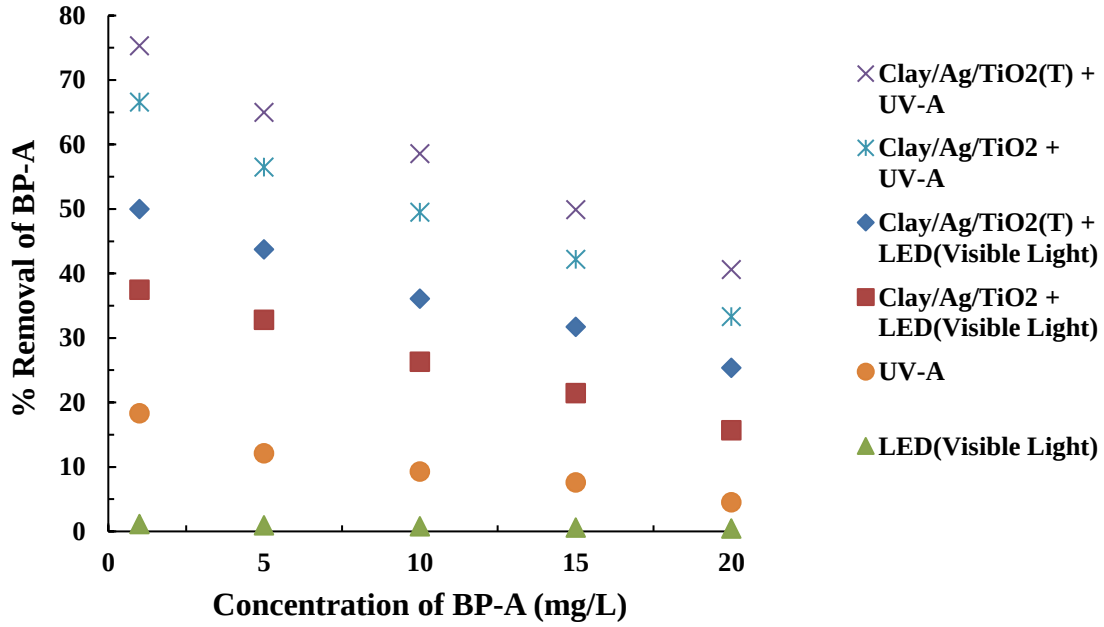

Figure 3.2.1.7.: Effect of concentration in the photocatalytic degradation of Bisphenol A (BP-A) (pH 8.0)

3.2.1.8. Effect of Concentration in the Photocatalytic Degradation of Rhodamine B (Rh-B) and Rhodamine 6G (Rh-6G)

The effect of initial concentration in the degradation of Rh-B and Rh-6G was studied by varying the concentration from 0.5 to 20.0 mg/L at constant pH 6.0. Using Clay/Au/TiO_2 and Clay/Au/TiO_2(T) photocatalyst, both the dyes solutions were treated under visible light and UV-A lamp for a total of 2 hrs. Figure 3.2.1.8. depicts the degradation results of Rh-B and Rh-6G with the change in initial dyes concentration. In brief, the percentage photocatalytic breakdown of Rh-B and Rh-6G is higher at lower initial dye concentrations (*Cf* Figure 3.2.1.8). More specifically, increasing the initial concentration of the Rh-B dye from 0.5 mg/L to 20.0 mg/L, the corresponding percentage degradation was decreased from 54.13% to 6.07% under visible light and from 76.26% to 17.64% under UV-A irradiation using photocatalyst Clay/Au/TiO_2(T). In case of Rh-6G, with an increase in the initial concentration of dye from 0.5 mg/L to 20.0 mg/L, the corresponding percentage removal of Rh-6G is reduced from 60.37% to 8.42% under visible light and from 84.68% to 19.66% under

UV-A light irradiations using photocatalyst Clay/Au/TiO_2(T). Jain et al reported photocatalytic degradation of Rh-B using TiO_2 in the occurrence of electron acceptor H_2O_2, also followed the same trends in the percentage removal with an increase in the dye concentrations (Jain et al., 2007). Similar results were obtained in the photocatalytic degradation of Rh-6G using ZnO-Ag nanoparticles prepared using pulsed laser ablation in liquid (PLAL) in which percentage removal was decreased drastically with an increase in the dye concentration (Yudasari et al., 2021).

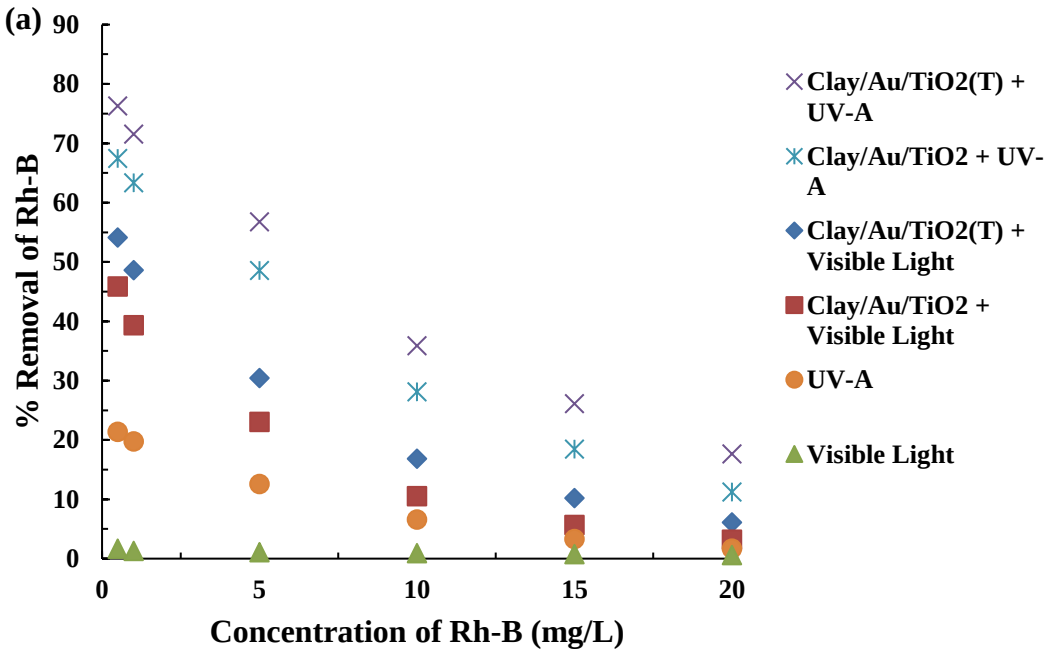

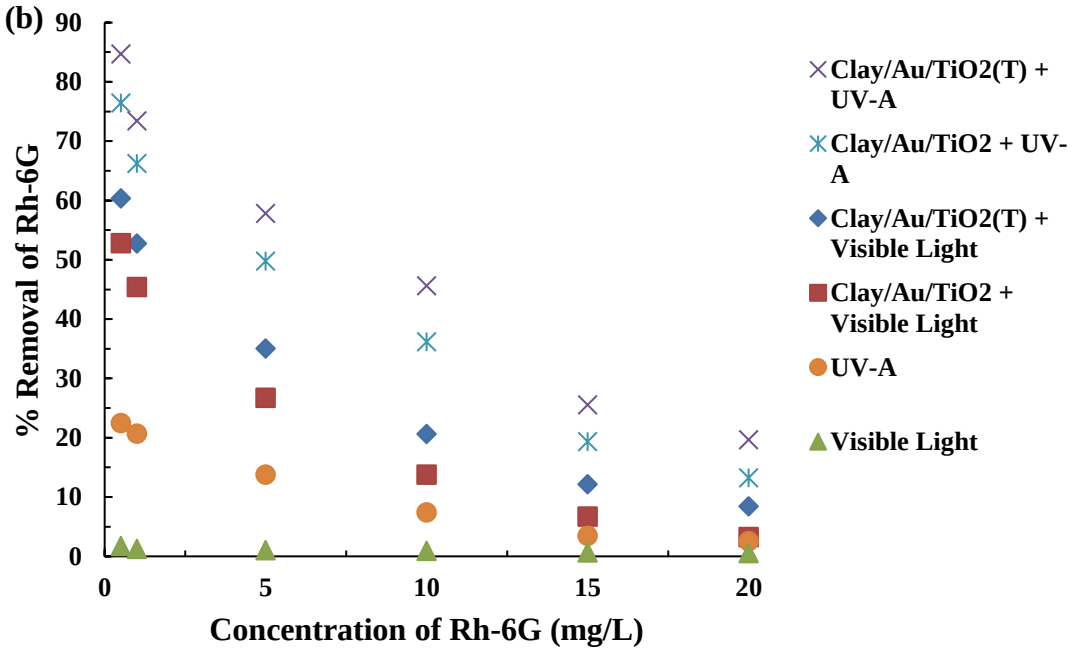

Figure 3.2.1.8.: Effect of concentration in the photocatalytic degradation of (a) Rh-B (pH 6.0) and (b) Rh-6G (pH 6.0)

3.2.1.9. Degradation Kinetics of Mordant Orange 1 (MO1)

The time dependence kinetics is carried out to assess the performance of Ag^0(NP)/TiO_2 nanocomposite photocatalysts in the elimination of MO1. The kinetic results at varied concentrations of MO1 are shown in Table 3.2.1.9. It is observed that degradation of MO1 proceeds through the pseudo-first-order rate equation. Further, the time dependent degradation kinetics of MO1 is favoured with the dilution i.e., increasing the concentration of the dyes causes a decrease in the rate constant values. Moreover, the rate of degradation of MO1 is faster using the UV-A light irradiations compared to the LED light irradiations. Similar results were reported previously where the degradation of methylene blue followed pseudo-first-order rate kinetics and the rate constant values were decreased increasing the methylene blue concentrations using graphene decorated TiO_2 (Acosta-Esparza et al., 2020).

Table 3.2.1.9.: Pseudo-first order rate constants in the photo-catalytic degradation of of MO1 [pH of solution: 6.0] using Ag^0(NP)/TiO_2 nanocomposite thin film under UV-A and LED (Visible light) irradiations.

Initial Concentration of MO1 (mg/L)	UV-A Irradiation		LED Light Irradiation	
	Rate constant $k_1x10^{-3}(s^{-1})$	R^2	Rate Constant $k_1x10^{-3}(s^{-1})$	R^2
0.5	7.0	0.965	4.1	0.998
1.0	5.9	0.993	3.4	0.982
5.0	4.0	0.987	2.5	0.999
10.0	2.9	0.9895	1.8	0.998
15.0	2.0	0.979	1.1	0.995
20.0	1.4	0.952	0.5	0.994

Additionally, the removal of MO1 is modelled to the Langmuir–Hinshelwood (L-H) rate kinetics using the standard equations. Therefore, the Langmuir–Hinshelwood (L-H) adsorption constant (k_r; mg/L/min) and the reaction rate constant (K; L/mg) were computed as 0.038 and 0.202 (R^2: 0.997 for UV-A) and 0.018 and 0.255 (R^2: 0.976 for LED), respectively.

3.2.1.10. Degradation Kinetics of Tetracycline (TC) and Sulfamethazine (SMZ)

The kinetic studies were carried out to determine the effectiveness of the photocatalyst (Clay/Ag/TiO_2 and Clay/Ag/TiO_2(T)), the efficiency of pollutant degradation, and the rate constant in the photocatalytic degradation reaction of TC and SMZ. The removal of TC and SMZ was obtained as a function of time and pollutant concentrations utilizing the LED (Visible Light) and UV-A light irradiation. The initial concentration of TC and SMZ was taken 5.0 mg/L at constant pH 10.0 and pH 6.0,

respectively. Straight lines were obtained while plotting the curve between $\ln(C_0/C_t)$ (where C_0 is the initial concentration of TC /or SMZ and C_t is the concentration of TC/SMZ at time 't') and 't' is the reaction time. The slope of straight lines yields the pseudo-first-order rate constant (k_1). Hence, at various pollutant concentrations, the k_1 values are computed and given in Table 3.2.1.10. The results showed that the kinetic data fitted well to the pseudo-first-order rate kinetics since reasonably high R^2 values were obtained for both the antibiotics. Furthermore, it is observed that the decrease in pollutant concentration favoured the rate constant values using both the photocatalysts viz., Clay/Ag/TiO_2 and Clay/Ag/TiO_2(T). Moreover, the rate constant values were significantly higher using UV-A light than the visible light (LED light) irradiation. Previous studies showed that the photocatalytic degradation of Alizarin Yellow dye followed the pseudo-first-order rate kinetics by utilizing Ag^0(NP)/TiO_2 catalyst (Lalliansanga et al., 2020).

The adsorption properties of TC and SMZ on the photocatalyst surface and the degradation process were modelled with a known Langmuir-Hinshelwood (L-H) adsorption isotherm at different initial concentrations (Khuzwayo and Chirwa, 2015). In case of TC, the rate constant 'k_r' (mg/L/min) and the L-H adsorption constant 'K' (L/mg) were obtained to be 0.136 and 0.064 (R^2: 0.995; for Clay/Ag/TiO_2(T)); 0.085 and 0.087 (R^2: 0.987; for Clay/Ag/TiO_2) respectively. In case of SMZ, the rate constant 'k_r' (mg/L/min) and the L-H adsorption constant 'K' (L/mg) were obtained to be 0.045 and 0.069 (R^2: 0.997; for Clay/Ag/TiO_2(T)); 0.029 and 0.085 respectively (R^2: 0.996; for Clay/Ag/TiO_2).

Table 3.2.1.10.: Pseudo-first order rate constants in the photo-catalytic degradation of TC [pH of solution: 10.0] and SMZ [pH of solution: 6.0] using Clay/Ag/TiO_2 and Clay/Ag/TiO_2(T) nanocomposite thin film under LED (Visible light) irradiations.

Initial Concentration of TC/or SMZ (mg/L)	TC				SMZ			
	Clay/Ag/TiO_2(T)		Clay/Ag/TiO_2		Clay/Ag/TiO_2(T)		Clay/Ag/TiO_2	
	Rate constant $k_1x10^{-3}(s^{-1})$	R^2	Rate Constant $k_1x10^{-3}(s^{-1})$	R^2	Rate constant $k_1x10^{-3}(s^{-1})$	R^2	Rate Constant $k_1x10^{-3}(s^{-1})$	R^2
0.5	8.6	0.872	7.4	0.899	3.0	0.952	2.4	0.974
1.0	7.6	0.892	6.1	0.935	2.7	0.945	2.1	0.977
5.0	6.7	0.898	5.3	0.902	2.3	0.967	1.8	0.970
10.0	5.5	0.897	4.1	0.940	2.0	0.926	1.5	0.938
15.0	4.8	0.883	3.6	0.892	1.7	0.909	1.2	0.923
20.0	4.1	0.894	3.1	0.879	1.3	0.951	0.9	0.944

3.2.1.11. Degradation kinetics of Bisphenol A (BP-A)

Kinetic studies were conducted to define the efficiency of BP-A degradation and the value of the reaction rate constant in the photocatalytic degradation of BP-A was computed at different concentrations of BP-A. The time dependence degradation of BP-A under LED (Visible Light) at pH 8.0 utilizing both the catalysts Clay/Ag/TiO_2 and Clay/Ag/TiO_2(T) were utilized to deduce the rate constant values.

Further, it is evident that the photocatalytic degradation of BP-A followed the pseudo-first-order rate kinetics. The pseudo-first-order rate constant values along with the R^2 values at varied BP-A concentrations, are returned in Table 3.2.1.11. It is evident that the dilution of BP-A favoured the rate constant values. It was reported previously that the photocatalytic breakdown of tetracycline in an aqueous solution followed the pseudo-first-order rate kinetics using the thin films Au^0(NP)/TiO_2 catalyst (Tiwari et al., 2019).

The photocatalytic degradation process of BP-A was modelled with a known Langmuir-Hinshelwood (L-H) adsorption isotherm at different concentrations to explore the properties of adsorption on the photocatalyst surface (L. Liu et al., 2019). The rate constant 'k_r' (mg/L/min) and the L-H adsorption constant 'K' (L/mg) for

nanocomposite Clay/Ag/TiO_2 thin film (R^2: 0.997) were computed as 0.036 and 0.057, respectively. On the other hand, for the nanocomposite Clay/Ag/TiO_2(T) thin film (R^2: 0.999), the rate constant 'k_r' (mg/L/min) and the L-H adsorption constant 'K' (L/mg) were found 0.051 and 0.063, respectively.

Table 3.2.1.11.: Pseudo-first order rate constants in the photo-catalytic degradation of BP-A [pH of solution: 8.0] using Clay/Ag/TiO_2 and Clay/Ag/TiO_2(T) nanocomposite thin film under LED (Visible light) irradiations.

Initial Concentration of BP-A (mg/L)	Clay/Ag/TiO_2		Clay/Ag/TiO_2(T)	
	Rate constant $k_1x10^{-3}(s^{-1})$	R^2	Rate Constant $k_1x10^{-3}(s^{-1})$	R^2
1.0	1.9	0.997	3.0	0.997
5.0	1.8	0.996	2.6	0.993
10.0	1.3	0.997	2.0	0.992
15.0	1.1	0.995	1.7	0.995
20.0	0.8	0.995	1.3	0.993

3.2.1.12. Degradation Kinetics of Rhodamine B (Rh-B) and Rhodamine 6G (Rh-6G)

The time dependence elimination data of these two dyes (pH 6.0) under the photocatalytic degradation utilizing the thin film catalysts Clay/Au/TiO_2(T) and Clay/Au/TiO_2 are fitted well to the pseudo-first-order rate equation (Equation 2.3).

Further, the pseudo-first-order rate constant values along with the R^2 values for these two dyes were computed, and shown in Table 3.2.1.12. Results inferred that the lowering the concentrations of dye, favoured the rate constant values. The photocatalytic removal of triclosan in aqueous solution followed the pseudo-first order rate kinetics using thin film Ag(NPs)/TiO_2 (Tiwari et al., 2020).

Further, the photocatalytic degradation of Rh-B and Rh-6G was modelled using a known Langmuir-Hinshelwood (L-H) adsorption isotherm at various concentrations (L. Liu et al., 2019). In case of Rh-B, the rate constant 'k_r' (mg/L/min) and the L-H adsorption constant 'K' (L/mg) were obtained 0.016 and 0.524 (R^2: 0.955; for Clay/Au/TiO_2(T)); 0.009 and 0.790 (R^2: 0.886; for Clay/Au/TiO_2), respectively. In case of Rh-6G, the rate constant 'k_r' (mg/L/min) and the L-H adsorption constant 'K' (L/mg) were found 0.022 and 0.468 (R^2: 0.985; for Clay/Au/TiO_2(T)); 0.011 and 0.922, respectively (R^2: 0.772; for Clay/Au/TiO_2).

Table 3.2.1.12.: Pseudo-first order rate constants in the photo-catalytic degradation of Rh-B and Rh-6G [pH of both the solution: 6.0] using Clay/Au/TiO_2(T) and Clay/Au/TiO_2 nanocomposite thin film under LED (Visible light) irradiations.

Initial Concentration of TC/SMZ (mg/L)	Rh-B				Rh-6G			
	Clay/Au/TiO2(T)		Clay/Au/TiO2		Clay/Au/TiO2(T)		Clay/Au/TiO2	
	Rate constant $k_1x10^{-3}(s^{-1})$	R^2	Rate Constant $k_1x10^{-3}(s^{-1})$	R^2	Rate constant $k_1x10^{-3}(s^{-1})$	R^2	Rate Constant $k_1x10^{-3}(s^{-1})$	R^2
0.5	6.4	0.999	5.1	0.998	8.3	0.990	6.6	0.997
1.0	5.6	0.998	4.1	0.999	6.9	0.987	5.4	0.995
5.0	3.1	0.999	2.3	0.998	3.8	0.992	2.8	0.993
10.0	1.5	0.999	1.0	0.997	2.1	0.993	1.4	0.985
15.0	0.9	0.999	0.5	0.997	1.2	0.990	0.7	0.981
20.0	0.5	0.998	0.3	0.998	0.8	0.993	0.3	0.981

3.2.1.13. Effect of Coexisting Ions in the Photocatalytic Degradation of Mordant Orange 1 (MO1)

Applicability of Ag^0(NP)/TiO_2 thin film photocatalyst in the removal of MO1 is further assessed in presence of variety of co-ions *viz.*, glycine, oxalic acid, $NaNO_3$, NaCl, $CuSO_4$, $NiCl_2$ and EDTA. The initial concentration of MO1 and co-existing ions was taken 5.0 mg/L and 50.0 mg/L, respectively (pH 6.0 and UV-A illumination for 2 hrs). The removal efficiency of MO1 for simultaneous presence of co-ions is shown in Figure 3.2.1.13. The removal efficiency of MO1 is affected in the presence of NaCl, EDTA and glycine. However, the other ions introduced have not significantly affected the degradation of MO1 in the photocatalytic reactor operations. The competitive sorption of Na^+ ions towards the TiO_2 surface caused decreased degradation of MO1 molecules in the photocatalytic degradation of these pollutants in aqueous medium (Sofyan et al., 2019; Yong et al., 2002). Glycine is also readily adsorbed on the TiO_2 surface through its zwitterion form, favourably by deprotonation of the carboxyl group, forming a (2 × 1) over layer at the catalyst surface, which inhibits the degradation of MO1 molecule in presence of glycine (Thompson and Yates, 2006).

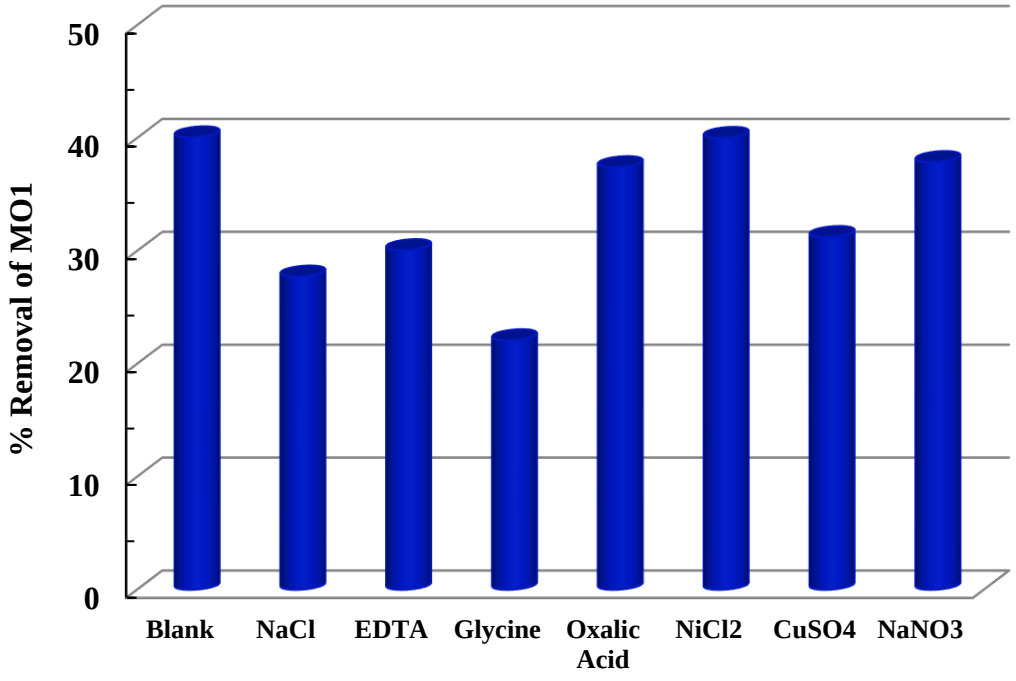

Figure 3.2.1.13.: Effect of Co-existing Ions (100.0 mg/L) in the photocatalytic degradation of MO1 [5.0 mg/L; pH:6.0] using Ag^0(NP)/TiO_2 under UV-A irradiation.

3.2.1.13.1. Degradation Mechanism of Mordant Orange 1 (MO1)

It is known that the photons carrying enough energy (hυ) may generate electron and hole pairs $(e^- - h^+)$ (Selvaraj and Li, 2006). However, titanium dioxide possessed wide band gap energy (3.2 eV) hence, excited predominantly by the photons at UV region. However, the doping of titanium dioxide by noble metals (Ag or Au) lowers apparent band gap energy. Noble metal nanoparticles generate a phenomenon called localised surface plasmon resonance, which enables TiO_2 photocatalysts to absorb light within the visible region and enhances the photo-excitation of electrons (Zangeneh et al., 2015). It also traps the newly generated electrons thus helping in reducing the charge recombination rate and allowing it to proceed further for photocatalytic reaction. Therefore, in order to demonstrate the possible mechanism involved in the elimination of MO1 using the nanocomposite photocatalyst, the investigation was extended in presence of several scavengers. 2-propanol and HCO_3^- compounds are known $^{\bullet}OH$ radical scavengers (Lalhriatpuia et al., 2016; Xu et al., 2015); whereas EDTA scavenges the h^+ of photocatalyst (Jia et al., 2016). Similarly, the sodium azide traps singlet oxygen which are generated in reaction of $O_2^{-\bullet}$ with h^+ (Xu et al., 2015). Thus, the degradation of MO1 (5.0 mg/L; pH 6.0) in presence of these scavengers is carried out using the UV-A irradiation for 2 hrs. The degradation efficiency of MO1 is shown as in Figure 3.2.1.13.1. The results imply that the 2-propanol, HCO_3^- and sodium azide greatly hampered the percentage degradation of MO1. This indicated that hydroxyl radicals are primarily involved in the degradation process. A sharp drop in the photocatalytic degradation of oxolinic acid (OA) using TiO_2/cellulosic paper catalysts in the presence of 2-propanol and EDTA was demonstrated elsewhere and inferred that reactive hydroxyl radicals are predominantly involved in the degradation process (Zeghioud et al., 2019). Additionally, NaN_3 suppressed the removal efficiency of MO1, inferring that singlet oxygen is taking part in the photocatalytic degradation reaction. Hence, these results showed that the

elimination mechanism of MO1 proceeds in two different possible pathways. First, the Ag(NPs) traps the newly generated electrons which helps in inhibiting the charge recombination and allows it to proceed further for reaction to form peroxide radical and hydroxyl radicals (R. Ahmad et al., 2016). Peroxide radicals are generated at the conduction band through interaction of trapped electrons and oxygen in presence of water, while hydroxyl radicals are generated at the valence band through the interaction of the H_2O and oxygen (Akpan and Hameed, 2009). Both the radicals then interacted with the pollutant molecule at the vicinity of the thin film photocatalyst, which results in the degradation of MO1 (Vogna et al., 2004; Tiwari et al., 2019). The other possible pathway is that Ag(NPs) absorbs light radiations resulting in the generation of electromagnetic fields as because of localized surface plasmon resonance (Lee et al., 2014). Further, Schottky barrier present with metal-semiconductor causes the excited electrons to move toward the electric field and the holes towards the opposite direction of the electric field. This inhibits the recombination of electron-hole pairs (D. Wang et al., 2018a). Further, the electron-hole pairs undergo further reaction to form peroxide radical and hydroxyl radical which take part in the degradation of MO1.

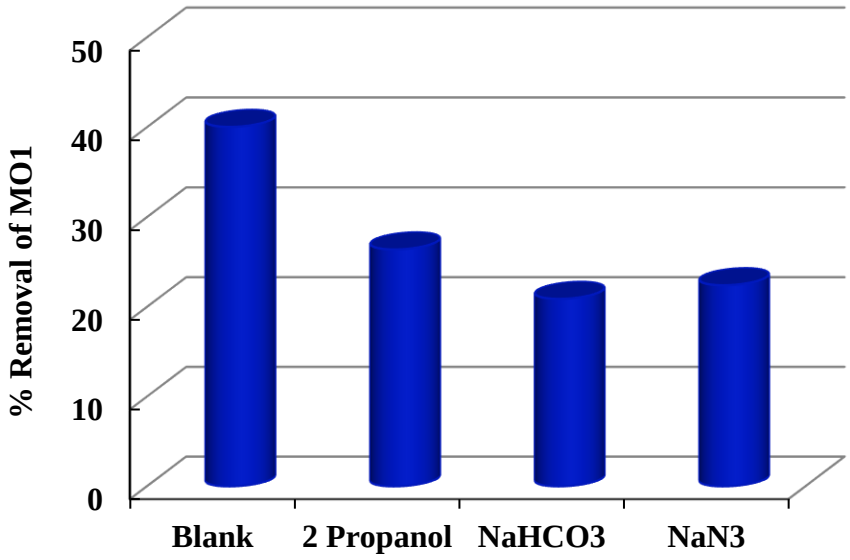

Figure 3.2.1.13.1.: Effect of Scavengers (500.0 mg/L) in the photocatalytic degradation of MO1 [5.0 mg/L; pH:6.0] using Ag^0(NP)/TiO_2 under UV-A irradiation.

3.2.1.14. Effect of Coexisting Ions in the Photocatalytic Degradation of Tetracycline (TC) and Sulfamethazine (SMZ)

The existence of coexisting ions in removing TC and SMZ provides useful input data in the treatment of real water samples. The studies are carried out in the presence of oxalic acid, glycine, $ZnCl_2$, NaCl, $NaNO_2$, $NaNO_3$, EDTA, and $CuSO_4$ in the photocatalytic degradation of TC and SMZ under LED (Visible Light) irradiation utilizing the Clay/Ag/TiO_2(T) catalyst. The initial pollutant concentration and pH were taken as 10.0 mg/L and pH 10.0 (for TC) and 10.0 mg/L and pH 6.0 (for SMZ), respectively. Each coexisting ion concentration was taken as 100.0 mg/L. Figure 3.2.1.14. show the removal of TC and SMZ in the presence of these co-ions. These ions showed varying effects in the removal of TC and SMZ. The presence of NaCl, EDTA, and glycine significantly affected the removal efficiency of TC.

On the other hand, in case of SMZ the removal efficiency was significantly hampered in the presence of oxalic acid, EDTA, and $CuSO_4$. This is because these ions compete with the pollutant molecules for sorption on the photocatalyst surface. Hence, it prevents the target molecule from reaching the photocatalyst surface and hinders the photocatalytic degradation of pollutant molecules. Additionally, the EDTA scavenges efficiently the photogenerated hole (h^+) in the TiO_2 photocatalysts, hence suppressing the generation of •OH (Xu et al., 2015; Yuan et al., 2019). Similarly, SO_4^{2-} showed a strong affinity towards the TiO_2 surface compared to the Cl^- ions. Hence, preferably are attracted by the catalyst surface over TC and SMZ. This results from the inhibition of TC and SMZ degradation (Dionysiou et al., 2000; Lin et al., 2016). Furthermore, SO_4^{2-} ions are recognized as an efficient h^+/•OH quencher (Selvam et al., 2007). This resulted in an apparent decrease in removal efficiency of TC and SMZ in the presence of $CuSO_4$.

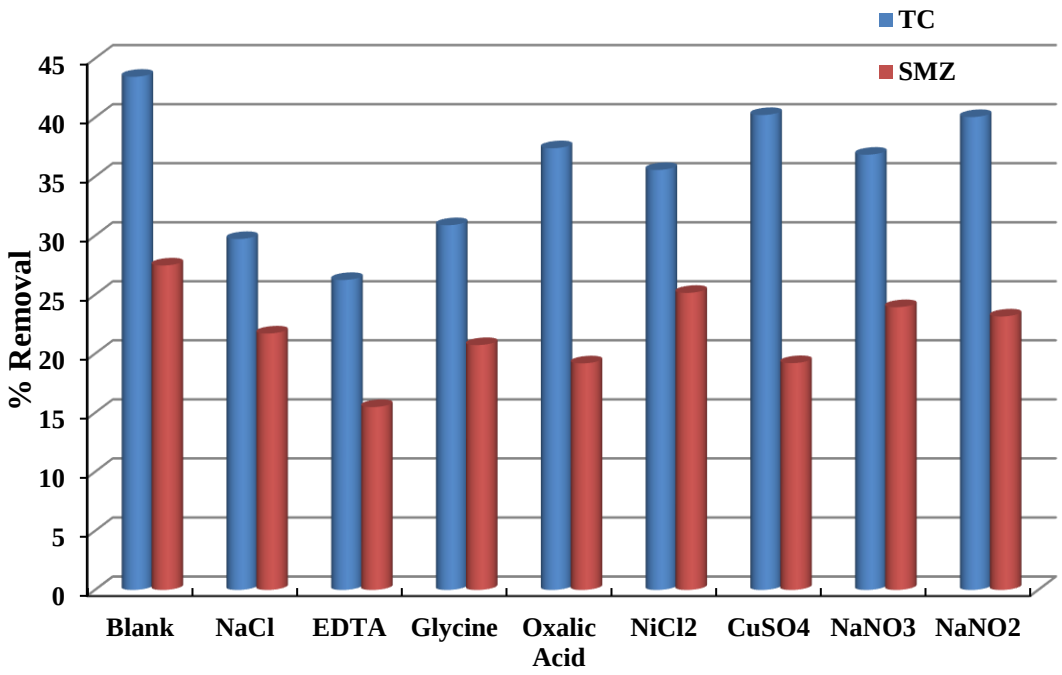

Figure 3.2.1.14.: Effect of Coexisting Ions (100.0 mg/L) in the photocatalytic degradation of TC [10.0 mg/L; pH:10.0] and SMZ [10.0 mg/L; pH:6.0] using Clay/Ag/TiO_2(T) under LED (Visible Light) irradiation.

3.2.1.14.1. Degradation Mechanism of Tetracycline (TC) and Sulfamethazine (SMZ)

The radical scavenger studies were extensively carried out to propose a plausible mechanism in the photocatalytic degradation of TC and SMZ. The HCO_3^- and 2-propanol are effective scavengers of the hydroxyl radicals (Xu et al., 2015). EDTA inhibits the generated h^+ of the photocatalyst (Jia et al., 2017). Similarly, the NaN_3 traps the singlet oxygen created by the reaction of $O_2^{\bullet -}$ radical with h^+. Singlet oxygen is a very reactive state of oxygen, capable of degrading organic compounds in an aqueous solution (Hussain et al., 2016). Therefore, the photocatalytic degradation of TC and SMZ (10.0 mg/L each) using Clay/Ag/TiO_2(T) photocatalyst under LED (Visible) light irradiation was conducted in the presence of various scavengers *viz.*, 2-propanol, $NaHCO_3$, and NaN_3 (1000.0 mg/L each). The percentage elimination of TC and SMZ in the presence of these scavengers is illustrated in Figure 3.2.1.14.1(a). The results indicated that the percentage elimination of TC and SMZ was significantly

hindered in the presence of 2-propanol and $NaHCO_3$. This revealed that the •OH radicals highly mediated the photocatalytic degradation of TC and SMZ.

Furthermore, previously it was observed that the addition of EDTA significantly suppressed the elimination of both these pollutants. These results showed that the degradation of TC and SMZ is predominantly proceeded through the •OH radicals. Additionally, the existence of NaN_3 also inhibited the degradation of both antibiotics, suggesting that singlet oxygen was involved in the oxidation of TC and SMZ.

Therefore, these results further enabled us to deduce the mechanism in the degradation of TC and SMZ. The absorption of light by the thin-film photocatalyst excites the electron from the VB to the CB (Díaz-Uribe et al., 2018). The excited electrons are trapped by the Ag^0(NPs) efficiently preventing the recombination of e^- /h^+ pairs. The electron trapped by the Ag^0(NPs) undergoes the formation of $O_2^{\bullet -}$ radical, which further facilitate the generation of •OH radicals. On the other hand, h^+ generated in the VB reacts with an oxygen molecule, which results the generation of $O_2^{\bullet -}$ radicals. This again leads to formation of •OH radical, as shown in Figure 3.2.1.14.1.(b) (Xu et al., 2012; Vogna et al., 2004). Moreover, the Ag^0(NP) itself absorbs light radiations and lead to the LSPR (localized surface Plasmon resonance) effect (D. Wang et al., 2018a). This causes the local excitation and simultaneous generation of e^-/h^+ pairs with Ag(NP). Moreover, the recombination of e^-/h^+ pairs were successively suppressed. This synergizes the degradation of TC and SMZ in the photocatalytic process (Figure 3.2.1.14.1(b)) (Saavedra et al., 2014; Xu et al., 2012).

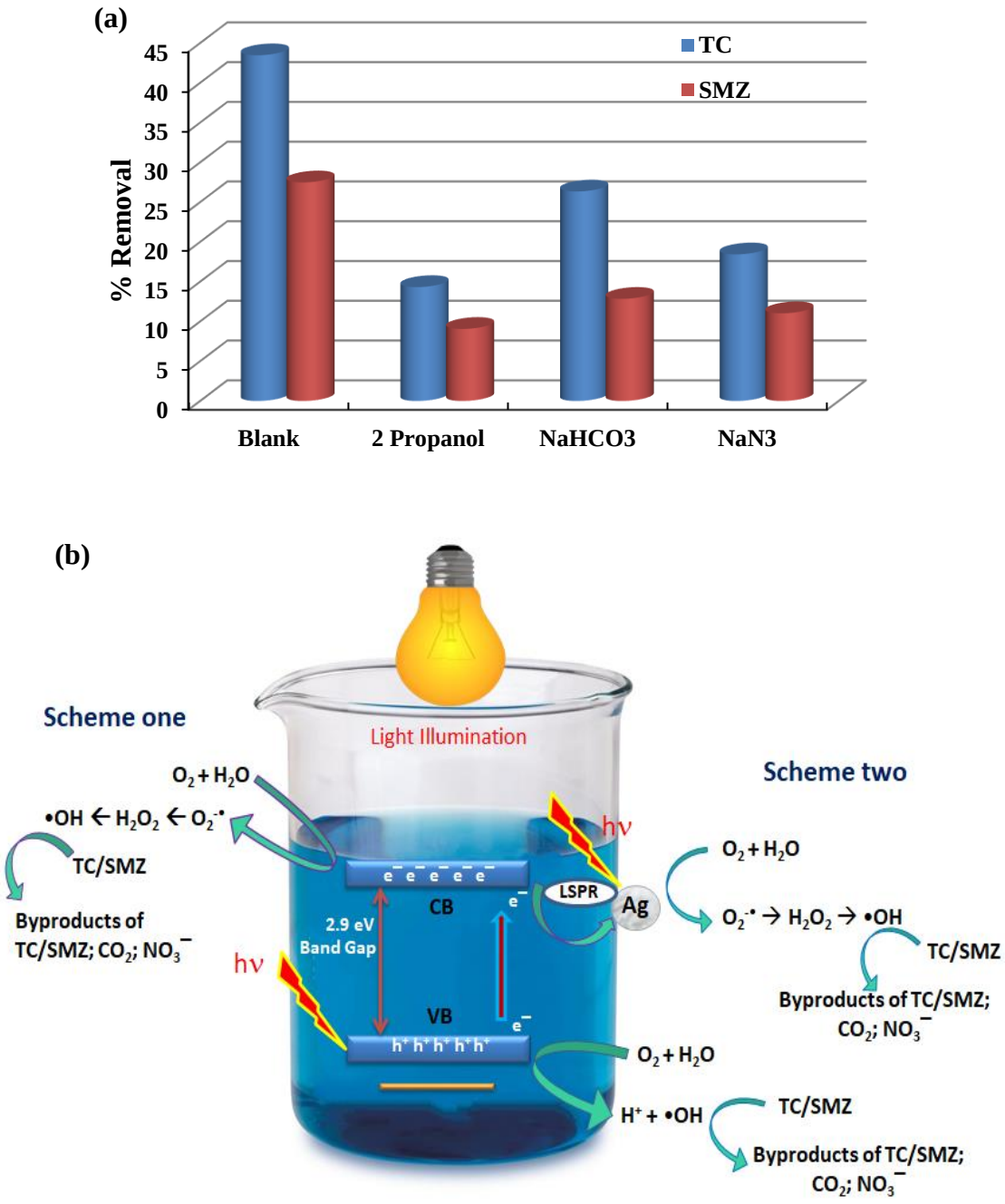

Figure 3.2.1.14.1.: (a) Effect of Scavengers (1000.0 mg/L) in the photocatalytic degradation of TC [10.0 mg/L; pH:10.0] and SMZ [10.0 mg/L; pH:6.0] using Clay/Ag/TiO_2(T) under LED (Visible Light) irradiation; (b) Schematic representation of the photocatalytic degradation of TC and SMZ using the Clay/Ag/TiO_2(T) thin film photocatalyst.

3.2.1.15. Effect of Coexisting Ions in the Photocatalytic Degradation of Bisphenol A (BP-A)

Studies were carried out to determine the photocatalytic removal of BP-A in the presence of several coexisting ions such as glycine, and oxalic acid, NaCl, EDTA, $NaNO_3$, $CuSO_4$, $NaNO_2$, and $ZnCl_2$. The thin film photocatalyst Clay/Ag/TiO_2(T) under LED (Visible Light) was employed and the initial concentration of BP-A was taken 10.0 mg/L at pH 8.0 and the concentrations of each ion was taken 100.0 mg/L. Figure 3.2.1.15 depicts the elimination of BP-A in the presence of these co-ions. As shown in Figure 3.2.1.15., the presence of various ions had varying effects in the elimination of BP-A. The percentage removal of BP-A was significantly suppressed in the presence of NaCl, $NaNO_3$, EDTA, and glycine. to stabilize the adsorption (Sowmiya and Senthilkumar, 2015). According to DFT molecular dynamics simulations, glycine is readily adsorbed on the TiO_2 surface through its zwitterion form, favourably by deprotonation of the carboxyl group, forming a (2 × 1) overlayer (Thompson and Yates, 2006). Sowmiya and Senthilkumar, proposed a binding model for TiO_2 and glycine in which the adsorbate binds to the TiO_2 surface through the -COOH end (by forming the oxygen bridge) and also to a surface oxygen ion through the $–NH_2$ end (by forming hydrogen bonding). Here, the hydrogen bonding through the amine group helps

Furthermore, various ions and molecules are capable of trapping radical species, which hampers the breakdown process. EDTA was reported to decrease the formation of •OH by reducing the generation of the hole (h^+) in TiO_2 photocatalysts (Xu et al., 2015; Yuan et al., 2019).

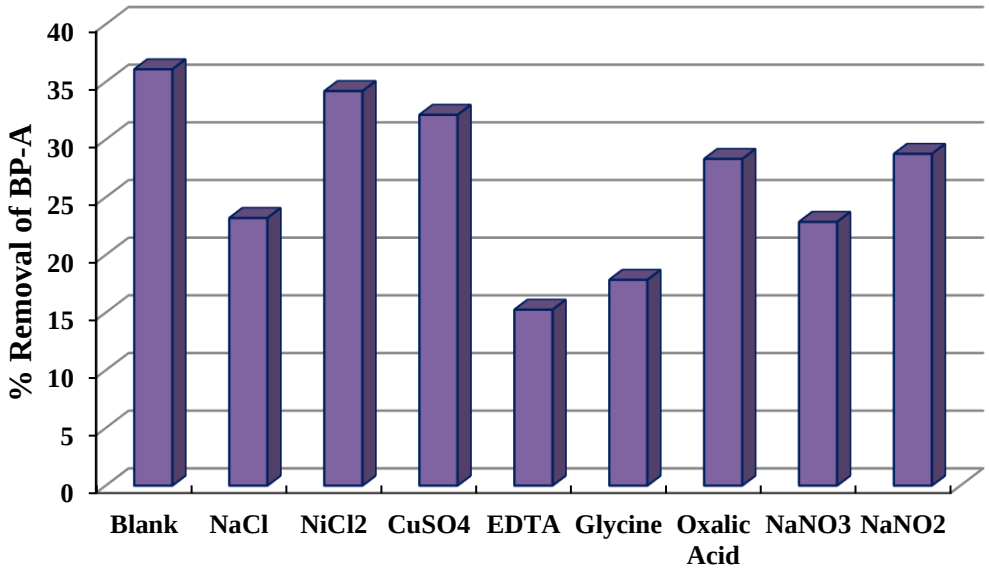

Figure 3.2.1.15.: Effect of Coexisting Ions (100.0 mg/L) in the photocatalytic degradation of BP-A [10.0 mg/L; pH: 8.0] using Clay/Ag/TiO_2(T) under LED (Visible Light) irradiation.

3.2.1.15.1. Degradation Mechanism of Bisphenol A (BP-A)

It is further important to investigate the mechanism involved in the degradation of BP-A under the photocatalytic reactor operations. Therefore, the photocatalytic elimination of BP-A (10.0 mg/L) was carried out in the presence of radical scavengers viz., $NaHCO_3$, 2-propanol, and NaN_3 (1000.0 mg/L each) utilizing Clay/Ag/TiO_2(T) photocatalyst under LED (Visible Light). Figure 3.2.1.15.1. shows the percentage elimination of BP-A in the presence of these scavengers. The percentage removal of BP-A was severely hampered in the presence of 2-propanol and $NaHCO_3$, as illustrated clearly in Figure 3.2.1.15.1. This demonstrated that •OH radicals were profoundly involved during the photocatalytic degradation of BP-A (Hussain et al., 2016). Also, the use of EDTA significantly inhibited the removal of the BP-A (contained within the coexisting ions). This indicated that the hole (h^+) was simultaneously taken part in the formation of •OH radicals and involved in the degradation of BP-A. Furthermore, the presence of NaN_3 caused suppression of the elimination of BP-A, implied that singlet oxygen was also involved in the oxidation process (Demyanenko et al., 2019).

Finally, the scavenging experiments revealed that in the presence of LED light, the Clay/Ag/TiO_2(T) thin-film photocatalyst caused photocatalytic degradation of BP-A via two distinct mechanisms. The photon causes the excitation of electrons from the VB to the CB in the photocatalyst. The excited electrons at the CB are then quickly trapped by Ag(NPs). This effectively disallowed the recombination of e^-/h^+ pairs. The trapped e^- by the Ag0(NPs) undergoes further reactions with H_2O and O_2, resulting in the formation of the $O_2^{\bullet-}$ radical. This further results in the generation of the •OH radical (Ajmal et al., 2014). Simultaneously, h^+ formed in the VB reacts with molecules of O_2, resulting in the generation of reactive $O_2^{\bullet-}$ radicals. This results in the formation of •OH radical (El Mragui et al., 2021). The second reaction mechanism is that the Ag^0(NP) absorbs photons of light and causes a phenomenon known as LSPR (localized surface Plasmon resonance) (Eom et al., 2013). The electrons get excited from their ground states, and there occurs rapid collective oscillation of electron density on the noble metals, which results in the induction of surface plasmons (Wang et al., 2018a; Zanella et al., 2018). When the wavelength of the incoming light radiation is dimensionally greater than the wavelength of the nanoparticles, then there is a resonance between the frequency of the electron cloud and the frequency of the incident light. This resulted in the generation of an electromagnetic field in the vicinity of the nanoparticles (Lal et al., 2007). As a result, the TiO_2 was stimulated locally, resulting in the formation of e^-/h^+ pairs. Thus, the •OH radicals, which are essential for BP-A degradation, were then produced simultaneously and synergised the oxidation of BP-A molecules.

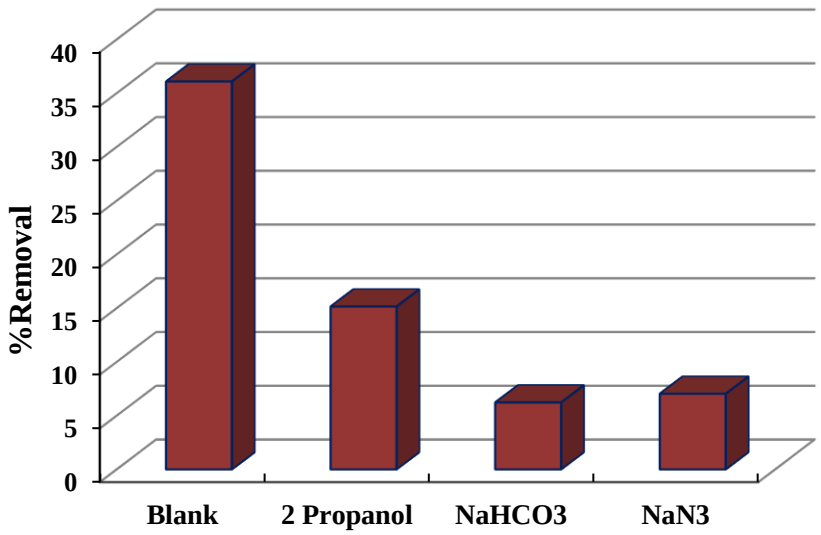

Figure 3.2.1.15.1.: Effect of Scavengers (1000.0 mg/L) in the photocatalytic degradation of BP-A [10.0 mg/L; pH: 8.0] using Clay/Ag/TiO_2(T) under LED (Visible Light) irradiation.

3.2.1.16. Effect of Coexisting Ions in the Photocatalytic Degradation of Rhodamine B (Rh-B) and Rhodamine 6G (Rh-6G)

Similarly, the photocatalytic removal of Rh-B and Rh-6G in the presence of several coexisting ions viz., glycine, $ZnCl_2$, oxalic acid, NaCl, $NaNO_2$, EDTA, $CuSO_4$ and $NaNO_3$ is carried out using the thin film photocatalyst Clay/Au/TiO_2(T) and under the LED light illumination. The initial concentration of Rh-B and Rh-6G was taken 10.0 mg/L at pH 6.0 and each ion's concentration was taken to 100.0 mg/L. Figure 3.2.1.16. demonstrates the removal of Rh-B and Rh-6G in the presence of these co-ions. The presence of various ions had variable effects in the removal of Rh-B and Rh-6G, as shown in Figure 3.2.1.16. The NaCl, $NiCl_2$, EDTA and glycine significantly suppressed the removal of Rh-B, however, the other co-ions showed insignificant effect in the photocatalytic degradation of these Rh-B. Similarly, the elimination of Rh-6G was also suppressed in the presence of NaCl, $NiCl_2$, EDTA, oxalic acid and glycine. Usually, the preferential sorption of ions on the photocatalyst's surface, prevents the sorption of target molecules on the catalyst surface hence, causing

reduced elimination (Sofyan et al., 2019; Yong et al., 2002). Additionally, different ions and molecules are having the ability to trap radical species, inhibiting the breakdown process. In TiO_2 photocatalysts, the EDTA scavenges the generation of •OH by lowering the formation of hole (h^+) (Meichtry et al., 2014). From DFT molecular dynamic studies, the surface of TiO_2 readily adsorbs the glycine molecules in its zwitterion state, with deprotonation of the carboxyl group (Thompson and Yates, 2006). Similarly, the competitive adsorption of Na^+ ions towards the TiO_2 surface inhibits the degradation efficiency of catalysts in presence of Na^+ (Sofyan et al., 2019; Yong et al., 2002). Direct oxidation/reduction of oxalic acid takes place at the TiO_2 surface by the formation of hole-electron pairs under light irradiation, which inhibits the target pollutant to be degraded (Mendive et al., 2015).

3.2.1.16.1. Degradation Mechanism of Rhodamine B (Rh-B) and Rhodamine 6G (Rh-6G)

In order to provide a probable mechanism involved during the degradation of Rh-B and Rh-6G, it is necessary to investigate the reaction steps that occur during the photocatalytic reaction. The hydroxyl radicals were known to scavenge by HCO_3^- and 2-propanol (S et al., 2012). EDTA suppresses the generation of h^+ during the reaction (Meichtry et al., 2014). Similarly, NaN_3 traps the singlet oxygen created by the reaction of the $O_2^{\bullet -}$ radical with h^+. Singlet oxygen is a highly reactive radical in an aqueous medium, capable of quickly removing organic molecules (Aldred et al., 2009). Therefore, photocatalytic degradation of Rh-B and Rh-6G (10.0 mg/L) was performed using Clay/Au/TiO_2(T) thin film photocatalyst in the presence of $NaHCO_3$, NaN_3 and 2-propanol (1000.0 mg/L each) under visible light irradiation. Figure 3.2.1.16. depicts the percentage removal of Rh-B and Rh-6G in the presence of these scavengers. With the addition of 2-propanol and $NaHCO_3$, the percentage removal of R-B and R-6G was considerably inhibited. This showed that •OH radicals are predominantly involved in the photocatalytic breakdown of both the dyes (Kaur et al., 2019). In addition, EDTA also suppressed the removal efficiency of both dyes (included in Coexisting ions). This implies that the holes (h^+) are also involved in the formation of •OH radicals, which are taking part in the removal of Rh-B and Rh-6G.

Furthermore, the addition of NaN_3 also significantly inhibited the degradation of both the dyes; it concluded that singlet oxygen was produced during the oxidation process (Nosaka et al., 2004). As a result, these studies demonstrated that the thin-film photocatalyst triggered photocatalytic degradation of Rh-B and R-6G via two distinct pathways in light. Excitation of electrons takes place from the valence band (VB) to the conduction band CB, when the light illuminates the semiconductor. The electrons excited at the CB were promptly taken by the Au(NPs), preventing the e^-/h^+ pair recombination. The trapped electrons at the Au^0(NPs) react again with H_2O and O_2, yielding the $O_2^{\bullet -}$ radical. Consequently, the •OH radical is generated (Ajmal et al., 2014). Simultaneously, h^+ produced in the VB interacts with O_2 molecules to produce an $O_2^{\bullet -}$ radical. As a result, the •OH radical is formed (El Mragui et al., 2021). Another possibility for the degradation mechanism is that Au^0(NP) absorbs incoming light radiation and generates LSPR (localised surface Plasmon resonance) effect, which is a collective oscillation of free conduction electrons of Au(NPs) (X. Li et al., 2009). These oscillating electrons, also called hot electrons, can jump to the conduction band of the TiO_2. This electron then interacts with oxygen molecules in the presence of water molecules, leading to the formation of •OH radicals.

Further, the •OH radicals then interact with the dye molecules, resulting in the photocatalytic breakdown of R-B and R-6G. The LSPR effect also leads to the generation of intense electric fields near the surface of metal NPs. This permits plasmonic Au(NPs) to behave as nanoantenna, concentrating and amplifying light in the vicinity of TiO_2 surface. This increases the light absorption in a nearby semiconductor (TiO_2) (Kumar et al., 2021).

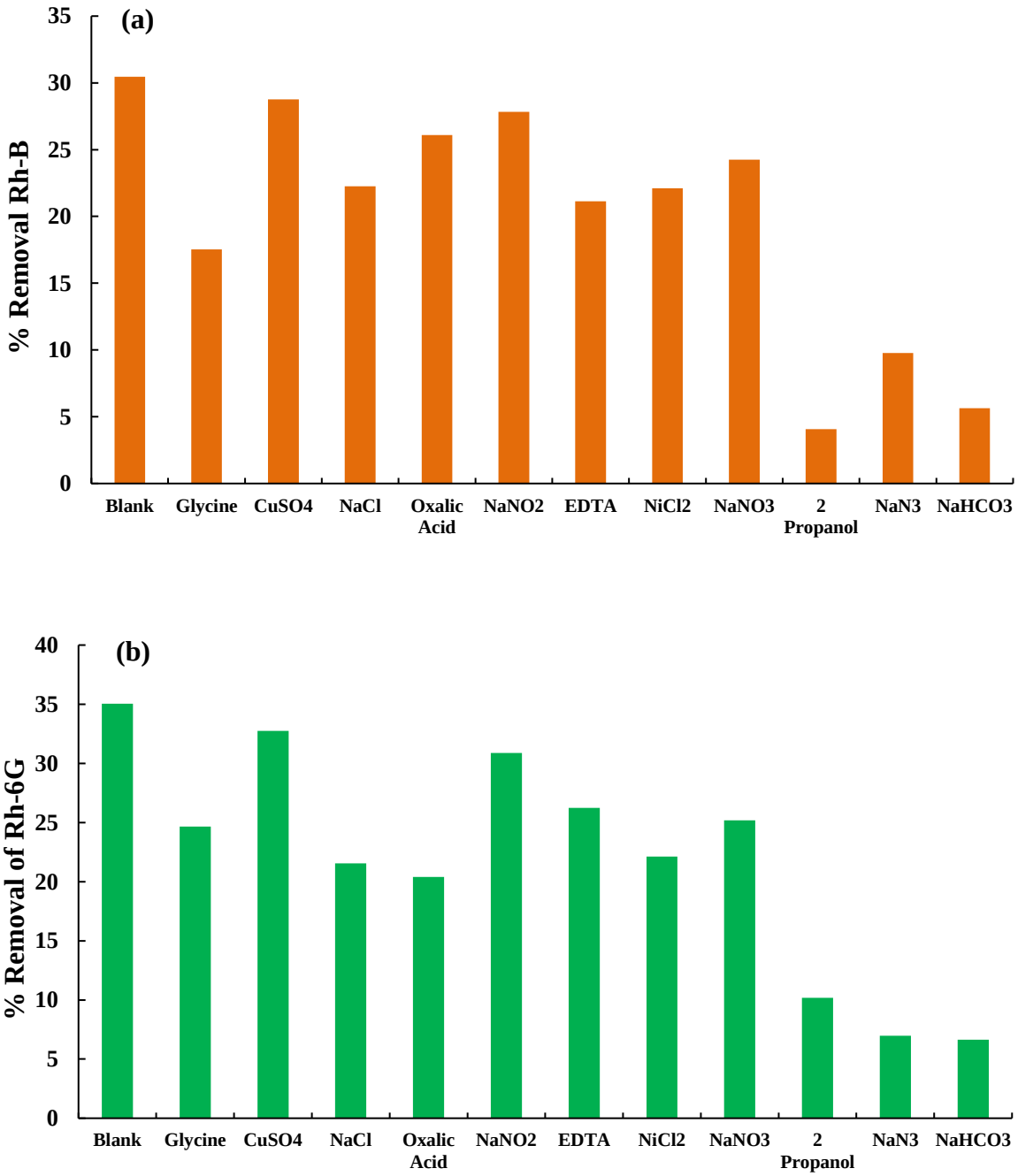

Figure 3.2.1.16.: Effect of Coexisting Ions (100.0 mg/L) and Scavengers (1000.0 mg/L) in the photocatalytic degradation of a) Rh-B [5.0 mg/L; pH:6.0] and b) Rh-6G [5.0 mg/L; pH:6.0] using Clay/Au/TiO_2(T) under LED (visible light) irradiation.

In order to study the possible degradation mechanism of Rh-B and Rh-6G, liquid chromatography-mass spectrometry (LC-MS) analyses were performed. Both the

dyes [5.0 mg/L; pH:6.0] were treated for 1 hrs under photocatalytic treatment using the Clay/Au/TiO_2(T) thin film catalyst under visible light irradiation. The initial solution and the treated solution of Rh-B and Rh-6G were analysed by the LC-MS, and the by-products formed in the degradation process were identified. The positive ion mode mass spectra were used to identify the compounds. On the basis of m/z values of by-products obtained during the course of treatment, a plausible degradation mechanism of Rh-B and Rh-6G is proposed in Figure 3.2.1.16.1. (a) and (b), respectively. It was observed that the degradation reaction of Rh-B and Rh-6G were induced by the hydroxyl radical (•OH). Mass peak at m/z 443 (Base peak) was observed for both the dye solutions i.e., Rh-B and Rh-6G (blank solution), and is attributed to the Rh-B and Rh-6G molecules of a chloride ion.

In case of Rh-B, peak at m/z 415 is assigned to the de-ethylated intermediates of Rh-B (Path 2). After losing a fragment of 74 mass units {$(C_2H_5)_2NH$}, it undergoes a decarboxylation reaction (Path 1). The hydroxyl radical (•OH) attacks the double bond on the aromatic ring and causes the molecules to undergo ring opening and are eventually decomposed into CO_2, NH_4^+ and H_2O. Further, the signal at m/z 74 was relatively strong. This peak suggests that the $(C_2H_5)_2NH$ fragment was not broken down into small molecules while the parent compounds are successfully decomposed into CO_2, NH_4^+ and H_2O.

In the case of Rh-6G, peak at m/z 415 is designated to the de-esterification (or hydrolysis) by-product of Rh-6G (Path 1 & 2), and the de-ethylated intermediates of Rh-6G (Path 3). The de-esterification by-product of Rh-6G then undergoes decarboxylation reaction followed by rearrangement reaction and gives the reaction intermediate with m/z 272. This undergoes ring opening with the production of CO_2, NH_4^+ and H_2O (Path 1). The de-esterification by-product of Rh-6G also undergoes with a fragmentation reaction in which benzoic acid is released as a by-product and the parent aromatic ring undergoes with ring opening with the formation of CO_2, NH_4^+ and H_2O (Path 2). Further, the de-ethylated intermediates of Rh-6G undergo ring opening with the elimination of CO_2, NH_4^+ and H_2O (Path 3).

The ring-opening of the intermediate from Paths 1, 2, and 3 leads to the generation of benzoic acid (m/z 122), oxalic acid (m/z 90), and other small molecules. These molecules are further oxidized by hydroxyl radical (•OH) and decomposed into CO_2 and H_2O. Similar by-products were also reported for R-B and R-6G, including gradual de-ethylation and breaking of the double bond of the benzene ring (Yang and Yang, 2018; Rajoriya et al., 2016).

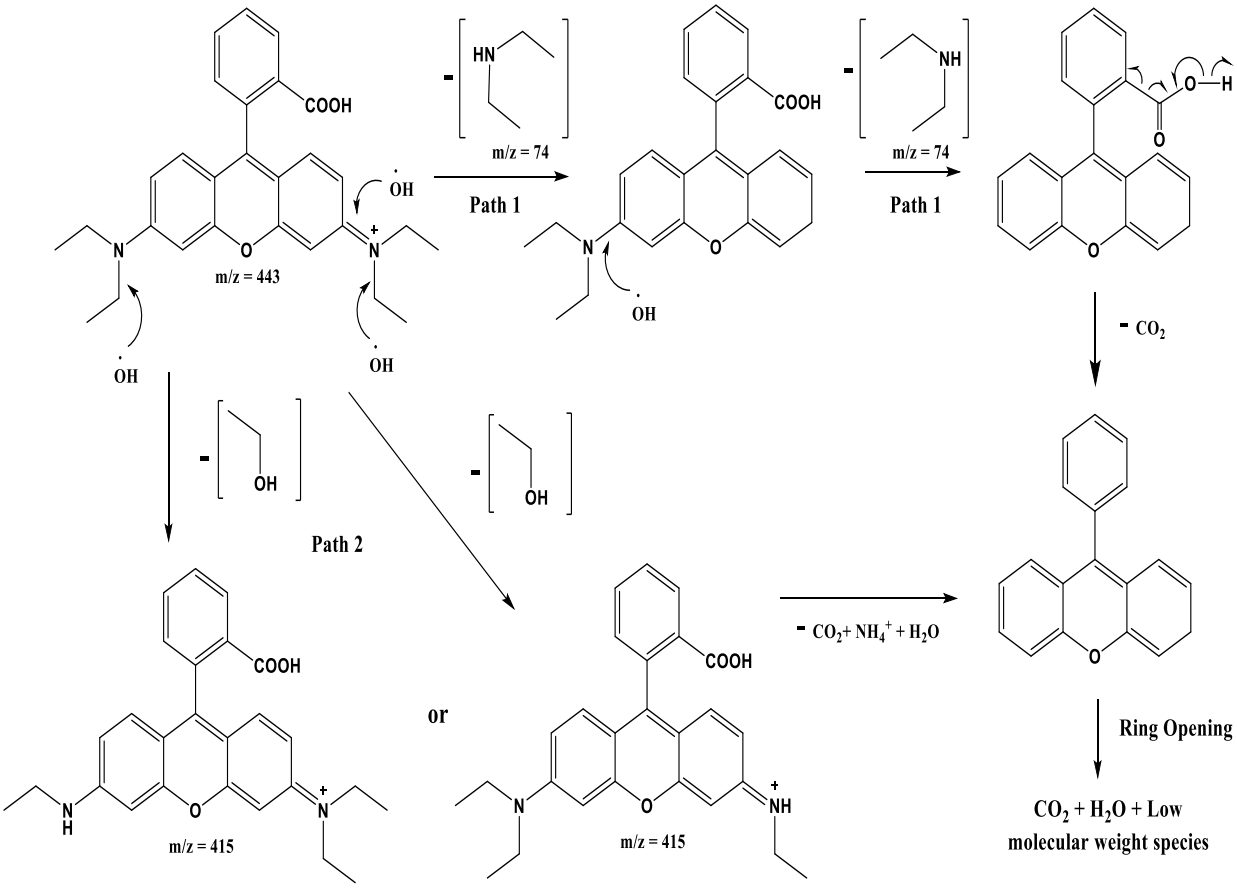

Figure 3.2.1.16.1.(a): Mechanism of the photocatalytic degradation of Rh-B [5.0 mg/L; pH:6.0] using Clay/Au/TiO_2(T) thin film under visible light irradiation.

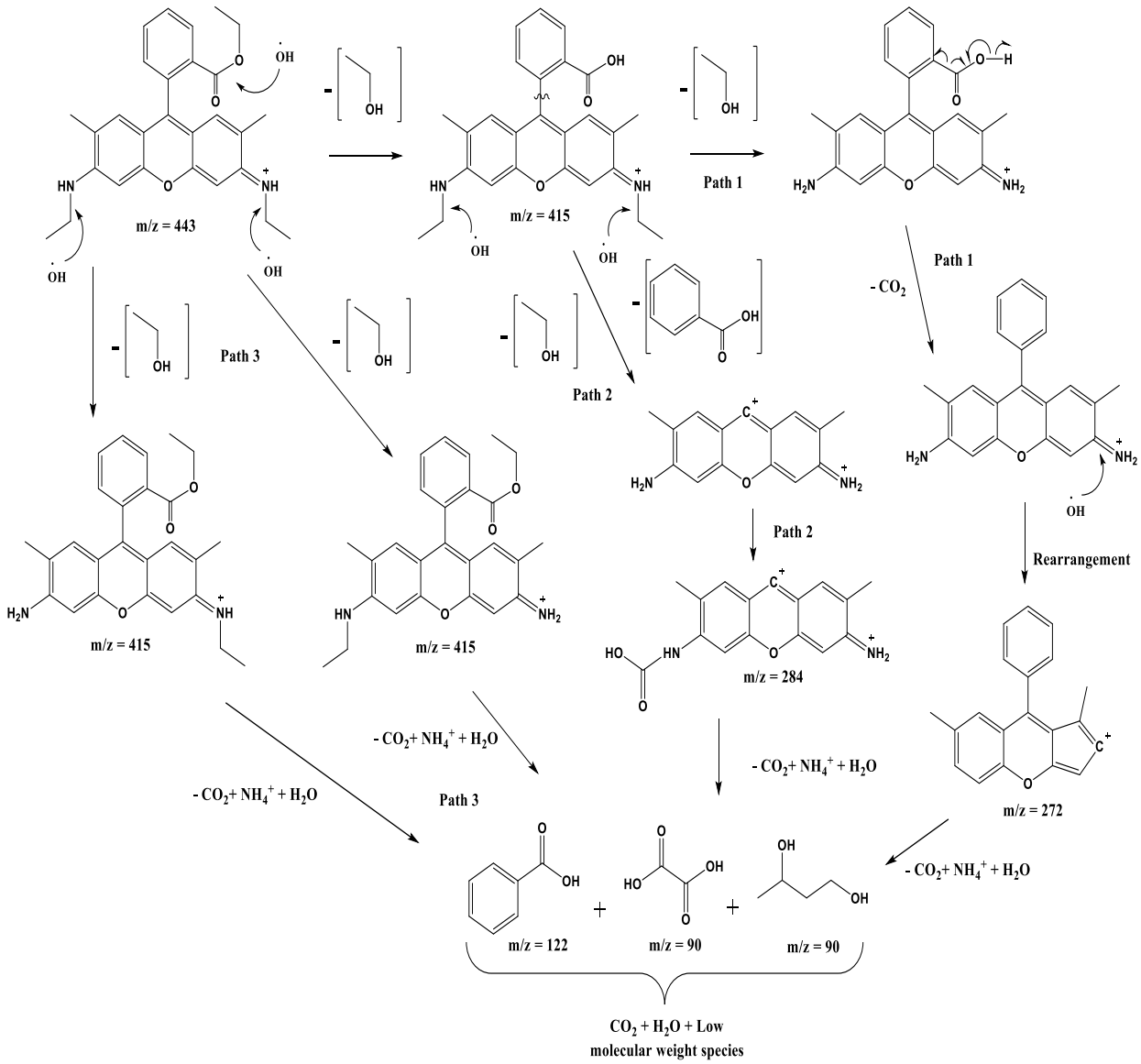

Figure 3.2.1.16.1.(b): Mechanism of the photocatalytic degradation of Rh-6G [5.0 mg/L; pH:6.0] using Clay/Au/TiO_2(T) thin film under visible light irradiation.

3.2.1.17. Reusability of Thin Film in the Photocatalytic Degradation of Mordant Orange 1 (MO1)

The efficacy of the photocatalyst largely depends on its reusability for successive reactor operations. Therefore, the reusability of Ag^0(NP)/TiO_2

nanocomposite thin film photocatalyst is carried out for repeated reactor operations in the elimination of MO1 (MO1 concentration: 5.0 mg/L; pH 6.0). The percentage elimination of MO1 as a function of repeated cycle of reactor operations is shown in Figure 3.2.1.17. The degradation efficiency of the photocatalyst is almost unaffected even at the end of six successive cycles of reactor operations. Quantitatively, the percentage degradation of MO1 is decreased only from 40.29% to 40.23% (i.e., 0.06%). The results show that the thin film catalyst is reasonably stable towards the reactor operations in photocatalytic degradation of MO1. Hence, the photocatalyst is shown to be employed for prolonged and sustainable operations.

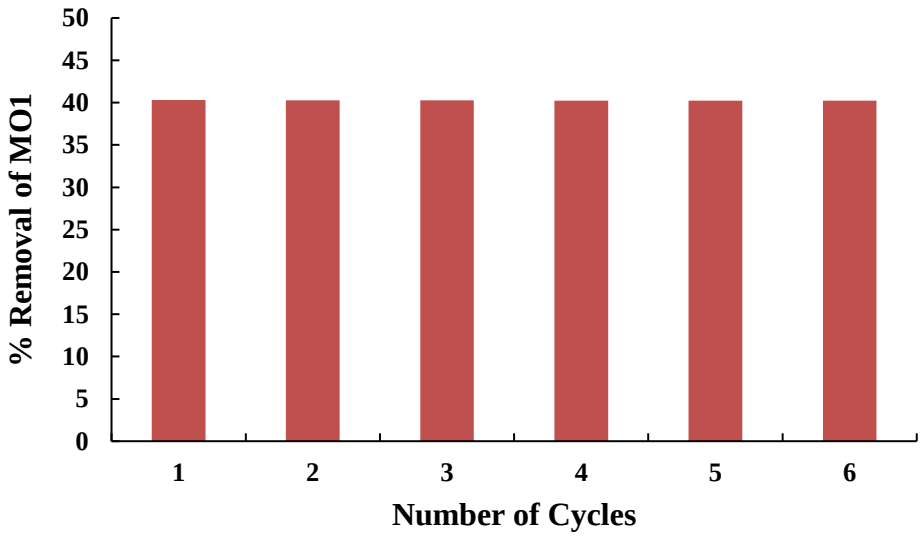

Figure 3.2.1.17.: Removal efficiency of MO1 (5.0 mg/L; pH 6.0) after 6 repeated cycles of Ag^0(NP)/TiO_2 catalyst operations.

3.2.1.18. Reusability of Thin Film in the Photocatalytic Degradation of Tetracycline (TC) and Sulfamethazine (SMZ)

The stability of the photocatalyst is essential and challenging for prolonged and sustainable use of catalysts in reactor operations. Therefore, the photocatalytic degradation of TC and SMZ in aqueous solutions was conducted for repeated reactor operations (six times) using the thin film Clay/Ag/TiO_2(T) catalyst under LED (Visible Light), and the results are shown in Figure 3.2.1.18. The repeated operations were

conducted, as usual; at the end of each cycle, the disk was rinsed with purified water and dried at 300°C for 1 hrs. The dried catalyst was again subjected to the subsequent reactor operations. The initial concentration and solution pH of TC was 10.0 mg/L and pH 10.0, respectively. Similarly, the solution pH and starting concentration of SMZ was maintained at pH 6.0 and 10.0 mg/L, respectively. The removal efficiency of TC and SMZ are shown in Figure 3.2.1.18. The results indicated that the catalyst is reasonably stable since the removal efficiency of TC and SMZ was not affected even after the six repeated operations. Quantitatively, completing the six cycles of operations caused only a 1.13 and 1.25% decrease in removal efficiency, respectively, for TC and SMZ. The results demonstrated that the nanocatalyst is reasonably stable and showed potential in the scale-up reactor operations. Previously it was reported that Fe-doped TiO_2 film showed reasonably good stability in the photocatalytic degradation of methylene blue as attempted for three repetitive time cycles (Bansode et al., 2015).

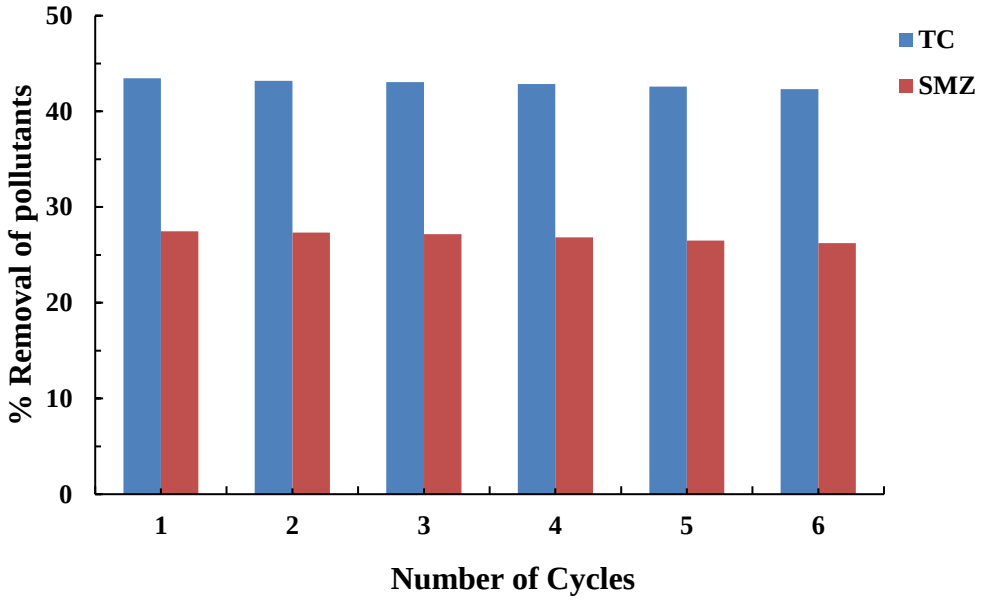

Figure 3.2.1.18.: Removal efficiency of TC (10.0 mg/L; pH 10.0) and SMZ (10.0 mg/L; pH 6.0) after 6 repeated cycles of Clay/Ag/TiO_2(T) catalyst operations.

3.2.1.19. Reusability of Thin Film in the Photocatalytic Degradation of Bisphenol A (BP-A)

The thin film Clay/Ag/TiO_2(T) catalyst was employed for the repeated photocatalytic degradation of BP-A under LED (Visible Light) irradiation. The results are displayed in Figure 3.2.1.19. After completion of each cycle, the thin film catalyst was cleaned with distilled water and then dried for 1 hrs at 300°C in a drying oven. The successive photocatalytic cycle was then carried out using the dried thin film. The initial concentration and pH of the solutions were kept at 10.0 mg/L and 8.0, respectively. Figure 3.2.1.19 inferred that even after 6 cycles of photocatalytic operations, the removal efficiency of the catalyst was almost unaffected at least in the elimination of BP-A. More specifically, the percentage of BP-A elimination was decreased only from 36.09% to 35.02% (i.e., a 1.07% decrease) at the end of the sixth cycle of operations. These results showed that the thin film photocatalyst is reasonably stable throughout the repeated photocatalytic operations. This increases the utility of thin-film in various wastewater treatment technologies for real implications (Tiwari et al., 2019).

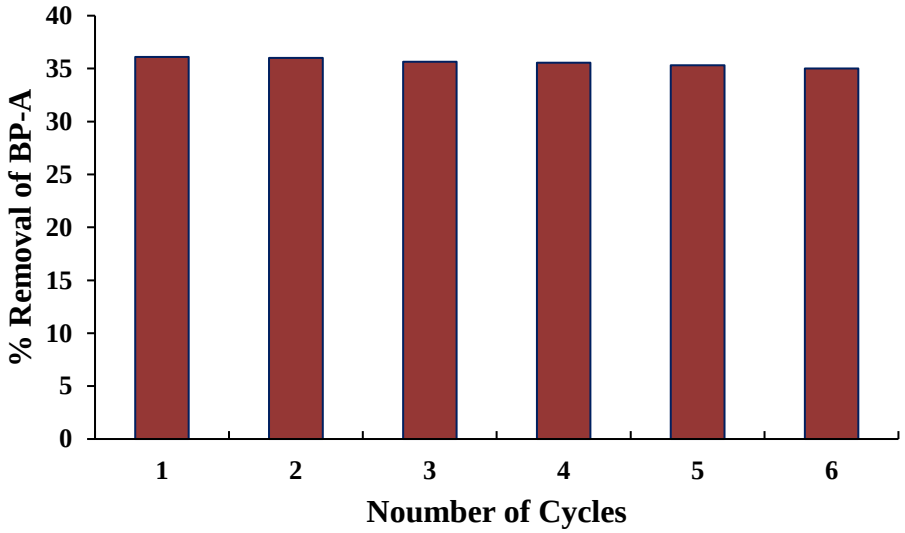

Figure 3.2.1.19.: Removal efficiency of BP-A (10.0 mg/L; pH 8.0) after 6 repeated cycles of Clay/Ag/TiO_2(T) catalyst operations.

3.2.1.20. Reusability of Thin Film in the Photocatalytic Degradation of Rhodamine B (Rh-B) and Rhodamine 6G (Rh-6G)

Extended and recurring photocatalytic activity is crucial for real-world applicability of photocatalysts. This would bring the extent of stability of the nanocomposite material. As a result, the photocatalytic degradation of Rh-B and Rh-6G in an aqueous solution was repeated six times using a thin film Clay/Au/TiO_2(T) catalyst and the results are shown in Figure 3.2.1.20(a) and (b). The pH and initial concentration of both the dyes solution (Rh-B and Rh-6G) were taken at pH 6.0 and 10.0 mg/L, respectively. The percentage efficiency of dye removal using the photocatalyst remained essentially constant even after 6 cycles of treatment (*Cf* Figure 3.2.1.20(a) and (b)). After six repeated cycles photocatalytic degradation reaction, the efficiency of Rh-B removal was decreased from 30.45 % to 29.43 % (a drop of 1.02%) (Figure 3.2.1.20(a)) and that of the efficiency of Rh-6G removal was decreased from 35.05 % to 34.12 % (a drop of 0.93%) (Figure 3.2.1.20(b)). These results revealed that both the thin film photocatalysts are reasonably stable even for repeated photocatalytic treatments.

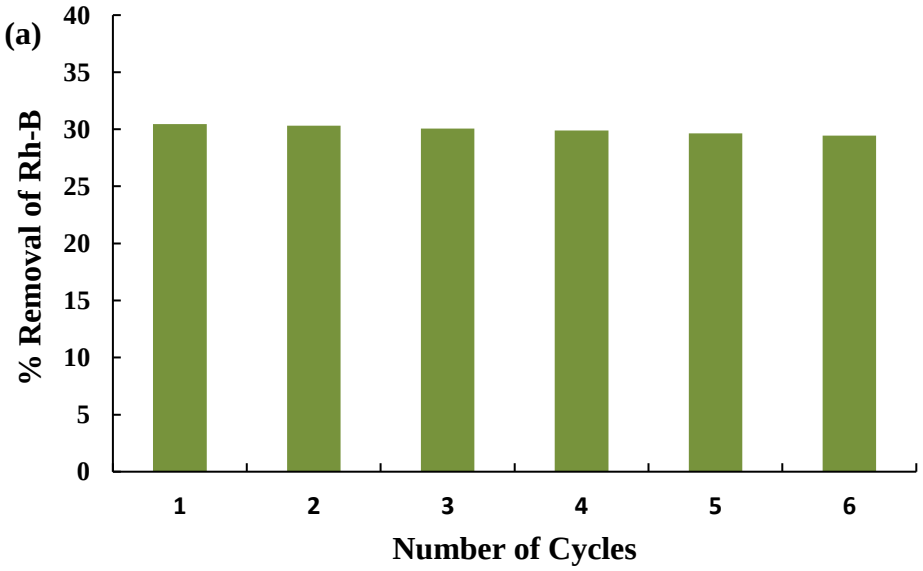

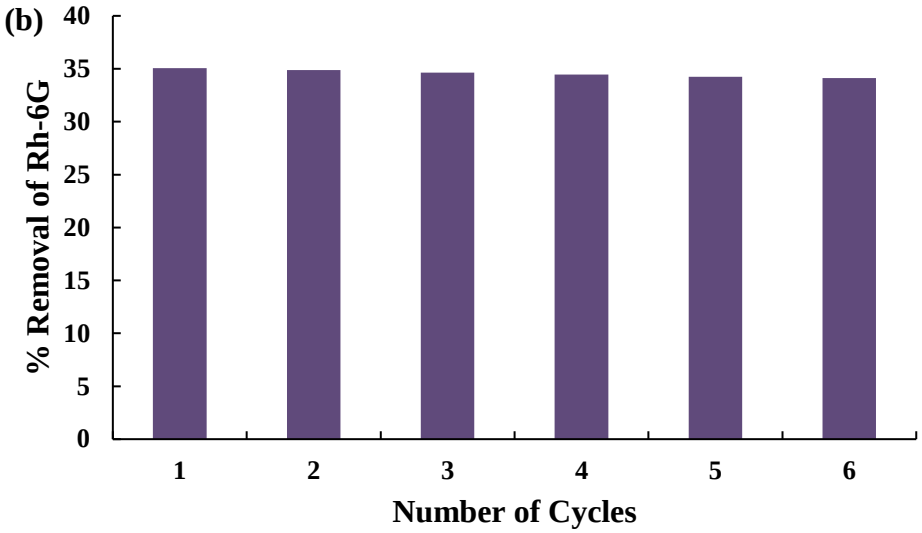

Figure 3.2.1.20: Removal efficiency of (a) Rh-B (5.0 mg/L; pH 6.0) and (b) Rh-6G (5.0 mg/L; pH 6.0) after 6 repeated cycles of Clay/Au/TiO_2(T) catalyst operations.

3.2.1.21. Mineralization of Mordant Orange 1 (MO1)

The extent of mineralization of pollutants in the photocatalytic treatment demonstrates the efficiency of operation. The percentage mineralization of MO1 is obtained at a wide range of concentration (1.0 to 20.0 mg/L; pH~6.0) using Ag^0(NP)/TiO_2 thin film catalyst. Results are shown in Figure 3.2.1.21, which indicated that decrease in concentration of MO1 from 20.0 to 1.0 mg/L had caused to increase the percentage mineralization of MO1 from 7.72 to 27.38% (for UV-A light) and from 4.12 to 17.1% (for LED light), respectively. These results further inferred that a single reactor operation enabled to significantly mineralize the percentage mineralization of MO1. The findings are similar to the concentration dependent studies conducted previously in the removal of MO1. On the other hand, the photolysis using the UV-A or LED irradiation showed almost negligible degradation of MO1. Therefore, the photocatalytic operations favoured the mineralization of MO1 using the Ag^0(NP)/TiO_2 nanocomposite thin film photocatalyst (Tiwari et al., 2015).

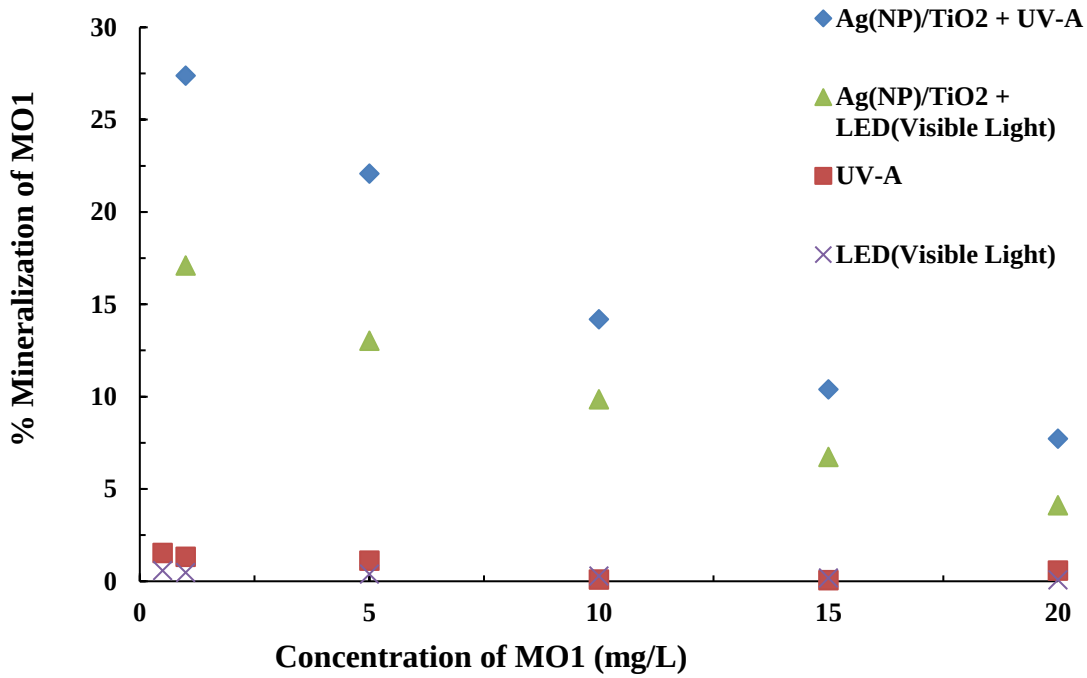

Figure 3.2.1.21.: Percentage mineralization of MO1 [pH:6.0] as a function of change in initial concentrations under photolytic and photocatalytic process using Ag^0(NP)/TiO_2 thin film.

3.2.1.22. Mineralization of Tetracycline (TC) and Sulfamethazine (SMZ)

Mineralization of pollutants in aqueous wastes is an important parameter in wastewater treatment strategies. Therefore, the mineralization of TC and SMZ was analysed using the NPOC (Non-Purgeable Organic Carbon) data. The NPOC was measured before and after the photocatalytic treatments. The concentrations of both the pollutants were increased from 0.5 to 20.0 mg/L, and solution pH was maintained at pH 10.0 and pH 6.0 for TC and SMZ, respectively. The reaction was carried out under LED (Visible Light) and UV-A light using both Clay/Ag/TiO_2 and Clay/Ag/TiO_2(T) catalysts. The pollutant solutions were treated for 2 hrs and 3 hrs, respectively, for TC and SMZ. The percentage mineralization of TC and SMZ as a function of pollutant concentrations is shown in Figures 3.2.1.22(a) and (b). Results showed that increasing the pollutant concentration caused a decrease in the mineralization percentage. Quantitatively, increasing the concentration of TC from 0.5

to 20.0 mg/L, the percentage mineralization was decreased from 31.3% to 18.2% (using the Clay/Ag/TiO_2(T) under LED (Visible Light)) and from 42.6% to 27.3% (using Clay/Ag/TiO_2(T) under UV-A light). On the other hand, increasing the SMZ concentration from 0.5 to 20.0 mg/L, the corresponding percentage mineralization was decreased from 20.1 to 10.4% (with Clay/Ag/TiO_2(T) under LED (Visible Light)) and from 34.2% to 21.8% (using Clay/Ag/TiO_2(T) under UV-A light). Furthermore, similar to the concentration dependence studies, the Clay/Ag/TiO_2(T) thin-film showed better catalytic efficacy in the percentage mineralization of these two pollutants as compared to the Clay/Ag/TiO_2 thin film. Moreover, the antibiotics were barely mineralized under photolysis using UV-A of LED (Visible light) irradiations. Thus, the mineralization studies inferred that the photocatalytic treatment of these recalcitrant pharmaceuticals enabled the mineralization of these two antibiotics significantly.

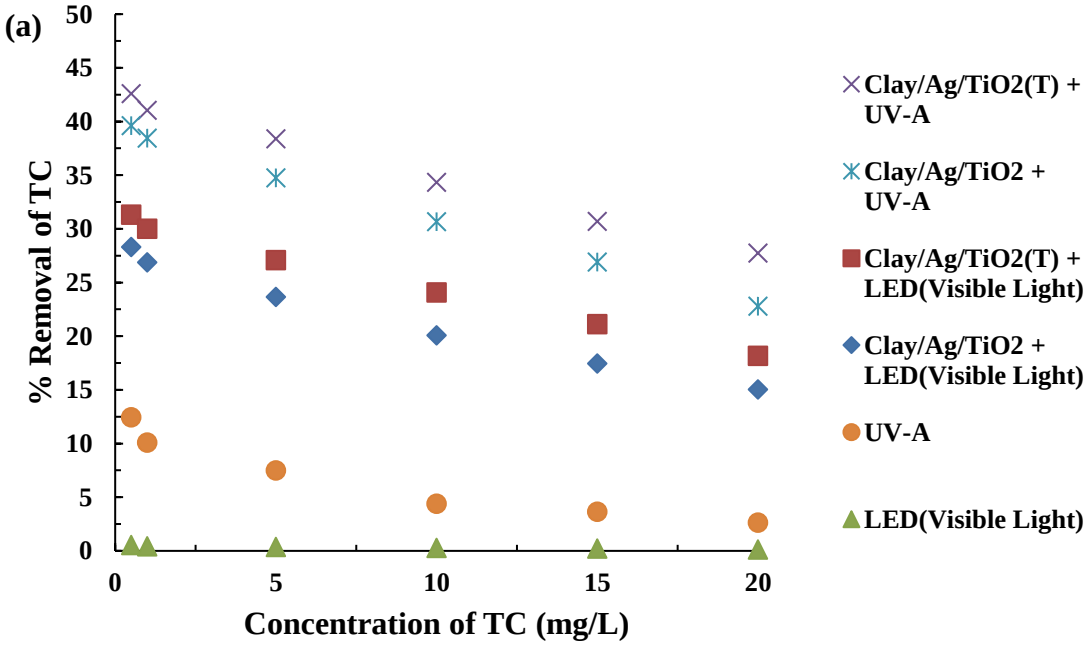

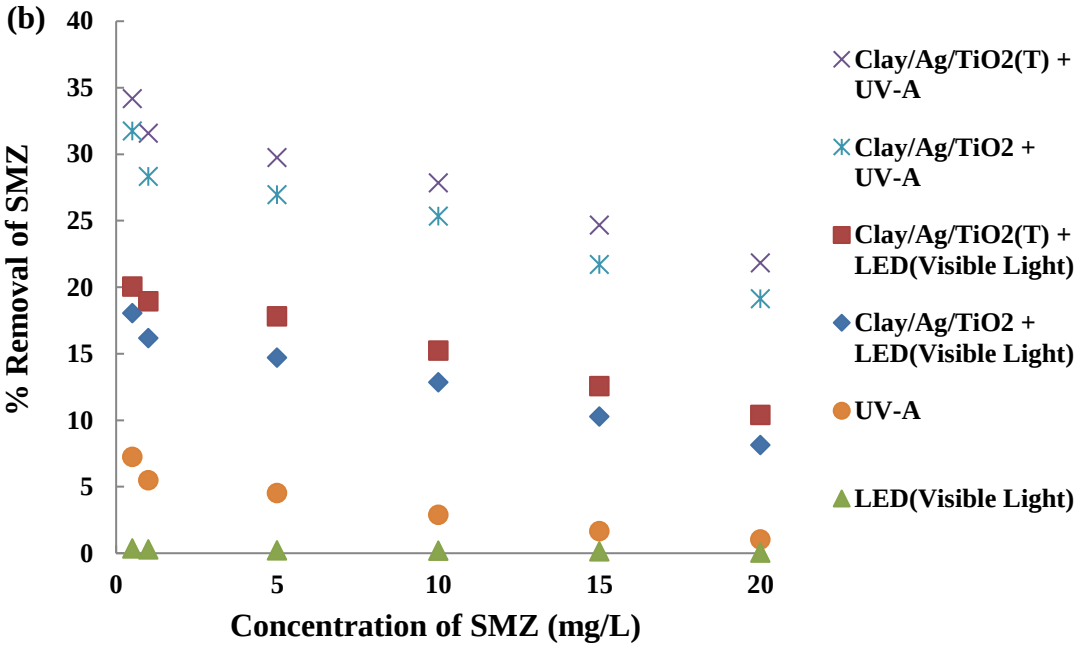

Figure 3.2.1.22: Percentage mineralization of (a) TC [pH:10.0]; and (b) SMZ [pH:6.0] as a function of change in initial concentrations under photolytic and photocatalytic process using Clay/Ag/TiO_2(T) thin film.

3.2.1.23. Mineralization of Bisphenol A (BP-A)

The mineralization of BP-A was obtained using the NPOC (Non-Purgeable Organic Carbon) data obtained for the treated and blank BP-A samples. The BP-A concentration was increased from 1.0 to 20.0 mg/L at 8.0. The pollutant solutions were photo catalytically treated for 4 hrs under LED (Visible Light) and UV-A light using Clay/Ag/TiO_2 and Clay/Ag/TiO_2(T) thin film catalysts. The percentage removal of NPOC as a function of BP-A concentrations is depicted in Figure 3.2.1.23. It indicated that the NPOC removal percentage was decreased with the increase in BP-A concentrations. More quantitatively, increasing the BP-A concentration from 1.0 to 20.0 mg/L, the corresponding NPOC percentage removal was decreased from 19.3% to 8.5% (using Clay/Ag/TiO_2 thin film) and from 27.5% to 14.3% (using Clay/Ag/TiO_2(T) thin-film) under LED (Visible Light). Similarly, the percentage of NPOC was decreased from 36.4% to 21.9% (using Clay/Ag/TiO_2 thin film) and from 45.8% to 26.2% (using Clay/Ag/TiO_2(T) thin-film) under UV-A light. Moreover,

compared to the photolytic reaction, the photocatalytic degradation reaction showed significantly enhanced mineralization of BP-A, which further indicated the applicability of thin film photocatalyst in the mineralization of BP-A in aqueous solutions. It was reported previously that a 20 hrs of treatment resulted with almost a complete mineralization (*Ca* 99%) of BP-A using TiO_2 under UV irradiation (Ohko et al., 2001).

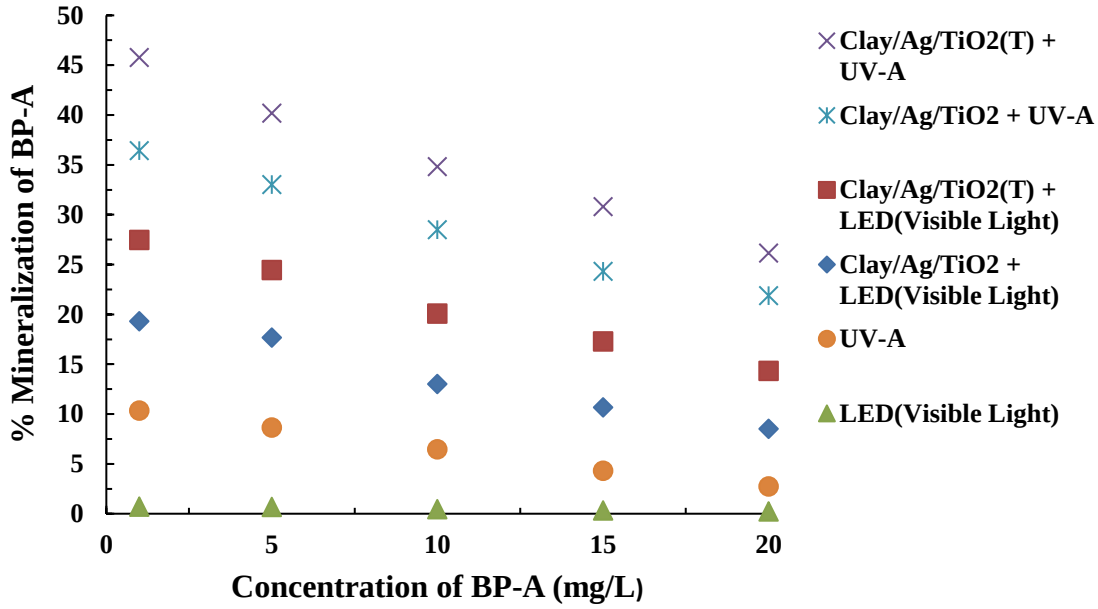

Figure 3.2.1.23.: Percentage mineralization of BP-A [pH:8.0] as a function of change in initial concentrations under photolytic and photocatalytic process using Clay/Ag/TiO_2(T) thin film.

3.2.1.24. Mineralization of Rhodamine B (Rh-B) and Rhodamine 6G (Rh-6G)

Similarly, the NPOC (Non-Purgeable Organic Carbon) data was obtained for various concentrations of treated Rh-B and Rh-6G samples. Both the dye solution concentration was increased from 0.5 to 20.0 mg/L at 6.0. The treated dye solutions were analysed after being treated for 2 hrs under visible light and UV-A light using Clay/Au/TiO_2 and Clay/Au/TiO_2(T) thin film catalysts. Figure 3.2.1.24. (a) and (b) show the percentage elimination of NPOC as a function of Rh-B and Rh-6G initial concentrations. It is revealed that, as the concentration of Rh-B and Rh-6G is

increased, the percentage removal of NPOC is decreased significantly. In case of Rh-B, when the concentration was increased from 0.5 to 20.0 mg/L, the percentage of NPOC removal was decreased from 29.37 % to 3.32 % (using Clay/Au/TiO_2(T) thin film) under visible light and from 41.12 % to 9.64 % (using Clay/Au/TiO_2(T) thin film) under UV-A light illumination.

On the other hand, increasing the Rh-6G concentrations from 0.5 to 20.0 mg/L caused for decrease in percentage NPOC removal from 33.25 % to 5.16 % (using Clay/Au/TiO_2(T) thin film) under visible light and from 43.16 % to 10.74 % (using Clay/Au/TiO_2(T) thin film) under UV-A light. Thus, according to the concentration dependent mineralization study, high mineralization percentage was achieved at lower dye concentrations under the photocatalytic treatment. Further, the Clay/Au/TiO_2(T) thin film is more efficient for the mineralization of Rh-B and Rh-6G as compared to the Clay/Au/TiO_2 thin film. Moreover, the photolysis showed insignificant mineralization of these dyes in the aqueous solutions. Hence, the photocatalytic operations enabled to achieve a significant mineralization of recalcitrant dyes in the aqueous medium, which enhances the applicability of catalysts in real implications.

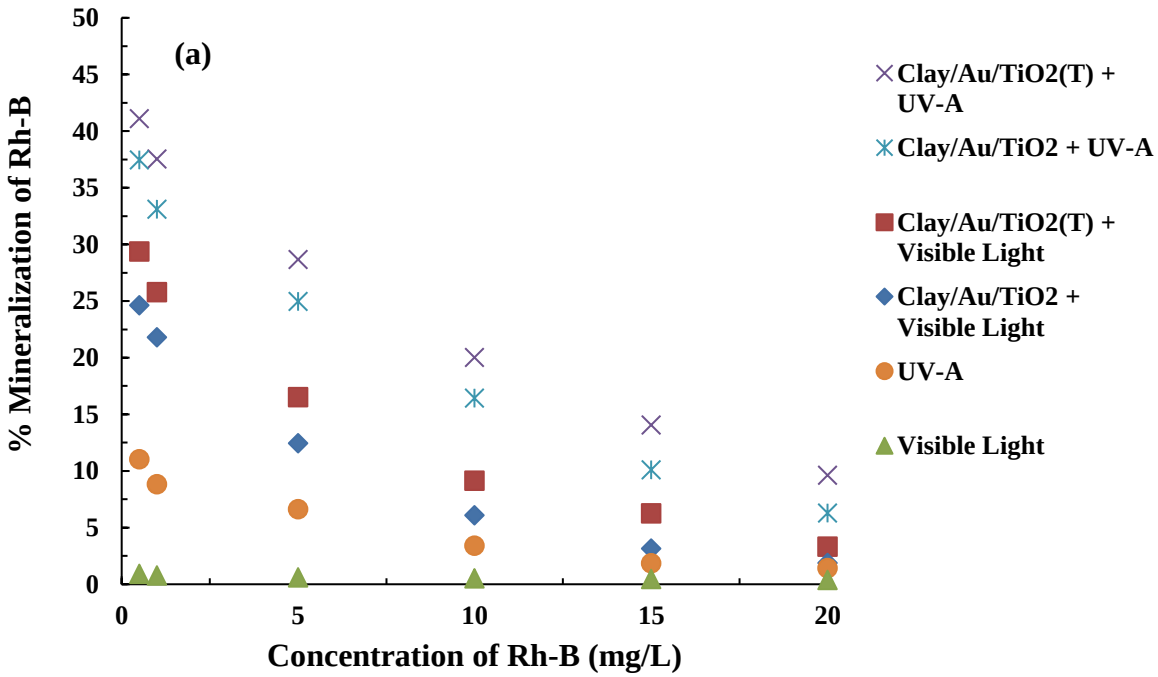

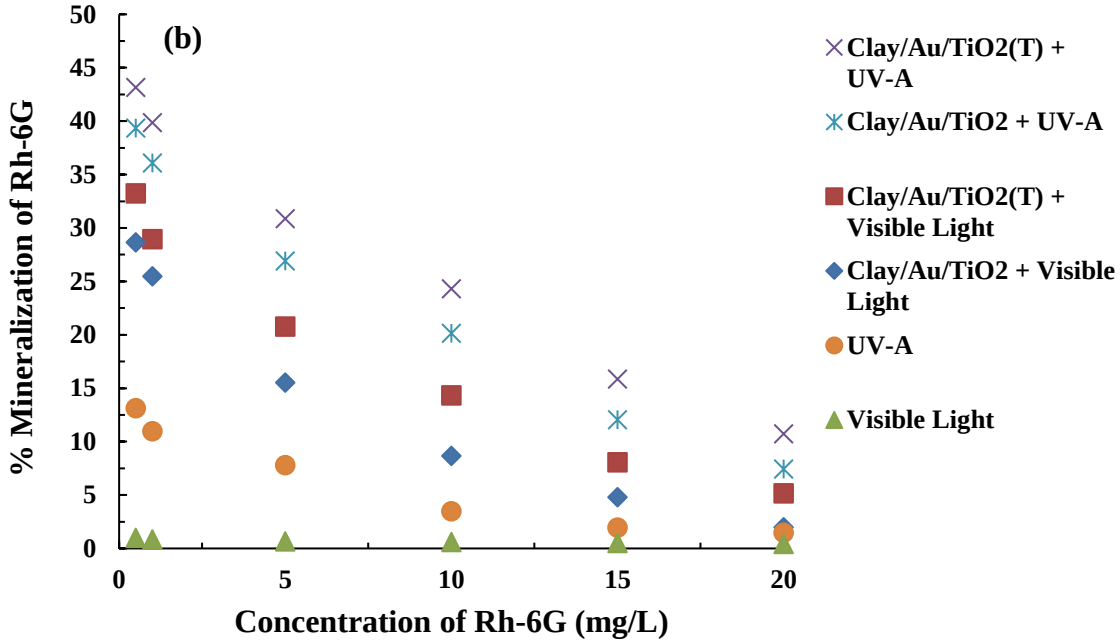

Figure 3.2.1.24.: Percentage mineralization of (a) Rh-B [pH:6.0]; and (b) Rh-6G [pH:6.0] as a function of change in initial concentrations under photolytic and photocatalytic process using.

3.2.1.25. Photocatalytic Degradation of Mordant Orange 1 (MO1) Tagged Real Water Samples

Applicability of fabricated thin film nano-catalyst depends largely on its utility to the real implications. Hence, the intended performance of Ag^0(NP)/TiO_2 thin film nano-catalyst in the elimination of MO1 was performed using the MO1 tagged real water samples. The real water was collected from Reiek Kai Site, Tlawng River (GPS: 23.7120° N, 92.6644° E). The water sample was analyzed for various physico/chemical parameters and results are shown in Table 3.2.1.25. The real water contained high concentrations of Fe, Ca and Zn. On the other hand, the TOC results indicated that the real water is contained with high inorganic carbon value with less NPOC value. Therefore, the water is having hardness, possibly, the presence of carbonate and bicarbonates of calcium are present. MO1 was tagged with real water having various concentrations of MO1 (0.5 to 20.0 mg/L; pH 6.0). Further, degradative

removal of MO1 is carried out using Ag^0(NP)/TiO_2 nanocomposite thin film catalyst under UV-A and LED light illuminations for 2 hrs. Percentage degradation of MO1 was obtained and compared with the result obtained with the purified water samples (*Cf* Figure 3.2.1.25.). The study revealed that the percentage degradation of MO1 is not significantly decreased in real water samples. This signifies the potential of nanocomposite thin film catalysts in the removal of MO1.

Table 3.2.1.25.: Various Physico-chemical Parametric Analysis of Reiek Kai Site, Tlawng River Water.

Parameters Studied	**Analytical Results**
pH	7.60
Conductivity	0.02 S/m
Resistivity	0.01 Mohm.cm
Salinity	0.12 PSU
Ox. Red. Potential	210.7 mV
Elements studied (AAS)	**(mg/L)**
Ni	0.0
Zn	0.53
Pb	0.08
Mn	0.01
Fe	0.20
Ca	2.34
Cu	0.0

TOC Analysis	**(mg/L)**
Inorganic Carbon	13.94
NPOC	2.49

Anions studied	**(mg/L)**
Nitrate	11.43

Fluoride	0.0
Sulphate	6.12
Phosphate	0.09

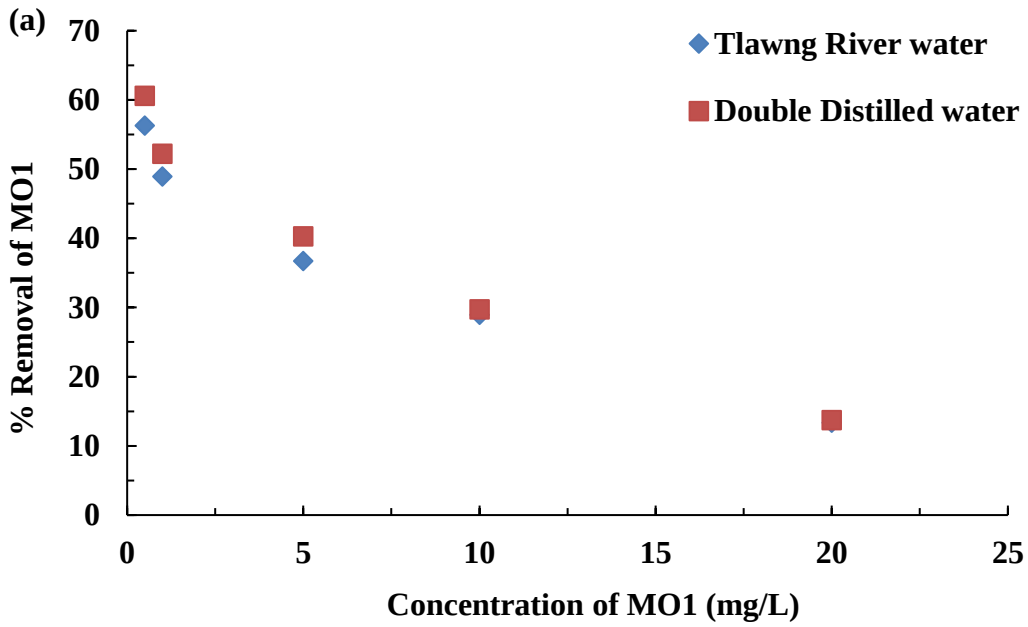

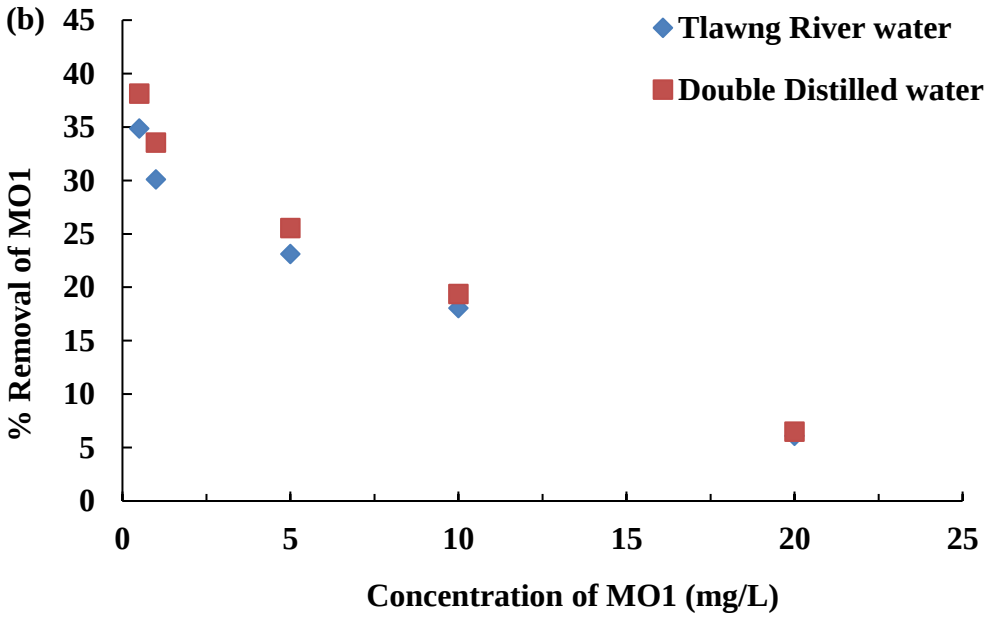

Figure 3.2.1.25.: Photocatalytic degradation of MO1(pH 6.0) in distilled water and real water (obtained from Tlawng river) using Ag^0(NP)/TiO_2 thin film catalyst under (a) UV-A and (b) LED light

3.2.1.26. Photocatalytic Degradation of Tetracycline (TC) and Sulfamethazine (SMZ) Tagged Real Water Samples.

Similarly, the applicability of thin film nanocatalyst Clay/Ag/TiO_2(T) in the real water implications are assessed using the catalyst in the degradation of TC and SMZ tagged river water samples. Therefore, the river water was collected from Tuipui River, Champhai District, Mizoram, India, (GPS location: 22.8795° N, 92.9357° E) and carefully analyzed for various physico-chemical parameters. The analyzed physicochemical parameters are returned in Table 3.2.1.26. It is evident from the analytical results that the river water is contained with relatively higher concentrations of Fe and Ca. Additionally, the TOC data revealed that the river water is having relatively high value of inorganic and organic carbon. The inorganic ions are within the permissible level.

Further, the river water was spiked with varying concentrations of TC and SMZ (0.5 to 20.0 mg/L) at pH 10.0 and 6.0, respectively. The photocatalytic degradation of TC and SMZ was carried out under LED (Visible light) light irradiation for 2 hrs and 3 hrs, respectively, utilizing the nanocomposite Clay/Ag/TiO_2(T) thin film. The removal efficiency of TC and SMZ was obtained and shown in Figure 3.2.1.26.(a) and (b). The results are well compared with the purified water treatment results. It is evident from Figure 3.2.1.26.(a) and (b) that the removal efficiency of TC and SMZ was not significantly affected in the river water samples. This inferred the potential use of nanocomposite thin film catalysts in the selective and efficient elimination of TC and SMZ in aqueous wastes.

Table 3.2.1.26.: Various Physico-chemical Parametric Analysis of Tuipui River Water.

Parameters Studied	**Analytical Results**
pH	7.13
Conductivity	0.02 S/m
Resistivity	0.03 Mohm.cm
Salinity	0.16 PSU
Ox. Red. Potential	198.0 mV
Elements studied (AAS)	**(mg/L)**
Ni	0.00
Zn	0.18
Pb	0.07
Mn	0.01
Fe	0.41
Ca	3.54
Cu	0.00

TOC Analysis	**(mg/L)**
Inorganic Carbon	11.53
NPOC	2.21

Anions studied	**(mg/L)**
Nitrate	1.95
Fluoride	0.39
Sulphate	7.0
Phosphate	0.86

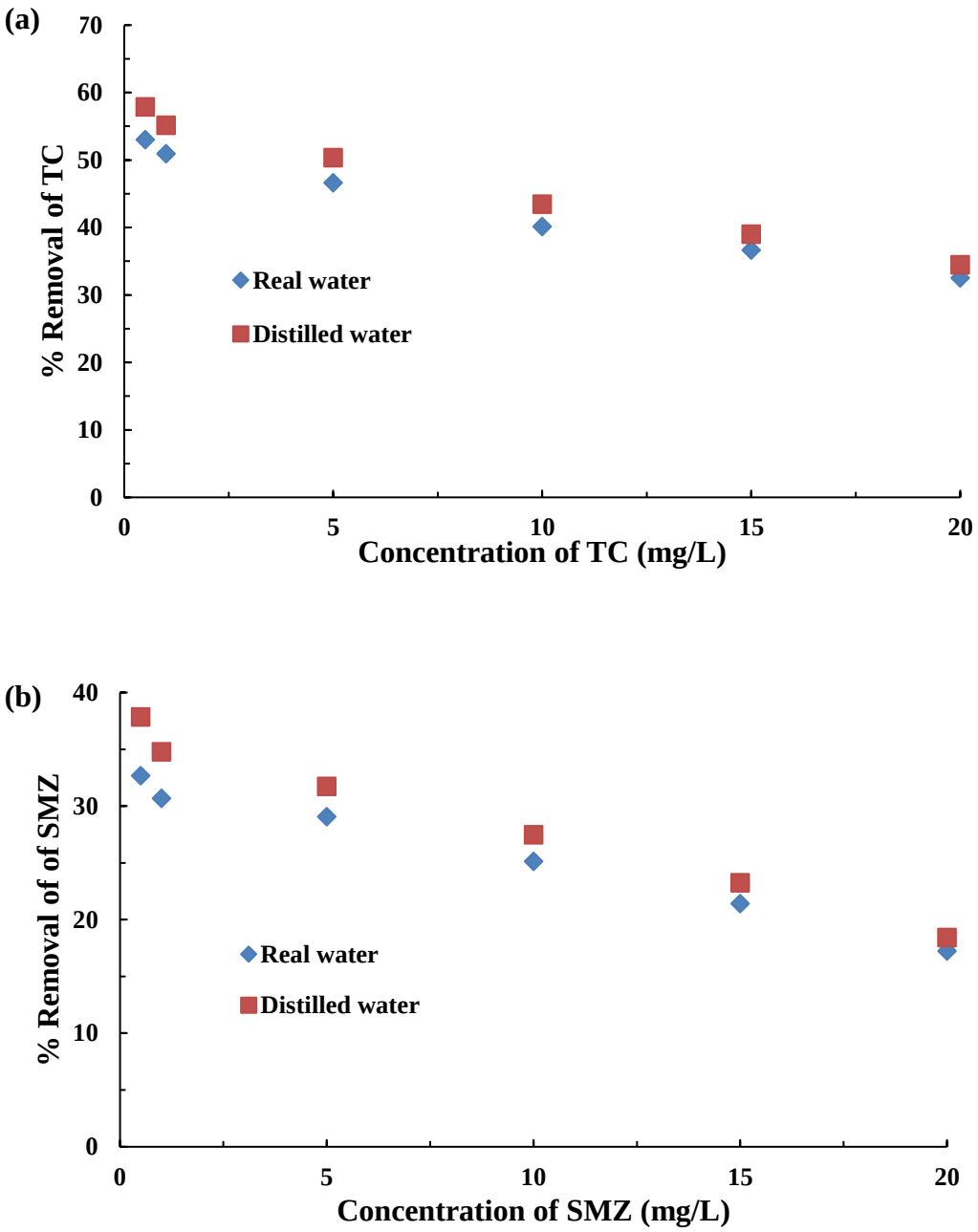

Figure 3.2.1.26.: Photocatalytic degradation of (a) TC (pH 10.0); and (b) SMZ (pH 6.0) in distilled water and real water (obtained from Tuipui river) using Clay/Ag/TiO_2(T) thin film catalyst under LED (Visible light)

3.2.1.27. Photocatalytic Degradation of Bisphenol A (BP-A) Tagged Real Water Samples.

The effectiveness of the developed thin-film nanocomposite depends on its application in natural water samples for real water treatment. Therefore, a natural water sample was collected from the Tiau (Indo-Myanmar Boundary) River in Champhai District, Mizoram, India (GPS location: 23.4713° N, 93.3220° E). The physico-chemical parameters of river water is shown in Table 3.2.1.27. The river water contained a relatively high content of total Fe, Ca, and Zn along with the inorganic carbon content. However, low value of NPOC and other inorganic anions are found in the river water samples.

Further, the river water is tagged with the known concentrations of BP-A (1.0 to 20.0 mg/L) at pH 8. The photocatalytic degradation of BP-A in natural water was carried out using a thin film nanocomposite Clay/Ag/TiO_2(T) catalyst under LED (Visible Light) irradiation for 4 hrs. The percentage degradation of BP-A is obtained and compared with the percentage removal of BP-A in the distilled water (*Cf* Figure 3.2.1.27.). It is evident from the results that the percentage elimination of BP-A in real water samples is minimally affected as compared to the distilled water results. This suggests that the thin film nanocomposite Clay/Ag/TiO_2(T) photocatalyst is promising in the real implications at least in the removal of emerging water contaminant BP-A from aqueous medium.

Table 3.2.1.27.: Various Physico-chemical Parametric Analysis of Tiau River Water.

Parameters Studied	**Analytical Results**
pH	6.82
Conductivity	0.03 S/m
Resistivity	0.03 Mohm.cm
Salinity	0.32 PSU
Ox. Red. Potential	123.26 mV
Elements studied (AAS)	**(mg/L)**

Ni	0.00
Zn	0.36
Pb	0.03
Mn	0.01
Fe	1.02
Ca	2.68
Cu	0.00

TOC Analysis	**(mg/L)**
Inorganic Carbon	8.63
NPOC	1.04

Anions studied	**(mg/L)**
Nitrate	2.8
Fluoride	0.14
Sulphate	5
Phosphate	0.18

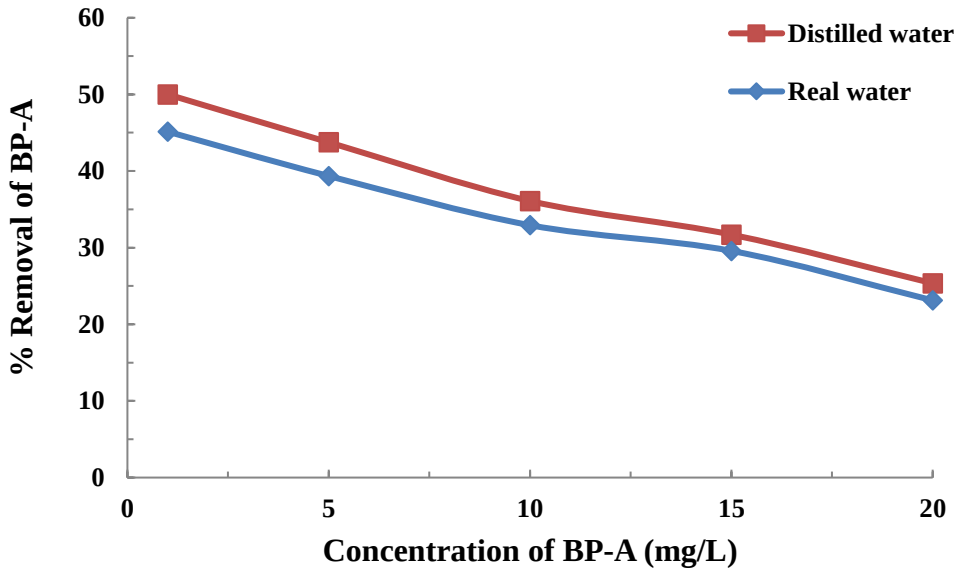

Figure 3.2.1.27.: Photocatalytic degradation of BP-A (pH 8.0) in distilled water and real water (obtained from Tiau river) using Clay/Ag/TiO_2(T) thin film catalyst under LED (Visible light)

3.2.1.28. Photocatalytic Degradation of Rhodamine B (Rh-B) and Rhodamine 6G (Rh-6G) Tagged Real Water Samples.

The use of fabricated thin film nanocatalyst in the real water determines the effectiveness of the catalyst in the real-world implications. As a result, the tagged Rh-B and Rh-6G solutions were prepared using the river water and employed for the photocatalytic degradation of these dyes. The river water was collected from the Serlui B river (Near Serlui B hydel Project), Kolasib District, Mizoram, India (GPS location: 24.3384° N, 92.7685° E). Table 3.2.1.28. shows the physical and chemical parameters of river water samples. The water is contained with rather high quantities of Fe, Ca, and Zn. The inorganic carbon concentration was quite high, while the NPOC content was relatively low. At a constant pH of 6, real water solutions of Rh-B and Rh-6G with varied concentrations (0.5 to 20.0 mg/L) were prepared. Further, the photocatalytic process was carried out using the nanocomposite Clay/Au/TiO_2(T) photocatalyst and pollutant solutions were illuminated with LED light for a period of 2 hrs. The photocatalytic elimination of Rh-B and Rh-6G in the river water samples were obtained and compared with the results obtained with distilled water samples [*Cf* Figure 3.2.1.28. (a) and (b)]. The percentage degradation of Rh-B and Rh-6G was not significantly reduced in the real water sample, (*Cf* Figure 3.2.1.28. (a) and (b)). This shows that fabricated thin film catalysts possessed potential in the real implications for the remediation of water contaminated with emerging dye contaminants. Moreover, the studies are the initial laboratory scale inputs useful for scaling up the process for large scale treatment of water contaminated with emerging water contaminants.

Table 3.2.1.28.: Various Physico-chemical Parametric Analysis of Serlui B river Water.

Parameters Studied	**Analytical Results**
pH	7.22
Conductivity	0.02 S/m
Resistivity	0.03 Mohm.cm
Salinity	0.25 PSU
Ox. Red. Potential	167.0 mV
Elements studied (AAS)	**(mg/L)**
Ni	0.00
Zn	0.48
Pb	0.07
Mn	0.01
Fe	0.20
Ca	1.98
Cu	0.00

TOC Analysis	**(mg/L)**
Inorganic Carbon	9.56
NPOC	2.33

Anions studied	**(mg/L)**
Nitrate	3.15
Fluoride	0.08
Sulphate	5.44
Phosphate	0.12

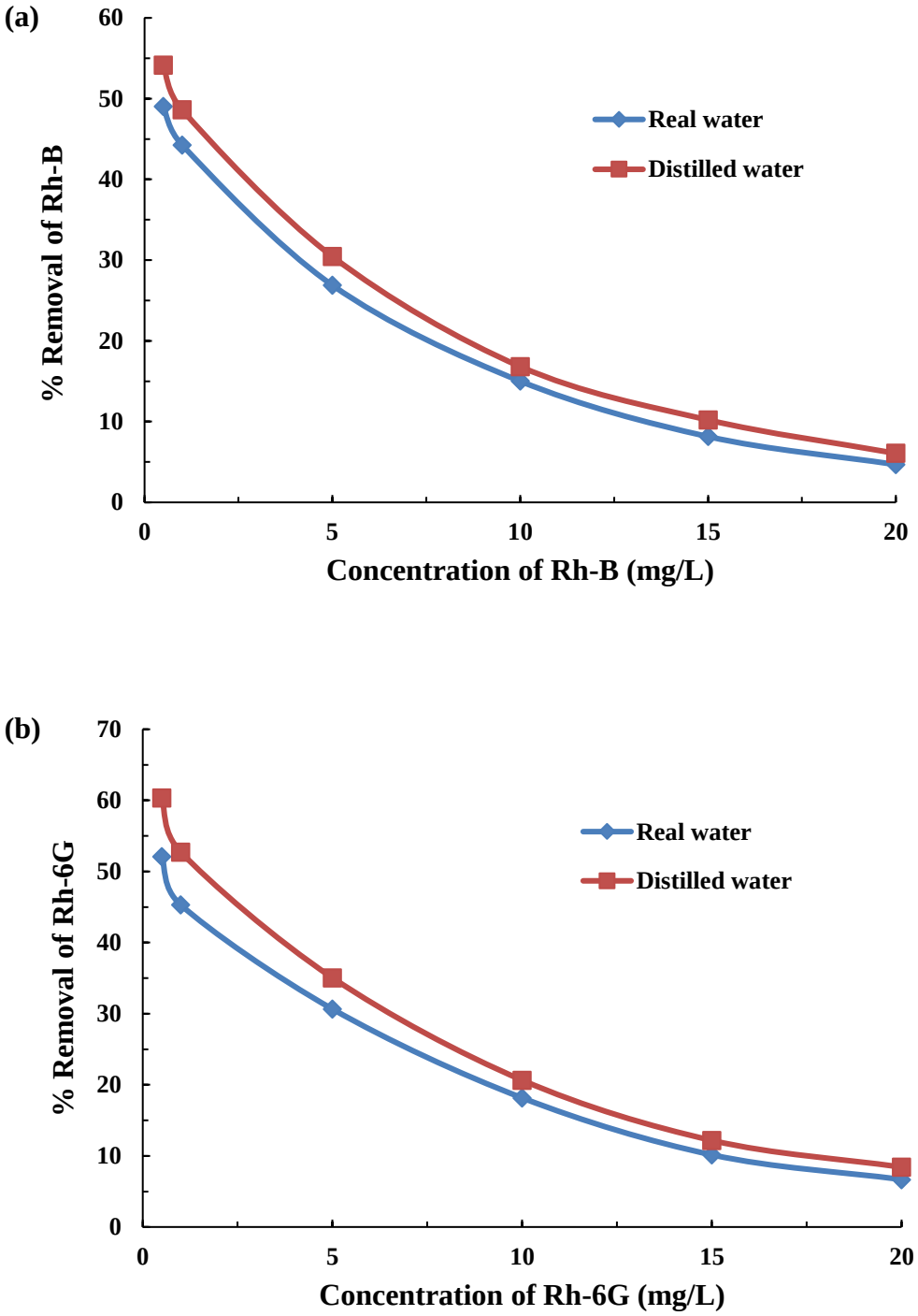

Figure 3.2.1.28.: Photocatalytic degradation of (a) Rh-B (pH 6.0); and (b) Rh-6G (pH 6.0) in distilled water and real water (obtained from Serlui B river) using Clay/Au/TiO_2(T) thin film catalyst under LED (Visible light)

CONCLUSION

4. CONCLUSION

Ag^0(NP) doped TiO_2 nanocomposite (Ag^0(NPs)/TiO_2), bentonite clay supported Ag^0(NP) doped TiO_2 nanocomposite (Clay/Ag/TiO_2 and Clay/Ag/TiO_2(T)) and bentonite clay supported Au^0(NP) doped TiO_2 nanocomposite (Clay/Au/TiO_2 and Clay/Au/TiO_2(T)) were synthesised using a facile template synthetic route using polyethylene glycol as filler medium. The thin film catalysts were fabricated by the simple dip coating process. The materials were characterized by advanced analytical methods. The SEM images of Ag^0(NPs)/TiO_2 showed that Ag spatially distributed within the titania network and the interplanar distance of Ag^0(NPs) was 0.15 nm. The AFM analysis indicated that the nanocomposite forms a heterogeneous structure on the glass substrate. The root mean square roughness (Rq) and mean roughness (Ra) of Ag^0(NPs)/TiO_2 catalyst was 16.952 nm and 12.250 nm, respectively. The diffuse reflectance spectra (DRS) for powder TiO_2 and Ag^0(NPs)/TiO_2 was obtained using UV-Vis spectrophotometer and the band gap energy of the material was obtained by converting the diffuse reflectance data in to its adsorption coefficient (α) values using Kubelka-Munk equation and the *Tauc's* relationship. The band gap energies for TiO_2 and Ag^0(NPs)/TiO_2 were determined to be 3.28 and 2.9 eV respectively. This clearly indicates that the presence of Ag^0(NPs) caused a reduction in the band gap energy of the nanocomposite material. On the other hand, the Clay/Ag/TiO_2 and Clay/Ag/TiO_2(T), the SEM images showed that fine grains of nanocomposite materials are evenly distributed on the substrate. Further, the TEM images showed that the Ag^0(NPs) are very distinctly distributed on the surface and formed cubical shape particles. Moreover, the AFM analyses showed that the mean roughness (R_a) of Clay/Ag/TiO_2 and Clay/Ag/TiO_2(T) thin-film was found to be 6.879 nm and 52.831 nm, respectively. The anatase phase of titanium dioxide was present in the synthesized materials. The N_2 adsorption/desorption results showed the H1 type hysteresis loops, which indicated that the porous material has a regular array of uniform spheres. The bandgap energies of Clay/Ag/TiO_2 and Clay/Ag/TiO_2(T) were found to be 2.85, and 2.9 eV, respectively. Similarly, in case of Clay/Au/TiO_2 and Clay/Au/TiO_2(T) composite materials, the SEM images revealed that both the thin films showed surface heterogeneous structure and the fine particles of Au/TiO_2 are dispersed on the substrate

surface. The TEM images revealed that the interplanar distance of the Au(NPs) was found to be 0.34 nm for both Clay/Au/TiO_2(T) and Clay/Au/TiO_2 solids. 3D-AFM analysis revealed that the mean roughness (R_a) and the root mean square roughness (R_q) of Clay/Au/TiO_2(T) were determined 1.165 nm and 1.454 nm, respectively, and 0.386 nm and 0.572 nm respectively for Clay/Au/TiO_2. DRS study revealed that doping of Au(NPs) with TiO_2 results in decrease of band energy from 3.24 to 2.85 and 2.88 eV for Clay/Au/TiO_2(T) and Clay/Au/TiO_2 respectively.

The photocatalytic degradation of micropollutants are carried out with several parametric studies to obtain the insights of mechanisms involved at the catalyst surface. The decrease in pH (from pH 10.0 to 4.0) has caused to increase the photocatalytic degradation efficiency of mordant orange 1 (MO1) (using Ag^0(NPs)/TiO_2) and bisphenol A (BP-A) (using Clay/Ag/TiO_2) (from pH 12.0 to 6.0). However, increase in solution pH from 4.0 to 10.0 significantly favoured the photocatalytic degradation efficiency of tetracycline (TC) (using Clay/Ag/TiO_2). Sulfamethazine (SMZ) (using Clay/Ag/TiO_2) and rhodamine B (Rh-B) (using Clay/Au/TiO_2) showed maximum degradation efficiency at pH ~6.0, while rhodamine 6G (Rh-6G) (using Clay/Au/TiO_2) showed its maximum degradation efficiency at pH ~8.0.

The decrease in pollutant concentrations (20.0 to 0.5 mg/L) significantly favoured the removal efficiency of MO1 (using Ag^0(NPs)/TiO_2), TC, SMZ and BP-A (using Clay/Ag/TiO_2), Rh-B and Rh-6G (using Clay/Au/TiO_2) under the photocatalytic treatment. With increase in pollutant concentrations from 0.5 to 20.0 mg/L, the percentage degradation of MO1 decreased from 60.6% to 13.7% (UV-A) and 38.14% to 6.5% (LED light). Further, the percentage degradation of TC decreased from 81.13% to 50.36% (UV-A) and 57.89 % to 34.46% (LED light). Furthermore, the percentage degradation of SMZ decreased from 64.58% to 36.21% (UV-A) and 37.83% to 18.42% (LED light). Moreover, the percentage degradation of BP-A decreased from 75.3% to 40.6% (UV-A) and 50.0% to 25.35% (LED light). Furthermore, the percentage degradation of Rh-B decreased from 76.26% to 17.64% (UV-A) and 54.13% to 6.07% (LED light). The percentage degradation of Rh-6G also decreased from 84.68% to 19.66% (UV-A) and 60.37% to 8.42% (LED light). These

results shows that the thin film photocatalysts could be used effectively at an extensively wide range of solution pH and concentration for the degradation of these micro-pollutants. Thus the thin film photocatalysts are highly effective in the degradation of these micro-pollutants in an aquatic environment. Further, the TOC (total organic carbon) data showed that the extent of mineralization of these pollutants was increased with decrease in the micropollutant concentrations. The decrease in concentration of pollutants from 20.0 to 0.5 mg/L has caused the percentage mineralization of MO1 to increase from 7.72% to 27.38% (UV-A) and 4.12% to 17.1% (LED light). Further, the percentage mineralization of TC increased from 27.3% to 42.6% (UV-A) and 18.2% to 31.3% (LED light). Furthermore, the percentage mineralization of SMZ increased from 21.8% to 34.2% (UV-A) and 10.4% to 20.1% (LED light). Moreover, the percentage mineralization of BP-A increased from 26.2% to 45.8% (UV-A) and 14.3% to 27.5% (LED light). Furthermore, the percentage mineralization of Rh-B increased from 9.64% to 41.12% (UV-A) and 3.32% to 29.37% (LED light). The percentage mineralization of Rh-6G also increased from 10.74% to 43.16% (UV-A) and 5.16% to 33.25% (LED light).

The degradation kinetics of mordant orange 1 (MO1), tetracycline (TC), sulfamethazine (SMZ), bisphenol A (BP-A), rhodamine B (Rh-B) and rhodamine 6G (Rh-6G) follow pseudo-first-order rate kinetics, and the degradation rate was utilized to fit the Langmuir-Hinshelwood isotherm. The photocatalytic degradations of MO1, TC, SMZ, BP-A, Rh-B and Rh-6G follow the L-H isotherm reasonably well. L-H adsorption constant 'K' (L/mg) and the reaction rate constant 'k_r' (mg/L/min) for MO1 were computed as 0.038 and 0.202 (R^2: 0.997 for UV-A) and 0.018 and 0.255 (R^2: 0.976 for LED), respectively. In case of TC, the rate constant 'k_r' (mg/L/min) and the L-H adsorption constant 'K' (L/mg) were obtained to be 0.136 and 0.064 (R^2: 0.995; for Clay/Ag/TiO_2(T)) respectively (using LED light). For SMZ, k_r (mg/L/min) and K (L/mg) were obtained to be 0.045 and 0.069 (R^2: 0.997; for Clay/Ag/TiO_2(T)) respectively (using LED light). In case of BP-A, k_r (mg/L/min) and K (L/mg) for Clay/Ag/TiO_2(T) thin film (R^2: 0.999) were found 0.051 and 0.063, respectively (using LED light). In Rh-B, k_r (mg/L/min) and K (L/mg) were obtained 0.016 and 0.524 (R^2: 0.955; for Clay/Au/TiO_2(T)), respectively (using LED light). In case of Rh-6G, the

rate constant 'k_r' (mg/L/min) and the L-H adsorption constant 'K' (L/mg) were again found to be 0.022 and 0.468 (R^2: 0.985; for Clay/Au/TiO_2(T)) respectively (using LED light). Further, the effect of co-existing ions and scavengers in the photocatalytic degradation of MO1 (using Ag^0(NPs)/TiO_2), TC, SMZ and BP-A (using Clay/Ag/TiO_2), Rh-B and Rh-6G (using Clay/Au/TiO_2) were studied. The removal efficiency of MO1 is affected in the presence of NaCl, EDTA and glycine. The scavengers such as 2-propanol, HCO_3^- and sodium azide hamperd significantly the percentage degradation of MO1. The presence of NaCl, EDTA, and glycine significantly affected the removal efficiency of TC. In case of SMZ the removal efficiency was significantly hampered in the presence of oxalic acid, EDTA, and $CuSO_4$. The percentage elimination of TC and SMZ was significantly hindered in the presence of scavengers such as 2-propanol and $NaHCO_3$. Moreover, the degradation efficiency of BP-A was significantly lowered in the presence of NaCl, $NaNO_3$, EDTA, glycine, 2-propanol and $NaHCO_3$. Furthermore, the Rh-B and Rh-6G degradation was suppressed in the presence of NaCl, $NiCl_2$, EDTA, oxalic acid, glycine, 2-propanol, HCO_3^- and sodium azide. These studies inferred that the degradation of these pollutants predominantly proceeded through the •OH radicals. Additionally, the singlet oxygen is also taking part in photocatalytic degradation reactions. The occurrence of several anions and cations affected the photocatalytic degradation of these micro-pollutants at varied levels. This is because these ions compete with the pollutant molecules for sorption on the photocatalyst surface. Hence, it prevented the target molecule from reaching the photocatalyst surface and hindered the photocatalytic degradation of pollutant molecules.

The repeated use of thin films, *viz.*, Ag^0(NPs)/TiO_2, Clay/Ag/TiO_2, Clay/Ag/TiO_2(T), Clay/Au/TiO_2 and Clay/Au/TiO_2(T) showed no substantial decline in percentage degradation of these micropollutants from aqueous solutions, which indicated that the thin films photocatalyst are fairly stable at least for six photocatalytic operations. Overall, the template synthesized photocatalysts Ag^0(NPs)/TiO_2, Clay/Ag/TiO_2(T) and Clay/Au/TiO_2(T) showed relatively enhanced photocatalytic efficiency than the corresponding non-template synthesized photocatalysts Clay/Ag/TiO_2 and Clay/Au/TiO_2. The efficiency of the photocatalytic process were

obtained to be remarkably higher than the photolytic process in the degradations of MO1 (using Ag^0(NPs)/TiO_2), TC, SMZ and BP-A (using Clay/Ag/TiO_2), Rh-B and Rh-6G (using Clay/Au/TiO_2). This emphasized that the thin film catalysts are having potential in the efficient degradation of several pollutants in the aqueous medium. Further, the photocatalytic degradation of these pollutants were carried in the real water samples and the removal efficiency of these pollutants was not affected as compared to the purified water degradation. These results further inferred the selectivity of catalyst in the degradation of these pollutants and wider implacability in real implications. The entire treatment process is relatively "greener" as devoid of 'no-waste' generation.

4.1. Future Perspective

The current study focuses on efficient and cost-effective treatment of water contaminated with emerging water contaminants *viz.*, mordant orange 1 (MO1), tetracycline (TC), sulfamethazine (SMZ), bisphenol A (BP-A), rhodamine B (Rh-B) and rhodamine 6G (Rh-6G) using thin film catalysts. The thin film photocatalysts *viz.*, Ag^0(NPs)/TiO_2, Clay/Ag/TiO_2, Clay/Ag/TiO_2(T), Clay/Au/TiO_2 and Clay/Au/TiO_2(T) were fabricated in facile process. The efficient and selective application of these photocatalysts are efficient in the break-down to significant mineralization of these micropollutants in the aqueous medium. The promising laboratory results are, possibly, utilised for large-scale treatment at a pilot plant conditions for real wastewater treatment. Moreover, the results are having greater applicability in scaling-up the unit operations for the development of robust and efficient waste water treatment technology.

The plasmonic noble metal-doped titanium dioxide photocatalysts showed fascinating and promising results in the efficient remediation of water contaminated with various pollutants. This is inherently a 'greener' with a 'no waste' approach and merits for technology development. However, challenges are still ahead to achieve the ultimate goal of these studies. Therefore, the future perspectives are follows: (i) The widespread use of a greener approach in the material synthesis is inevitable to accomplish the entire process, i.e., from synthesis to applications is environment

friendly. (ii) The optimized shape and size of the nanocomposites need to be regulated precisely for efficient catalytic operations. (iii) Although, the thin film catalyst are cost effective, however, with enhanced efficiency and repeated use of catalyst may further enables the cost-effectiveness of catalyst in real implications; (iv) Although study addressed partly the molecular level insights, however, further insights at molecular levels could provide greater insights into the reaction mechanism and the interaction of pollutant molecules at the catalyst surface. (v) The laboratory-scale investigations need extensive trials for implications in real/or complex matrix treatment at the large scale or pilot scale treatment.

REFERENCES

Abdelhay, A., Jum'h, I., Albsoul, A., Abu Arideh, D., Qatanani, B., (2020). Performance of electrochemical oxidation over BDD anode for the treatment of different industrial dye-containing wastewater effluents. *J. Water Reuse Desalination.*, **11**: 110–121.

Abdel-Messih, M.F., Ahmed, M.A., El-Sayed, A.S., (2013). Photocatalytic decolorization of Rhodamine B dye using novel mesoporous SnO2–TiO2 nano mixed oxides prepared by sol–gel method. *J. Photochem. Photobiol. Chem.*, **260**: 1–8.

Ackerman, L., Noonan, G., Heiserman, W., Roach, J., Limm, W., Begley, T., (2010). Determination of Bisphenol A in US Infant Formulas: Updated Methods and Concentrations. *J. Agric. Food Chem.*, **58**: 2307–13.

Acosta-Esparza, M.A., Rivera, L.P., Pérez-Centeno, A., Zamudio-Ojeda, A., González, D.R., Chávez-Chávez, A., Santana-Aranda, M.A., Santos-Cruz, J., Quiñones-Galván, J.G., (2020). UV and Visible light photodegradation of methylene blue with graphene decorated titanium dioxide. *Mater. Res. Express*, **7**: 035504.

Ahmad, R., Ahmad, Z., Khan, A., Mastoi, N., Aslam, M., Kim, J., (2016). Photocatalytic Systems as an Advanced Environmental Remediation: Recent Developments, Limitations and new Avenues for Applications. *J. Environ. Chem. Eng.*, **4**: 4143–4164.

Ahmad, T., Ahmad, K., Alam, M., (2016b). Characterization of Water Treatment Plant's Sludge and its Safe Disposal Options. *Procedia Environ. Sci., Waste Management for Resource Utilisation.*, **35**: 950–955.

Ajmal, A., Majeed, I., Malik, R., Iqbal, M., Nadeem, M., Hussain, I., Yousuf, S., Zeshan, Mustafa, G., Zafar, M.I., Nadeem, M., (2016). Photocatalytic degradation of textile dyes on Cu2O-CuO/TiO2 anatase powders. *J. Environ. Chem. Eng.*, **4**.

Ajmal, A., Majeed, I., Malik, R.N., Idriss, H., Nadeem, M.A., (2014). Principles and mechanisms of photocatalytic dye degradation on TiO2 based photocatalysts: a comparative overview. *RSC Adv.*, **4**: 37003–37026.

Akpan, U.G., Hameed, B.H., (2009). Parameters affecting the photocatalytic degradation of dyes using TiO2-based photocatalysts: a review. *J. Hazard. Mater.*, **170:** 520–529.

Alapi, T., Dombi, A., (2007). Comparative study of the UV and UV/VUV-induced photolysis of phenol in aqueous solution. *J. Photochem. Photobiol. Chem.*, **188**: 409–418.

Aldred, E.M., Buck, C., Vall, K., (2009). Free radicals, in: Aldred, E.M., Buck, C., Vall, K. (Eds.), Pharmacology. Churchill Livingstone, Edinburgh., **7**: 41–52.

Alford, R., Simpson, H.M., Duberman, J., Hill, G.C., Ogawa, M., Regino, C., Kobayashi, H., Choyke, P.L., (2009). Toxicity of organic fluorophores used in molecular imaging: literature review. *Mol. Imaging.*, **8**: 341–354.

Al-Hajji, L.A., Ismail, A.A., Bumajdad, A., Alsaidi, M., Ahmed, S.A., Almutawa, F., Al-Hazza, A., (2020). Construction of Au/TiO2 Heterojunction with high photocatalytic performances under UVA illumination. *Ceram. Int.*, **46**: 20155–20162.

Ali, H., (2010). Biodegradation of Synthetic Dyes—A Review. *Water. Air. Soil Pollut.*, **213**: 251–273.

Alkaim, A., Aljeboree, A., Alrazaq, N.A., Jaafer, S., Hussein, F., lilo, A.J., (2014). Effect of pH on Adsorption and Photocatalytic Degradation Efficiency of Different Catalysts on Removal of Methylene Blue. *Asian J. Chem.*, **26**: 8445–8448.

Allen, S.J., McKay, G., Porter, J.F., (2004). Adsorption isotherm models for basic dye adsorption by peat in single and binary component systems. *J. Colloid Interface Sci.*, **280**: 322–333.

Alotaibi, M.R., Mahmoud, M.H.H., (2022). Promptness of tetracycline pollutant degradation via CuCo2O4@ZrO2 nanocomposites photocatalyst. *Opt. Mater.*, **126**: 112200.

Ameta, R., K. Chohadia, A., Jain, A., Punjabi, P.B., (2018). Fenton and Photo-Fenton Processes, in: Ameta, S.C., Ameta, R. (Eds.), Advanced Oxidation Processes for Waste Water Treatment. *Academic Press*, **3**: 49–87.

Amin, S., Pazouki, M., Hosseinnia, A., (2009). Synthesis of TiO 2–Ag nanocomposite with sol–gel method and investigation of its antibacterial activity against E. coli. *Powder Technol.*, **196**: 241–245.

Angel, R., Durán-Álvarez, J.C., Zanella, R., (2018). TiO2-Low Band Gap Semiconductor Heterostructures for Water Treatment Using Sunlight-Driven Photocatalysis. *Titanium Dioxide - Material for a Sustainable Environment*

Angulo-Ibáñez, A., Goitandia, A.M., Albo, J., Aranzabe, E., Beobide, G., Castillo, O., Pérez-Yáñez, S., (2021). Porous TiO2 thin film-based photocatalytic windows for an enhanced operation of optofluidic microreactors in CO_2 conversion. *iScience.*, **24**: 102654.

Antonelli, D.M., Ying, J.Y., (1995). Synthesis of Hexagonally Packed Mesoporous TiO2 by a Modified Sol–Gel Method. *Angew. Chem. Int. Ed. Engl.*, **34**: 2014–2017.

Arany, E., Szabó, R.K., Apáti, L., Alapi, T., Ilisz, I., Mazellier, P., Dombi, A., Gajda-Schrantz, K., (2013). Degradation of naproxen by UV, VUV photolysis and their combination. *J. Hazard. Mater.*, **262**: 151–157.

Arora, S., (2014). Textile Dyes: It's Impact on Environment and its Treatment. *J. Bioremediation Biodegrad.*, **5**.

Asha, K.K., Sankar, T.V., Viswanathan Nair, P.G., (2007). Effect of tetracycline on pancreas and liver function of adult male albino rats. *J. Pharm. Pharmacol.*, **59:** 1241–1248.

Augugliaro, V., Baiocchi, C., Prevot, A.B., García-López, E., Loddo, V., Malato, S., Marcí, G., Palmisano, L., Pazzi, M., Pramauro, E., (2002). Azo-dyes photocatalytic degradation in aqueous suspension of TiO2 under solar irradiation. *Chemosphere*, **49**: 1223–1230.

Backer, H.D., (2017). Chapter 7 - Water Disinfection, in: Sanford, C.A., Pottinger, P.S., Jong, E.C. (Eds.), The Travel and Tropical Medicine Manual (Fifth Edition). *Elsevier*, : 91–111.

Bahnemann, D., (2004). Photocatalytic water treatment: solar energy applications. *Sol. Energy*, **77**: 445.

Ballesteros-Gómez, A., Rubio, S., Pérez-Bendito, D., (2009). Analytical methods for the determination of bisphenol A in food. *J. Chromatogr. A.*, **1216**: 449–69.

Bansode, A., More, S., Bhoraskar, S., Mathe, V., (2015). Reusable thin film photocatalyst of Fe-doped TiO2 deposited by ECR plasma. *Surf. Interface Anal.*, **47**.

Barakat, N., Abdelwahab, N., Mohammed, A., Mohamed, S., (2020). Ag-decorated TiO2 nanofibers as Arrhenius equation-incompatible and effective photocatalyst for water splitting under visible light irradiation. *Colloids Surf. Physicochem. Eng. Asp.*, **604**: 125307.

Barakat, N.A.M., Kanjwal, M.A., Chronakis, I.S., Kim, H.Y., (2013). Influence of temperature on the photodegradation process using Ag-doped TiO2 nanostructures: Negative impact with the nanofibers. *J. Mol. Catal. Chem*., **366**: 333–340.

Bashiri, R., Mohammed, N., Kait, C., (2017). Advancement of Sol-Gel–Prepared TiO2 Photocatalyst. *Intech Open Sci.,* **8:** 151-167

Bauer, R., Fallmann, H., (1997). The Photo-Fenton Oxidation — A cheap and efficient wastewater treatment method. *Res. Chem. Intermed.,* **23**: 341–354.

Behera, S.K., Kim, H.W., Oh, J.-E., Park, H.-S., (2011). Occurrence and removal of antibiotics, hormones and several other pharmaceuticals in wastewater treatment plants of the largest industrial city of Korea. *Sci. Total Environ.*, **409**: 4351–4360.

Beltrán, F.J., García-Araya, J.F., Acedo, B., (1994). Advanced oxidation of atrazine in water—II. Ozonation combined with ultraviolet radiation. *Water Res.,* **28**: 2165–2174.

Ben Saber, N., Mezni, A., Alrooqi, A., Altalhi, T., (2021). Fabrication of efficient Au@TiO2/rGO heterojunction nanocomposite: Boosted photocatalytic activity under ultraviolet and visible light irradiation. *J. Mater. Res. Technol*., **12**: 2238–2246.

Bendjabeur, S., Zouaghi, R., Kaabeche, nour el houda, Sehili, T., (2017). Parameters Affecting Adsorption and Photocatalytic Degradation Behavior of Gentian Violet under UV Irradiation with Several Kinds of TiO2 as a Photocatalyst. *Int. J. Chem. React. Eng.* **15**.

Bhatkhande, D.S., Kamble, S.P., Sawant, S.B., Pangarkar, V.G., (2004). Photocatalytic and photochemical degradation of nitrobenzene using artificial ultraviolet light. *Chem. Eng. J.*, **102**: 283–290.

Bilgin, M., Yurtsever, M., Karadagli, F., (2020). Microplastic removal by aerated grit chambers versus settling tanks of a municipal wastewater treatment plant. *J. Water Process Eng.*, **38**: 101604.

Bligaard, T., Nørskov, J. K., (2008). Heterogeneous Catalysis, in: Nilsson, A., Pettersson, L.G.M., Nørskov, Jens K. (Eds.), Chemical Bonding at Surfaces and Interfaces. *Elsevier, Amsterdam,* **4**: 255–321.

Bodaghi, H., Mostofi, Y., Oromiehie, A., Ghanbarzadeh, B., Ghasimi Hagh, Z., (2015). Synthesis of clay–TiO2 nanocomposite thin films with barrier and photocatalytic properties for food packaging application. *J. Appl. Polym. Sci.,* **132.**

Boehler, M., Zwickenpflug, B., Hollender, J., Ternes, T., Joss, A., Siegrist, H., (2012). Removal of micropollutants in municipal wastewater treatment plants by powder-activated carbon. *Water Sci. Technol. J. Int. Assoc. Water Pollut. Res.,* **66**: 2115–2121.

Bolong, N., Ismail, A.F., Salim, M.R., Matsuura, T., (2009). A review of the effects of emerging contaminants in wastewater and options for their removal. *Desalination*., **239**: 229–246.

Boxi, Dr.S., Paria, S., (2015). Visible Light Induced Enhanced Photocatalytic Degradation of Organic Pollutants in Aqueous Media Using Ag Doped Hollow TiO2 Nanospheres. *RSC Adv.*, **5**: 37657–37668.

Boxi, S.S., Paria, S., (2015). Visible light induced enhanced photocatalytic degradation of organic pollutants in aqueous media using Ag doped hollow TiO2 nanospheres. *RSC Adv.,* **5**: 37657–37668.

Brandt, M.J., Johnson, K.M., Elphinston, A.J., Ratnayaka, D.D., (2017). Chapter 11 - Disinfection of Water, in: Brandt, M.J., Johnson, K.M., Elphinston, A.J., Ratnayaka, D.D. (Eds.), Twort's Water Supply (Seventh Edition). Butterworth-Heinemann, Boston., 475–511.

Buxton, G.V., Greenstock, C.L., Helman, W.P., Ross, A.B., (1988). Critical Review of rate constants for reactions of hydrated electrons, hydrogen atoms and

hydroxyl radicals (·OH/·O− in Aqueous Solution. *J. Phys. Chem.*, **17**: 513–886.

Cao, Z., Zhu, S., Qu, H., Qi, D., Ziener, U., Yang, L., Yan, Y., Yang, H., (2014). Preparation of visible-light nano-photocatalysts through decoration of TiO2 by silver nanoparticles in inverse miniemulsions. *J. Colloid Interface Sci.*, **435C**: 51–58.

Carballa, M., Omil, F., Lema, J.M., Llompart, M., García-Jares, C., Rodríguez, I., Gómez, M., Ternes, T., (2004). Behavior of pharmaceuticals, cosmetics and hormones in a sewage treatment plant. *Water Res.*, **38**: 2918–2926.

Carmen, Z., Daniel, S., (2012). Textile Organic Dyes – Characteristics, Polluting Effects and Separation/Elimination Procedures from Industrial Effluents – A Critical Overview, in: Puzyn, T. (Ed.), Organic Pollutants Ten Years After the Stockholm Convention - Environmental and Analytical Update. *InTech.*

Cervantes-Avilés, P., Camarillo Piñas, N., Ida, J., Cuevas-Rodríguez, G., (2017). Influence of wastewater type on the impact generated by TiO2 nanoparticles on the oxygen uptake rate in activated sludge process. *J. Environ. Manage.*, **190**: 35–44.

Chaidez, C., Soto, M., Jimenez, M., (2014). Water: waste, recycling and irrigation in fresh produce processing, in: Hoorfar, J. (Ed.), Global Safety of Fresh Produce, Woodhead Publishing Series in Food Science, Technology and Nutrition. *Woodhead Publishing*, **9**: 119–132.

Chao, H.E., Yun, Y.U., Xingfang, H.U., Larbot, A., (2003). Effect of silver doping on the phase transformation and grain growth of sol-gel titania powder. *J. Eur. Ceram. Soc.*, **23**: 1457–1464.

Chavoshani, A., Hashemi, M., Mehdi Amin, M., Ameta, S.C., (2020). Chapter 1 - Introduction, in: Chavoshani, A., Hashemi, M., Mehdi Amin, M., Ameta, S.C. (Eds.), *Micropollutants and Challenges. Elsevier*, 1–33.

Chen, D., Cheng, Y., Zhou, N., Chen, P., Wang, Y., Li, K., Huo, S., Cheng, P., Peng, P., Zhang, R., Wang, L., Liu, H., Liu, Y., Ruan, R., (2020). Photocatalytic degradation of organic pollutants using TiO2-based photocatalysts: A review. *J. Clean. Prod.*, **268**: 121725.

Chen, H., (2006). Recent Advances in Azo Dye Degrading Enzyme Research. *Curr. Protein Pept. Sci.,* **7**: 101–111.

Chen, Y.-W., Hsu, Y.-H., (2021). Effects of Reaction Temperature on the Photocatalytic Activity of TiO2 with Pd and Cu Cocatalysts. *Catalysts*., **11**: 966.

Chen, Z., Wang, D., Dao, G., Shi, Q., Yu, T., Guo, F., Wu, G., (2021). Environmental impact of the effluents discharging from full-scale wastewater treatment plants evaluated by a hybrid fuzzy approach. *Sci. Total Environ.,* **790**: 148212.

Cheneviere, Y., Caps, V., Tuel, A., (2010). Gold-catalyzed oxidation of substituted phenols by hydrogen peroxide. *Appl. Catal. Gen.,* **387**: 129–134.

Chiang, K., Lim, T.M., Tsen, L., Lee, C.C., (2004). Photocatalytic degradation and mineralization of bisphenol A by TiO2 and platinized TiO2. *Appl. Catal. Gen*., **261**: 225–237.

Choi, K.-J., Kim, S.-G., Kim, S.-H., (2008). Removal of antibiotics by coagulation and granular activated carbon filtration. *J. Hazard. Mater.,* **151**: 38–43.

Chong, M.N., Jin, B., Chow, C., Saint, C., (2010). Recent Developments in Photocatalytic Water Treatment Technology: A Review. *Water Res.,* **44**: 2997–3027.

Chusaksri, S., Lomda, J., Saleepochn, T., Sutthivaiyakit, P., (2011). Photocatalytic degradation of 3,4-dichlorophenylurea in aqueous gold nanoparticles-modified titanium dioxide suspension under simulated solar light. *J. Hazard. Mater.,* **190**: 930–937.

Clescerl, L.S., Greenberg, A.E., Eaton, A.D., (1999). Standard Methods for Examination of Water and Wastewater (20th ed.). *Washington, DC: American Public Health Association,* ISBN 0–87553–235–7. Method 5310A.

Constantin, L.A., Nitoi, I., Cristea, N.I., Constantin, M.A., (2018). Possible degradation pathways of triclosan from aqueous systems via TiO2 assisted photocatalyis. *J. Ind. Eng. Chem.,* **58**: 155–162.

Daughton, C.G., Ternes, T.A., (1999). Pharmaceuticals and personal care products in the environment: agents of subtle change. *Environ. Health Perspect.,* **107(6)**: 907–938.

Demir Kivrak, H., Saleh, D., Alpaslan, D., Caglar, A., Selçuk, K., Dudu, T., Aktas, N., (2021). Quantum size effect of cadmium-doped titanium dioxide photocatalysts towards methylene blue degradation and electrooxidation. *Int. J. Environ. Sci. Technol.,* **161.**

Demyanenko, A.V., Bogomolov, A.S., Dozmorov, N.V., Svyatova, A.I., Pyryaeva, A.P., Goldort, V.G., Kochubei, S.A., Baklanov, A.V., (2019). Singlet Oxygen 1O2 in Photocatalysis on TiO2. Where Does It Come from? *J. Phys. Chem. C*., **123**: 2175–2181.

Dias, F.F., Oliveira, A.A.S., Arcanjo, A.P., Moura, F.C.C., Pacheco, J.G.A., (2016). Residue-based iron catalyst for the degradation of textile dye via heterogeneous photo-Fenton. *Appl. Catal. B Environ. Complete.,* 136–142.

Díaz-Uribe, C., Viloria, J., Cervantes, L., Vallejo, W., Navarro, K., Romero, E., Quiñones, C., (2018). Photocatalytic Activity of Ag-TiO2 Composites Deposited by Photoreduction under UV Irradiation. *Int. J. Photoenergy,* e6080432.

Ding, Q., Song, X., Yuan, M., Sun, R., Zhang, J., Yin, L., Pu, Y., (2022). Removal of microcystins from water and primary treatment technologies – A comprehensive understanding based on bibliometric and content analysis, 1991–2020. *J. Environ. Manage.,* **305**: 114349.

Dinh, C.-T., Yen, H., Kleitz, F., Do, T.-O., (2014). Three-Dimensional Ordered Assembly of Thin-Shell Au/TiO2 Hollow Nanospheres for Enhanced Visible-Light-Driven Photocatalysis. *Angew. Chem. Int. Ed.,* **53**: 6618–6623.

Dionysiou, D.D., Suidan, M.T., Bekou, E., Baudin, I., Laîné, J.-M., (2000). Effect of ionic strength and hydrogen peroxide on the photocatalytic degradation of 4-chlorobenzoic acid in water. *Appl. Catal. B Environ*., **26**: 153–171.

Doll, T.E., Frimmel, F.H., (2003). Fate of pharmaceuticals—photodegradation by simulated solar UV-light. *Chemosphere.,* **52**: 1757–1769.

Dong, C., Xing, M., Zhang, J., (2020). Recent Progress of Photocatalytic Fenton-Like Process for Environmental Remediation. *Front. Environ. Chem.,* **1**.

Donohue, J.M., (2003). Water Conditioning, Industrial, in: Meyers, R.A. (Ed.), *Encyclopedia of Physical Science and Technology (Third Edition). Academic Press, New York,* 671–697.

Dutschke, M., Schnabel, T., Schütz, F., Springer, C., (2022). Degradation of chlorinated volatile organic compounds from contaminated ground water using a carrier-bound TiO2/UV/O3-system. *J. Environ. Manage.*, **304**: 114236.

Dwivedi, A., (2017). Researches In Water Pollution: A Review. *International Research Journal of Natural and Applied Sciences.,* **4(1).**

Mugunthan, E., Saidutta, M.B., Jagadeeshbabu, P.E., (2018). Visible light assisted photocatalytic degradation of diclofenac using TiO2-WO3 mixed oxide catalysts. *Environ. Nanotechnol. Monit. Manag*., **10**: 322–330.

Eggins, B.R., (1998). Photoelectrochemistry of oxalate on particulate TiO2 electrodes. *J. Electroanal. Chem.,* **1–2**: 61–72.

El Mragui, A., Zegaoui, O., Esteves da Silva, J.C.G., (2021). Elucidation of the photocatalytic degradation mechanism of an azo dye under visible light in the presence of cobalt doped TiO2 nanomaterials. *Chemosphere*, **266**: 128931.

Emeline, A.V., Kuznetsov, V.N., Ryabchuk, V.K., Serpone, N., (2013). Heterogeneous Photocatalysis: Basic Approaches and Terminology, in: Suib, S.L. (Ed.), New and Future Developments in Catalysis. *Elsevier, Amsterdam,* **1**: 1–47.

Eom, H., Jung, J.-Y., Shin, Y., Kim, S., Choi, J.-H., Lee, E., Jeong, J.-H., Park, I., (2013). Strong localized surface plasmon resonance effects of Ag/TiO2 core–shell nanowire arrays in UV and visible light for photocatalytic activity. *Nanoscale,* **6**: 226–234.

Fajrina, N., Tahir, M., (2019). A critical review in strategies to improve photocatalytic water splitting towards hydrogen production. *Int. J. Hydrog. Energy.*, **44**: 540–577.

Falah, M., MacKenzie, K., Knibbe, R., Page, S., Hanna, J., (2016). New composites of nanoparticle Cu (I) oxide and titania in a novel inorganic polymer (geopolymer) matrix for destruction of dyes and hazardous organic pollutants. *J. Hazard. Mater.* **318**: 772-782.

Farombi, E.O., Ugwuezunmba, M.C., Ezenwadu, T.T., Oyeyemi, M.O., Ekor, M., (2008). Tetracycline-induced reproductive toxicity in male rats: effects of vitamin C and N-acetylcysteine. *Exp. Toxicol. Pathol. Off. J. Ges. Toxikol. Pathol*., **60**: 77–85.

Florenza, X., Sales Solano, A., Centellas, F., Martinez-Huitle, C.A., Brillas, E., Garcia-Segura, S., (2014). Degradation of the azo dye Acid Red 1 by anodic oxidation and indirect electrochemical processes based on Fenton's reaction chemistry. Relationship between decolorization, mineralization and products. *Electrochimica Acta*, **142**: 276–288. https://doi.org/10.1016/j.electacta.2014.07.117

Foo, K.Y., Hameed, B.H., (2010). Decontamination of textile wastewater via TiO2/activated carbon composite materials. *Adv. Colloid Interface Sci*. **159**: 130–143.

Forgacs, E., Cserháti, T., Oros, G., (2004). Removal of synthetic dyes from wastewaters: a review. *Environ. Int.*, **30**: 953–971.

Fromenty, B., Pessayre, D., (1995). Inhibition of mitochondrial beta-oxidation as a mechanism of hepatotoxicity. *Pharmacol. Ther*., **67**: 101–154.

Fu, C., Li, M., Li, H., Li, C., Wu, X. guo, Yang, B., (2017). Fabrication of Au nanoparticle/TiO2 hybrid films for photoelectrocatalytic degradation of methyl orange. *J. Alloys Compd.*, **692**: 727–733.

Fu, G., Vary, P.S., Lin, C.-T., (2005). Anatase TiO2 Nanocomposites for Antimicrobial Coatings. *J. Phys. Chem. B*, **109**: 8889–8898.

Fu, Y., Viraraghavan, T., (2001). Fungal decolorization of dye wastewaters: a review. Bioresour. Technol., **79**: 251–262.

Fujishima, A., Honda, K., (1972). Electrochemical Photolysis of Water at a Semiconductor Electrode. *Nature*., **238**: 37–38.

Fukahori, S., Fujiwara, T., Ito, R., Funamizu, N., (2011). pH-Dependent adsorption of sulfa drugs on high silica zeolite: Modeling and kinetic study. *Desalination*, **275**: 237–242.

Fukugami, Y., Sato, T., (2000). Synthesis and photochemical properties of Cd0.8Zn0.2S pillared H1−xCa2−xLaxNb3O10. *J. Alloys Compd.*, **312**: 111–116.

Gao, M., Zhu, L., Ong, W.L., Wang, J., Ho, G.W., (2015). Structural design of TiO2-based photocatalyst for H2 production and degradation applications. *Catal. Sci. Technol.*, **5**: 4703–4726.

Gaya, U.I., Abdullah, A.H., (2008). Heterogeneous photocatalytic degradation of organic contaminants over titanium dioxide: A review of fundamentals, progress and problems. *J. Photochem. Photobiol. C Photochem. Rev.*, **9**: 1–12.

Ge, L., Xu, M., Fang, H., (2006). Preparation and characterization of silver and indium vanadate co-doped TiO2 thin films as visible-light-activated photocatalyst. *J. Sol-Gel Sci. Technol.*, **40**: 65–73.

Glaze, W.H., Kang, J.-W., Chapin, D.H., (1987). The Chemistry of Water Treatment Processes Involving Ozone, Hydrogen Peroxide and Ultraviolet Radiation. *Ozone Sci. Eng.*, **9**: 335–352.

Gleick, P., Wolff, G., Cooley, H., Palaniappan, M., (2007). The World's Water 2006-2007: The Biennial Report on Freshwater Resources. *Bibliovault OAI Repos. Univ. Chic. Press.*

Gleick, P.H., (2000). The World's Water 2000-2001: The Biennial Report On Freshwater Resources. *Island Press.*

Green, I.X., Tang, W., Neurock, M., Yates, J.T., (2012). Localized Partial Oxidation of Acetic Acid at the Dual Perimeter Sites of the Au/TiO2 Catalyst—Formation of Gold Ketenylidene. *J. Am. Chem. Soc.*, **134**: 13569–13572.

Grosso, D., Soler-Illia, G.J. de A.A., Crepaldi, Eduardo.L., Cagnol, F., Sinturel, C., Bourgeois, A., Brunet-Bruneau, A., Amenitsch, H., Albouy, P.A., Sanchez, C., (2003). Highly Porous TiO2 Anatase Optical Thin Films with Cubic Mesostructure Stabilized at 700 °C. *Chem. Mater.*, **15**: 4562–4570.

Guo, Q., Zhou, C., Ma, Z., Yang, X., (2019). Fundamentals of TiO2 Photocatalysis: Concepts, Mechanisms, and Challenges. *Adv. Mater.*, **31**: 1901997.

Gürses, A., Açıkyıldız, M., Güneş, K., Gürses, M.S., (2016). Dyes and Pigments: Their Structure and Properties, in: Dyes and Pigments, SpringerBriefs in Molecular Science. Springer International Publishing, *Cham, pp.*, 13–29.

Gwo, S., Chen, H.-Y., Lin, M.-H., Sun, L., Li, X., (2016). Nanomanipulation and controlled self-assembly of metal nanoparticles and nanocrystals for plasmonics. *Chem. Soc. Rev.*, **45**: 5672–5716.

Hamrouni, A., Azzouzi, H., Rayes, A., Palmisano, L., Ceccato, R., Parrino, F., (2020). Enhanced Solar Light Photocatalytic Activity of Ag Doped TiO2-Ag3PO4 Composites. *Nanomater. Basel Switz.*, **10**: E795.

Handoko, C., G. Moustakas, N., Peppel, T., Springer, A., Oropeza, F., Huda, A., Bustan, M., Bambang, Y., Gulo, F., Strunk, J., (2019). Characterization and Effect of Ag(0) vs. Ag(I) Species and Their Localized Plasmon Resonance on Photochemically Inactive TiO2. *Catalysts*., **9:** 323.

He, S., Li, D., Wang, F., Zhang, C., Yue, C., Huang, Y., Xie, L., Zhang, Y.T., Mu, J., (2022). Parental exposure to sulfamethazine and nanoplastics alters the gut microbial communities in the offspring of marine madaka (Oryzias melastigma). *J. Hazard. Mater.*, **423**: 127003.

Hernández-Leal, L., Temmink, H., Zeeman, G., Buisman, C.J.N., (2011). Removal of micropollutants from aerobically treated grey water via ozone and activated carbon. *Water Res.*, **45**: 2887–2896.

Hichem, Z., Khellaf, N., Amrane, A., Djelal, H., Elfalleh, W., Rtimi, S., (2017). Photocatalytic performance of TiO2 impregnated polyester for the degradation of Reactive Green 12: Implications of the surface pretreatment and the microstructure. *J. Photochem. Photobiol. Chem.*, **346**.

Hoigné, J., (1997). Inter-calibration of OH radical sources and water quality parameters. *Water Sci. Technol., Oxidation Technologies for Water and Wastewater Treatment*, **35**: 1–8.

Hou, W., Hung, W.H., Pavaskar, P., Goeppert, A., Aykol, M., Cronin, S.B., (2011). Photocatalytic Conversion of CO2 to Hydrocarbon Fuels via Plasmon-Enhanced Absorption and Metallic Interband Transitions. *ACS Catal.*, **1**: 929–936.

Hua, W., Bennett, E.R., Letcher, R.J., (2006). Ozone treatment and the depletion of detectable pharmaceuticals and atrazine herbicide in drinking water sourced from the upper Detroit River, Ontario, Canada. *Water Res.*, **40**: 2259–2266.

Hussain, M., Tariq, S., Ahmad, M., Sun, H., Maaz, K., Ali, G., Hussain, S.Z., Iqbal, M., Karim, S., Nisar, A., (2016). AgTiO2 nanocomposite for environmental and sensing applications. *Mater. Chem. Phys. C*, 194–203.

IARC, n.d. Some Flame Retardants and Textile Chemicals, and Exposures in the Textile Manufacturing Industry.

Isari, A.A., Payan, A., Fattahi, M., Jorfi, S., Kakavandi, B., (2018). Photocatalytic degradation of rhodamine B and real textile wastewater using Fe-doped TiO2

anchored on reduced graphene oxide (Fe-TiO2/rGO): Characterization and feasibility, mechanism and pathway studies. *Appl. Surf. Sci.*, **462**: 549–564.

Isidoro, O.-R., Rafael, H., Alejandro, M., Carlos, G., Luis, E.-A., Enric, B., Ignasi, S., Karen, E., (2019). TiO2/Au/TiO2 multilayer thin-film photoanodes synthesized by pulsed laser deposition for photoelectrochemical degradation of organic pollutants. *Sep. Purif. Technol.* **224**: 189–198.

Ismail, N., Wee, S.Y., Aris, A.Z., (2017). Multi-class of endocrine disrupting compounds in aquaculture ecosystems and health impacts in exposed biota. *Chemosphere*, **188**: 375–388.

Jackson, R.B., Carpenter, S.R., Dahm, C.N., McKnight, D.M., Naiman, R.J., Postel, S.L., Running, S.W., (2001). Water In A Changing World. *Ecol. Appl.*, **11**: 1027–1045.

Jafari-Kang, A., Brown, A., Wong, C., Yuan, Q., (2017). Removal of Antibiotic Sulfamethoxazole by Anoxic/Anaerobic/Oxic Granular and Suspended Activated Sludge Processes. *Bioresour. Technol.*, **251**.

Jain, R., Mathur, M., Sikarwar, S., Mittal, A., (2007). Removal of the hazardous dye rhodamine B through photocatalytic and adsorption treatments. *J. Environ. Manage.* **85**: 956–964.

Jang, J.S., Kim, H.G., Lee, J.S., (2012). Heterojunction semiconductors: A strategy to develop efficient photocatalytic materials for visible light water splitting. *Catal. Today*, **185**: 270–277.

Jayakumar, A., Wurzer, C., Soldatou, S., Edwards, C., Lawton, L.A., Mašek, O., (2021). New directions and challenges in engineering biologically-enhanced biochar for biological water treatment. *Sci. Total Environ.*, **796**: 148977.

Jia, C., Wang, Y., Zhang, C., Qin, Q., Kong, S., Salomon, K., (2012). Photocatalytic Degradation of Bisphenol A in Aqueous Suspensions of Titanium Dioxide. *Environ. Eng. Sci.*, **29**: 630–637.

Jia, Y., Liu, J., Cha, S., Choi, S., Park, Y., Liu, C., (2016). Magnetically separable Au-TiO2/nanocube ZnFe2O4 composite for chlortetracycline removal in wastewater under visible light. *J. Ind. Eng. Chem.*, **47**.

Jia, Y., Liu, J., Cha, S., Choi, S., Park, Y.C., Liu, C., (2017). Magnetically separable Au-TiO2/nanocube ZnFe2O4 composite for chlortetracycline removal in wastewater under visible light. *J. Ind. Eng. Chem. C*, 303–314.

Jiang, H., Wang, Q., Chen, P., Zheng, H., Shi, J., Shu, H., Liu, Y., (2022). Photocatalytic degradation of tetracycline by using a regenerable (Bi)BiOBr/rGO composite. *J. Clean. Prod.*, **339**: 130771.

Jin, Z., Wang, Q., Zheng, W., Cui, X., (2016). Highly Ordered Periodic Au/TiO2 Hetero-Nanostructures for Plasmon-Induced Enhancement of the Activity and Stability for Ethanol Electro-oxidation. *ACS Appl. Mater. Interfaces*, **8**: 5273–5279.

Jung, K.-W., Choi, B.H., Hwang, M.-J., Jeong, T.-U., Ahn, K.-H., (2016). Fabrication of granular activated carbons derived from spent coffee grounds by entrapment in calcium alginate beads for adsorption of acid orange 7 and methylene blue. *Bioresour. Technol.*, **219**: 185–195.

Kafle, B.P., (2020). Theory and instrumentation of absorption spectroscopy: UV–VIS spectrophotometry and colorimetry. *Chemical Analysis and Material Characterization by Spectrophotometry*, *Elsevier*, **2**: 17–38.

Kang, J., Liu, H., Zheng, Y.-M., Qu, J., Chen, J.P., (2010). Systematic study of synergistic and antagonistic effects on adsorption of tetracycline and copper onto a chitosan. *J. Colloid Interface Sci.*, **344**: 117–125.

Kang, J.-H., Kondo, F., Katayama, Y., (2006). Human exposure to bisphenol A. *Toxicology*, **226**: 79–89.

Kang, Z., Yan, X., Zhao, L., Liao, Q., Zhao, K., Du, H., Zhang, Xiaohui, Zhang, Xueji, Zhang, Y., (2015). Gold nanoparticle/ZnO nanorod hybrids for enhanced reactive oxygen species generation and photodynamic therapy. *Nano Res.*, **6**, 2004–2014.

Karale, R.S., Manu, B., Shrihari, S., (2014). Fenton and Photo-fenton Oxidation Processes for Degradation of 3-Aminopyridine from Water. *APCBEE Procedia, 5th International Conference on Chemical, Biological and Environmental Engineering - ICBEE 2013 & 2nd International Conference on Civil Engineering - ICCEN 2013.*, **9**: 25–29.

Kaur, G., Singh, H., Singh, J., (2021). UV-vis spectrophotometry for environmental and industrial analysis. *Green Sustainable Process for Chemical and Environmental Engineering and Science,* **2**: 49–68.

Kaur, H., Hippargi, G., Pophali, G.R., Bansiwal, A.K., (2019). Treatment methods for removal of pharmaceuticals and personal care products from domestic wastewater, Waste Management and Treatment Technology. Butterworth-Heinemann, **6**: 129–150.

Kecili, R., Hussain, C.M., (2018). Mechanism of Adsorption on Nanomaterials. *Nanomaterials in Chromatography. Elsevier.,* **4**: 89–115.

Kepa, U., Stanczyk-Mazanek, E., Stepniak, L., (2008). The use of the advanced oxidation process in the ozone + hydrogen peroxide system for the removal of cyanide from water. *Desalination, European Desalination Society and Center for Research and Technology Hellas (CERTH),* **223**: 187–193.

Khan, H., Khalil, A.K., Khan, A., (2019). Photocatalytic degradation of alizarin yellow in aqueous medium and real samples using chitosan conjugated tin magnetic nanocomposites. *J. Mater. Sci. Mater. Electron.,* **30**: 21332–21342.

Khlyustova, A., Khomyakova, N., Sirotkin, N., Marfin, Y., (2016). The Effect of pH on OH Radical Generation in Aqueous Solutions by Atmospheric Pressure Glow Discharge. *Plasma Chem. Plasma Process*., **36**: 1229–1238.

Khuzwayo, Z., Chirwa, E.M.N., (2015). Modelling and simulation of photocatalytic oxidation mechanism of chlorohalogenated substituted phenols in batch systems: Langmuir–Hinshelwood approach. *J. Hazard. Mater*., **300**: 459–466.

Kibanova, D., Trejo, M., Destaillats, H., Cervini-Silva, J., (2009). Synthesis of hectorite–TiO2 and kaolinite–TiO2 nanocomposites with photocatalytic activity for the degradation of model air pollutants. *Appl. Clay Sci.*, **42**: 563–568.

Kikkawa, R., Fujikawa, M., Yamamoto, T., Hamada, Y., Yamada, H., Horii, I., (2006). In vivo hepatotoxicity study of rats in comparison with in vitro hepatotoxicity screening system. *J. Toxicol. Sci.*, **31**: 23–34.

Kim, G., Choi, H.J., Kim, H., Kim, J., Monllor-Satoca, D., Kim, M., Park, H., (2016). Temperature-boosted photocatalytic H2 production and charge transfer

kinetics on TiO2 under UV and visible light. *Photochem. Photobiol. Sci.*, **15**: 1247–1253.

Kirstein, I.V., Gomiero, A., Vollertsen, J., (2021). Microplastic pollution in drinking water. *Curr. Opin. Toxicol.*, **28**: 70–75.

Kočí, K., Obalová, L., Matějová, L., Plachá, D., Lacný, Z., Jirkovský, J., Šolcová, O., (2009). Effect of TiO2 particle size on the photocatalytic reduction of CO2. *Appl. Catal. B Environ.*, **89**: 494–502.

Kornbrust, D., Barfknecht, T., (1985). Testing of 24 food, drug, cosmetic, and fabric dyes in the in vitro and the in vivo/in vitro rat hepatocyte primary culture/DNA repair assays. *Environ. Mutagen.* **7**: 101–120.

Kosek, K., Luczkiewicz, A., Fudala-Książek, S., Jankowska, K., Szopińska, M., Svahn, O., Tränckner, J., Kaiser, A., Langas, V., Björklund, E., (2020). Implementation of advanced micropollutants removal technologies in wastewater treatment plants (WWTPs) - Examples and challenges based on selected EU countries. *Environ. Sci. Policy.*, **112**: 213–226.

Kovalova, L., Siegrist, H., von Gunten, U., Eugster, J., Hagenbuch, M., Wittmer, A., Moser, R., McArdell, C.S., (2013). Elimination of Micropollutants during Post-Treatment of Hospital Wastewater with Powdered Activated Carbon, Ozone, and UV. *Environ. Sci. Technol.*, **47**: 7899–7908.

Krasner, S.W., Westerhoff, P., Chen, B., Rittmann, B.E., Amy, G., (2009). Occurrence of disinfection byproducts in United States wastewater treatment plant effluents. *Environ. Sci. Technol.*, **43**: 8320–8325.

Krishnan, B., Mahalingam, S., (2017). Ag/TiO2/bentonite nanocomposite for biological applications: Synthesis, characterization, antibacterial and cytotoxic investigations. *Adv. Powder Technol. Int. J. Soc. Powder Technol. Jpn.*, **28**: 2265–2280.

Kubota, M., Matsui, M., Chiku, H., Kasashima, N., Shimojoh, M., Sakaguchi, K., (2005). Cell Adsorption and Selective Desorption for Separation of Microbial Cells by Using Chitosan-Immobilized Silica. *Appl. Environ. Microbiol.*, **71**: 8895–8902.

Kumar, Ajay, Choudhary, P., Kumar, Ashish, Camargo, P., Krishnan, V., (2021). Recent Advances in Plasmonic Photocatalysis Based on TiO 2 and Noble

Metal Nanoparticles for Energy Conversion, Environmental Remediation, and Organic Synthesis. *Small,* **18**: 2101638.

Kuo, C.-Y., Wu, C.-H., Lin, H.-Y., (2010). Photocatalytic degradation of bisphenol A in a visible light/TiO2 system. *Desalination*, **256**: 37–42.

Kusiak-Nejman, E., Morawski, A.W., (2019). TiO2/graphene-based nanocomposites for water treatment: A brief overview of charge carrier transfer, antimicrobial and photocatalytic performance. *Appl. Catal. B Environ.*, **253**: 179–186.

Lal, S., Link, S., Halas, N.J., (2007). Nano-optics from sensing to waveguiding. *Nat. Photonics*, **1**: 641–648.

Lalhriatpuia, C., Tiwari, A., Shukla, A., Tiwari, D., Lee, S.M., (2016). Nanopillars TiO2 thin film photocatalyst application in the remediation of aquatic environment. *Korean J. Chem. Eng*., **33**: 3367–3373.

Lalhriatpuia, C., Tiwari, D., Tiwari, A., Lee, S.-M., (2015). Immobilized Nanopillars-TiO2 in the efficient removal of micro-pollutants from aqueous solutions: Physico-chemical studies. *Chem. Eng. J*., **281**: 782–792.

Lalliansanga, Tiwari, D., Tiwari, A., Shukla, A., Kim, D.-J., Yoon, Y.-Y., Lee, S.-M., (2020). Facile synthesis and characterization of nanocomposite Au0(NPs)/titanium dioxide: Photocatalytic degradation of Alizarin Yellow. *J. Ind. Eng. Chem*., **82:** 153–163.

Langmuir, I., (1918). The adsorption of gases on plane surfaces of glass, mica and platinum. *J. Am. Chem. Soc.*, **40**: 1361–1403.

Lara-Martín, P.A., González-Mazo, E., Petrovic, M., Barceló, D., Brownawell, B.J., (2014). Occurrence, distribution and partitioning of nonionic surfactants and pharmaceuticals in the urbanized Long Island Sound Estuary (NY). *Mar. Pollut. Bull.*, **85**: 710–719.

Laws, E.A., (2000). Aquatic pollution: an introductory text. *Wiley, New York.*

Ledjeri, A., Yahiaoui, I., Kadji, H., Aissani-Benissad, F., Amrane, A., Fourcade, F., (2017). Combination of the Electro/Fe3+/peroxydisulfate (PDS) process with activated sludge culture for the degradation of sulfamethazine. *Environ. Toxicol. Pharmacol.* **53**: 34.

Lee, C.-G., Javed, H., Zhang, D., Kim, J.-H., Westerhoff, P., Li, Q., Alvarez, P.J.J., (2018). Porous Electrospun Fibers Embedding TiO2 for Adsorption and

Photocatalytic Degradation of Water Pollutants. *Environ. Sci. Technol.*, **52**: 4285–4293.

Lee, H., Lee, Y., Hwang, E., Park, J., (2014). Enhanced Surface Plasmon Effect of Ag/TiO2 Nanodiodes on Internal Photoemission. *J. Phys. Chem. C*, **118**: 5650–5656.

Lee, Y.H., Matthews, R.D., Pavlostathis, S.G., (2006). Biological decolorization of reactive anthraquinone and phthalocyanine dyes under various oxidation-reduction conditions. *Water Environ. Res. Res. Publ. Water Environ. Fed.*, **78**: 156–169.

Lemus, J., Martin-Martinez, M., Palomar, J., Gomez-Sainero, L., Gilarranz, M.A., Rodriguez, J.J., (2012). Removal of chlorinated organic volatile compounds by gas phase adsorption with activated carbon. *Chem. Eng. J.*, **211–212**: 246–254.

Leong, K.H., Gan, B.L., Ibrahim, S., Saravanan, P., (2014). Synthesis of surface plasmon resonance (SPR) triggered Ag/TiO2 photocatalyst for degradation of endocrine disturbing compounds. *Appl. Surf. Sci., Photocatalytic materials for energy and environmental applications*, **319**: 128–135.

Lepper, M.H., Wolfe, C.K., Zimmerman, H.J., Caldwell, E.R., Spies, H.W., Dowling, H.F., (1951). Effect of large doses of aureomycin on human liver. *AMA Arch. Intern. Med.*, **88**: 271–283.

Li, C., Sun, T., Zhang, D., Zhang, X., Qian, Y., Zhang, Y., Lin, X., Liu, J., Zhu, L., Wang, X., Shi, Z., Lin, Q., (2022). Fabrication of ternary Ag/La-black TiO2−x photocatalyst with enhanced visible-light photocatalytic activity for tetracycline degradation. *J. Alloys Compd.*, **891**: 161960.

Li, G., Lv, L., Fan, H., Ma, J., Li, Y., Wan, Y., Zhao, X., (2010). Effect of the agglomeration of TiO2 nanoparticles on their photocatalytic performance in the aqueous phase. *J. Colloid Interface Sci.*, **348**: 342–7.

Li, J., Suyoulema, Wang, W., Sarina, (2009). A study of photodegradation of sulforhodamine B on Au–TiO2/bentonite under UV and visible light irradiation. *Solid State Sci.*, **11**: 2037–2043.

Li, M., Wang, C., Gonzalez, M., Qiang, Z., (2016). Sulfamethazine degradation in water by the VUV/UV process: Kinetics, mechanism and antibacterial activity

determination based on a mini- fluidic VUV/UV photoreaction system. *Water Res.* **108**: 348–355.

Li, S., Hu, J., (2016). Photolytic and photocatalytic degradation of tetracycline: Effect of humic acid on degradation kinetics and mechanisms. *J. Hazard. Mater.*

Li, S., Peng, L., Yang, C., Song, S., Xu, Y., (2022). Cometabolic biodegradation of antibiotics by ammonia oxidizing microorganisms during wastewater treatment processes. *J. Environ. Manage.*, **305**: 114336.

Li, W., Li, B., Meng, M., Cui, Y., Wu, Y., Zhang, Y., Dong, H., Feng, Y., (2019). Bimetallic Au/Ag decorated TiO2 nanocomposite membrane for enhanced photocatalytic degradation of tetracycline and bactericidal efficiency. *Appl. Surf. Sci.*, **487**: 1008–1017.

Li, X., Jiang, L., Zhan, Q., Qian, J., He, S., (2009). Localized surface plasmon resonance (LSPR) of polyelectrolyte-functionalized gold-nanoparticles for bio-sensing. *Colloids Surf. Physicochem. Eng. Asp.*, **332**: 172–179.

Li, X., Song, Y., Jia, M., Wang, F., Bian, Y., Jiang, X., (2021). Sorption and desorption characteristics of sulfamethazine in three different soils before and after removal of organic matter. *Pedosphere*, **31**: 796–806.

Li, X.Z., Li, F.B., (2001). Study of Au/Au3+-TiO2 Photocatalysts toward Visible Photooxidation for Water and Wastewater Treatment. *Environ. Sci. Technol.* **35**: 2381–2387.

Lin, C.-C., Cheng, Y.-J., (2021). Effectiveness of using nanoscale zero-valent iron and hydrogen peroxide in degrading sulfamethazine in water. *J. Taiwan Inst. Chem. Eng.*, **118**: 179–186.

Lin, C.-C., Wu, M.-S., (2018). Feasibility of using UV/H2O2 process to degrade sulfamethazine in aqueous solutions in a large photoreactor. *J. Photochem. Photobiol. Chem.*, **367**: 446–451.

Lin, L., (2013). Photocatalytic oxidation for degradation of VOCs. *Open J. Inorg. Chem.*, **03**: 14–25.

Lin, L., Wang, H., Luo, H., Xu, P., (2016). Photocatalytic Treatment of Desalination Concentrate Using Optical Fibers Coated With Nanostructured Thin Films:

Impact of Water Chemistry and Seasonal Climate Variations. *Photochem. Photobiol*., **92**: 379–387.

Lin, Y., Zhou, M., Wang, G., Li, H., Wei, Y., Lou, Y., Zhang, D., Ji, L., (2022). Degradation and transformation pathways of sulfamethazine by pre-oxidation disinfection process. *J. Environ. Chem. Eng.*, **10**: 107194.

Linley, S., Liu, Y., Ptacek, C.J., Blowes, D.W., Gu, F.X., (2014). Recyclable Graphene Oxide-Supported Titanium Dioxide Photocatalysts with Tunable Properties. *ACS Appl. Mater. Interfaces*, **6**: 4658–4668.

Liu, C., Lei, Z., Yang, Y., Wang, H., Zhang, Z., (2013). Improvement in settleability and dewaterability of waste activated sludge by solar photocatalytic treatment in Ag/TiO2-coated glass tubular reactor. *Bioresour. Technol.*, **137**: 57–62.

Liu, G., Ji, J., Huang, H., Xie, R., Feng, Q., Shu, Y., Zhan, Y., Fang, R., He, M., Liu, S., Ye, X., Leung, D.Y.C., (2017). UV/H2O2: An efficient aqueous advanced oxidation process for VOCs removal. *Chem. Eng. J.*, **324**: 44–50.

Liu, H., Qi, Z., Liu, C., (2021). Inhibition mechanisms of humic acid and protein on the degradation of sulfamethazine by horseradish peroxidase. *Colloids Surf. Physicochem. Eng. Asp.*, **629**: 127473.

Liu, H., Yang, Y., Kang, J., Fan, M., Qu, J., (2012). Removal of tetracycline from water by Fe-Mn binary oxide. *J. Environ. Sci*., **24**: 242–247.

Liu, J., Dong, M., Zuo, S., Yu, Y., (2009). Solvothermal preparation of TiO2/montmorillonite and photocatalytic activity. *Appl. Clay Sci.*, **43**: 156–159.

Liu, J., Zhang, G., (2014). Recent advances in synthesis and applications of clay-based photocatalysts: A review. *Phys. Chem. Chem. Phys. PCCP*, **16**: 8178–8192.

Liu, L., Luo, X.-B., Ding, L., Luo, S.-L., (2019). Application of Nanotechnology in the Removal of Heavy Metal From Water, in: Luo, X., Deng, F. (Eds.), Nanomaterials for the Removal of Pollutants and Resource Reutilization, *Micro and Nano Technologies*., **4**: 83–147.

Liu, X., Ji, H., Li, S., Liu, W., (2019). Graphene modified anatase/titanate nanosheets with enhanced photocatalytic activity for efficient degradation of sulfamethazine under simulated solar light. *Chemosphere*, **233**: 198–206.

Liu, Y., Liu, X., Dong, W., Zhang, L., Kong, Q., Wang, W., (2017). Efficient Adsorption of Sulfamethazine onto Modified Activated Carbon: A Plausible Adsorption Mechanism. *Sci. Rep*., 7.

Liu, Y., Wang, P., Gojenko, B., Yu, J., Wei, L., Luo, D., Xiao, T., (2021). A review of water pollution arising from agriculture and mining activities in Central Asia: Facts, causes and effects. *Environ. Pollut.*, **291**: 118209.

Liu, Z., Kanjo, Y., Mizutani, S., (2009). Removal mechanisms for endocrine disrupting compounds (EDCs) in wastewater treatment — physical means, biodegradation, and chemical advanced oxidation: A review. *Sci. Total Environ.,* **407**: 731–748.

Lu, H., Li, Q., Feng, W., (2022). Application Progress of O3/UV Advanced Oxidation Technology in the Treatment of Organic Pollutants in Water. *Sustainability.,* **14**: 1556.

Lucas, P., Cabral, C., Colford, J., (2011). Dissemination of Drinking Water Contamination Data to Consumers: A Systematic Review of Impact on Consumer Behaviors. *PloS One*., **6**: e21098.

Luo, Y., Guo, W., Ngo, H.H., Nghiem, L.D., Hai, F.I., Zhang, J., Liang, S., Wang, X.C., (2014). A review on the occurrence of micropollutants in the aquatic environment and their fate and removal during wastewater treatment. *Sci. Total Environ.,* **473–474**: 619–641.

Luttrell, T., Halpegamage, S., Tao, J., Kramer, A., Sutter, E., Batzill, M., (2014). Why is anatase a better photocatalyst than rutile- Model studies on epitaxial TiO2 films. *Sci. Rep.,* **4**: 4043.

Madhavan, J., Theerthagiri, J., Balaji, D., Sunitha, S., Choi, M.Y., Ashokkumar, M., (2019). Hybrid Advanced Oxidation Processes Involving Ultrasound: An Overview. *Molecules*., **24**: 3341.

Malato, S., Fernández-Ibáñez, P., Maldonado, M.I., Blanco, J., Gernjak, W., (2009). Decontamination and disinfection of water by solar photocatalysis: Recent overview and trends. *Catal. Today,* **147**: 1–59.

Mallakpour, S., Nikkhoo, E., (2014). Surface modification of nano-TiO2 with trimellitylimido-amino acid-based diacids for preventing aggregation of nanoparticles. *Adv. Powder Technol.,* **25**: 348–353.

Manea, E., Robescu, L.D., Presura, E., (2016). Limitations In Evaluating Wastewater Treatment Plants Carbon Footprint. 450–453.

Mansouri, L., Tizaoui, C., Geissen, S.-U., Bousselmi, L., (2019). A comparative study on ozone, hydrogen peroxide and UV based advanced oxidation processes for efficient removal of diethyl phthalate in water. *J. Hazard. Mater.*, **363**: 401–411.

Mantzavinos, D., Psillakis, E., (2004). Enhancement of biodegradability of industrial wastewaters by chemical oxidation pre-treatment. *J. Chem. Technol. Biotechnol.*, **79**: 431–454.

Maurya, N.S., Mittal, A.K., Cornel, P., Rother, E., (2006). Biosorption of dyes using dead macro fungi: Effect of dye structure, ionic strength and pH. *Bioresour. Technol.*, **97**: 512–521.

McFarland, A.D., Haynes, C.L., Mirkin, C.A., Van Duyne, R.P., Godwin, H.A., (2004). Color My Nanoworld. *J. Chem. Educ.*, **81**: 544A.

McGregor, D.B., Brown, A.G., Howgate, S., McBride, D., Riach, C., Caspary, W.J., (1991). Responses of the L5178Y mouse Lymphoma cell forward mutation assay. V: 27 coded chemicals. *Environ. Mol. Mutagen.*, **17**: 196–219.

Medvedev, Z.A., Crowne, H.M., Medvedeva, M.N., (1988). Age related variations of hepatocarcinogenic effect of azo dye (3'-MDAB) as linked to the level of hepatocyte polyploidization. *Mech. Ageing Dev.*, **46**: 159–174.

Mehrjouei, M., Müller, S., Möller, D., (2015). A review on photocatalytic ozonation used for the treatment of water and wastewater. *Chem. Eng. J.*, **263**: 209–219.

Meichtry, J.M., Colbeau-Justin, C., Custo, G., Litter, M.I., (2014). Preservation of the photocatalytic activity of TiO2 by EDTA in the reductive transformation of Cr(VI). Studies by Time Resolved Microwave Conductivity. *Catal. Today*, **224**: 236–243.

Mendioroz, S., Pajares, J.A., Benito, I., Pesquera, C., Gonzalez, F., Blanco, C., (1987). Texture evolution of montmorillonite under progressive acid treatment: change from H3 to H2 type of hysteresis. *Langmuir*, **3**: 676–681.

Mendive, C.B., Bredow, T., Schneider, J., Blesa, M., Bahnemann, D., (2015). Oxalic acid at the TiO2 /water interface under UV(A) illumination: Surface reaction mechanisms. *J. Catal.*, **322**: 60–72.

Merényi, G., Lind, J., Naumov, S., Sonntag, C. von, (2010). Reaction of Ozone with Hydrogen Peroxide (Peroxone Process): A Revision of Current Mechanistic Concepts Based on Thermokinetic and Quantum-Chemical Considerations. *Environ. Sci. Technol.*, **44**: 3505–3507.

Min, B., Heo, J., Youn, N., Joo, O., Lee, H., Kim, J., Kim, H.S., (2009). Tuning of the photocatalytic 1,4-dioxane degradation with surface plasmon resonance of gold nanoparticles on titania. *Catal. Commun.*, **10**: 712–715.

Mirsalis, J.C., Tyson, C.K., Steinmetz, K.L., Loh, E.K., Hamilton, C.M., Bakke, J.P., Spalding, J.W., (1989). Measurement of unscheduled DNA synthesis and S-phase synthesis in rodent hepatocytes following in vivo treatment: testing of 24 compounds. *Environ. Mol. Mutagen.*, **14**: 155–164.

Miyoshi, H., Mori, H., Yoneyama, H., (2002). Light-induced decomposition of saturated carboxylic acids on iron oxide incorporated clay suspended in aqueous solutions. *ACS Publ.*

Mogal, S., Gandhi, G., Mishra, M., Tripathi, S., Shripathi, T., Joshi, P., Shah, D., (2014). Single-Step Synthesis of Silver-Doped Titanium Dioxide: Influence of Silver on Structural, Textural, and Photocatalytic Properties. *Ind. Eng. Chem. Res.*, **53**: 5749–5758.

Moran, S., (2018). Dirty water unit operation design: Biological processes. An Applied Guide to Water and Effluent Treatment Plant Design. *Butterworth-Heinemann*, **14**: 171–202.

Moussavi, G., Pourakbar, M., Shekoohiyan, S., Satari, M., (2018). The photochemical decomposition and detoxification of bisphenol A in the VUV/H2O2 process: Degradation, mineralization, and cytotoxicity assessment.

Mudge, S.M., Ball, A.S., (1964). Sewage, *Environmental Forensics. Academic Press, Burlington*, **3**: 35–53.

Muhd Julkapli, N., Bagheri, S., Bee Abd Hamid, S., (2014). Recent Advances in Heterogeneous Photocatalytic Decolorization of Synthetic Dyes. *Sci. World J.*, e692307.

Munter, R., (2001). Advanced oxidation processes–current status and prospects. Estonian Academy Publishers.

Mutou, Y., Ibuki, Y., Terao, Y., Kojima, S., Goto, R., (2006). Chemical change of chlorinated bisphenol A by ultraviolet irradiation and cytotoxicity of their products on Jurkat cells. *Environ. Toxicol. Pharmacol.*, **21**: 283–289.

Nakano, K., Obuchi, E., Nanri, M., (2004). Thermo-Photocatalytic Decomposition of Acetaldehyde Over Pt-TiO2/SiO2. *Chem. Eng. Res. Des.*, **82**: 297–301.

Nakata, K., Fujishima, A., (2012). TiO2 photocatalysis: Design and applications. *J. Photochem. Photobiol. C Photochem. Rev.*, **13**: 169–189.

Nasseri, S., Mahvi, A.H., Seyedsalehi, M., Yaghmaeian, K., Nabizadeh, R., Alimohammadi, M., Safari, G.H., (2017). Degradation kinetics of tetracycline in aqueous solutions using peroxydisulfate activated by ultrasound irradiation: Effect of radical scavenger and water matrix. *J. Mol. Liq.*, **241**: 704–714.

Nawawi, W.I., Zaharudin, R., Mohd Ishak, M.A., Ismail, K., Ahmad, Z., (2016). The Preparation and Characterization of Immobilized TiO2/PEG by Using DSAT as a Support Binder. *Appl. Sci.*, **7**: 24.

Nazar, M.F., Shah, S.S., Khosa, M.A., (2010). Interaction of Azo Dye with Cationic Surfactant Under Different pH Conditions. *J. Surfactants Deterg.*, **13**: 529–537.

Nestmann, E.R., Douglas, G.R., Matula, T.I., Grant, C.E., Kowbel, D.J., (1979). Mutagenic activity of rhodamine dyes and their impurities as detected by mutation induction in Salmonella and DNA damage in Chinese hamster ovary cells. *Cancer Res.* **39**: 4412–4417.

Newcombe, G., (2006). Removal of natural organic material and algal metabolites using activated carbon. *Interface Science and Technology, Interface Science in Drinking Water Treatment. Elsevier.*, **8**: 133–153.

Ng, H., Elimelech, M., (2004). Influence of Colloidal Fouling on Rejection of Trace Organic Contaminants by Reverse Osmosis. *J. Membr. Sci.*, **244**: 215–226.

Ni, M., Leung, M.K.H., Leung, D.Y.C., Sumathy, K., (2007). A review and recent developments in photocatalytic water-splitting using TiO2 for hydrogen production. *Renew. Sustain. Energy Rev.*, **11**: 401–425.

Niu, J., Ding, S., Zhang, L., Zhao, J., Feng, C., (2013). Visible-light-mediated Sr-Bi2O3 photocatalysis of tetracycline: Kinetics, mechanisms and toxicity assessment. *Chemosphere,* **93**

Nosaka, Y., Daimon, T., Nosaka, A., Murakami, Y., 2004. Singlet oxygen formation in photocatalytic TiO2 aqueous suspension. *Phys. Chem. Chem. Phys.*, **6**: 2917–2918.

Ohko, Y., Ando, I., Niwa, C., Tatsuma, T., Yamamura, T., Nakashima, T., Kubota, Y., Fujishima, A., (2001). Degradation of Bisphenol A in Water by TiO2 Photocatalyst. *Environ. Sci. Technol.*, **35**: 2365–2368.

Ohno, T., Sarukawa, K., Tokieda, K., Matsumura, M., (2001). Morphology of a TiO2 Photocatalyst (Degussa, P-25) Consisting of Anatase and Rutile Crystalline Phases. *J. Catal.*, **203**: 82–86.

Omrani, N., Nezamzadeh-Ejhieh, A., (2020). A comprehensive study on the mechanism pathways and scavenging agents in the photocatalytic activity of BiVO4/WO3 nano-composite. *J. Water Process Eng.*, **33**: 101094.

Ono, Y., Sekiguchi, K., Sankoda, K., Nii, S., Namiki, N., (2020). Improved ultrasonic degradation of hydrophilic and hydrophobic aldehydes in water by combined use of atomization and UV irradiation onto the mist surface. *Ultrason. Sonochem.* **60**: 104766.

Orlov, A., Chan, M.S., Jefferson, D.A., Zhou, D., Lynch, R.J., Lambert, R.M., (2006). Photocatalytic degradation of water-soluble organic pollutants on TiO2 modified with gold nanoparticles. *Environ. Technol.*, **27**: 747–752.

Orlov, A., Jefferson, D., Tikhov, M., Lambert, R., (2007). Enhancement of MTBE photocatalytic degradation by modification of TiO2. *Catal. Commun.*, **8**: 821–824.

Oros-Ruiz, S., Zanella, R., Prado, B., (2013). Photocatalytic degradation of trimethoprim by metallic nanoparticles supported on TiO2-P25. *J. Hazard. Mater.*, **263**: 28–35.

Ozawa, K., Emori, M., Yamamoto, Susumu, Yukawa, R., Yamamoto, Shingo, Hobara, R., Fujikawa, K., Sakama, H., Matsuda, I., (2014). Electron–Hole Recombination Time at TiO2 Single-Crystal Surfaces: Influence of Surface Band Bending. *J. Phys. Chem. Lett.*, **5**: 1953–1957.

Ozekin, K., Westerhoff, P., Amy, G.L., Siddiqui, M., (1998). Molecular Ozone and Radical Pathways of Bromate Formation during Ozonation. *J. Environ. Eng.*, **124**: 456–462.

Pal, M., Pal, U., Jiménez, J.M.G.Y., Pérez-Rodríguez, F., (2012). Effects of crystallization and dopant concentration on the emission behavior of TiO2:Eu nanophosphors. *Nanoscale Res. Lett*., **7**: 1.

Pal, P., (2017). Chapter 2 - Chemical Treatment Technology, in: Pal, P. (Ed.), Industrial Water Treatment Process Technology. *Butterworth-Heinemann*, 21–63.

Panagiotaras, D., Stathatos, E., Papoulis, D., (2014). Silver Modified TiO2/Halloysite Thin Films for Decontamination of Target Pollutants. *Int. J. Chem. Mol. Eng.* **8**: 914–920.

Passos, L.C., Saraiva, M.F.S., (2019). Detection in UV-visible spectrophotometry: Detectors, detection systems, and detection strategies. *Measurement*., **135**: 896–904.

Pawlak, Z. (Ed.), (2003). Environmental Issues. *Tribology and Interface Engineering Series, Tribochemistry of Lubricating Oils. Elsevier*., **7**: 267–300.

Pelaez, M., de la Cruz, A.A., O'Shea, K., Falaras, P., Dionysiou, D.D., (2011). Effects of water parameters on the degradation of microcystin-LR under visible light-activated TiO2 photocatalyst. *Water Res.*, **45**: 3787–3796.

Pera-Titus, M., García-Molina, V., Baños, M.A., Giménez, J., Esplugas, S., (2004). Degradation of chlorophenols by means of advanced oxidation processes: a general review. *Appl. Catal. B Environ.*, **47**: 219–256.

Percy, A.J., Moore, N., Chipman, J.K., (1989). Formation of nuclear anomalies in rat intestine by benzidine and its biliary metabolites. *Toxicology*, **57**: 217–223.

Pereira, V.J., Linden, K.G., Weinberg, H.S., (2007). Evaluation of UV irradiation for photolytic and oxidative degradation of pharmaceutical compounds in water. *Water Res.*, **41**: 4413–4423.

Perini, J.A. de L., Silva, B.C. e., Tonetti, A.L., Nogueira, R.F.P., (2017). Photo-Fenton degradation of the pharmaceuticals ciprofloxacin and fluoxetine after anaerobic pre-treatment of hospital effluent. *Environ. Sci. Pollut. Res.*, **24**: 6233–6240.

Perini, J.A.L., Tonetti, A.L., Vidal, C., Montagner, C., Nogueira, R., (2018). Simultaneous degradation of ciprofloxacin, amoxicillin, sulfathiazole and

sulfamethazine, and disinfection of hospital effluent after biological treatment via photo-Fenton process under ultraviolet germicidal irradiation.

Pinkston, K., Sedlak, D., (2004). Transformation of aromatic ether-and amine-containing pharmaceuticals during chlorine disinfection. *Environ. Sci. Technol.,* **38**: 4019–4025.

Pintado-Herrera, M., González-Mazo, E., Lara-Martin, P.A., (2014). Atmospheric pressure gas chromatography-time-of-flight-mass spectrometry (APGC-ToF-MS) for the determination of regulated and emerging contaminants in aqueous samples after stir bar sorptive extraction (SBSE). *Anal. Chim. Acta*., **851**

Pulido Melián, E., González Díaz, O., Ortega Méndez, A., López, C.R., Nereida Suárez, M., Doña Rodríguez, J.M., Navío, J.A., Fernández Hevia, D., Pérez Peña, J., (2013). Efficient and affordable hydrogen production by water photo-splitting using TiO2-based photocatalysts. *Int. J. Hydrog. Energy*., **38**: 2144–2155.

Qiu, P., Park, B., Choi, J., Thokchom, B., Pandit, A., Khim, J., (2018). A review on heterogeneous sonocatalyst for treatment of organic pollutants in aqueous phase based on catalytic mechanism. *Ultrason. Sonochem.,* **45**

Rajabizadeh, K., Yazdanpanah, G., Dowlatshahi, S., Malakootian, M., (2020). Photooxidation Process Efficiency (UV/O3) for P-nitroaniline Removal from Aqueous Solutions. *Ozone Sci. Eng.*, **42**: 420–427.

Rajoriya, S., Bargole, S., Saharan, V., (2016). Degradation of a cationic dye (Rhodamine 6G) using hydrodynamic cavitation coupled with other oxidative agents: Reaction mechanism and pathway. *Ultrason. Sonochem*., 34.

Ran, Y., Qingmin, C., Maorun, F., (2019). Chlorine Dioxide Generation Method and Its Action Mechanism for Removing Harmful Substances and Maintaining Quality Attributes of Agricultural Products. *Food Bioprocess Technol.*, **12**: 1110–1122.

Reghunath, S., Pinheiro, D., Kr, S.D., (2021). A review of hierarchical nanostructures of TiO2: Advances and applications. *Appl. Surf. Sci. Adv.,* **3**: 100063.

Rengaraj, S., Li, X.Z., (2006). Enhanced photocatalytic activity of TiO2 by doping with Ag for degradation of 2,4,6-trichlorophenol in aqueous suspension. *J. Mol. Catal. Chem.,* **243**: 60–67.

Reza, K.M., Kurny, A., Gulshan, F., (2017). Parameters affecting the photocatalytic degradation of dyes using TiO2: a review. *Appl. Water Sci.*, **7**: 1569–1578.

Richardson, S.D., Willson, C.S., Rusch, K.A., (2004). Use of Rhodamine water tracer in the marshland upwelling system. *Ground Water*, **42**: 678–688.

Rivera-Utrilla, J., Sánchez-Polo, M., Ferro-García, M.Á., Prados-Joya, G., Ocampo-Pérez, R., (2013). Pharmaceuticals as emerging contaminants and their removal from water. A review. *Chemosphere*, **93**: 1268–1287.

Rochat, J., Demenge, P., Rerat, J.C., (1978). Toxicologic study of a fluorescent tracer: rhodamine B. *Toxicol. Eur. Res. Rech. Eur. En Toxicol.*, **1**: 23–26.

Rossner, A., Snyder, S.A., Knappe, D.R.U., (2009). Removal of emerging contaminants of concern by alternative adsorbents. *Water Res.*, **43**: 3787–3796.

Rtimi, S., Pulgarin, C., Sanjines, R., Kiwi, J., (2013). Innovative semi-transparent nanocomposite films presenting photo-switchable behavior and leading to a reduction of the risk of infection under sunlight. *RSC Adv.*, **3**: 16345–16348.

Rycenga, M., Cobley, C.M., Zeng, J., Li, W., Moran, C.H., Zhang, Q., Qin, D., Xia, Y., (2011). Controlling the Synthesis and Assembly of Silver Nanostructures for Plasmonic Applications. *Chem. Rev.*, **111**: 3669–3712.

Sowmya, R. S., Madhu, G. M., Hashir, M., (2018). Studies on Nano-Engineered TiO2 Photo Catalyst for Effective Degradation of Dye. IOP Conf. *Ser. Mater. Sci. Eng.*, **310**: 012026.

Siqi, L., Nan, Z., Zi-Rong, T., Yi-jun, X., (2012). Synthesis of one-dimensional CdS@TiO_2 core-shell nanocomposites photocatalyst for selective redox: the dual role of TiO_2 shell. *ACS Appl. Mater. Interfaces*, 4.

Shanthakumar, S., Chiampo, F., (2020). UV Light-Irradiated Photocatalytic Degradation of Coffee Processing Wastewater Using TiO2 as a Catalyst. *Environments*, **7**: 47.

Saavedra, J., Doan, H., Pursell, C., Grabow, L., Chandler, B., (2014). The critical role of water at the gold-titania interface in catalytic CO oxidation. *Science*, 345.

Sabnis, R.W., (2015). Handbook of Fluorescent Dyes and Probes. *John Wiley & Sons*.

Sagadevan, S., Vennila, S., Muthukrishnan, L., Murugan, B., Anita Lett, J., Shahid, M.M., Fatimah, I., Akbarzadeh, O., Mohammad, F., Johan, M.R., (2020).

Improved antimicrobial efficacy and photocatalytic performance of gold decorated titanium dioxide nanohybrid. *Optik*, **224**: 165515.

Saharan, V.K., Pinjari, D.V., Gogate, P.R., Pandit, A.B., (2014). Chapter 3 - Advanced Oxidation Technologies for Wastewater Treatment: An Overview, in: Ranade, V.V., Bhandari, V.M. (Eds.), Industrial Wastewater Treatment, Recycling and Reuse. *Butterworth-Heinemann, Oxford,* 141–191.

Sangiorgi, N., Aversa, L., Tatti, R., Verucchi, R., Sanson, A., (2017). Spectrophotometric method for optical band gap and electronic transitions determination of semiconductor materials. *Opt. Mater.*, **64**: 18–25.

Schneider, J., Matsuoka, M., Takeuchi, M., Zhang, J., Horiuchi, Y., Anpo, M., Bahnemann, D.W., (2014). Understanding TiO2 Photocatalysis: Mechanisms and Materials. *Chem. Rev.*, **114**: 9919–9986.

Scialdone, O., Randazzo, S., Galia, A., Silvestri, G., (2009). Electrochemical oxidation of organics in water: Role of operative parameters in the absence and in the presence of NaCl. *Water Res.*, **43**: 2260–2272.

Sclafani, A., Herrmann, J.-M., (1998). Influence of metallic silver and of platinum-silver bimetallic deposits on the photocatalytic activity of titania (anatase and rutile) in organic and aqueous media. *J. Photochem. Photobiol. Chem.*, **113**: 181–188.

Selene, C.-H., Chou, J., (2003). Concise International Chemical Assessment Document 53: Hydrogen sulfide: Human health aspects. *IPCS Concise Int. Chem. Assess. Doc.*

Selvam, K., Muruganandham, M., Inbasekaran, M., Swaminathan, M., (2007). The influence of inorganic oxidants and metal ions on semiconductor sensitized photodegradation of 4-fluorophenol. *Chem. Eng. J.*, **128**: 51–57.

Selvaraj, R., Li, X., (2006). Enhanced Photocatalytic Activity of TiO2 by Doping with Ag for Degradation of 2,4,6-Trichlorophenol in Aqueous Suspension. *J. Mol. Catal. Chem.*, **243**.

Shanthakumar, S., Chiampo, F., (2020). UV Light-Irradiated Photocatalytic Degradation of Coffee Processing Wastewater Using TiO2 as a Catalyst. *Environments,* **7**: 47.

Shawabkeh, R.A., Tutunji, M.F., (2003). Experimental study and modeling of basic dye sorption by diatomaceous clay. *Appl. Clay Sci.*, **1–2**: 111–120.

Shen, C., Meng, Q., Schmelzer, E., Bader, A., (2009). Gel entrapment culture of rat hepatocytes for investigation of tetracycline-induced toxicity. *Toxicol. Appl. Pharmacol.,* **238:** 178–187.

Shoueir, K., Kandil, S., El-hosainy, H., El-Kemary, M., (2019). Tailoring the surface reactivity of plasmonic Au@TiO2 photocatalyst bio-based chitosan fiber towards cleaner of harmful water pollutants under visible-light irradiation. *J. Clean. Prod.*

Silva, C.P., Otero, M., Esteves, V., (2012). Processes for the elimination of estrogenic steroid hormones from water: a review. *Environ. Pollut. Barking Essex 1987,* **165**: 38–58.

Sing, K.S.W., (1984). Reporting Physisorption Data for Gas/Solid Systems with Special Reference to the Determination of Surface Area and Porosity. *Pure Appl. Chem*., **54(11)**: 2201–2218.

Singer, P.C., (1990). Assessing Ozonation Research Needs in Water Treatment. *J. Am. Water Works Assoc.*, **82**: 78–88.

Siqi, L., Nan, Zi-Rong, T., Yj, X., (2012). Synthesis of one-dimensional CdS@TiO_2 core-shell nanocomposites photocatalyst for selective redox: the dual role of TiO_2 shell. *ACS Appl. Mater. Interfaces.,* **4.**

Sithamparanathan, E., Kujawa-Roeleveld, K., Soedarso, J.A.R., Sutton, N.B., Grolle, K., Bruning, H., Rijnaarts, H.H.M., (2021). Sorption of micropollutants to hydroponic substrata: Effects of physico-chemical properties. *Environ. Adv*., **4**: 100049.

So, C., Cheng, M.Y., Yu, J., Wong, P.K., (2002). Degradation of azo dye Procion Red MX-5B by photocatalytic oxidation. *Chemosphere*, **46**: 905–12.

Sofianou, M.-V., Boukos, N., Vaimakis, T., Trapalis, C., (2014). Decoration of TiO2 anatase nanoplates with silver nanoparticles on the {101} crystal facets and their photocatalytic behaviour. *Appl. Catal. B Environ.*, **158–159**: 91–95.

Sofyan, N., Ridhova, A., Yuwono, A.H., Sianturi, M., (2019). Effect of NaCl Addition on Nano Rosette Tio2 Crystal Growth during Hydrothermal Deposition. *Int. J. Technol.*, **10**: 1235.

Solonenko, O.P., Ando, Y., Nishiyama, H., Kindole, D., Smirnov, A.V., Golovin, A.A., Uehara, S., Nakajima, T., (2018). Synthesis of thick photocatalytic titania surface layers by solution plasma spraying and subsequent treatment by pulsed laminar plasma jet. *Surf. Coat. Technol.*, **333**: 39–51.

Sonawane, R., Hegde, S., Dongare, M., (2003). Preparation of Titanium(IV) Oxide Thin Film Photocatalyst by Sol–Gel Dip Coating. *Mater. Chem. Phys.*, **77**: 744–750.

Sossalla, N.A., Nivala, J., Reemtsma, T., Schlichting, R., König, M., Forquet, N., van Afferden, M., Müller, R.A., Escher, B.I., (2021). Removal of micropollutants and biological effects by conventional and intensified constructed wetlands treating municipal wastewater. *Water Res.*, **201**: 117349.

Sousa-Castillo, A., Comesaña-Hermo, M., Rodríguez-González, B., Pérez-Lorenzo, M., Wang, Z., Kong, X.-T., Govorov, A.O., Correa-Duarte, M.A., (2016). Boosting Hot Electron-Driven Photocatalysis through Anisotropic Plasmonic Nanoparticles with Hot Spots in Au–TiO2 Nanoarchitectures. *J. Phys. Chem. C.*, **120**: 11690–11699.

Sowmiya, M., Senthilkumar, K., (2015). Adsorption of proline, hydroxyproline and glycine on anatase (001) surface: a first-principle study. *Theor. Chem. Acc*., 135.

Sowmya, S R., Madhu, GM., M., Hashir, M., (2018). Studies on Nano-Engineered TiO2 Photo Catalyst for Effective Degradation of Dye. *IOP Conf. Ser. Mater. Sci. Eng.*, **310**: 012026.

Su, C.-C., Pukdee-Asa, M., Ratanatamskul, C., Lu, M.-C., (2011). Effect of operating parameters on decolorization and COD removal of three reactive dyes by Fenton's reagent using fluidized-bed reactor. *Desalination.*, **278**: 211–218.

Su, R., Tiruvalam, R., He, Q., Dimitratos, N., Kesavan, L., Hammond, C., Lopez-Sanchez, J.A., Bechstein, R., Kiely, C.J., Hutchings, G.J., Besenbacher, F., (2012). Promotion of Phenol Photodecomposition over TiO2 Using Au, Pd, and Au–Pd Nanoparticles. *ACS Nano*, **6**: 6284–6292.

Sun, W., Chen, L., Tian, J., Wang, J., He, S., (2013). Degradation of a monoazo dye Alizarin Yellow GG in aqueous solutions by gamma irradiation:

Decolorization and biodegradability enhancement. *Radiat. Phys. Chem.*, **83**: 86–89.

Sun, Z., Chen, Y., Ke, Q., Yang, Y., Yuan, J., (2002). Photocatalytic degradation of cationic azo dye by TiO2/bentonite nanocomposite. *J. Photochem. Photobiol. Chem.*, **149:** 169–174.

Suzuki, T., Nakagawa, Y., Takano, I., Yaguchi, K., Yasuda, K., (2004). Environmental Fate of Bisphenol A and Its Biological Metabolites in River Water and Their Xeno-estrogenic Activity. *Environ. Sci. Technol.*, **38**: 2389–96.

Tahir, K., Ahmad, A., Li, B., Khan, A.U., Nazir, S., Khan, Shafiullah, Khan, Z.U.H., Khan, Shahab, (2016). Preparation, characterization and an efficient photocatalytic activity of Au/TiO2 nanocomposite prepared by green deposition method. *Mater. Lett.*, **178**: 56–59.

Tatsuma, T., Nishi, H., Ishida, T., (2017). Plasmon-induced charge separation: chemistry and wide applications. *Chem. Sci.*, **8**: 3325–3337.

Thaler, S., Haritoglou, C., Choragiewicz, T., Messias, A., Baryluk, A., May, C., Rejdak, R., Fiedorowicz, M., Zrenner, E., Schuettauf, F., (2008). In Vivo Toxicity Study of Rhodamine 6G in the Rat Retina. *Invest. Ophthalmol. Vis. Sci.*, **49**: 2120–6.

Thomas, M., Natarajan, T., (2018). TiO2-High Surface Area Materials Based Composite Photocatalytic Nanomaterials for Degradation of Pollutants: A Review. *Photocatalytic Nanomaterials for Environmental Applications.*

Thompson, T.L., Yates, J.T., (2006). Surface Science Studies of the Photoactivation of TiO2 New Photochemical Processes. *Chem. Rev.*, **106**: 4428–4453.

Tiwari, A., Shukla, A., Lalliansanga, Tiwari, D., Lee, S., (2018). Nanocomposite thin films Ag0(NP)/TiO2 in the efficient removal of micro-pollutants from aqueous solutions: A case study of tetracycline and sulfamethoxazole removal. *J. Environ. Manage.*, **220**: 96–108.

Tiwari, A., Shukla, A., Lalliansanga, Tiwari, D., Lee, S.-M., (2019). Au-nanoparticle/nanopillars TiO2 meso-porous thin films in the degradation of tetracycline using UV-A light. *J. Ind. Eng. Chem.*, **69**: 141–152.

Tiwari, A., Shukla, A., Lalliansanga, Tiwari, D., Lee, S.M., (2020). Synthesis and characterization of Ag0(NPs)/TiO2 nanocomposite: insight studies of triclosan removal from aqueous solutions. *Environ. Technol.*, **41**: 3500–3514.

Tiwari, D., Lalhriatpuia, C., Lalhmunsiama, L., Lee, S.-M., Kong, S.-H., (2015). Efficient application of nano-TiO2 thin films in the photocatalytic removal of Alizarin Yellow from aqueous solutions. *Appl. Surf. Sci.*, **353**: 275–283.

Tixier, C., Bogaerts, P., Sancelme, M., Bonnemoy, F., Twagilimana, L., Cuer, A., Bohatier, J., Veschambre, H., (2000). Fungal biodegradation of a phenylurea herbicide, diuron: Structure and toxicity of metabolites. *Pest Manag. Sci.*, **56:** 455–462.

Tsukamoto, D., Shiraishi, Y., Sugano, Y., Ichikawa, S., Tanaka, S., Hirai, T., (2012). Gold Nanoparticles Located at the Interface of Anatase/Rutile TiO2 Particles as Active Plasmonic Photocatalysts for Aerobic Oxidation. *J. Am. Chem. Soc.*, **134:** 6309–6315.

Turchi, C., (1990). Photocatalytic degradation of organic water contaminants: Mechanisms involving hydroxyl radical attack. *J. Catal.*, **122**: 178–192.

Tuzen, M., Sari, A., Saleh, T., (2017). Response surface optimization, kinetic and thermodynamic studies for effective removal of rhodamine B by magnetic AC/CeO2 nanocomposite. *J. Environ. Manage.*, **206**: 170–177.

Ulhaq, I., Ahmad, W., Ahmad, I., Yaseen, M., Ilyas, M., (2021). Engineering TiO2 supported CTAB modified bentonite for treatment of refinery wastewater through simultaneous photocatalytic oxidation and adsorption. *J. Water Process Eng.*, **4:** 102239.

Vader, J.S., van Ginkel, C.G., Sperling, F.M.G.M., de Jong, J., de Boer, W., de Graaf, J.S., van der Most, M., Stokman, P.G.W., (2000). Degradation of ethinyl estradiol by nitrifying activated sludge. *Chemosphere.*, **41**: 1239–1243.

Verma, A.K., Dash, R.R., Bhunia, P., (2012). A review on chemical coagulation/flocculation technologies for removal of colour from textile wastewaters. *J. Environ. Manage.*, **93**: 154–168.

Vogna, D., Marotta, R., Napolitano, A., Andreozzi, R., d'Ischia, M., (2004). Advanced oxidation of the pharmaceutical drug diclofenac with UV/H2O2 and ozone. *Water Res.*, **38**: 414–422.

Wadley, S., Waite, T.D., (2002). Photo-Fenton oxidation of pesticides. *Water Supply*., **2**: 249–256.

Wainwright, M., (2011). Dyes for the medical industry, in: Handbook of Textile and Industrial Dyeing. *Elsevier*, 204–230.

Wallace, B., Purcell, M., Furlong, J., (2002). Total organic carbon analysis as a precursor to disinfection byproducts in potable water: Oxidation technique considerations. *J. Environ. Monit.*, **4**: 35–42.

Walsh, G.E., Bahner, L.H., Horning, W.B., (1980). Toxicity of textile mill effluents to freshwater and estuarine algae, crustaceans and fishes. *Environ. Pollut. A.*, **21:** 169–179.

Wang, D., Pillai, S.C., Ho, S.-H., Zeng, J., Li, Y., Dionysiou, D.D., (2018a). Plasmonic-based nanomaterials for environmental remediation. *Appl. Catal. B Environ.*, **237**: 721–741.

Wang, F., Stahl, S.S., (2020). Electrochemical Oxidation of Organic Molecules at Lower Overpotential: Accessing Broader Functional Group Compatibility with Electron−Proton Transfer Mediators. *Acc. Chem. Res.*, **53:** 561–574.

Wang, F., Wang, Y., Li, Y., Cui, X., Zhang, Q., Xie, Z., Liu, H., Feng, Y., Lv, W., Liu, G., (2018b). The facile synthesis of a single atom-dispersed silver-modified ultrathin g-C3N4 hybrid for the enhanced visible-light photocatalytic degradation of sulfamethazine with peroxymonosulfate. *Dalton Trans.*, **47**: 6924–6933.

Wang, G., Dai, J., Luo, Q., Deng, N., (2021). Photocatalytic degradation of bisphenol A by TiO2@aspartic acid-β-cyclodextrin@reduced graphene oxide. *Sep. Purif. Technol*., **254**: 117574.

Wang, H., You, T., Shi, W., Li, J., Guo, L., (2012). Au/TiO2/Au as a Plasmonic Coupling Photocatalyst. *J. Phys. Chem. C*, **116**: 6490–6494.

Wang, L., Zhang, C., Gao, F., Mailhot, G., Pan, G., (2017). Algae decorated TiO2/Ag hybrid nanofiber membrane with enhanced photocatalytic activity for Cr(VI) removal under visible light. *Chem. Eng. J.*, **314**: 622–630.

Wang, M., Han, J., Xiong, H., Guo, R., Yin, Y., (2015). Nanostructured Hybrid Shells of r-GO/AuNP/m-TiO2 as Highly Active Photocatalysts. *ACS Appl. Mater. Interfaces.*, **7**: 6909–6918.

Wang, R., Ji, M., Zhai, H., Liu, Y., (2020). Occurrence of phthalate esters and microplastics in urban secondary effluents, receiving water bodies and reclaimed water treatment processes. *Sci. Total Environ.*, **737**: 140219.

Warner, A.J., Hathaway-Schrader, J.D., Lubker, R., Davies, C., Novince, C.M., (2022). Tetracyclines and bone: Unclear actions with potentially lasting effects. *Bone*, **159**: 116377.

Weber, R.S., Ramasamy, K.K., (2020). Electrochemical Oxidation of Lignin and Waste Plastic. *ACS Omega*., **5**: 27735–27740.

Wen, D., Wu, Z., Tang, Y., Li, M., Qiang, Z., (2018). Accelerated degradation of sulfamethazine in water by VUV/UV photo-Fenton process: Impact of sulfamethazine concentration on reaction mechanism. *J. Hazard. Mater.*, **344**: 1181–1187.

Westerhoff, P., Yoon, Y., Snyder, S., Wert, E., (2005). Fate of Endocrine-Disruptor, Pharmaceutical, and Personal Care Product Chemicals during Simulated Drinking Water Treatment Processes. *Environ. Sci. Technol.*, **39**: 6649–6663.

Wojcieszak, D., Mazur, M., Kaczmarek, D., Morgiel, J., Poniedzialek, A., Domaradzki, J., Czeczot, A., (2015). Influence of the structural and surface properties on photocatalytic activity of TiO2: Nd thin films. *Pol. J. Chem. Technol.*, **17**: 103–111.

Wu, J., Uchida, S., Fujishiro, Y., Yin, S., Sato, T., (1999). Synthesis and photocatalytic properties of HTaWO6/(Pt,TiO2) and HTaWO6/(Pt,Fe2O3) nanocomposites. *Int. J. Inorg. Mater.*, **1**: 253–258.

Wu, T.-S., Wang, K., Li, G.-D., Sun, S.-Y., Sun, J., Chen, J., (2010). Montmorillonite-Supported Ag/TiO2 Nanoparticles: An Efficient Visible-Light Bacteria Photodegradation Material. *ACS Appl. Mater. Interfaces*, **2**: 544–50.

Xiang, Y., Gonsior, M., Schmitt-Kopplin, P., Shang, C., (2020). Influence of the UV/H2O2 Advanced Oxidation Process on Dissolved Organic Matter and the Connection between Elemental Composition and Disinfection Byproduct Formation. *Environ. Sci. Technol.*, **54**: 14964–14973.

Xiong, Z., Ma, J., Ng, W.J., Waite, T.D., Zhao, X.S., (2011). Silver-modified mesoporous TiO2 photocatalyst for water purification. *Water Res.*, **45**: 2095–2103.

Xu, D., Liu, K., Shi, W., Chen, M., Luo, B., Xiao, L., Gu, W., (2015). Ag-decorated K2Ta2O6 nanocomposite photocatalysts with enhanced visible-light-driven degradation activities of tetracycline (TC). *Ceram. Int.*, **41**: 4444–4451.

Xu, H., Hao, Z., Feng, W., Wang, T., Fu, X., (2022). The floating photocatalytic spheres loaded with weak light-driven TiO2-based catalysts for photodegrading tetracycline in seawater. *Mater. Sci. Semicond. Process.* **144**: 106610.

Xu, J., Xiao, X., Ren, F., Wu, W., Dai, Z., Cai, G., Zhang, S., Zhou, J., Mei, F., Jiang, C., (2012). Enhanced photocatalysis by coupling of anatase TiO2 film to triangular Ag nanoparticle island. *Nanoscale Res. Lett.*, **7**: 239.

Xu, J.J., Henstock, P.V., Dunn, M.C., Smith, A.R., Chabot, J.R., de Graaf, D., (2008). Cellular imaging predictions of clinical drug-induced liver injury. *Toxicol. Sci. Off. J. Soc. Toxicol.*, **105**: 97–105.

Yamamoto, A., Mizuno, Y., Teramura, K., Shishido, T., Tanaka, T., (2013). Effects of reaction temperature on the photocatalytic activity of photo-SCR of NO with NH3 over a TiO2 photocatalyst. *Catal. Sci. Technol.* **3**: 1771–1775.

Yamamoto, T., Yasuhara, A., Shiraishi, H., Nakasugi, O., (2001). Bisphenol A in hazardous waste landfill leachates. *Chemosphere*, **42**: 415–418.

Yang, H., Yang, J., (2018). Photocatalytic degradation of rhodamine B catalyzed by TiO2 films on a capillary column. *RSC Adv.*, **8**: 11921–11929.

Yang, W., Tang, Z., Zhou, F., Zhang, W., Song, L., (2013). Toxicity studies of tetracycline on Microcystis aeruginosa and Selenastrum capricornutum. *Environ. Toxicol. Pharmacol.*, **35**: 320–324.

Yasumori, A., Yamazaki, K., Shibata, S., Yamane, M., (1994). Preparation of TiO_2 Fine Particles Supported on Silica Gel as Photocatalyst. *J. Ceram. Soc. Jpn.* **102**: 702–707.

Ye, S., Wang, R., Wu, M.-Z., Yuan, Y.-P., (2015). A review on g-C3N4 for photocatalytic water splitting and CO2 reduction. *Appl. Surf. Sci.*, **358**: 15–27.

Yong, C.W., Smith, W., Kendall, K., (2002). Surface contact studies of NaCl and TiO2: molecular dynamics simulation studies. *J. Mater. Chem.*, **12**: 2807–2815.

Yu, J., Kiwi, J., Wang, T., Pulgarin, C., Rtimi, S., (2019). Evidence for a dual mechanism in the TiO2/CuxO photocatalyst during the degradation of sulfamethazine under solar or visible light: Critical issues. *J. Photochem. Photobiol. Chem.*, **375**: 270–279.

Yuan, R., Zhu, Y., Zhou, B., Hu, J., (2019). Photocatalytic oxidation of sulfamethoxazole in the presence of TiO2: Effect of matrix in aqueous solution on decomposition mechanisms. *Chem. Eng. J.*, **359**: 1527–1536.

Yudasari, N., Anugrahwidya, R., Tahir, D., Suliyanti, M.M., Herbani, Y., Imawan, C., Khalil, M., Djuhana, D., (2021). Enhanced photocatalytic degradation of rhodamine 6G (R6G) using ZnO–Ag nanoparticles synthesized by pulsed laser ablation in liquid (PLAL). *J. Alloys Compd.*, **886**: 161291.

Yun, H., Lee, H., Kim, N., Yi, J., (2009). Characterization of photocatalytic performance of silver deposited TiO2 nanorods. *Electrochem. Commun.*, **11(2)**: 363-366.

Zanella, R., Avella, E., Ramírez-Zamora, R.M., Castillón-Barraza, F., Durán-Álvarez, J.C., (2018). Enhanced photocatalytic degradation of sulfamethoxazole by deposition of Au, Ag and Cu metallic nanoparticles on TiO2. *Environ. Technol*. **39**: 2353–2364.

Zangeneh, H., Zinatizadeh, A.A.L., Habibi, M., Akia, M., Hasnain Isa, M., (2015). Photocatalytic oxidation of organic dyes and pollutants in wastewater using different modified titanium dioxides: A comparative review. *J. Ind. Eng. Chem.*, **26**: 1–36.

Zeghioud, H., Kamagate, M., Coulibaly, L.S., Rtimi, S., Assadi, A.A., (2019). Photocatalytic degradation of binary and ternary mixtures of antibiotics: reactive species investigation in pilot scale. *Chem. Eng. Res. Des*., **144**: 300–309.

Zhang, M.-H., Dong, H., Zhao, L., Wang, D.-X., Meng, D., (2019). A review on Fenton process for organic wastewater treatment based on optimization perspective. *Sci. Total Environ.*, **670**: 110–121.

Zhang, X., Chen, Y.L., Liu, R.-S., Tsai, D.P., (2013). Plasmonic photocatalysis. *Rep. Prog. Phys.*, **76**: 046401.

Zhang, Y., Wang, D., Zhang, G., (2011). Photocatalytic degradation of organic contaminants by TiO2/sepiolite composites prepared at low temperature. *Chem. Eng. J*., **173**: 1–10.

Zhao, Q.-E., Wen, W., Xia, Y., Wu, J.-M., (2018). Photocatalytic activity of TiO2 nanorods, nanowires and nanoflowers filled with TiO2 nanoparticles. *Thin Solid Films*., **648**.

Zhong, S.-F., Yang, B., Xiong, Q., Cai, W.-W., Lan, Z.-G., Ying, G.-G., (2022). Hydrolytic transformation mechanism of tetracycline antibiotics: Reaction kinetics, products identification and determination in WWTPs. *Ecotoxicol. Environ. Saf.*, **229**: 113063.

Zhou, X., Liu, G., Yu, J., Fan, W., (2012). Surface plasmon resonance-mediated photocatalysis by noble metal-based composites under visible light. *J. Mater. Chem*., **22**: 21337–21354.

Zucca, P., Vinci, C., Sollai, F., Rescigno, A., Sanjust, E., (2008). Degradation of Alizarin Red S under mild experimental conditions by immobilized 5,10,15,20-tetrakis(4-sulfonatophenyl)porphine–Mn(III) as a biomimetic peroxidase-like catalyst. *J. Mol. Catal. Chem.*, **288**: 97–102.

BIO-DATA

1. NAME : CVL Hmingmawia

2. DATE OF BIRTH : 24th June, 1993.

3. FATHER'S NAME : C Hrangliana

4. PERMANENT ADDRESS : C-3, Dawr Veng, Vengthlang, Champhai, Mizoram 796321.

5. EDUCATIONAL QUALIFICATIONS:

Qualification	Year of Passing	Board/University	Subjects	Marks %	Division
HSLC	2010	Mizoram Board of School Education	English, Mizo, Mathematics, Science, Social sciences	58.8	Second
HSSLC	2013	Mizoram Board of School Education	English, Mizo, Biology, Physics, Chemistry	68.8	First
B.Sc (Chemisty)	2016	Mizoram University	Chemistry, Botany, Zoology	81.75	First
M.Sc (Chemistry)	2018	University of Hyderabad	General Chemistry (Project in Organic Chemistry)	65.5	First

List of Publications

A. Journals

1. **Chhakchhuak Vanlalhmingmawia**, Chhakchhuak Lalhriatpuia, Diwakar Tiwari†, Dong-Jin Kim (2022). Noble metal-doped TiO_2 thin films in the efficient removal of Mordant Orange-1: insights of degradation process. *Environmental Science and Pollution Research*, **29**: 51732–51743. https://doi.org/10.1007/s11356-021-17568-2. (**Published**)

2. **Chhakchhuak Vanlalhmingmawia[1],** Diwakar Tiwari[1, †], Seung Mok Lee[2,† †], (2023). Engineering Clay supported Au doped TiO_2 thin film for the efficient degradation of Rhodamine B and Rhodamine 6G under Visible Light irradiation: Reaction Mechanism and Pathway. *Environmental Engineering Research*, **28(4)***: 220430.* https://doi.org/10.4491/eer.2022.430 (**Published**)

3. **Chhakchhuak Vanlalhmingmawia,** Seung-Mok Lee, Diwakar Tiwari†, (2023). Plasmonic Noble Metal Doped Titanium Dioxide Nanocomposites: Newer and Exciting Materials in the Remediation of Aquatic Environment Contaminated with Micropollutants. *Journal of Water Process Engineering*, **51**: 103360. https://doi.org/10.1016/j.jwpe.2022.103360 (**Published**)

4. **Chhakchhuak Vanlalhmingmawia,** Diwakar Tiwari†, (2023). Novel Cubical Ag(NP) Decorated Titanium dioxide Supported Bentonite Thin film in the Efficient Removal of Bisphenol A Using Visible Light. *Environmental Science and Pollution Research* (**Published**)

5. Levia Lalthazuala, Lalhmunsiama*, **Chhakchhuak Vanlalhmingmawia,** Diwakar Tiwari†, Suk Soon Choi** and Seung-Mok Lee***,†(2022). Newer Insights on Ferrate(VI) Reactions with Various Water pollutants: A Review. *Applied Chemical Engineering*, **33**: 3. https://doi.org/10.14478/ace.2022.1030. (**Published**)

6. Lalhmunsiama, Ralte Malsawmdawngzela*, **Chhakchhuak Vanlalhmingmawia*,** Diwakar Tiwari*,† and Yiyong Yoon**,†(2022). Advancement of clay and clay-based materials in the remediation of aquatic environment contaminated with heavy

metal toxic ions and micro-pollutants. *Applied Chemical Engineering*, **33**: 5. https://doi.org/10.14478/ace.2022.1089. (**Published**)

7. **Chhakchhuak Vanlalhmingmawia,** Dong-Jin Kim, Diwakar Tiwari†, (2022). Novel cubical silver (NP) decorated nanocatalyst thin films in the efficient removal of antibiotics: Insights of photocatalytic treatment of TC and SMZ. *Environmental Research* (**Accepted**)

B. Conference/ Seminar

1. Presented 'Potential of Iron Pillared Clay as Active Nanocatalyst for Rapid Decolorization of Methylene Blue' at International Conference on Chemistry & Environmental Sustainability (ICCES-2019) on 19th to 22nd February, 2019 which was organized by Department of Chemistry, Mizoram university Aizawl, Mizoram, India.

2. Presented 'Nanocomposite Ag^0(NP)/TiO_2Thin Film in the Efficient Removal of Dye from Aqueous Solutions: Physico-chemical Studies' at National Conference on Functional Materials and Applications- 2019 (NCFMA- 2019) on 22nd to 23rd November 2019, organized by Department of BS&HSS (Physics), National Institute of Technology, Aizawl, Mizoram, India.

3. Presented 'Clay Supported Noble Metal Doped TiO_2 Photocatalyst for the Efficient Removal of Tetracycline from Aqueous Solution' at the 2nd Annual Convention of North East (India) Academy of Science and Technology (NEAST) & International Seminar on Recent Advances in Science and Technology (ISRAST), 16th -18th November 2020, Organized NEAST, Mizoram University, Aizawl, Mizoram, India.

4. Presented 'Novel nanocomposite thin films for efficient degradation of Rhodamine B and Rhodamine 6G under visible light irradiation: Reaction Mechanism and Pathway studies' at Mizoram Science Congress 2022 on 24-25 November 2022, Organized by Mizoram Science, Technology, and Innovation Council (MISTIC) in collaboration with Mizo Academy of Sciences (MAS), Mizoram Science Society

(MSS), Science Teachers' Association, Mizoram (STAM), Geological Society of Mizoram (GSM), Mizoram Mathematics Society (MMS), Biodiversity and Nature Conservation Network (BIOCONE) and Mizoram Information & Technology Society (MITS); Aizawl, Mizoram, India.

ISSN **1614-7499** (Online) | Environmental science and pollution research international |

Environmental Science and Pollution Research

Editor-in-Chief
Philippe Garrigues

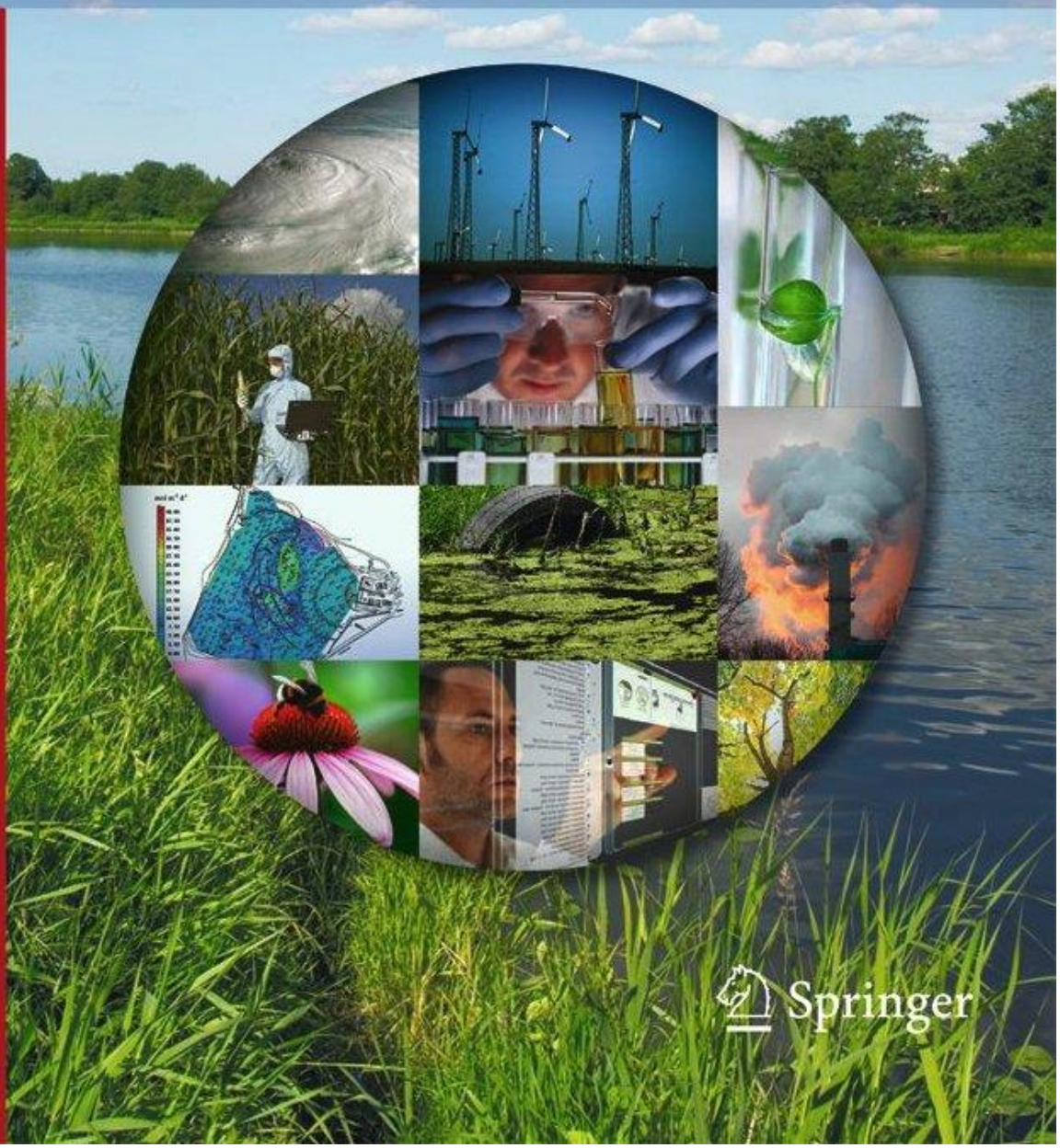

Official Organ of the EuCheMS Division of Chemistry and the Environment (EuCheMS DCE)

Springer

Environmental Science and Pollution Research (2022) 29:51732–51743
https://doi.org/10.1007/s11356-021-17568-2

RESEARCH ARTICLE

Noble metal-doped TiO_2 thin films in the efficient removal of Mordant Orange-1: insights of degradation process

Chhakchhuak Vanlalhmingmawia[1] · Chhakchhuak Lalhriatpuia[2] · Diwakar Tiwari[1] · Dong-Jin Kim[3]

Received: 1 July 2021 / Accepted: 12 November 2021 / Published online: 5 March 2022

Abstract

Nanocomposite Ag^0(NPs)/TiO_2 is synthesised in a facile template method enabling nanoparticles of reduced Ag evenly distributed within the titania network. The morphological studies of nanocomposites were extensively performed employing SEM/EDX (scanning electron microscopy/energy dispersive X-ray), TEM (transmission electron microscopy) and AFM (atomic force microscopy). Moreover, the bandgap energies of materials were obtained using the diffuse reflectance spectrometer (DRS). The newer insights in the photocatalytic elimination of Mordant Orange-1 (MO1) was obtained using the nanocomposite thin film for various parametric studies utilising the UV-A and LED illuminations. The kinetics of degradation of MO1 was performed, and the rate constant was favoured at lower concentrations of MO1. Moreover, the elimination efficiency of MO1 was favoured with a decrease in solution pH. The NPOC results inferred that a fairly good extent of MO1 was mineralised using a thin-film catalyst for both the UV-A and LED illuminations. The minimal effect of several co-ions demonstrated the applicability of thin films in the elimination of MO1, and the stability of the thin film has shown the potential applicability of thin-film catalysts. Further, the mechanism of photocatalytic degradation was demonstrated with the radical scavenger studies and ascertained the reaction pathways.

Keywords Insights of degradation · Kinetic studies · Mineralisation of Mordant Orange-1 · Mordant Orange-1 · Nanocomposite · Surface plasmon resonance

Introduction

The contamination of aquatic environments with innumerable dye compounds is a greater environmental concern. Several dyes, dye precursors are seemingly known as carcinogenic/mutagenic (Matouq et al. 2014). The main entry route of synthetic dyes in water bodies is through the effluent discharged from the industries viz., textile, paper, leather, paint, food, cosmetics, pharmaceuticals, hair colourings, etc. (Verma et al. 2012; Papić et al. 2004). It was reported that the annual dye production exceeds 7×10^5 tons (Lee et al. 2006; Riera-Torres et al. 2010), and nearly 10–15% of the total dyes are directly entering through the effluents during the synthesis and dyeing processes (Husain 2006; Gupta and Suhas 2009; Hai et al. 2007). Moreover, textile dyes estimated at around 2.8×10^5 tons are eventually released into the water bodies through the industrial effluents every year (Jin et al. 2007; H et al. 2017). Synthetic dyes are refractory in nature as they are trivially biodegradable in nature and are known to be highly stable against some oxidising agents (Sadeghzade-Attar 2018). Hence, such dyes are often escaped from the current wastewater treatment plants and entered into the water bodies which caused serious and adverse effects to the aquatic environment (Jung et al. 2016; Su et al. 2011; Muhd Julkapli et al. 2014). Azo dye compounds are known to be highly toxic causing several health issues such as allergy, skin diseases, cancer, defect in embryo development, etc. (Rosu et al. 2017; Alves de Lima et al. 2007; Hatch and Maibach 1995). Therefore, complete and efficient removal of dye compounds from the water

Responsible Editor: Sami Rtimi

✉ Diwakar Tiwari
Ediw_tiwari@yahoo.com

[1] Department of Chemistry, School of Physical Sciences, Mizoram University, Aizawl 796004, India

[2] Department of Chemistry, Pachhunga University College, Mizoram University, Aizawl 796001, India

[3] Department of Environment Science and Biotechnology, Hallym University, Chuncheon 24252, Republic of Korea

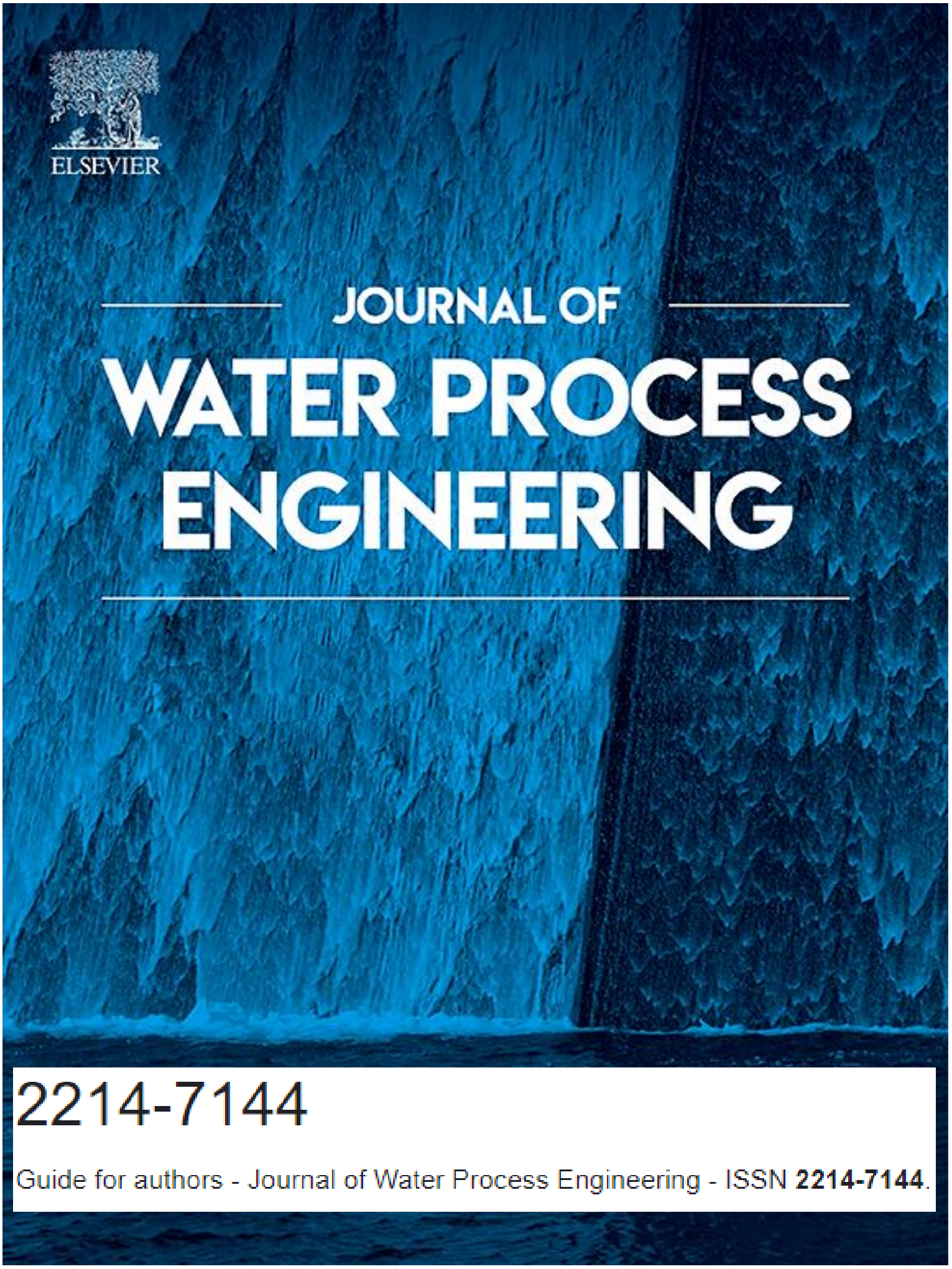

2214-7144

Guide for authors - Journal of Water Process Engineering - ISSN **2214-7144**.

Journal of Water Process Engineering 51 (2023) 103360

Contents lists available at ScienceDirect

Journal of Water Process Engineering

journal homepage: www.elsevier.com/locate/jwpe

Plasmonic noble metal doped titanium dioxide nanocomposites: Newer and exciting materials in the remediation of water contaminated with micropollutants

Chhakchhuak Vanlalhmingmawia [a], Seung Mok Lee [b], Diwakar Tiwari [a,*]

[a] Department of Chemistry, School of Physical Sciences, Mizoram University, Aizawl 796004, India
[b] Department of Biosystems and Convergence Engineering, Catholic Kwandong University, Gangneung 25601, Republic of Korea

ARTICLE INFO

Keywords:
Plasmonic materials
Noble metal(NPs) doped TiO_2
Decontamination
Reaction mechanism of degradation
Photocatalysts
LSPR

ABSTRACT

The noble metal nanoparticles doped semiconductor titanium dioxide have received greater attention and showed enhanced applicability and utility in the diverse field of research. Applications of these materials in the environmental sciences, specifically in the decontamination of aquatic environments contaminated with various micropollutants, is an emerging area of research. These materials have shown promising features that attracted global interest. The noble metals viz., Au, Ag, Pt, and Pd are extensively included in the review article for their use removing of various micropollutants contaminating the aquatic environment. Synthesis and characterization of these materials are essential for their insightful understanding of remediation processes. Various preparatory methods of materials and their photocatalytic efficiency, along with the mechanistic aspects, are critically evaluated in the review. The critical components of the catalyst for possible implications are the materials' shape, size, textural distribution, loaded amount of noble metal nanoparticles, and the band gap energy of materials. Further, the role of the light sources in photocatalytic operations is crucial and better optimized for greater output. Moreover, the practical aspects of these materials are extensively studied for their stability/reusability in prolonged operations, selectivity for real implications, and large-scale/or pilot-scale implications. Insights into the catalytic processes, particularly the radical identification, by-products formed, and reaction pathways, provide a more profound and molecular-level understanding of the processes. These input results pave the way for implementing the laboratory trials toward possible technology developments.

1. Introduction

Micropollutants such as pesticides, endocrine-disrupting chemicals (EDCs), personal care products, pharmaceuticals, polychlorinated biphenyl (PCBs), polycyclic aromatic hydrocarbons (PAHs), and dyes are the class of emerging water pollutants and shown global attention in recent time. They are widely dispersed in industrial and municipal wastewater effluents and finally to the water bodies [1]. These micropollutants in water bodies pose a severe risk to the ecological system. Thus, it must be treated efficiently to prevent aquatic environment contamination [2,3]. Excessive and uncontrolled release of these micropollutants from municipal waste and industries and improper treatments result in an additional load of these contaminants to the water bodies [4].

Among micropollutants, the pharmaceuticals are extensively used for humans and livestock in curing various diseases. Moreover, antibiotics are the most common micropollutants since they are widely used in modern medication. These are employed for therapeutic development and inhibit microbes while leaving intact cells [5]. These compounds are extensively used to prevent many common diseases and to control parasites [6]. Global antibiotic consumption exceeds billions of tablets annually [7], and around 70 billion were produced in 2010 [8]. A significant amount of antibiotics is excreted through urine and feces, and they are thus finally entered into the aquatic environment. The animals or humans readily consume the polluted water, increasing antibiotic-resistant genes' growth [9].

Similarly, endocrine-disrupting chemicals (EDC) cause impairment in the reproductive organs of aquatic animals [10,11]. The EDCs interact with the body's regular secretory chemicals, which results in a change in metabolism, release, synthesis, and operation process. EDCs also inhibit

* Corresponding author.
E-mail address: diw_tiwari@yahoo.com (D. Tiwari).

https://doi.org/10.1016/j.jwpe.2022.103360
Received 24 July 2022; Received in revised form 13 November 2022; Accepted 16 November 2022

Environmental Engineering Research

eISSN : 2005-968X
pISSN : 1226-1025

Environmental Engineering Research

An International Journal of the Korean Society of Environmental Engineers (KSEE)

Environ. Eng. Res. 2023; 28(4): 220430
https://doi.org/10.4491/eer.2022.430

pISSN 1226-1025
eISSN 2005-968X

Research

Novel nanocomposite thin films for efficient degradation of Rhodamine B and Rhodamine 6G under visible light irradiation: Reaction Mechanism and Pathway studies

Chhakchhuak Vanlalhmingmawia[1], Swamy Sreenivasa[2], Diwakar Tiwari[1,†], Seung Mok Lee[4,†]

[1]*Department of Chemistry, School of Physical Sciences, Mizoram University, Aizawl-796004, India*
[2]*Department of Studies and Research in Chemistry, Tumkur University, Tumakuru- 572103, India*
[3]*Department of Biosystems and Convergence Engineering, Catholic Kwandong University, Gangneung 25601, Republic of Korea*

Received August 8, 2022 **Revised** October 5, 2022 **Accepted** October 11, 2022

ABSTRACT

The present investigation aims to synthesize the novel nanocomposite thin film and utilize the material to remove emerging dyes efficiently (i.e., Rhodamine B (R-B) and Rhodamine 6G (R-6G)), in an aqueous solution using LED visible light and UV-A light. A facile synthetic route was adopted to obtain the TiO_2-supported bentonite and *in situ* decorated with Au nanoparticles (NPs) thin film. The advanced analytical techniques characterizes the materials. The laboratory scale reactor was utilized for efficient degradation of R-B and R-6G using thin film catalysts. The percentage removal of R-B was 54.13% (visible light) and 76.26% (UV-A light) and the R-6G, was removed 60.37% (visible light) and 84.68% (UV-A light) at the initial pollutant concentration of 0.5 mg/L and at pH 6.0 using the thin film photocatalyst. The parametric studies demonstrated the insights of degradation mechanisms in photocatalytic operations. A significant mineralization of these dyes is achieved, and the repeated use in reactor operations indicated the catalysts' stability. After six repeated cycles of photocatalytic reaction, the efficacy of catalyst was decreased by 1.02% only (for R-G) and 0.93% only (for R-6G). A plausible reaction pathway was proposed, and the real implications showed higher selectivity of the catalyst.

Keywords: Degradation Pathway, Insights of Degradation, Mineralization of Dyes, Nanocomposite Material, Rhodamine B, Rhodamine 6G

Graphical Abstract

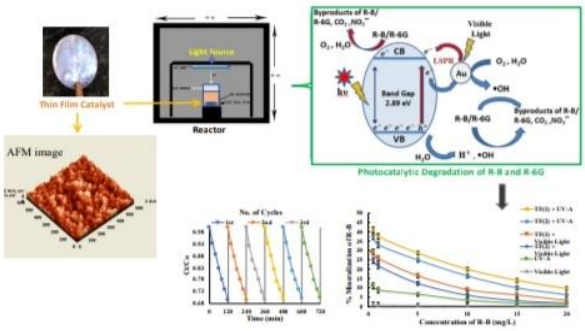

† Corresponding author
E-mail: diw_tiwari@yahoo.com (D.T.), leesm@cku.ac.kr (S.M.L.)
Tel: +91-9862323015 (D.T.), +82-10-88917635 (S.M.L.)
Fax: +91-389-2330834 (D.T.)
ORCID: 0000-0002-9177-9704 (D.T.), 0000-0003-0240-4888 (S.M.L.)

Applied Chemical Engineering

2018 . Vol 1 . No 1

ISSN

2578-2010 (Online)

Indexing & Archiving

Scopus

CNKI 中国知网 www.cnki.net 中国知识基础设施工程

EuroPub

Academic Resource Index ResearchBib

ROOTINDEXING

PORTICO

EnPress

1

Appl. Chem. Eng., Vol. 33, No. 5, October 2022, 00-00
https://doi.org/10.14478/ace.2022.1089

Article

Advancement of Clay and Clay-based Materials in the Remediation of Aquatic Environment Contaminated with Heavy Metal Toxic Ions and Micro-pollutants

Lalhmunsiama, Ralte Malsawmdawngzela*, Chhakchhuak Vanlalhmingmawia*, Diwakar Tiwari*,† and Yiyong Yoon,†**

Department of Industrial Chemistry, School of Physical Sciences Mizoram University, Aizawl 796004, India
**Department of Chemistry, School of Physical Sciences Mizoram University, Aizawl 796004, India*
***Department of Biosystems and Convergence Engineering, Catholic Kwandong University, 도시명 우편번호, Korea*
(Received August 24, 2022; Revised September 14, 2022; Accepted September 15, 2022)

Abstract

Clay minerals are natural materials that show widespread applications in various branches of science, including environmental sciences, in particular, the remediation of water contaminated with various water pollutants. The modified clays and minerals attracted the attention of researchers in the recent past since the modified materials are seemingly more useful and efficient for removing emerging water contaminants. Therefore, the modified engineered materials having multi functionalities have received greater interest from researchers. The advanced clay-based materials are highly effective in the remediation of water contaminated with organic and inorganic contaminants, and these materials showed enhanced selectivity towards the specific pollutants. The review inherently discusses various methods employed in the modification of clays and addresses the challenges in synthesizing the advanced engineered materials precursor to natural clay minerals. The changes in physical and chemical properties, as investigated by various characterization techniques before and after the modifications, are broadly explained. Further, the implications of these materials for decontamination waterbodies as contaminated with potential water pollutants are extensively discussed. Additionally, the insights involved in the removal of organic and inorganic pollutants are discussed in the review. Furthermore, the future perspectives and specific challenges in the scaling up of the treatment methods in the technology development are included in this communication.

Keywords: *Advanced clay based materials, Sorption mechanism, Micro-pollutants, Heavy metals, Synthesis of advanced materials*

1. Introduction

Rapid industrialization and urbanization resulted in the deleterious quality of fresh water. The occurrence of toxic heavy metals and emerging micro-pollutants in water resources is increased tremendously with the advent of enhanced industrial and anthropogenic activities, including the mining industry, electroplating industry, pesticides, metal rinse processes, tanning industry, textile industry, batteries, metal smelting, paper industry, electrolysis applications etc.[1,2]. Many heavy metals, including mercury, lead, copper, cadmium, arsenic, chromium, and many other (toxic) metals, are excessively released, which causes serious environmental and public health issues[3,4]. The primary sources, permissible levels in drinking water, and health effects of heavy metals are given in Table 1. The heavy metals are persistent and non-biodegradable; hence, even at low concentrations posing serious environmental concerns. The presence of these contaminants in waterbodies resulted in a slow accumulation in the biological systems, both in marine and human lives. Hence, eliminating these heavy metals is a viable and effective solution to safeguard the human and aquatic environment[5].

Similarly, excess release of harmful endocrine-disrupting chemicals (EDCs), pharmaceuticals, dyes, personal care products etc. are entering the aquatic environment through various anthropogenic activities[6,7]. Micro-pollutants are usually detected at trace quantities ranging from μg/L to ng/L in waterbodies, including river and lake waters. Since the traditional wastewater treatment plants are not specifically designed to eliminate these emerging pollutants at low levels. Moreover, their potential persistency and bioactivity caused an additional pollutant load to the water bodies, which needs efficient removal of these emerging contaminants from the aquatic environment. Different types of micro-pollutants and their effects on human health are summarized in Table 2. Due to extensive and continuous usage of these pollutants with unmanaged disposal in the water bodies, they are detected in the aquatic environment. Therefore, these micro-pollutants pose several health issues in humans and living organisms and received a global concern [8,9].

Removing of toxic heavy metals and micro-pollutants from water bodies is of great environmental concern. A literature survey reveals that several methods, including chemical precipitation, evaporation, re-

† Corresponding Author: Diwakar Tiwari: Department of Chemistry, School of Physical Sciences Mizoram University, Aizawl 796004, India;
Yiyong Yoon: Department of Biosystems and Convergence Engineering, Catholic Kwandong University, 도시명 우편번호, Korea
Tel: Diwakar Tiwari: +91-9862323015; Yiyong Yoon: +82-유선번호
e-mail: Diwakar Tiwari: diw_tiwari@yahoo.com; Yiyong Yoon: yoonyy@cku.ac.kr

pISSN: 1225-0112 eISSN: 2288-4505

Appl. Chem. Eng., Vol. 33, No. 3, June 2022, 00-00
https://doi.org/10.14478/ace.2022.1030

Review

Newer Insights on Ferrate(VI) Reactions with Various Water Pollutants: A review

Levia Lalthazuala, Lalhmunsiama*, Chhakchhuak Vanlalhmingmawia, Diwakar Tiwari†, Suk Soon Choi and Seung-Mok Lee***,†**

Department of Chemistry, Mizoram University, Aizawl-796004, India
**Department of Industrial Chemistry, Mizoram University, Aizawl-796004, India*
***Department of Biological and Environmental Engineering, Semyung University, Jecheon 27136, Republic of Korea*
****Department of Environmental Engineering, Catholic Kwandong University, Gangneung 25601, Republic of Korea*
(Received May 13, 2022; Revised May 27, 2022; Accepted May 27, 2022)

Abstract

Ferrate (VI) [Fe(VI)] has multi-functional features, which includes potential oxidant, coagulant, and disinfectant features. Therefore, because of these distinctive properties, numerous studies have examined the synthesis of ferrate (VI) and its possible applications in a wide variety of areas. This review details different methods of ferrate synthesis that have been examined to date, including wet chemical, electrochemical, and thermal methods. This paper also discusses in depth the recent advancements that have been achieved in ferrate (VI) oxidation and the synergistic effect of the oxidative properties of ferrate (VI) in the presence of various compounds or materials. Moreover, this review examines the methods of ferrate (VI) application used to degrade various types of water pollutants and its reaction mechanism. The optimized experimental conditions and interactions mechanisms of ferrate (VI) with micro-pollutants, dyes, and other organic compounds are also elaborated upon to provide greater insight for future studies. Lastly, the limitations of and prospects for ferrate use in the treatment of polluted water are described.

Keywords: *High-valent iron (Fe(VI)), mineralization, micro-pollutants, mechanism, synthesis of high purity Fe(VI), insights of reactions*

1. Introduction

Urbanization and the rapid growth of various types of industry have led to a significant upsurge in the production of recalcitrant pollutants, thus affecting the aquatic eco-system and resulting in environmental pollution[1−3]. Studies have shown that natural water is now contaminated with various pollutants, such as pesticides, volatile organic carbons, pathogenic microbes, pharmaceuticals, and personal care products[4−6]. These pollutants negatively affect biodiversity, human health, and marine ecosystems[7−9]. The need for water treatment necessitates the development of novel procedures to remove organic pollutants, and micro-pollutants in particular, as those are primarily persistent in nature[10,11]. The conventional approaches, including the photocatalytic, adsorption, filtration processes, are constrained by limited efficiency, generation of toxic byproducts, time consuming, etc.[12]. On the other hand, ferrate (VI) delivers multi-functional with high efficiency showed enhanced applicability. Further, the ferrate (VI) treatment was devoid with toxic by-products that implied it safer and environment friendly treatment[13]. Therefore, the application of ferrate (VI) for wastewater treatment is an attractive process, as it has been shown to be both environmentally friendly and relatively efficient[14].

The application of advanced oxidation processes to remove organic micro-pollutants has attracted increasing interest because they are capable of efficiently removing pharmaceuticals, dyes, and hormonal drug from aqueous waste[7,15]. Ozonation and Fenton reactions have been shown to be effective in removing hazardous organic chemicals; however, compared to its parent molecule, ozone generates additional hazardous intermediates[16]. Chemical oxidation using peroxydisulfate and permanganate are widely used to degrade several organic pollutants, but the oxidation pathways are found to be highly pH dependent and the oxidation efficiency oxidant is limited[17]. It has been further reported that sulfate and its degradation products provide significant risks of secondary exposure[17]. Moreover, oxidation using permanganate has a drawback in that the manganese oxide generated during the oxidation of permanganate contributes to the blockage of the filter pores, which consequently suppresses the efficacy of water treatment[18,19].

There are multiple ferrate (VI) treatment approaches in reaction systems (single and multiple treatment and/or encapsulation) that have been further suggested for advance implications of ferrate (VI). The advantages of using ferrate (VI) for SST (Sewage Sludge Treatment)

† Corresponding Author: Seung-Mok Lee: Department of Environmental Engineering Catholic Kwandong University, Gangneung 25601, Republic of Korea; Diwakar Tiwari: Department of Chemistry Mizoram University, Aizawl-796004, India
Tel: Seung-Mok Lee: +82-유선 전화번호; Diwakar Tiwari: +91-9862323015
e-mail: Seung-Mok Lee: leesm@cku.ac.kr; Diwakar Tiwari: diw_tiwari@yahoo.com

pISSN: 1225-0112 eISSN: 2288-4505

PARTICULARS OF THE CANDIDATE

NAME OF THE CANDIDATE	:	CVL Hmingmawia
DEGREE	:	Doctor of Philosophy (Ph.D.)
DEPARTMENT	:	Department of Chemistry
TITLE OF THESIS	:	Photocatalytic Degradation of Micropollutants Using Thin Films Fabricated with Advanced Materials
DATE OF ADMISSION	:	9th August, 2018

APPROVAL OF RESEARCH PROPOSAL:

1. BOS	:	23th April, 2019
2. SCHOOL BOARD	:	8th May, 2019
3. MZU REGISTRATION NUMBER	:	1807307
4. Ph.D REGISTRATION NO. & DATE	:	MZU/Ph.D./1222 of 09.08.2018

Head

Department of Chemistry

ABSTRACT

PHOTOCATALYTIC DEGRADATION OF MICROPOLLUTANTS USING THIN FILMS FABRICATED WITH ADVANCED MATERIALS

AN ABSTRACT SUBMITTED IN PARTIAL FULFILMENT OF THE REQUIREMENTS FOR THE DEGREE OF DOCTOR OF PHILOSOPHY

CVL HMINGMAWIA

MZU REGISTRATION NUMBER : 1807307

Ph.D REGISTRATION NUMBER : MZU/Ph.D./1222 of 09.08.2018

DEPARTMENT OF CHEMISTRY

SCHOOL OF PHYSICAL SCIENCES

SEPTEMBER, 2022

PHOTOCATALYTIC DEGRADATION OF MICROPOLLUTANTS USING THIN FILMS FABRICATED WITH ADVANCED MATERIALS

BY

CVL HMINGMAWIA

Department of Chemistry

Under the supervision of

Prof. DIWAKAR TIWARI

Submitted

In partial fulfilment of the requirement of the Degree of Doctor of Philosophy in Chemistry of Mizoram University, Aizawl.

ABSTRACT

The most valuable natural resource on the planet is water. However, the water resources are unethically and improperly treated. Therefore, a reliable fresh and clean water resource remains a global concern. Finite freshwater resources are under tremendous stress, which results in unsustainable exploitation and rising water demand for numerous human activities. Further, global climate change, growing urbanisation, agricultural and industrial activity caused massive release of wastewater contained with refractory contaminants and solid wastes. Over the last few decades, the volume of hazardous wastes deposited in aquatic environments has increased significantly. Furthermore, massive increase in pollutant load has resulted in widespread water quality degradation/deterioration around the world, limiting availability of clean or fresh water. About 2 billion people lack access to clean/fresh water, according to the World Bank and the World Health Organization, and around 1 billion people are unable to get their daily basic needs. Each year, 3.5 million people die in the developing nations due to the insufficient water supply, sanitation, and hygiene related issues.

The increased amount of wastewater carrying a wide range of toxic and hazardous chemicals along with pathogens poses a serious threat to human health, aquatic life and the environment in general. Diarrheal illness is one of a prominent water borne disease; expected to cause 1.5 million children's death below the age of five years. Furthermore, the increasing global shortages of clean water, as well as the catastrophic environmental repercussions of wastewater, need an urgent treatment and reduction of such wastewaters. Due to rigorous environmental regulations and norms, it is now required that wastewater collected from municipalities and communities need to be appropriately treated in order to meet the mandated and stringent water quality requirements before being disposed-off into lakes or rivers. Several monitoring agencies stated that the pharmaceuticals and dyes are widely detected in the waterbodies.

Tetracycline (TC) is a widely prescribed antibiotic for the treatment of bacterial infections like pneumonia, gonorrhoea, amoebic infections, respiratory tract infections, Rocky Mountain spotted fever and syphilis. It is also used to treat acne vulgaris, as well as other skin conditions such as perioral dermatitis and rosacea. It enters the water bodies as active metabolites, unmetabolized drugs and breakdown products by excretion and direct runoff. It is known fact that over 90% of antibiotics are excreted through the urine and up to 75% in animal faeces, implying that 70%-80% of antibiotics enter into the sewage system in their parent form. However, the conventional sewage treatment system is unable to eliminate it completely; hence, resulting in residual antibiotics in the treated wastewater effluents. Sulfamethazine (SMZ) is also one of the most often detected antibiotics in water bodies. It is potentially harmful to marine species, affects animal reproduction, and interrupts the human endocrine system, hence; the presence of SMZ in water bodies is a serious environmental concern. Bisphenol A (BP-A) is a common organic compound used as a raw material and intermediary in the production of epoxy resins, polycarbonate plastics and food packaging. It is regarded as a typical chemical of endocrine disrupting chemicals (EDC) that leads to damage in the reproductive organs of aquatic organisms.

Dyes such as Mordant Orange-1 (MO1), Rhodamine B (Rh-B) and Rhodamine 6G (Rh-6G) are extensively utilized in the pharmaceutical, food, cosmetic, textile, paint, tannery, paper and pulp, and paper industries for dyeing the materials. Such dyes enter the water bodies through effluent discharged by these industries, as well as those from dye manufacturing plants. Therefore, the dye industries posing serious environmental concerns due to the discharge of dye compounds into the aquatic environment and lead to a major threat to the aquatic environment's living species

Despite advancements in wastewater treatment, conventional water treatment systems are not able to completely eliminate such harmful micro-pollutants. The treatment process entails a number of time-consuming steps that necessitate the use of a range of chemicals. Perhaps the most important disadvantage is the potential of environmental issues to arise as a result of these activities. Hypochlorite, chlorine and ozone are among the chemical oxidants typically employed in wastewater treatment.

Because of their easy availability, possibly cost effectiveness and relative efficiency as oxidants, these chemicals are widely used. However, the by-products produced appear to be hazardous, their application in such environmental remediation raises various health issues. Furthermore, the use of ozone and chlorine in wastewater treatment is linked to the formation of toxic disinfection by-products (DBPs) such as bromate and trihalomethanes. Numerous by-products are potentially carcinogens or mutagens, making them potentially more dangerous than the original compounds. Another disadvantage of current wastewater treatment systems is the production of excessive sludge, which frequently encompasses numerous types of harmful substances, making pollutants removal a serious concern.

Therefore, there is a growing concern on developing effective and efficient waste water treatment methods, which is feasible, cost-effective, environment friendly, and sustainable. "Advanced Oxidation Process (AOPs)" is one of the alternative methods, which relies on heterogeneous photocatalysis using the TiO_2 semiconductor as a photocatalyst. The basis of AOPs lies on the *in situ* formation of reactive species, such as hydroxyl radicals, which rapidly oxidises a variety of organic contaminants non-selectively. Titania (TiO_2) has a variety of applications, which is primarily due to its unique qualities, that include high thermal and chemical stability, biocompatibility, low toxicity, cost effectiveness, ease of manufacturing and tailored material. The use of TiO_2 semiconductor in photocatalytic processes is found to be a cost-effective, environment friendly, and long-term treatment technique that aligns with the 'zero' waste strategy. Despite numerous advantages, TiO_2 possesses a number of limitations that limit its wider implications in the treatment processes. TiO_2 has a large band gap energy (3.2 eV) that requires harmful UV-C radiation to excite the semiconductor. Moreover, a high electron-hole pair recombination rate limits the efficiency of catalysts in wastewater treatment processes. The e^-/h^+ pairs are having very short lifespans, and without the presence of suitable scavengers, recombination dissipates the stored energy within a few nanoseconds. However, a suitable modification improves the applicability of TiO_2 in the wastewater treatment.

Doping of Ag or Au nanoparticles with TiO_2 has shown a substantial importance due to the surface plasmon resonance (SPR) phenomenon. The Ag or Au

nanoparticles decorated TiO_2 are able to absorb light towards the visible region, which causes a localised electric field near the TiO_2 surface, resulting in the efficient generation of electron-hole pairs at the TiO_2 surface. Furthermore, the noble metal nanoparticles on TiO_2 surface operate as a co-catalyst, assisting the efficient separations of electron and hole pairs. The presence of Ag^0(NPs) effectively restricts the electrons excited from TiO_2 and leaves the holes for organic compound degradation reactions. It also causes a delay in their wavelength response when they approach the visible range. Furthermore, silver nanoparticles efficiently promote electron excitation by generating a local electric field, with surface plasmon resonance effect in metallic silver nanoparticles, which show an enhanced electric field. Similarly, the Au^0(NPs) doped TiO_2 exhibit an intense visible light absorption and the surface plasmon resonance effect (SPR) of their free electrons.

Recently, interest lies on the advanced nanocomposite material based on the natural clay and TiO_2 for the removal of micro-pollutants. Bentonite clay is an aluminium silicate in which two silica tetrahedral sheets fused to one alumina octahedral sheet. Clay is a porous material showing high surface area, which offers an excellent support material. Moreover, clays are abundant, non-toxic, cost effective, and more importantly are found environment friendly. The potential applicability of the bentonite clay supported TiO_2 and further decorated with Ag or Au nanoparticles for the degradation of emerging micro-pollutants (mordant orange 1 (MO1), tetracycline (TC), sulfamethazine (SMZ), bisphenol A (BP-A), rhodamine B (Rh-B) and rhodamine 6G (Rh-6G)) in an aqueous solutions is presented in this work.

Ag^0(NP) doped TiO_2 nanocomposite (Ag^0(NPs)/TiO_2), bentonite clay supported Ag^0(NP) doped TiO_2 nanocomposite (Clay/Ag/TiO_2 and Clay/Ag/TiO_2(T)) and bentonite clay supported Au^0(NP) doped TiO_2 nanocomposite (Clay/Au/TiO_2 and Clay/Au/TiO_2(T)) were synthesised using a facile template synthetic route using polyethylene glycol as filler medium. The thin film catalysts were fabricated by a simple dip coating process. The materials were characterized by advanced analytical methods such as scanning electron microscopy (SEM), transmission electron microscopy (TEM), X-ray diffraction (XRD), atomic force microscopy (AFM), Brunauer-Emmett-Teller (BET) and diffuse reflection spectroscopic (DRS) analyses.

The SEM images of Ag^0(NPs)/TiO_2 showed that Ag(NPs) were spatially distributed within the titania network and the interplanar distance of Ag^0(NPs) was 0.15 nm. The AFM analysis indicated that the nanocomposite forms a heterogeneous structure on the glass substrate. BET analysis revealed that the root mean square roughness (R_q) and mean roughness (R_a) of Ag^0(NPs)/TiO_2 catalyst was 16.952 nm and 12.250 nm, respectively. The diffuse reflectance spectra (DRS) for powder TiO_2 and Ag^0(NPs)/TiO_2 was obtained using UV-Vis spectrophotometer and the band gap energy of the material was obtained by converting the diffuse reflectance data in to its absorption coefficient (α) values using Kubelka-Munk equation and the *Tauc's* relationship. The band gap energies for TiO_2 and Ag^0(NPs)/TiO_2 were determined to be 3.28 and 2.9 eV, respectively. This clearly indicated that the presence of Ag^0(NPs) caused to reduce the band gap energy of the nanocomposite material. On the other hand, the Clay/Ag/TiO_2 and Clay/Ag/TiO_2(T), the SEM images showed that fine grains of nanocomposite materials were evenly distributed on the substrate. Further, the TEM images showed that the Ag^0(NPs) are very distinctly distributed on the surface and formed cubical shape particles. Moreover, the AFM analyses showed that the mean roughness (R_a) of Clay/Ag/TiO_2 and Clay/Ag/TiO_2(T) thin-film was found to be 6.879 nm and 52.831 nm, respectively. The anatase phase of titanium dioxide was present in the synthesized materials. The N_2 adsorption/desorption results showed the H1 type hysteresis loops, which indicated that the porous material has a regular array of uniform spheres. The band gap energies of Clay/Ag/TiO_2 and Clay/Ag/TiO_2(T) were found to be 2.85, and 2.9 eV, respectively. Similarly, in case of Clay/Au/TiO_2 and Clay/Au/TiO_2(T) composite materials, the SEM images revealed that both the thin films showed heterogeneous surface structure and the fine particles of Au/TiO_2 are dispersed on the substrate surface. The TEM images revealed that the interplanar distance of the Au(NPs) was found to be 0.34 nm for both Clay/Au/TiO_2(T) and Clay/Au/TiO_2 solids. 3D-AFM analysis revealed that the mean roughness (R_a) and the root mean square roughness (R_q) of Clay/Au/TiO_2(T) were determined 1.165 nm and 1.454 nm, respectively, and 0.386 nm and 0.572 nm, respectively for Clay/Au/TiO_2. DRS study revealed that doping of Au(NPs) with TiO_2 results in decrease of band energy from 3.24 to 2.85 and 2.88 eV for Clay/Au/TiO_2(T) and Clay/Au/TiO_2 respectively.

The photocatalytic degradation of micropollutants are carried out using the thin film catalysts under LED (Visible Light) and UV-A light with several parametric studies to obtain the insights of mechanisms involved at the catalyst surface. The decrease in pH (from pH 10.0 to 4.0) has caused to increase the photocatalytic degradation efficiency of mordant orange 1 (MO1) (using Ag^0(NPs)/TiO_2) and bisphenol A (BP-A) (using Clay/Ag/TiO_2) (from pH 12.0 to 6.0). However, increase in solution pH from 4.0 to 10.0 significantly favoured the photocatalytic degradation efficiency of tetracycline (TC) (using Clay/Ag/TiO_2). Sulfamethazine (SMZ) (using Clay/Ag/TiO_2) and rhodamine B (Rh-B) (using Clay/Au/TiO_2) showed maximum degradation efficiency at pH ~6.0, while rhodamine 6G (Rh-6G) (using Clay/Au/TiO_2) showed its maximum degradation efficiency at pH ~8.0.

The decrease in pollutant concentrations (20.0 to 0.5 mg/L) significantly favoured the removal efficiency of MO1 (using Ag^0(NPs)/TiO_2), TC, SMZ and BP-A (using Clay/Ag/TiO_2), Rh-B and Rh-6G (using Clay/Au/TiO_2) under the photocatalytic treatment. With an increase in pollutant concentrations from 0.5 to 20.0 mg/L, the percentage degradation of MO1 was decreased from 60.6% to 13.7% (UV-A) and 38.14% to 6.5% (LED light). Further, the percentage degradation of TC was decreased from 81.13% to 50.36% (UV-A) and 57.89 % to 34.46% (LED light). Furthermore, the percentage degradation of SMZ was decreased from 64.58% to 36.21% (UV-A) and 37.83% to 18.42% (LED light). Moreover, the percentage degradation of BP-A was decreased from 75.3% to 40.6% (UV-A) and 50.0% to 25.35% (LED light). Furthermore, the percentage degradation of Rh-B was decreased from 76.26% to 17.64% (UV-A) and 54.13% to 6.07% (LED light). The percentage degradation of Rh-6G was decreased from 84.68% to 19.66% (UV-A) and 60.37% to 8.42% (LED light). These results show that the thin films photocatalyst could be used effectively at an extensively wide range of solution pH and concentration for the degradation of these micro-pollutants. Thus the thin film photocatalysts are highly efficient in the degradation of these micro-pollutants in the aquatic environment. Further, the TOC (total organic carbon) data showed that the extent of mineralization of these pollutants was increased with a decrease in the micropollutants concentrations. The decrease in concentration of pollutants from 20.0 to 0.5 mg/L has caused the

percentage mineralization of MO1 to increase from 7.72% to 27.38% (UV-A) and 4.12% to 17.1% (LED light). Further, the percentage mineralization of TC was increased from 27.3% to 42.6% (UV-A) and 18.2% to 31.3% (LED light). Furthermore, the percentage mineralization of SMZ was increased from 21.8% to 34.2% (UV-A) and 10.4% to 20.1% (LED light). Moreover, the percentage mineralization of BP-A was increased from 26.2% to 45.8% (UV-A) and 14.3% to 27.5% (LED light). Furthermore, the percentage mineralization of Rh-B was increased from 9.64% to 41.12% (UV-A) and 3.32% to 29.37% (LED light). The percentage mineralization of Rh-6G was increased from 10.74% to 43.16% (UV-A) and 5.16% to 33.25% (LED light).

The degradation kinetics of mordant orange 1 (MO1), tetracycline (TC), sulfamethazine (SMZ), bisphenol A (BP-A), rhodamine B (Rh-B) and rhodamine 6G (Rh-6G) followed pseudo-first-order rate kinetics, and the degradation rate was utilized to fit the Langmuir-Hinshelwood isotherm. The photocatalytic degradations of MO1, TC, SMZ, BP-A, Rh-B and Rh-6G follow the L-H isotherm reasonably well. Further, the effect of co-existing ions and scavengers in the photocatalytic degradation of MO1 (using Ag^0(NPs)/TiO_2), TC, SMZ and BP-A (using Clay/Ag/TiO_2), Rh-B and Rh-6G (using Clay/Au/TiO_2) were studied. The removal efficiency of MO1 was affected in the presence of NaCl, EDTA and glycine. The scavengers such as 2-propanol, HCO_3^- and sodium azide hampered significantly the percentage degradation of MO1. The presence of NaCl, EDTA, and glycine significantly affected the removal efficiency of TC. In case of SMZ the removal efficiency was significantly hampered in the presence of oxalic acid, EDTA, and $CuSO_4$. The percentage elimination of TC and SMZ was significantly hindered in the presence of scavengers such as 2-propanol and $NaHCO_3$. Moreover, the degradation efficiency of BP-A was lowered in the presence of NaCl, $NaNO_3$, EDTA, glycine, 2-propanol and $NaHCO_3$. Similarly, the Rh-B and Rh-6G degradation was suppressed in the presence of NaCl, $NiCl_2$, EDTA, oxalic acid, glycine, 2-propanol, HCO_3^- and sodium azide. These studies inferred that the degradation of these pollutants predominantly proceeded through the •OH radicals. Additionally, the singlet oxygen is also taking part in photocatalytic degradation reactions. The occurrence of several anions and cations affected the photocatalytic

degradation of these micro-pollutants at varied levels. This is because these ions compete with the pollutant molecules for sorption on the photocatalyst surface. Hence, it prevented the target molecule from reaching the photocatalyst surface and hindered the photocatalytic degradation of pollutant molecules.

The repeated use of thin films, *viz*., Ag^0(NPs)/TiO_2, Clay/Ag/TiO_2, Clay/Ag/TiO_2(T), Clay/Au/TiO_2 and Clay/Au/TiO_2(T) showed no substantial decline in percentage degradation of these micropollutants from aqueous solutions, which indicated that the thin films photocatalyst are fairly stable at least for six photocatalytic operations. Overall, the template synthesized photocatalysts Ag^0(NPs)/TiO_2, Clay/Ag/TiO_2(T) and Clay/Au/TiO_2(T) showed relatively enhanced photocatalytic efficiency than the corresponding non-template synthesized photocatalysts Clay/Ag/TiO_2 and Clay/Au/TiO_2. The efficiency of the photocatalytic process were obtained to be remarkably higher than the photolytic process in the degradations of MO1 (using Ag^0(NPs)/TiO_2), TC, SMZ and BP-A (using Clay/Ag/TiO_2), Rh-B and Rh-6G (using Clay/Au/TiO_2). This emphasized that the thin film catalysts are having potential in the efficient degradation of several pollutants in the aqueous medium. Further, the photocatalytic degradation of these pollutants were carried in the real water samples and the removal efficiency of these pollutants was not affected as compared to the purified water degradation. These results further inferred the selectivity of catalyst in the degradation of these pollutants and wider implacability in real implications. The entire treatment process is relatively "greener" as devoid with ‘no-waste’ generation.